SYNTHESIS, ELECTROCHEMISTRY, AND PHYSICAL STUDIES OF GRAPHITE ELECTRODES WITH CHEMICALLY MODIFIED SURFACES AND COPPER COMPLEXES WITH MACROCYCLIC LIGANDS

Thesis by

Carl Anthony Koval

In Partial Fulfillment of the Requirements

for the Degree of

Doctor of Philosophy

California Institute of Technology

Pasadena, California

1979

(Submitted November 20, 1978)

To my wife,

Joan

and

to my parents,

Anne and Bernard.

Acknowledgements

If a man must serve two masters, he should try to find two people like my advisors Fred Anson and Bob Gagné. I thank Fred and Bob for their interest, suggestions and encouragement, and especially for their understanding about my divided responsibilities.

My work at Caltech has allowed me to collaborate with several postdocs, namely Alan Brown, Wayne Smith, Noboru Oyama and Tom Smith. I enjoyed these interactions and learned much from them. Indeed, I have enjoyed working with everyone in the Anson and Gagné groups.

I thank the following people and places for providing friendship and social diversions: fellow Hash Marker and Clubhouse Member Bruce Parkinson; drinking and hiking companions Judy Allison and Malcolm Boyd; tennis opponent Peter Armentrout; beautiful places, Yosemite, Kings Canyon, and Sequoia National Parks; fellow hackers Pete Wolczanski, Rich Threlkel and Bill Jones; comedian and confidante Dave Erwin; iron pumpers Cliff Spiro and Bob Kreh; good neighbors David and Susan Andersen; and UCLA comrades Jean Campbell and Peter Bird. In a similar vein, I thank all the East Coast friends and relatives whose visits kept homesickness to a minimum.

Thanks to Beth Cooper for typing this thesis.

I especially want to acknowledge my close friend, Tom Upton. Besides keeping me sane for these four years, he and his wife Nancy

provided me with a home while I was in the throes of writing up.

Finally, I thank my wife Joan. Without her encouragement I never would have come to Caltech and without her companionship I would not have stayed.

Abstract

The attachment of various molecules to graphite surfaces and the electrochemistry exhibited by the attached species are discussed in Part I.

Section I-A

Aromatic compounds such as 9,10-phenanthrenequinone are irreversibly adsorbed onto pyrolytic graphite electrodes. Cyclic voltammetry is used to illustrate the differences in electrochemical response between surface and solution species. Integration of the current used to oxidize or reduce the molecules on the surface affords measurement of surface concentrations, which are typically 10^{-10} to 10^{-11} moles/cm^2. The use of differential pulse voltammetry to study surface electrochemistry is introduced.

Section I-B

Procedures are presented for attaching pyridinepentaammineruthenium(II) complexes to graphite electrodes by covalent bonding and irreversible adsorption. Cyclic voltammetry and differential pulse voltammetry are used to compare the electrochemical behavior of the attached complexes and to measure surface concentrations. Different orientations of the anisotropic graphite affect the quantity of reactant that can be attached as well as the voltammetric responses. On "edge plane" pyrolytic graphite the covalently bound and irreversibly adsorbed ruthenium complexes reach coverages of 1.5×10^{-10} and 1.6×10^{-9} moles/cm^2, respectively. The coverage for

the adsorbed complex on "basal plane" graphite is 3.5×10^{-10} moles/cm^2. The covalent attachment procedure is unsuccessful on this surface, presumably due to the lack of surface oxides. Attachment by irreversible adsorption yields larger quantities of complex on the electrode surface but the covalently attached complex persists on the surface for a longer time; $t_{1/2}$ = 313 and 1080 min, respectively.

Design of a holder used for rapid mounting of graphite discs for electrochemical use is included.

Section I-C

The catalytic reduction of oxygen in acidic aqueous solution at several modified pyrolytic graphite surfaces is examined using a rotating ring-disc electrode. Surfaces coated with 9,10-phenanthrenequinone and Ru(III)(edta) afford no catalysis. Adsorbed Fe(III) protoporphyrin IX catalyzes the reduction of oxygen to water at ~0.2 V. Catalytic properties of modified graphite and platinum surfaces are compared.

The synthesis, electrochemistry and physical properties of a variety of Cu(II) and Cu(I) complexes are presented in Part II. The physical studies reveal several unusual properties of the Cu(I) complexes.

Section II-A

Measurements of formal reduction potentials are compared for several inorganic systems using cyclic voltammetry, d.c. polarography, differential pulse voltammetry, and potentiometry. For the type of copper complexes

being studied, d.c. polarography is judged to be the most reliable technique, especially in the electrochemical measurement of CO binding constants. The potential of the oxidation of ferrocene to ferricenium ion is suggested as a practical reference against which to report the potentials of other couples.

Section II-B

The synthesis of an oxo-bridged copper(II)-copper(I) mixed-valence ion and its carbon monoxide adduct is reported along with preliminary observations concerning electronic and electron paramagnetic resonance spectra of the ions.

Section II-C

More complete physical studies of the mixed-valence system introduced in Section II-B are presented. Electrochemistry is used to synthesize the copper(I)-copper(I) state of the molecule and to obtain formal reduction potentials (-0.518 V and -0.908 V) for the two copper atoms. The CO binding constant for the copper(II)-copper(I) complex is measured polarographically and found to be 2.82×10^4. All complexes are characterized by elemental analysis, infra-red spectroscopy, magnetic susceptibility and electronic spectroscopy. Temperature-dependent electron paramagnetic resonance spectra of the mixed-valence complex provide an estimated intramolecular electron transfer rate of 2.2×10^{10} sec^{-1} at 298°K.

Table of Contents

Introduction to Research on Graphite Electrodes with Chemically Modified Surfaces

Research in the area of modified electrode surfaces has expanded rapidly since 1975 (1-14). Prior to 1975, only two papers by Hubbard and Lane (8) contained material similar to the work being done in this field today. While modified electrodes are of interest for a variety of reasons, the research described herein originated as part of a collaborative effort to discover an electrode that would reversibly reduce molecular oxygen to water (15).

The ability to reduce oxygen to water rapidly at its thermodynamic potential, +1.23 V versus NHE, would constitute a major breakthrough in the area of fuel cells and air batteries. Most electrodes require a large amount of overpotential to effect oxygen reduction and do so only by producing hydrogen peroxide; this is an energetically unfavorable route (16). Platinum is the best material for oxygen reduction. There is evidence that reduction of O_2 at platinum electrodes proceeds directly to H_2O (17); however, platinum is too expensive for practical use in fuel cells.

Rather than searching for new electrode materials, the efforts of the collaboration were to be aimed at synthesizing molecular catalysts capable of: a) being attached to inexpensive electrode materials, b) rapidly reducing oxygen to water, and c) being reactivated by the electrode at ~+1.0 V. The formation and functioning of such a modified electrode is diagrammed below:

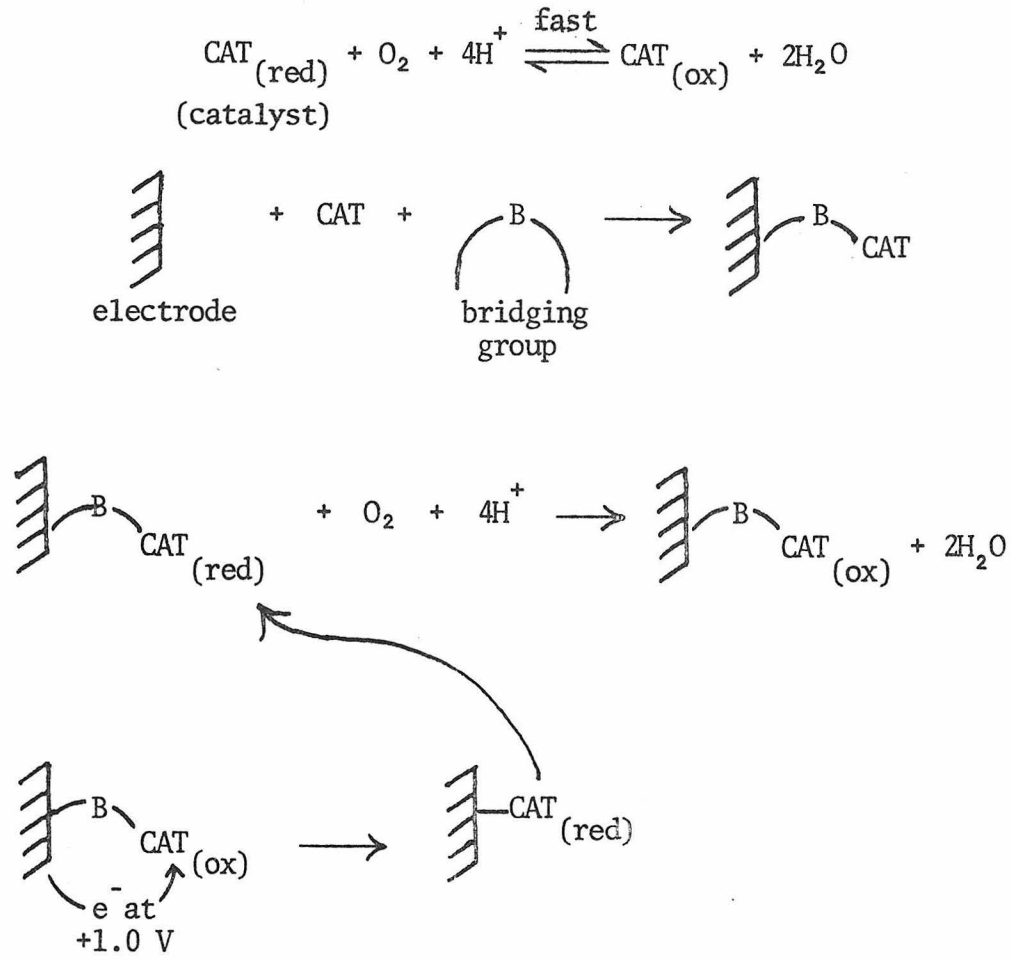

While other partners in the collaboration were to attempt catalyst synthesis, the Anson group was to investigate methods of catalyst attachment and to select electrochemical techniques suitable for detecting surface species and evaluating their ability to reduce oxygen. Initial efforts were directed toward attachment of two classes of compounds, flat aromatic organic complexes and ruthenium complexes, to graphite eletrodes. The attachment of these types of compounds was desirable because the first potential catalysts likely to emerge from the collaboration would be metallo-porphyrins and multi-nuclear ruthenium ammine complexes.

For a variety of reasons pyrolytic graphite was selected as the material to be used in all attempted attachments. A form of pure carbon, graphite is conducting and inexpensive. It has been widely used as a working electrode in electrochemical studies of diffusing species. Most importantly, graphite is anisotropic, being composed of sheets of aromatic carbon atoms with the layers held together by Van der Waals forces. The two possible orientations of graphite are called "basal plane" or "edge plane" depending on whether the flat sheets or jagged edges are exposed. Organic dyes are known to adsorb strongly to the basal planes of graphite, while the edge planes contain a variety of carbon-oxygen functional groups which could be used in covalent attachment of catalysts (18).

Considerable early effort involved attempts to use finely powdered or microcrystalline graphite as an electrode. Powdered graphite has a large surface-area/mass ratio; seemingly, electrode surfaces constructed from these materials would hold easily-detected amounts of catalysts. Unfortunately, only carbon paste electrodes (19) could be made from powdered graphite and the role of the pasting agent, Nujol, in attachment procedures was unclear. Furthermore, this material was so porous that all reagents were trapped within and could only be removed after prodigious washing.

The opposite of microcrystalline graphite is highly ordered pyrolytic graphite, HOPG, which consists of large pieces of graphite ordered nearly as well as in a single crystal. This material

would have been ideal for distinguishing differences in basal and edge faces with respect to various attachment procedures; however, HOPG is nearly impossible to machine or mount as a working electrode.

The material eventually used was a form of graphite that was visibly anisotropic but which contained sufficient lattice disorder to allow machining. It could be mounted successfully with either primarily basal planes (1c) or edge planes (1b) exposed.

At the time of this author's Admission to Candidacy (March 1976) two papers dealing with modified electrodes, other than Hubbard and Lane's, had appeared in the literature. Miller et al. induced chirality in the product of an organic electro-synthetic reaction by attaching an optically-active molecule to a graphite electrode (11a). Murray et al. used silane chemistry to attach several organic molecules to SnO_2 electrodes and then detected their presence with ESCA (12a). In neither case was the attached species detected electrochemically. At Caltech, A. P. Brown and this author were obtaining electrochemical responses from molecules irreversibly adsorbed on graphite electrodes. Electro-active organic molecules such as 9,10-phenanthrenequinone and 3,3'-dimethoxybenzidine, and iron(III) protoporphyrin IX were detected by cyclic voltammetry and differential pulse voltammetry. The results of this work were published (1c) and are included as Section I-A of this thesis (20).

While the irreversible adsorption discussed above occurs spontaneously, it proved to be much more difficult to attach ruthenium complexes to graphite by means of a covalent bond.

Synthesis of the necessary ruthenium complexes was a major problem in itself. Eventually, a ruthenium pentaammine pyridine complex was attached by way of an amide bond. This work has also been published (1b) and constitutes Section I-B of this thesis. Because 9,10-phenanthrenequinone adsorbed so tenaciously on graphite attempts were made to modify this molecule into a ligand capable of complexing with $Ru(NH_3)_5(H_2O)^{2+}$ and anchoring it to the electrode (20). While these efforts failed, Brown was able to synthesize such a molecule from phenanthrene (1d), although phenanthrene adsorbs less strongly than its quinone form and has no electrochemistry. Comparisons of the electrochemistry of anchored and covalently-attached ruthenium are also included in Section I-B.

From 1976 to the present, many papers dealing with modified electrodes have appeared (1-10, 11b-f, 12b-j, 13, 14). Several attachment strategies have been used to affix organic and inorganic molecules to electrodes. The advances in this area suggest that if a good oxygen reduction catalyst existed, it could be successfully attached to an electrode. Therefore, one remaining task necessary for the O_2-collaboration was the development of procedures for evaluating surface-bound catalysts. The rotating ring-disc technique was used for this purpose and this work is presented in Section I-C.

References

1. a) Alan P. Brown and Fred C. Anson, Anal. Chem. 49, 1589 (1977); b) Carl Koval and F. C. Anson, Anal. Chem. 50, 223 (1978); c) Alan P. Brown, Carl Koval and Fred C. Anson, J. Electroanal. Chem. 72, 379 (1976); d) Alan P. Brown and Fred C. Anson, J. Electroanal. Chem. 83, 203, (1977); 3) Noboru Oyama, Alan P. Brown and Fred C. Anson, J. Electroanal. Chem. 87, 435 (1978); f) Noboru Oyama and Fred C. Anson, J. Electroanal. Chem. 88, 289 (1978).

2. N. R. Armstrong and D. D. Hawn, J. Phys. Chem. 82, 1288 (1978).

3. a) A. J. Bard and A. Merz, J. Am. Chem. Soc. 100, 3222 (1978); b) A. J. Bard and A. Merz, J. Electroanal. Chem. 75, 487 (1977).

4. A. Diaz, J. Am. Chem. Soc. 99, 3838 (1977).

5. L. R. Faulkner and Hiroyasu Tachikawa, J. Am. Chem. Soc. 100, 4380 (1978).

6. a) M. Fujihira, T. Matsue and T. Osa, Chem. Lett. 875 (1976); b) T. Osa and M. Fujihira, Nature, 264, 349 (1976); c) M. Fujihira, N. Oihishi, and T. Osa, Nature, 268, 226 (1977).

7. H. L. Landrum, R. T. Salmon, and F. M. Hawkridge, J. Am. Chem. Soc. 99, 3154 (1977).

8. a) A. T. Hubbard and R. F. Lane, J. Phys. Chem. 77, 1401 (1973); b) A. T. Hubbard and R. F. Lane, J. Phys. Chem. 77, 1411 (1973).

9. a) N. R. Armstrong, A. W. Lin, M. Fujihara and T. Kuwana, Anal. Chem. 48, 741 (1976); b) J. F. Evans and T. Kuwana, Anal. Chem. 49, 1632 (1977); c) D. C. Tse and T. Kuwana, Anal. Chem. 50, 640 (1978); d) A. M. Yacynyah and T. Kuwana, Anal. Chem. 50, 1315 (1978); e) J. F. Evans, T. Kuwana, M. T. Henne, and G. P. Royer, J. Electroanal. Chem. 80, 409 (1977); f) A. C. Lin, P. Yeh, A. M. Yacynych, and T. Kuwana, J. Electroanal. Chem. 84, 411 (1977); g) M. C. Fujihira, T. Osa, D. Hursh, and T. Kuwana, J. Electroanal. Chem. 88, 285 (1978).

10. S. Mazur, T. Matusinovic and K. Cammann, J. Am. Chem. Soc. 99, 3888 (1977).

11. a) B. F. Watkins, J. R. Behling, E. Kariv and L. L. Miller, J. Am. Chem. Soc. 97, 3459 (1975); b) B. E. Firth, L. L. Miller, M. Mitani, T. Rodgers, J. Lennox, and R. W. Murray, J. Am. Chem. Soc. 98, 8271 (1976); c) B. E. Firth and L. L. Miller, J. Am. Chem. Soc. 98, 8272 (1976); d) L. L. Miller and M. R. VanDe Mark, J. Am. Chem. Soc. 100, 639 (1978); e) M. R. VanDe Mark and L. L. Miller, J. Am. Chem. Soc. 100, 3223 (1978); f) L. L. Miller and M. R. Van De Mark, J. Electroanal. Chem. 88, 437 (1978).

12. a) P. R. Moses, L. Wier, and R. W. Murray, Anal. Chem. 47, 1882 (1975); b) C. M. Elliot and R. W. Murray, Anal. Chem. 48,

1247 (1976); c) R. G. Davis and R. W. Murray, Anal. Chem. 49, 194 (1977); d) P. R. Moses, L. M. Wier, J. C. Lennox, H. O. Finklea, J. R. Lenhard, and R. W. Murray, Anal. Chem. 50, 576 (1978); e) P. R. Moses and R. W. Murray, J. Electroanal. Chem. 77, 393 (1977); f) J. R. Lenhard and R. W. Murray, J. Electroanal. Chem. 78, 195 (1977); g) J. C. Lennox and R. W. Murray, J. Electroanal. Chem. 78, 395 (1977); h) D. F. Untereker, J. C. Lennox, L. M. Weir, P. R. Moses, and R. W. Murray, J. Electroanal. Chem. 81, 309 (1977); i) P. R. Moses and R. W. Murray, J. Am. Chem. Soc. 98, 7435 (1976); j) J. C. Lennox and R. W. Murray, J. Am. Chem. Soc. 100, 3710 (1978).

13. a) R. J. Burt, G. J. Leigh, and C. J. Pickett, J. Am. Chem. Soc. Chem. Comm. 940, (1976); b) G. J. Leigh and C. J. Pickett, J. Chem. Soc. Dalton, 1797 (1977).

14. a) R. G. Austin, A. B. Bocarsly, J. M. Bolts, O. Haas, K. D. Legg, L. Nadjo, and M. C. Palazzotto, J. Am. Chem. Soc. 100, 1602 (1978); b) R. G. Austin, A. B. Bocarsly, J. M. Bolts, O. Haas, K. D. Legg, L. Nadjo, and M. C. Palazzotto, J. Electroanal. Chem. 87, 429 (1978).

15. F. C. Anson, M. Boudart, J. P. Collman, H. Taube, H. G. Tennent. A proposal concerning this research was originally submitted to and funded by NSF-RANN.

16. J. O'M Bockris and S. Srinivasan, Fuel Cells: Their Electrochemistry, McGraw-Hill, Inc. N.Y. (1969) and references therein.

17. A. Damjonovic, M. A. Genshaw and J. O'M Bockris, J. Electrochem. Soc. 114, 466 (1967).

18. J. S. Mattson and H. B. Mark, Activated Carbon, Marcel Dekker, Inc., N.Y. (1971) and references therein.

19. R. N. Adams, Anal. Chem. 30, 1576 (1958).

20. Only the work with 9,10-phenanthrenequinone and the attempts to use differential pulse voltammetry as a quantitative technique are due to this author.

SECTION I-A

Illustrative Electrochemical Behavior of Reactants Irreversibly Adsorbed on Graphite Electrode Surfaces

Alan P. Brown, Carl Koval and Fred C. Anson

Contribution No. 5340 from the A. A. Noyes Laboratory,
California Institute of Technology,
Pasadena, California 91125
(Received 24 May 1976)

Chemically modified electrode surfaces are the focus of considerable current research in a number of laboratories [1-3]. Ample evidence for the successful attachment of various compounds to the surface of platinum [1], graphite [2] and tin oxide [3] electrodes has been offered, however, the direct observation of the electrochemical behavior of such surface species for extended periods in solutions free of the attached reactants has been reported in only one instance [1]. We have found it possible to observe the electrochemistry of reactants which are irreversibly adsorbed on the surface of graphite electrodes by employing differential pulse voltammetry [4] or slow sweep cyclic voltammetry. The former technique provides an especially good signal-to-noise ratio which allows low surface coverages of reactants to be monitored.

In the present studies we have relied upon the tendency of certain classes of reactants to adsorb very strongly on graphite electrodes to produce electroactive surface species which could be examined in the absence of any diffusing reactant. It proved possible to influence the electrochemistry of these adsorbed reactants by altering the composition (pH, ligand concentration, etc.) of the (reactant free) solutions in which their electrochemistry was inspected, thus demonstrating their

susceptibility to chemical modification in the adsorbed state. The results we have so far obtained suggest many possibilities for elaboration and extensions, a number of which we are currently pursuing.

Experimental

The carbon electrodes employed were either vitreous carbon (Tokai Ltd., Japan) or pyrolitic graphite (Union Carbide Corporation, Parma, Ohio). The rod-shaped electrodes were mounted in glass tubes by means of heat-shrinkable polyolefin tubing to give exposed discs of area ca. 0.2 cm^2. The vitreous carbon was polished before use with silica powder. The pyrolitic graphite was cleaved just before use with a razor blade.

In most experiments, reactants were adsorbed by exposing the electrode to solutions of the reactant for several minutes followed by washing with (undeaerated) distilled water. The electrochemical behavior of the adsorbed reactants was recorded in reactant-free, deaerated supporting electrolyte solutions.

The electrolysis cell and apparatus for recording cyclic voltammograms were conventional. Potentials were measured and are reported with respect to the saturated calomel electrode. Electrode areas were 0.2 cm^2.

Differential pulse voltammograms were obtained with a standard Princeton Applied Research Model 174 instrument with the following settings: Pulse amplitude: 10 mV; d.c. potential scan rate: 5 mV/sec; "drop time": 0.5 sec (i.e., pulse repetition rate: 2 sec^{-1}).

9,10-Phenanthrenequinone was recrystallized from benzene. The iron(III) tetraphenylporphyrin chloride and iron(III) protoporphyrin IX chloride were commercial materials which were used as received. Supporting electrolyte salts and buffers were reagent grade materials used without further purification.

Results and Discussion

Figure 1 shows a set of cyclic voltammograms which result when a pyrolitic graphite or vitreous carbon electrode is placed in a solution containing 10^{-6} M 9,10-phenanthrenequinone and 3×10^{-4} M $Ru(NH_3)_6^{3+}$. The voltammograms were recorded at increasing times following the immersion of the electrode in the solution. The phenanthrenequinone/phenanthrenehydroquinone and $Ru(NH_3)_6^{3+/2+}$ couples give rise to the pairs of waves centered at +175 mV and -200 mV, respectively. The peak currents of the former couple increase in magnitude as more and more of the quinone has time to diffuse to the electrode and adsorb on its surface. At the same

Figure 1

Cyclic voltammograms obtained with a pyrolitic graphite electrode in a solution containing 0.3 mM $Ru(NH_3)_6^{3+}$ and 0.001 mM 9,10-phenanthrene-quinone. Scan rate: 20 mV/sec; supporting electrolyte: 1 M CF_3COOH; electrode area: 0.2 cm^2. Minutes of exposure of the freshly cleaved electrode to the solution (which was stirred by bubbling nitrogen between scans): a - 2, b - 8, c - 20, d - 47, 3 - 84.

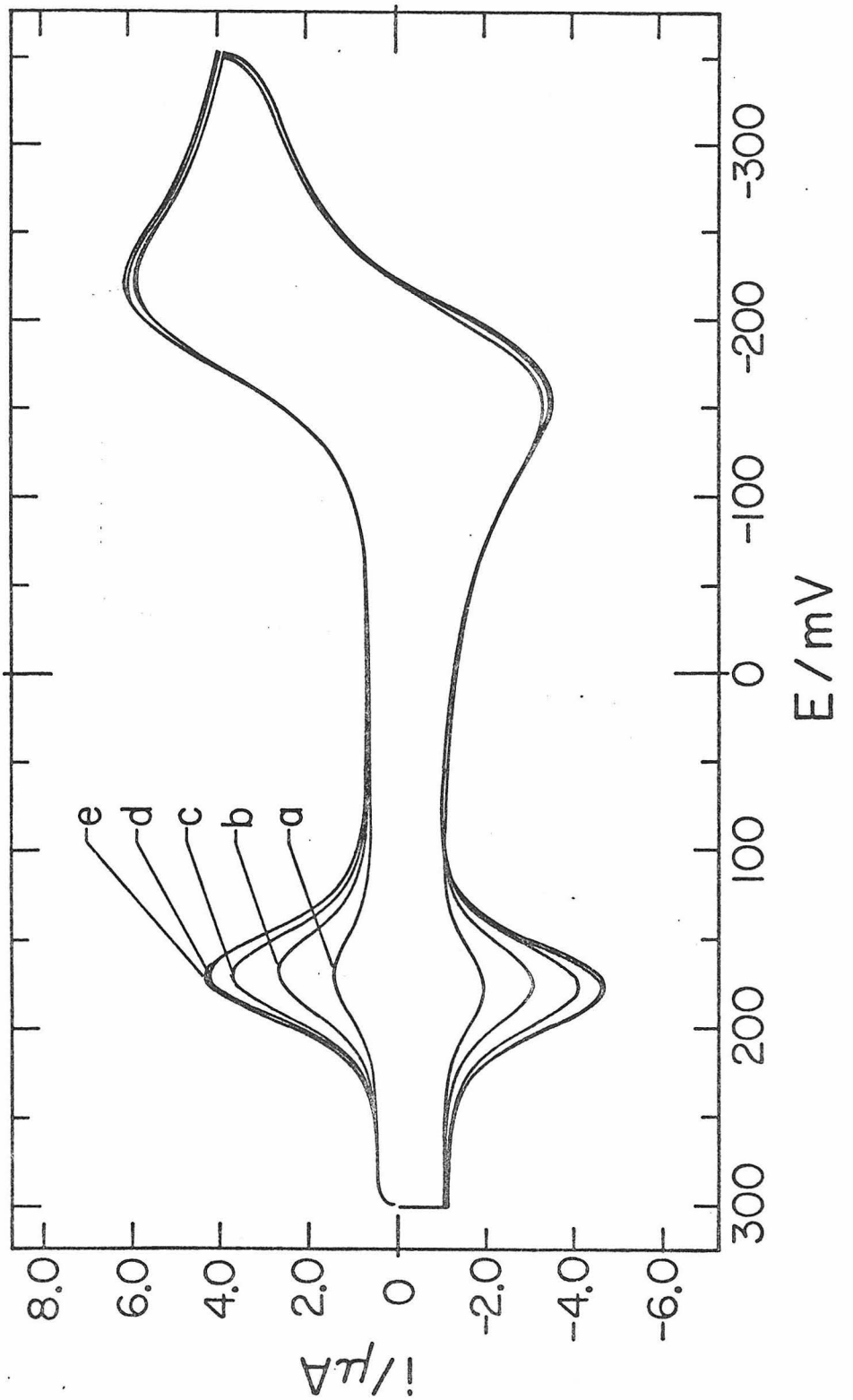

Figure 1

time there is virtually no change in the peaks corresponding to the non-adsorbing $Ru(NH_3)_6^{3+/2+}$ couple. (Note that the current resulting from unadsorbed, diffusing quinone is negligibly small in this 10^{-6} M solution.) The test was made to demonstrate that accumulation of the quinone occurs on the electrode surface and not by absorption into micropores or crevices in the electrode or its seal. The latter would lead to a comparable enhancement for both the ruthenium and quinone couples.

The two sets of waves in Figure 1 have the differing shapes and forward and reverse peak separations that are expected for adsorbed and diffusing reactants. The peak potentials for the $Ru(NH_3)_6^{3+/2+}$ waves are separated by ca. the 58 mV expected for a simple one-electron nernstian couple present in solution. The much smaller peak separation and more symmetrical wave shapes exhibited by the quinone/hydroquinone couple are consistent with both the reactant and product remaining on the surface [5,6]. (The behavior is very similar to that observed with dissolved reactants in thin-layer cells [7]).

The $Ru(NH_3)_6^{3+/2+}$ waves in Figure 1 do not differ significantly from those obtained in the absence of the adsorbed quinone. This outer-sphere redox couple is apparently able to exchange electrons with the electrode

through the layer of adsorbed hydroquinone present on the graphite at the potentials where $Ru(NH_3)_6^{3+}$ is reduced.

If the electrode used in Figure 1 is removed from the solution, washed with excess water and placed in a supporting electrolyte free of both reactants, a cyclic voltammogram such as the one shown in Figure 2 results. The area under either wave corresponds to the presence of ca. 2.5×10^{-10} moles cm^{-2} (geometric area) of quinone on the electrode surface which approximates monolayer coverage. The adsorbed 9,10-phenanthrenequinone leaves the electrode surface very slowly. The magnitude of the peak current decreases over a period of many hours. The rate of removal appears to be approximately first order with a half-life of 7 to 9 hours. The waves can be eliminated immediately if the electrode surface is renewed by cleaving (pyrolitic graphite) or polishing (vitreous carbon).

9,10-Phenanthrenequinone adsorbed on graphite exhibits readily detectable cyclic voltammograms because of the high coverage obtained with this reactant and the fact that two electrons are involved in its reduction. The peak current is proportional to the square of the number of electrons transferred for a nernstian process involving reactants and products confined to the electrode surface [5,6]. With smaller quantities of adsorbed reactants whose

Figure 2

Cyclic voltammogram obtained after the adsorption depicted in Figure 1 was complete and the electrode was removed, washed, and transferred to a solution containing only 1 M CF_3COOH.
Scan rate: 20 mV/sec.

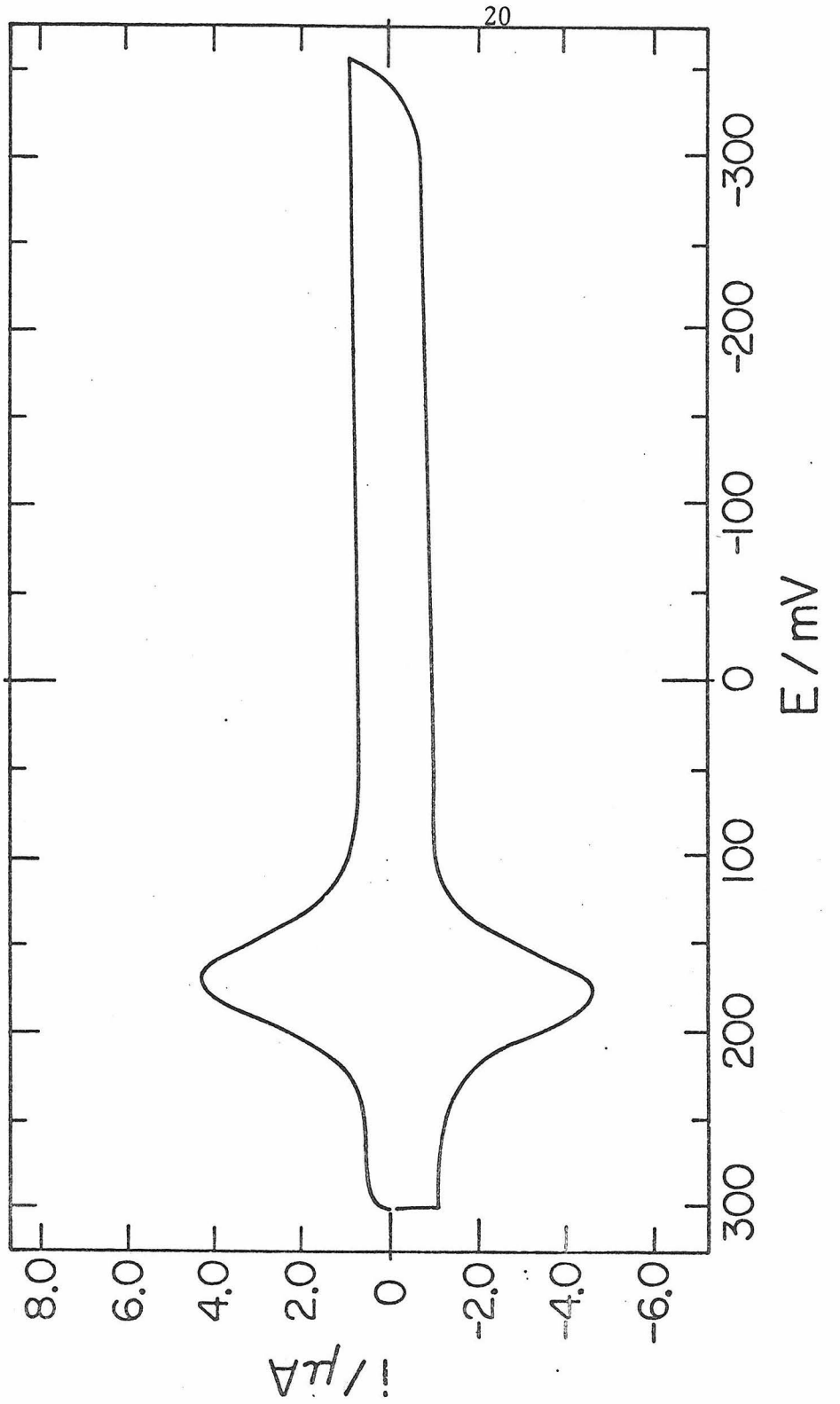

Figure 2

reactions involve only one electron, less well defined cyclic voltammograms result. For example, Figure 3A shows the cyclic voltammogram obtained when iron(III) tetraphenylporphyrin is adsorbed on the electrode. The amount of this larger molecule which is adsorbed is only about 10^{-11} moles cm^{-2} (estimated from the cyclic voltammogram assuming that the reaction involves one electron). Figure 3B shows the differential pulse voltammogram obtained with the same electrode. The relative improvement in the ratio of the peak current to background current is apparent. Similar improvements in sensitivity have been obtained with a number of adsorbed reactants and the differential pulse technique appears to be generally useful for examining the behavior of new systems.

The strength of the adsorption of various reactants on graphite appears to correlate with the number of aromatic centers in the adsorbing molecule. Thus N,N,-N′,N′-tetramethyl-p-phenylenediamine, having one aromatic ring, showed no detectable irreversible adsorption onto vitreous carbon electrodes from a saturated solution in 1 M $HClO_4$. By contrast o-dianisidine (3,3′-dimethoxybenzidine), with two aromatic rings, was readily adsorbed from 1 M $HClO_4$.

Figure 3

Cyclic (A) and differential pulse (B) voltammograms of iron(III) tetraphenylporphyrin adsorbed on a vitreous carbon electrode. Adsorption for 5 minutes from a saturated solution of the porphyrin in dimethyl formamide. Voltammograms recorded in 1 M HCl as supporting electrolyte. Cyclic scan rate: 5 mV/sec.

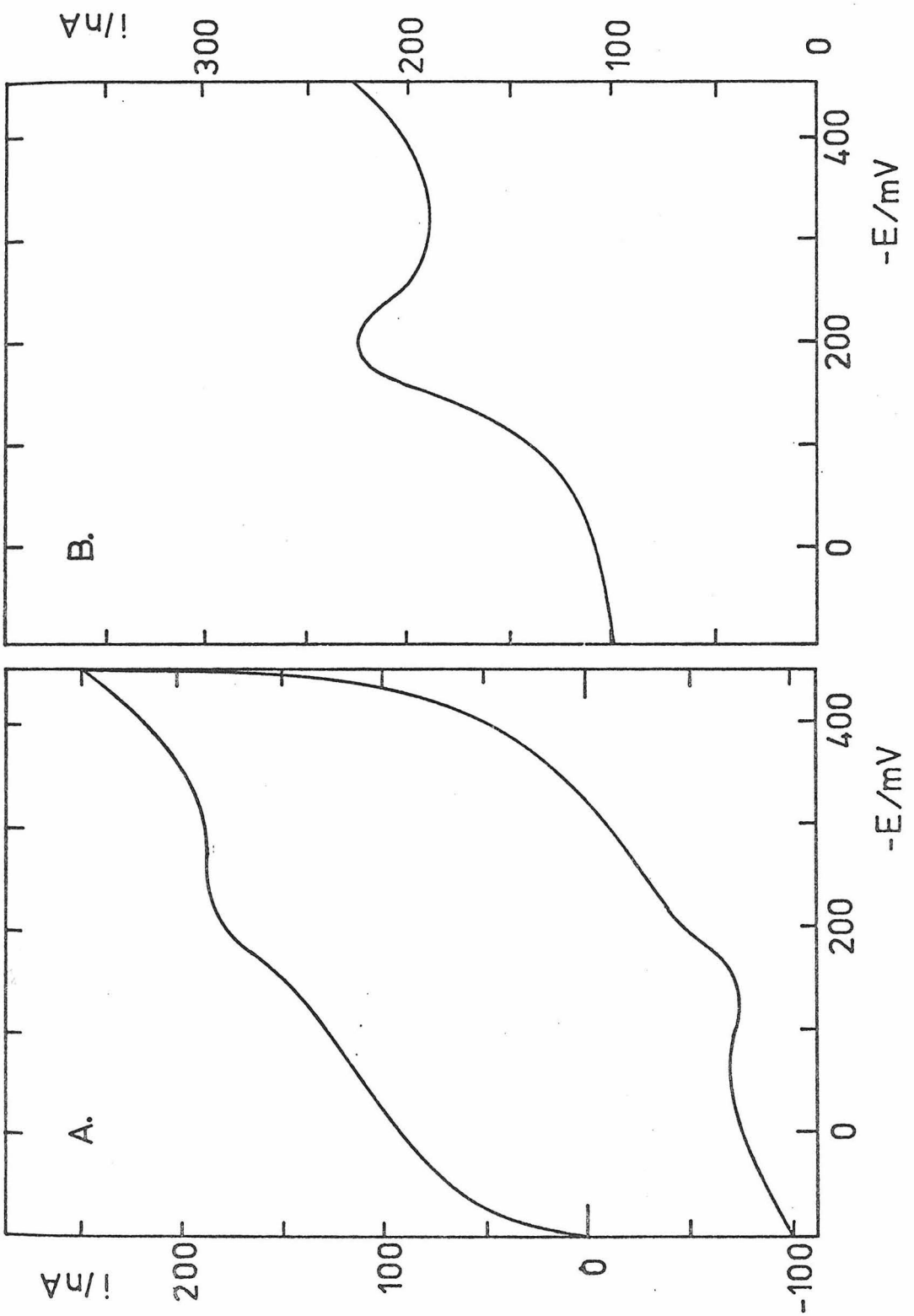

Figure 3

Cyclic and differential pulse voltammograms for iron(III) protoporphyrin IX adsorbed on a vitreous carbon electrode are shown in Figure 4. This area under half of the cyclic voltammogram corresponds to the presence of ca. 10^{-10} moles cm^{-2} of reactant assuming a one-electron electrode reaction. That a one-electron process is involved was confirmed by measuring the sweep rate dependence of the cathodic peak current. The ratio of the slope of a plot of peak current vs. sweep rate to the area under a voltammogram (at any convenient sweep rate) can be shown to equal $\frac{nF}{4RT}$. The measured value of this ratio was ca. 0.23 $\frac{F}{RT}$ suggesting that n = 1.

The electrochemistry of both the adsorbed 9,10-phenanthrenequinone and iron protoporphyrin IX could be altered by changing the pH of the electrolyte in which the voltammograms were recorded. Figure 5 shows the pH dependence of the differential pulse peak potentials for both adsorbed reactants. The shift of ca. 60 mV per pH unit resembles the behavior observed with iron protoporphyrin IX in homogeneous solution [8]. The cyclic voltammetric behavior of 9,10-phenanthrenequinone in homogeneous solution has not been reported. We found its homogeneous electrochemistry to be complicated by a separation into two closely spaced waves at pH values above 1; similar behavior of the surface species

Figure 4

Cyclic (A) and differential pulse (B) voltammograms of iron(III) protoporphyrin IX adsorbed on a vitreous carbon electrode. Adsorption for 5 minutes from a saturated solution of the porphyrin in 0.1 M $Na_2B_4O_7$. Voltammograms recorded in 0.1 M $Na_2B_4O_7$ as supporting electrolyte. Cyclic scan rate: 5 mV/sec.

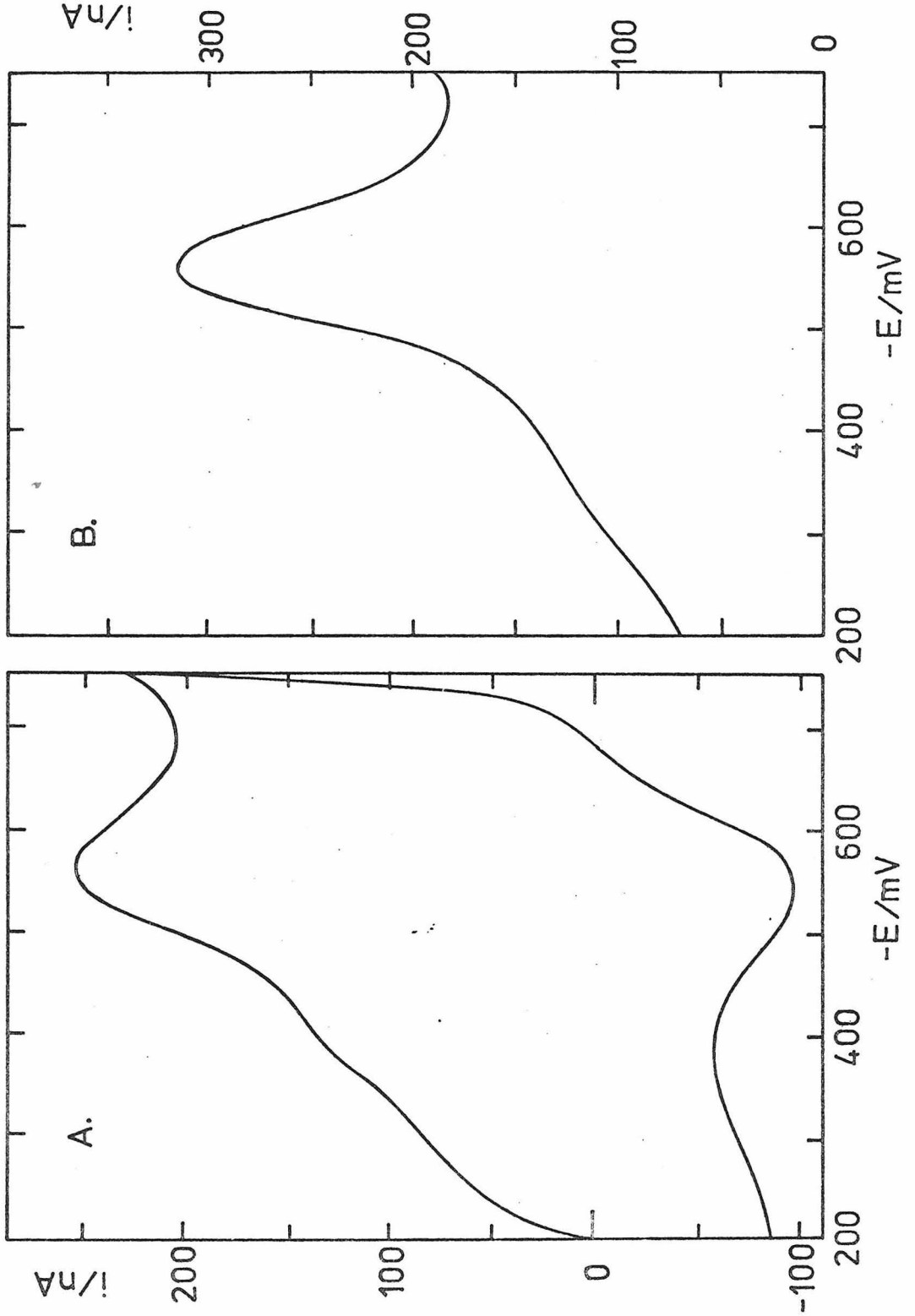
i/nA
300
200
100
0
B.
200
400
600
-E/mV
i/nA
200
100
0
-100
A.
200
400
600
-E/mV

Figure 4

Figure 5

Differential pulse voltammetric peak potentials for 9,10-phenanthrenequinone (○) and iron(III) protoporphyrin IX (□) as a function of the pH of supporting electrolyte buffers.

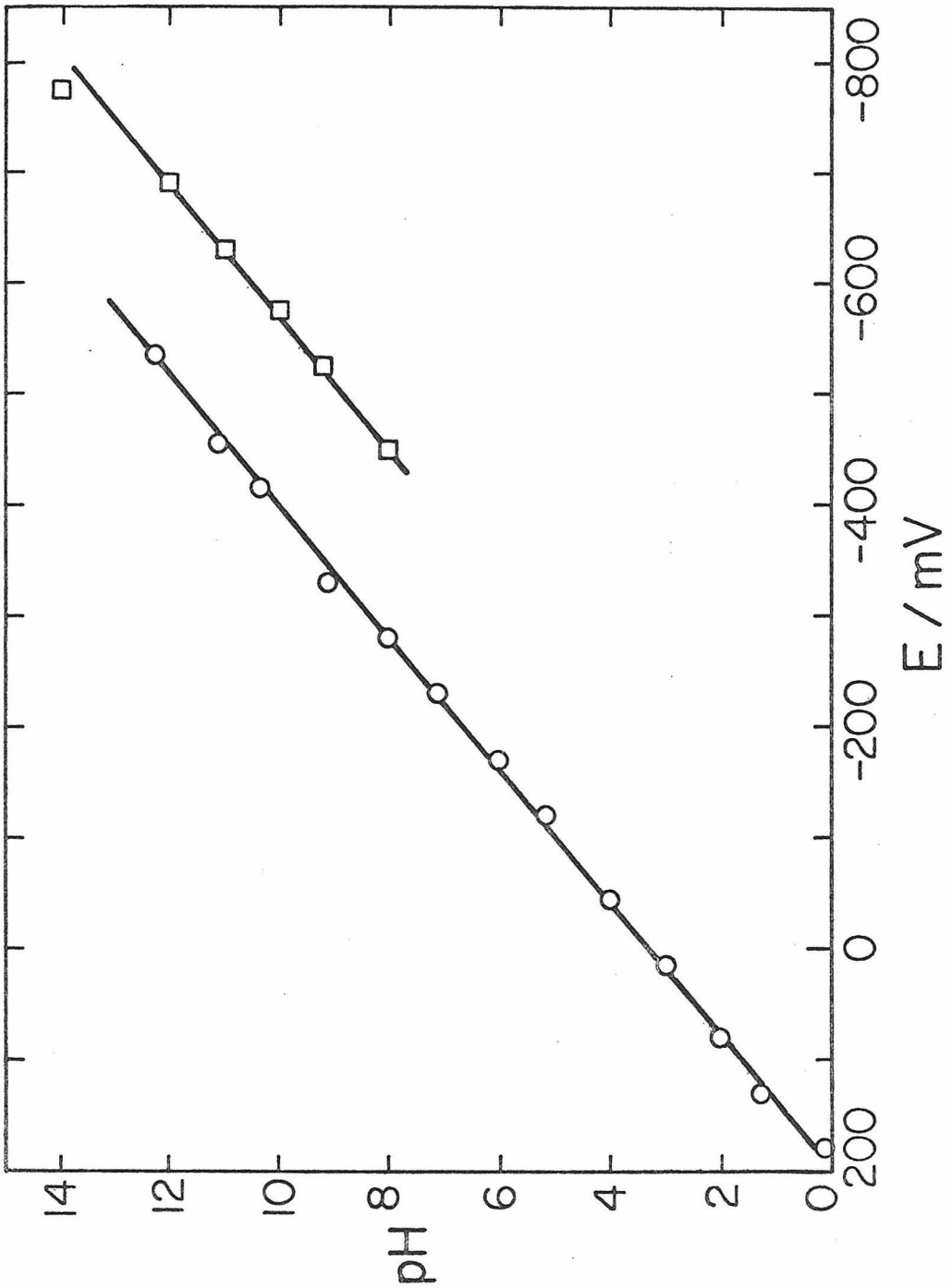

Figure 5

results when the quinone is adsorbed from such solutions. However, only a single wave is obtained in supporting electrolytes of all pH when the adsorption is carried out from solutions containing 1 M H^+. The 60 mV slope obtained in Figure 5 resembles the homogeneous behavior of similar anthraquinones [9] and is reasonable for the expected 2-electron 2-proton reduction reaction. The fact that the differential pulse peak potential depended only on the pH of the electrolyte in which the voltammogram was recorded is evidence of the chemical accessibility of the adsorbed quinone.

Experiments were conducted with the protoporphyrin IX to test whether the iron center in the adsorbed complex was susceptible to ligand substitution. It was found that in a borate buffer (pH 10) the addition of 1 M chloride ion had no effect on the peak potential but saturation of the electrolyte with carbon monoxide caused an anodic shift of 50 mV in the peak potential which could be reversed by subsequent saturation with argon. Similar anodic shifts in peak potentials also resulted when imidazole or pyridine were added to the supporting electrolytes in modest concentrations (0.01 - 0.1 M). At higher concentrations these strong axial ligands [10] tended to strip the adsorbed porphyrin from the electrode surface.

The general responses of the adsorbed molecules to changes in the homogeneous concentrations of protons and potential axial ligands are understandable in terms of the homogeneous chemistry of the same molecules. However, the evidence does not prove that identical chemistry is involved on the surface and in solution. It would not be surprising to encounter surface chemistry which differs substantially from that in the solution phase with other reactants or alternative modes of attachment to the surface.

The small wave that can just be discerned in Figure 4 at potentials anodic of the main wave is enhanced when the adsorption is carried out from solutions in which the porphyrin is known to exist as a monomeric species. Figure 6 shows a series of differential pulse voltammograms that resulted when the porphyrin was adsorbed from the aqueous layer produced by equilibrating 1 M HCl with a dilute (< 1 mM) chloroform solution of the porphyrin[11,12]. The decay of the prewave suggests that it may represent a second form of adsorbed porphyrin which is less strongly attached. If the adsorption is carried out from glacial acetic acid where the porphyrin is also monomeric [13], similar behavior results although the peak potential of the prewave is shifted slightly.

Figure 6

Differential pulse voltammograms for iron(III) protoporphyrin IX adsorbed on vitreous carbon from the aqueous layer resulting when a dilute chloroform solution of the porphyrin was equilibrated with 1 M HCl [11]. Supporting electrolyte: 0.1 M $Na_2B_4O_7$. The voltammograms were recorded successively on the same electrode, in the order shown. The elapsed time between each recording was approximately 5 minutes.

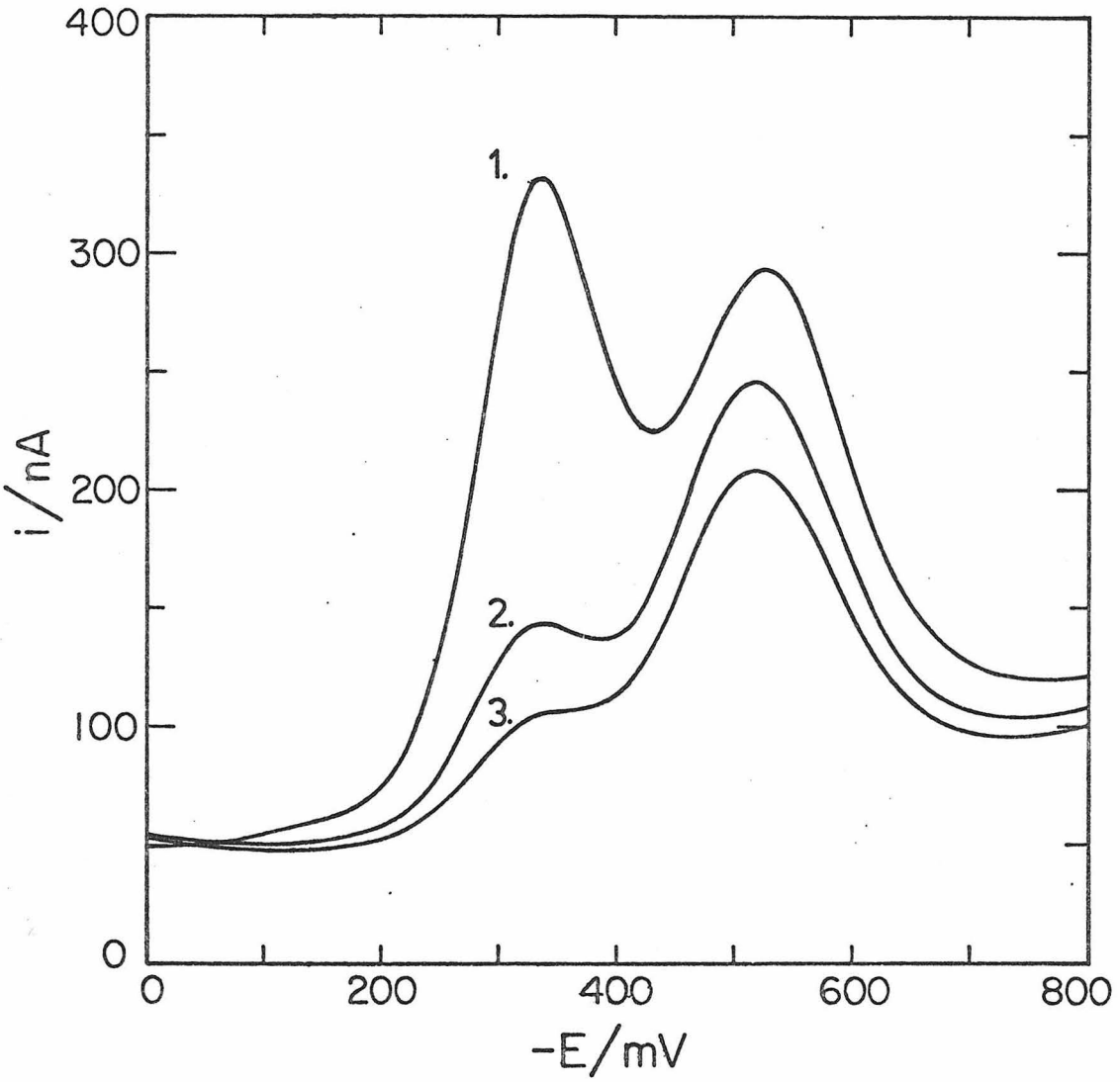

Figure 6

A further indication of the differences in the two forms of the attached porphyrin appears when small amounts of oxygen are introduced as shown in Figure 7. The current at potentials near the prewave grows as the oxygen concentration is increased while the more cathodic wave remains unaffected. In the absence of adsorbed porphyrin and with comparable oxygen concentrations, the peak due to the reduction of the oxygen occurs at potentials about 200 mV more negative so that the adsorbed porphyrin appears to provide a modest catalysis of the oxygen reduction reaction.

It is somewhat surprising that differential pulse voltammetry, a technique designed to discriminate against capacitive charging currents, should prove so useful in measuring currents which flow to charge the faradaic pseudocapacitance arising from adsorbed reactants. The effectiveness is in fact dependent upon the presence of some uncompensated resistance in the circuit controlled by the PAR 174 instrument. A theoretical analysis of the peak currents to be expected in differential pulse voltammetry with nernstian reactants bound to electrode surfaces in the presence of uncompensated resistance [14] shows that the relationship between peak currents and the quantity of attached reactant will not be linear in general. However, approximate linearity is predicted

Figure 7

Differential pulse voltammogram for oxygen reduction at a vitreous carbon electrode on which iron protoporphyrin IX is adsorbed. Supporting electrolyte: 0.1 M $Na_2B_4O_7$. Voltammograms were recorded after introduction of increasing quantities of oxygen. The largest peak current is ca. one-fifth as large as that obtained in an air-saturated solution.

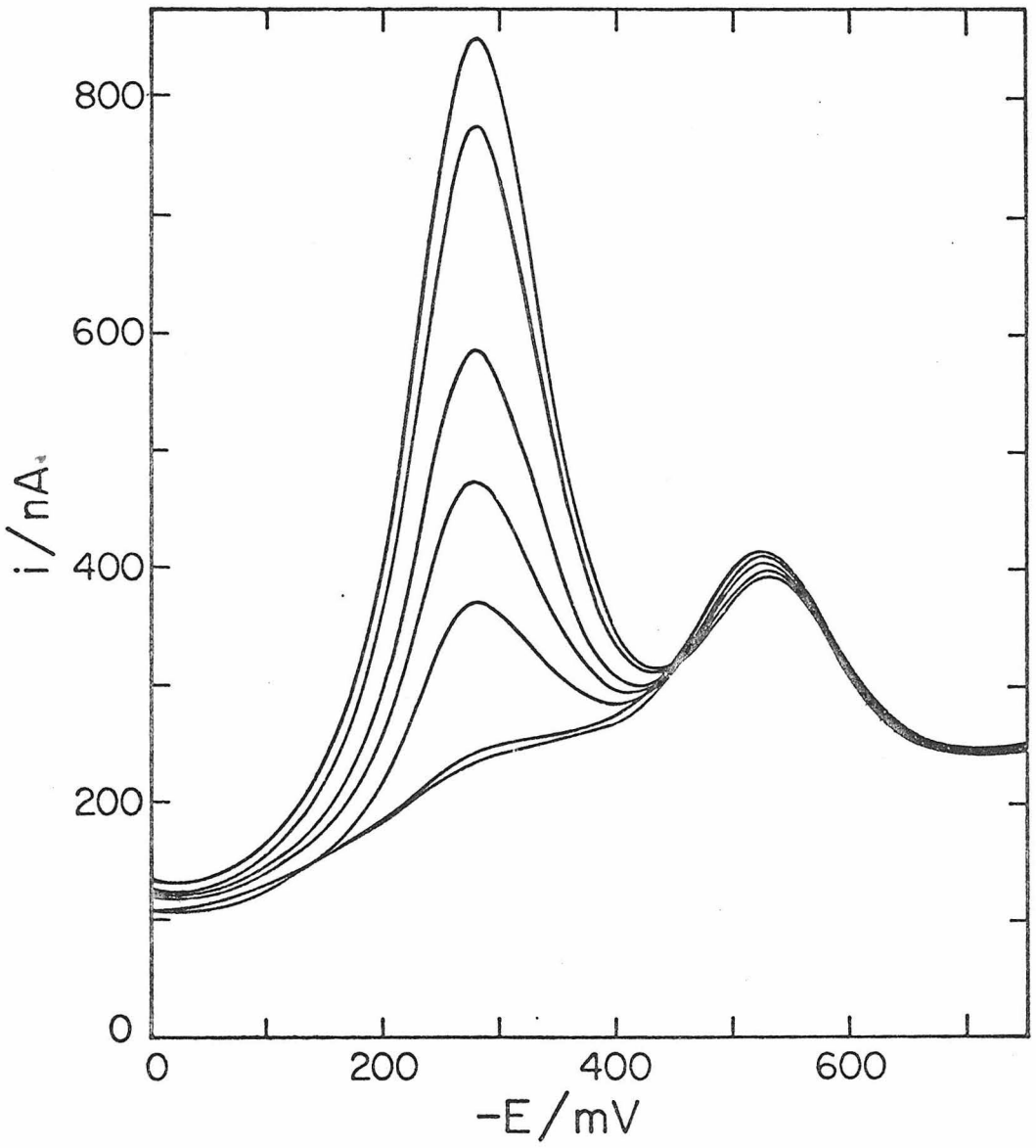

Figure 7

within certain ranges of surface concentration and uncompensated resistance. Figure 8 shows plots of both the differential pulse and cyclic voltammetric peak currents vs. the quantity of adsorbed 9,10-phenanthrene-quinone under conditions where the uncompensated resistance present in the cell was approximately 100 ohms. The linearity of the cyclic voltammetric data is to be expected [5,6]. The corresponding linearity, zero-intercept and larger slope of the plot of the differential pulse data are encouraging observations which suggest that the more sensitive differential pulse technique can provide quantitative as well as qualitative electrochemical information about reactants attached to electrode surfaces.

Acknowledgment

This work was stimulated by, and benefited considerably from, several unpublished research reports prepared by James French and Theodore Bednarski at Hercules Research Center, Inc. Howard Tennent was also a generous source of much invaluable experimental information and encouragement. This work was supported by a grant from NSF-RANN.

Figure 8

Differential pulse (a) and cyclic (b) voltammetric peak currents vs. quantity of 9,10-phenanthrenequinone adsorbed on a pyrolitic graphite electrode. The quantity adsorbed was estimated by integration of the cyclic voltammetric current-potential curves. Supporting electrolyte: 1 M CH_3COOH. The lines are the result of least-squares regression of the data. Cyclic scan rate: 10 mV/sec.

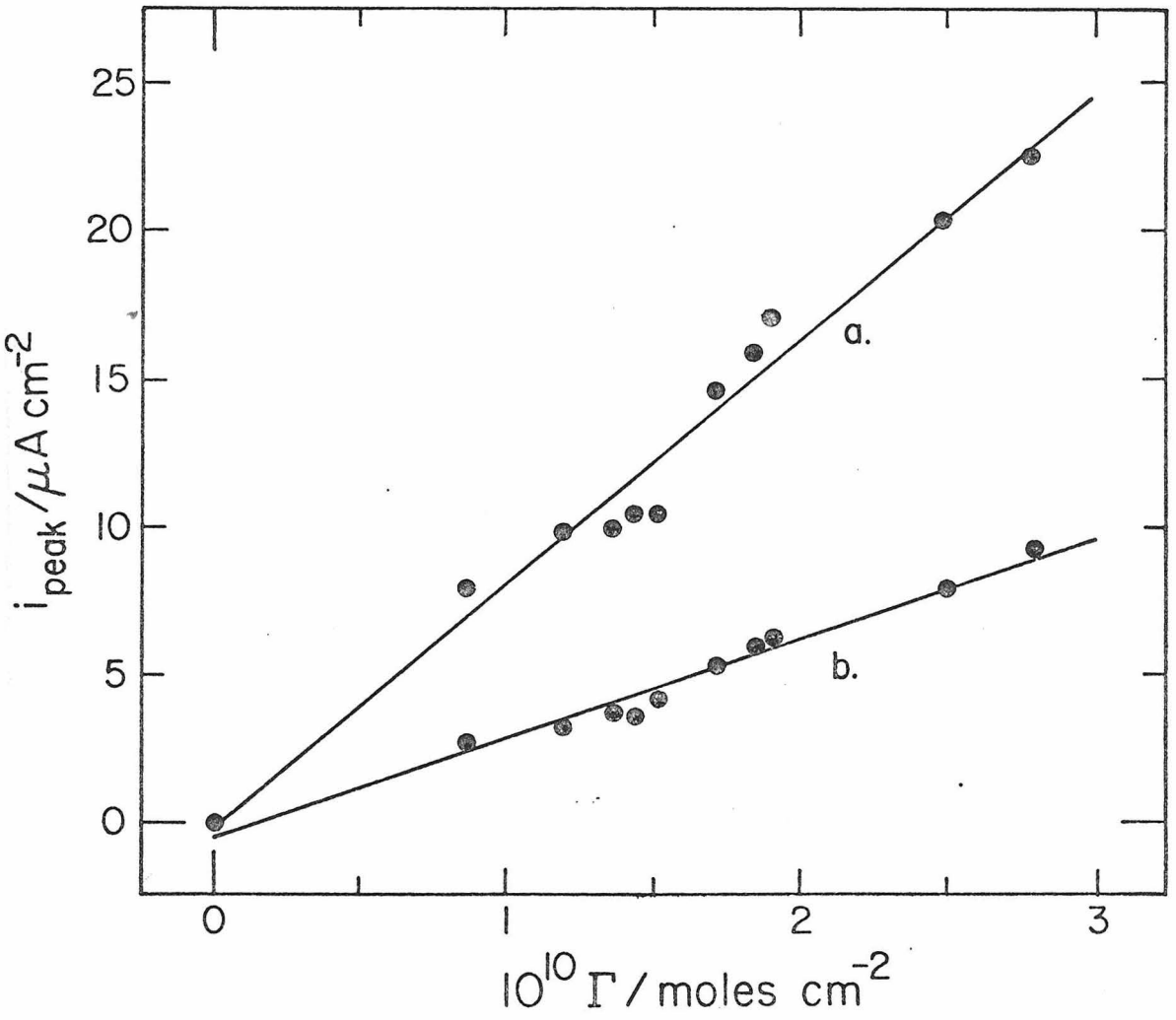

Figure 8

References

1 R. F. Lane and A. T. Hubbard, J. Phys. Chem., 77 (1973) 1401, 1411.

2 B. F. Watkins, J. R. Behling, E. Kariv, and L. L. Miller, J. Am. Chem. Soc., 97 (1975) 3549.

3 P. P. Moses, L. Wier, and R. W. Murray, Anal. Chem., 47 (1975) 1882.

4 J. B. Flato, Anal. Chem., 44 (11) (1972) 75A.

5 E. Laviron, Bull. Soc. Chim. Fr., (1967) 3717.

6 H. A. Laitinen, C. A. Vincent, and T. J. Bednarski, J. Electrochem. Soc., 115 (1968) 1024.

7 A. T. Hubbard and F. C. Anson in, "Electroanalytical Chemistry," A. J. Bard, ed., M. Dekker Inc., New York, 1970, Vol. 4.

8 T. M. Bednarski and J. Jordon, J. Am. Chem. Soc., 89 (1967) 1552.

9 N. H. Furman and G. Stone, J. Am. Chem. Soc., 70 (1948) 3055.

10 D. G. Davis and D. L. Orleron, Anal. Chem., 38 (1966) 179; D. Lexa, M. Momenteau, J. Mispelter, and J. M. Lhoste, Bioelectrochem. Bioenergetics, 1 (1974) 108.

11 F. R. Hopf, D. Möbius, and D. G. Whitten, J. Am. Chem. Soc., 98 (1976) 1584.

12 E. B. Fleischer and T. S. Srivastava, J. Am. Chem. Soc., 91 (1969) 2403.

13 W. H. Fuehsman, H. H. Bernstein, and D. P. Tempest, Bioinorg. Chem., 4 (1975) 177.

14 A. P. Brown and F. C. Anson, Anal. Chem. 49 (1977) 1589.

SECTION I-B

Electrochemistry of the Ruthenium(3+,2+) Couple Attached to Graphite Electrodes

Carl A. Koval and Fred C. Anson

Arthur A. Noyes Laboratory,
California Institute of Technology,
Pasadena, California 91125

A number of schemes for the attachment of a variety of molecules to electrode surfaces have been proposed and tested recently (1-12). In only a few instances have the attached molecules exhibited the long-lived, reversible electrochemical behavior that would be essential for effective catalysis of charge transfer reactions involving less reactive substrates to be realized. In preliminary experiments (4) directed at such an objective we reported some examples of reactants containing multiple aromatic rings (e.g., 9,10-phenanthrenequinone, iron protoporphyrin IX, and iron tetraphenylporphyrin), which attach themselves to graphite electrodes by spontaneous, irreversible adsorption. In media free of attached reactant, these surface species remain adsorbed for hours and can be cycled repeatedly between oxidation states electrochemically. The tendency of sufficiently large, aromatic molecules to adsorb on graphite has also been exploited to attach a simple transition metal complex, $Ru(NH_3)_5L^{2+}$ (L is the large, aromatic ligand), to a graphite electrode and to examine its electrochemical behavior in the attached state (12).

In the present paper, methods similar to those described by Miller and co-workers (2) were used to attach the same ruthenium redox couple to graphite electrodes by coordinating the metal to a pyridine ligand which was,

in turn, covalently linked to the graphite surface. The objective was to compare the two methods of attachment with respect to the electrochemical behavior of the redox center and to the longevity of the attachment.

EXPERIMENTAL

Materials

Graphite. The pyrolytic graphite was commercially available material (Union Carbide Corp., Parma, Ohio). It was obtained in the form of cylindrical rods in which the layered (basal) planes of graphite were either parallel or perpendicular to the axis of the rod. In the former case surfaces cut perpendicular to the rod axis presumably contain a large number of "edge" carbon atoms and will be termed edge pyrolytic graphite (EPG). In the latter case, cut surfaces contain mostly basal planes and are termed basal pyrolytic graphite (BPG).

Complexes. $[Ru(NH_3)_5Cl]Cl_2$ was prepared from $Ru(NH_3)_6Cl_3$ by standard procedures (13). $[Ru(NH_3)_5L](PF_6)_2$ where L = pyridine, 4-aminomethylpyridine, (AMP), (insert drawing 1) and N-(4-picolinic)-benzamide, (PBA), (insert drawing 2) were synthesized by adaptation of a procedure described in reference (14): To a solution of $Ru(NH_3)_5(OH_2)^{2+}$, generated by reduction of $Ru(NH_3)_5Cl^{2+}$ with zinc amalgam, a five-fold excess of L was added and the reaction allowed to proceed for ca. 1 hour. The resulting solution was

DRAWINGS

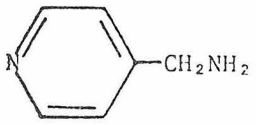

1 - AMP

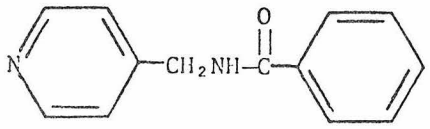

2 - PBA

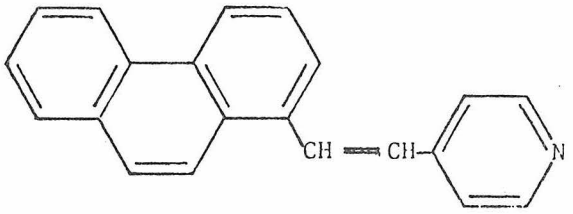

3 - PPE

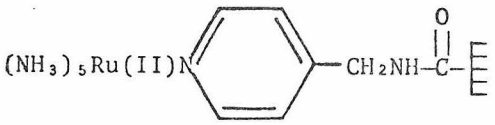

4 - $(NH_3)_5Ru(II)(CAAMP)$

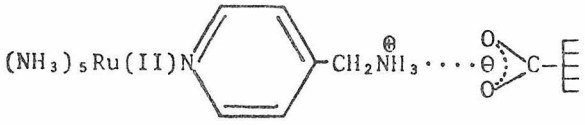

5

filtered and the desired complex precipitated by addition of solid NH_4PF_6.

The ligand, PBA, was synthesized by the reaction of benzoyl chloride and 4-aminomethylpyridine in benzene. The crude product was recrystalized from benzene yielding white needles which gave the following elemental analysis (%): C, 73.69, H, 5.79, and N, 13.13. Calculated for $C_{13}H_{12}N_2O$ C, 73.56, H, 5.70 and N, 13.20. The preparation of the ligand, 1-(9-phenanthrene)-2-(4-pyridine)-ethene, (PPE), (insert drawing 3) and its ruthenium complex have been described (12).

Other chemicals, solvents and supporting electrolytes were reagent grade and were used as received.

Apparatus. Cyclic voltammograms and differential pulse voltammograms were obtained by means of a Princeton Applied Research Model 174 Polarographic Analyzer. Conventional two-compartment cells were employed with a platinum wire auxiliary electrode and a saturated calomel reference electrode. Both BPG and EPG electrodes were in the form of disks. Disks were obtained from rods of basal plane pyrolytic graphite by slicing with a razor blade. Those from edge pyrolytic graphite rods were cut on a lathe. Both types of electrode were mounted in the Teflon holder shown in Figure 1. The O-ring seal defines a reasonably reproducible surface area of ca. 0.12 cm^2

Figure 1

Teflon holder for pyrolitic graphite disk electrodes.

ELECTRODE HOLDER FOR PYROLYTIC GRAPHITE DISKS

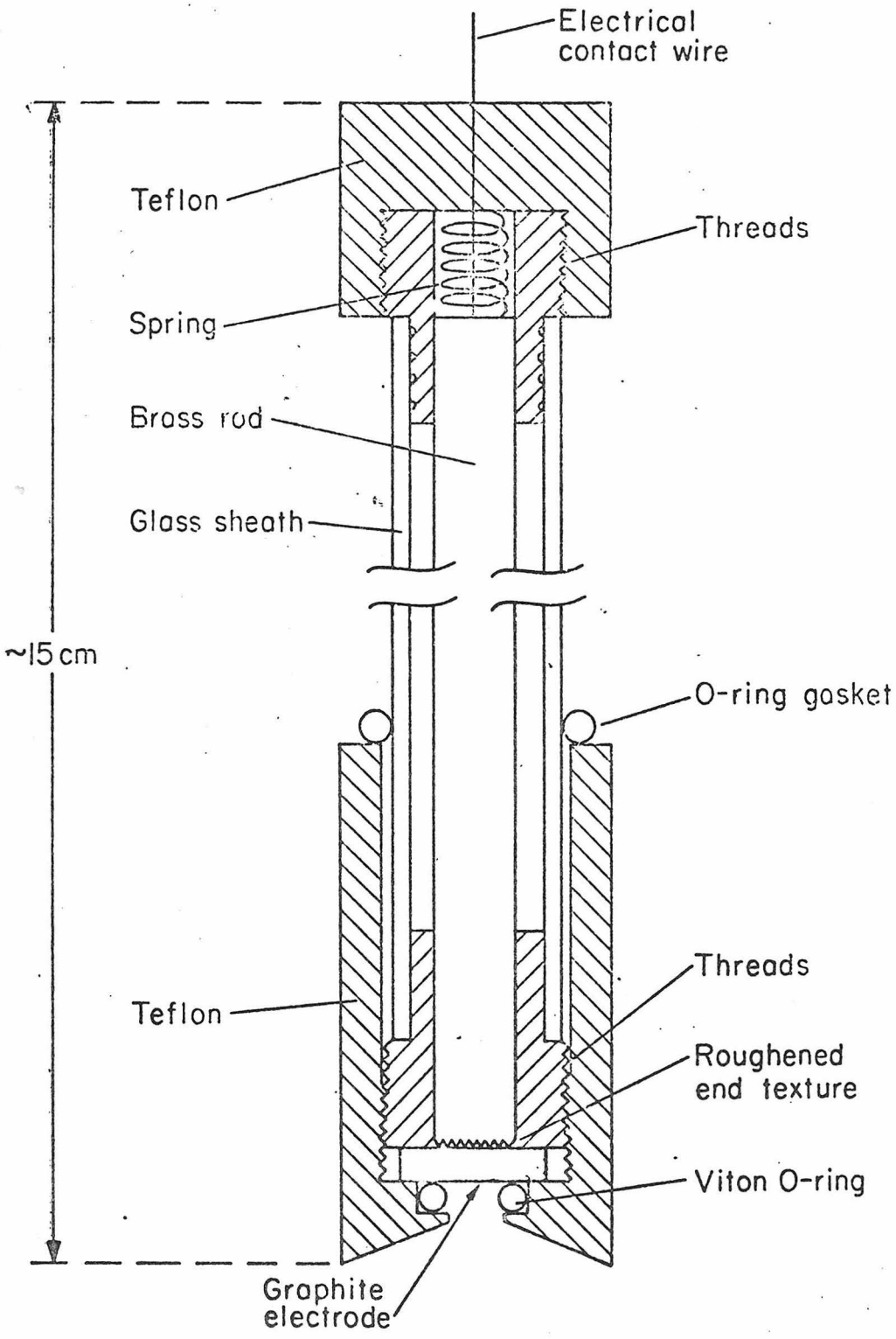

Figure 1

and there was no evidence of the solution leaking under the O-ring even after several hours of use. The holder allows electrodes to be mounted in less than one minute which is highly desirable when a large number of electrodes is being screened. The electrode surface is recessed ca. 2 mm below the outer orifice of the removable Teflon cap but it did not prove difficult to stir the solution well enough to ensure that the solution layer at the electrode surface was representative of the bulk solution composition.

Procedures. The graphite discs were subjected to various treatments designed to clean and oxidize the surface, to attach ligands to the surface and to form ruthenium complexes with the attached ligands.

Treatment I - EPG disks were abraded in air with clean, AG2-400 silicon carbide paper (Minnesota Mining & Manufacturing Co., Minneapolis, Minnesota) to expose fresh graphite. The surfaces of these discs were flat but visibly rough. They were not polished further for fear of decreasing the number of exposed "edge" carbon sites. Loose graphite particles were removed by vigorous washing with water and the disks were dried under vacuum. Treatments of BPG electrodes began with cleavage of a thin layer from the surface to expose fresh graphite instead of abrading the surface with silicon carbide paper. Both types of disks were then heated in air at 400° C for four hours, cooled, treated in a Soxhlet extractor with distilled water for twelve hours and dried under vacuum.

Treatment II - Disks from Treatment I were subjected to Soxhlet extraction with benzene for twelve hours and dried under vacuum.

Treatment III - Disks from Treatment I were stirred overnight in a refluxing solution of benzene (10 ml.) containing 2 ml of 4-amminomethylpyridine. The disks were rinsed with several portions of benzene and then subjected to twelve hours of Soxhlet extraction with benzene, removed and dried under vacuum.

Treatment IV - Disks from Treatment I were stirred in a refluxing mixture of benzene (5 ml.) and thionyl chloride (5 ml.) for eight hours, rinsed with pure benzene and then subjected to Treatment III.

Treatment V - A 0.01 M solution of $Ru(NH_3)_5OH_2^{2+}$ was prepared by dissolving $[Ru(NH_3)_5Cl]Cl_2$ in a 0.1 M solution of sodium trifluoracetate (pH 6 - 7) and reducing the Ru(III) to Ru(II) at a stirred mercury pool electrode at -700 mV vs. S.C.E. under argon. The resulting solution was transferred under argon to a second vessel containing the disk electrodes which were soaked in the solution for 30 minutes, rinsed thoroughly with water and air dried.

Electrochemical measurements were conducted at room temperature (22 ±2° C) in solutions freed of oxygen by

bubbling with argon that had been passed through a vanadium(II) solution. All potentials are quoted vs. the saturated calomel electrode (S.C.E.)

RESULTS

Relevant Formal Potentials of Unattached Ruthenium Complexes. Formal potentials for the couple $Ru(III)(NH_3)_5X + e^- = Ru(II)(NH_3)_5X$ have been measured in a variety of supporting electrolytes for a considerable number of hetero-ligands, X (15,16). Those most relevant to the present study are collected in Table I and include values, measured as part of the present study, for complexes for which no previous potentials were available in the desired acidic electrolyte. Supporting electrolytes consisting of 1 M acids were employed in the present case in order to shift the inevitably present, pH-dependent waves associated with oxidation and reduction of the graphite electrode surface out of the potential region characteristic of the ruthenium complexes investigated. Differential pulse voltammetry was used to measure the formal potentials in Table I using EPG electrodes which had been subjected to Treatment I (see Experimental section). The width at half-peak height of the differential pulse voltammograms was typically 90 to 95 mV compared with the expected 90.4 mV for a one-

TABLE I. Formal Redox Potentials of Some Selected Complexes of Ru(III) - Ru(II)

Complex	E^f, mV vs. SCE	Supporting Electrolyte	Reference
$Ru(NH_3)_6^{3+,2+}$	-194	0.1F $NaBF_4$	(15)
	-191	1 M HTFA	this work
	-210	1 M HCl	this work
$Ru(NH_3)_5py^{3+,2+}$	60	0.1F NaTFA - 0.1F HTFA	(15)
	48	1F HTFA	this work
	26	1F HCl	this work
$Ru(NH_3)_5L^{3+,2+}$			
L = AMP	95	1F HTFA	this work
	76	1F HCl	this work
L = PBA	44	1F HTFA	this work
	23	1F HCl	this work
$Ru(NH_3)_5OH_2^{3+,2+}$	-179	0.1F NaTFA - 0.1F HTFA	(15)
$Ru(NH_3)_5Cl^{2+,3+}$	-287	0.2F NaTFA	(15)

py = pyridine

HTFA = Trifluoroacetic acid

NaTFA - Sodium trifluoroacetate

electron nernstian reaction, indicating that high electron transfer rates prevail between the dissolved complexes and the EPG graphite electrodes. The small differences in the formal potentials in Table I for hydrochloric acid and trifluoroacetic acid supporting electrolytes are most likely reflections of differences in the extent of ion pairing between the cationic reactants and the supporting electrolyte anions in the two cases.

Attachment of $Ru(II)(NH_3)_5^{2+}$ to Graphite Electrode Surfaces by Means of a Covalently Bound, Pendant Pyridine Ligand. Graphite disks were subjected to Treatments III and IV (see Experimental section) in order to produce a surface containing 4-aminomethylpyridine groups and to Treatment V to attach the $Ru(NH_3)_5^{2+}$- moiety to the pendant pyridine ligand. The likely surface chemistry is indicated in Figure 2.

Figure 2

The likely surface chemistry involved in the attachment of $Ru(II)(NH_3)_5^{2+}$ to graphite electrode surfaces.

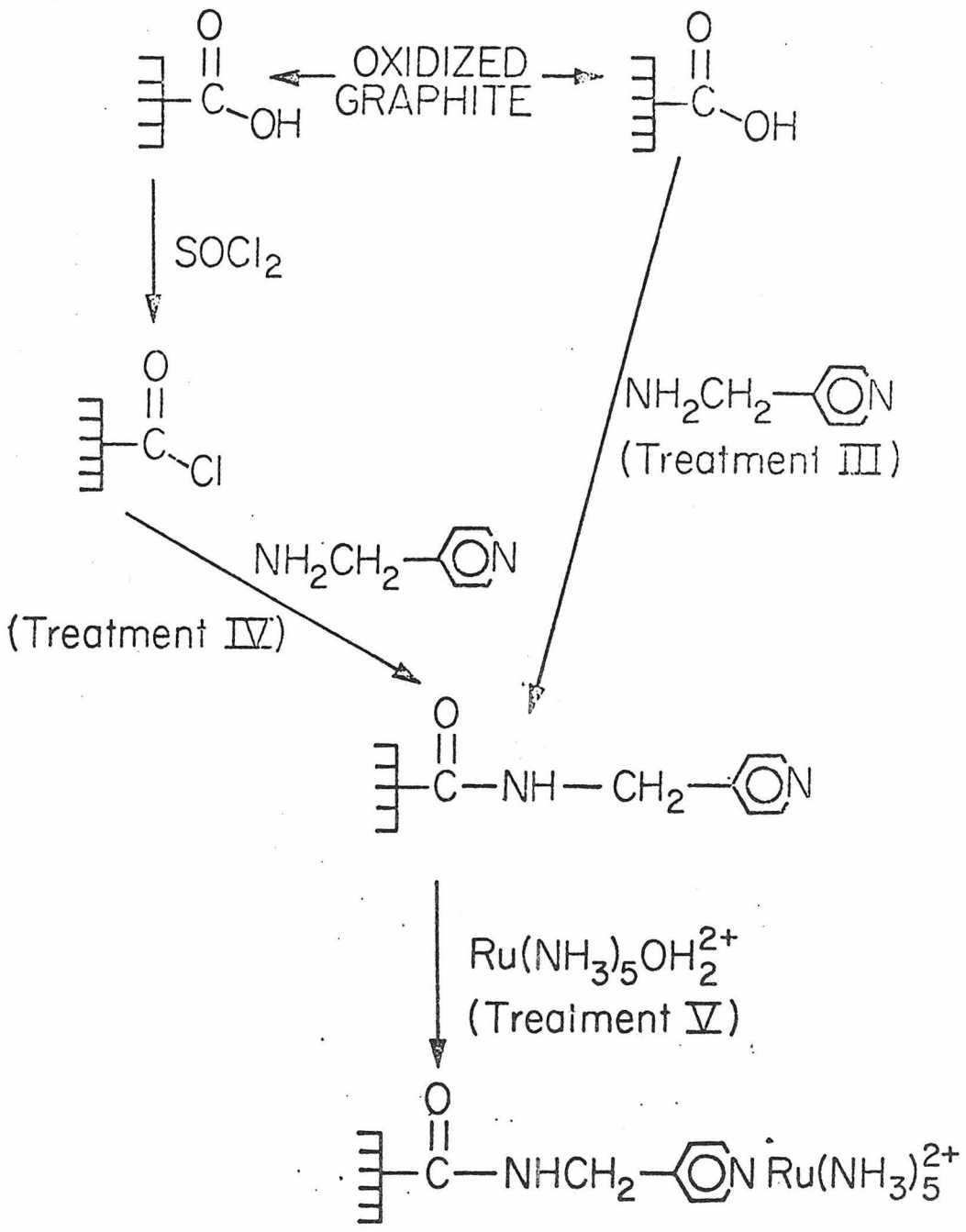
OXIDIZED GRAPHITE
SOCl2
NH2CH2
(Treatment III)
NH2CH2
(Treatment IV)
Ru(NH3)5OH2 2+
(Treatment V)
Ru(NH3)5 2+

Figure 2

The unabraded graphite disks with chiefly basal planes exposed (BPG) showed no detectable attachment under any of the reaction conditions investigated. By contrast, attachment to EPG disks was successful. Figure 3 shows typical differential pulse voltammograms recorded at EPG disks following the treatments used to achieve attachment of the Ru(II) complex. The surfaces of the disks show no apparent changes to the eye at any stage of the treatments and the differential pulse voltammograms recorded at any point prior to Treatment V are virtually identical (Figure 3). However, disks subjected to Treatments III and IV and then soaked in a solution of $Ru(NH_3)_5OH_2^{2+}$, i.e., Treatment V, yield a prominent differential pulse voltammetric peak centered at ca. +135 mV.

Cyclic voltammograms recorded at EPG disks that have undergone Treatments III and V or IV and V are displayed in Figure 4. The waves have the symmetric shape characteristic of a surface redox couple (11); however, the peak potentials are not identical. They differ by 40 mV (Figure 4A). Furthermore, the width at half peak height is 145 mV (Figure 4A or 4B) compared to the theoretical value of 90 mV (17). The area under the waves in Figure 4 corresponds to a surface concentration of 4.6×10^{-10} moles cm^{-2} (geometric area).

Repeated scanning of these waves between the potential limits shown causes no change in their size or shape. However, if the electrode potential is maintained in the range between +0.5 and 1.0 volt for several minutes, the peak current

Figure 3

Different pulse voltammograms recorded at EPG discs. The discs have undergone the treatments indicated (see Experimental section). Supporting electrolyte: 1 M Trifluoroacetic acid. Scan rate: 2 mV sec^{-1}. Modulation amplitude: 5 mV.

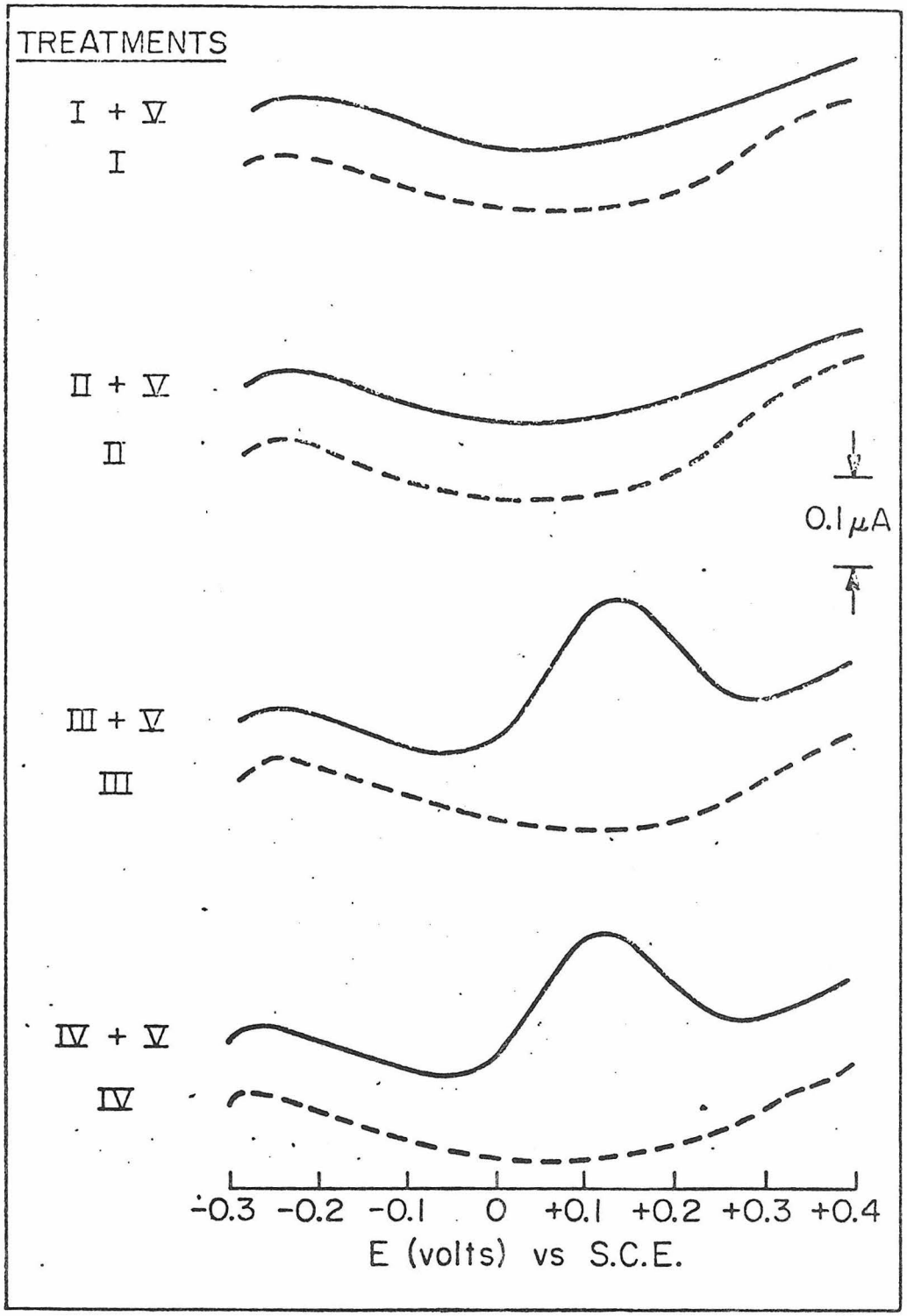
TREATMENTS
I + V
I
II + V
II
0.1 μA
III + V
III
IV + V
IV
-0.3 -0.2 -0.1 0 +0.1 +0.2 +0.3 +0.4
E (volts) vs S.C.E.

Figure 3

Figure 4

Cyclic voltammograms of covalently attached $Tu(NH_3)_5(CAAMP)$. Supporting electrolyte: 1 M Trifluoroacetic acid. Scan rates: A, 0.1 volt sec^{-1}, B, 5.0 volt sec^{-1}.

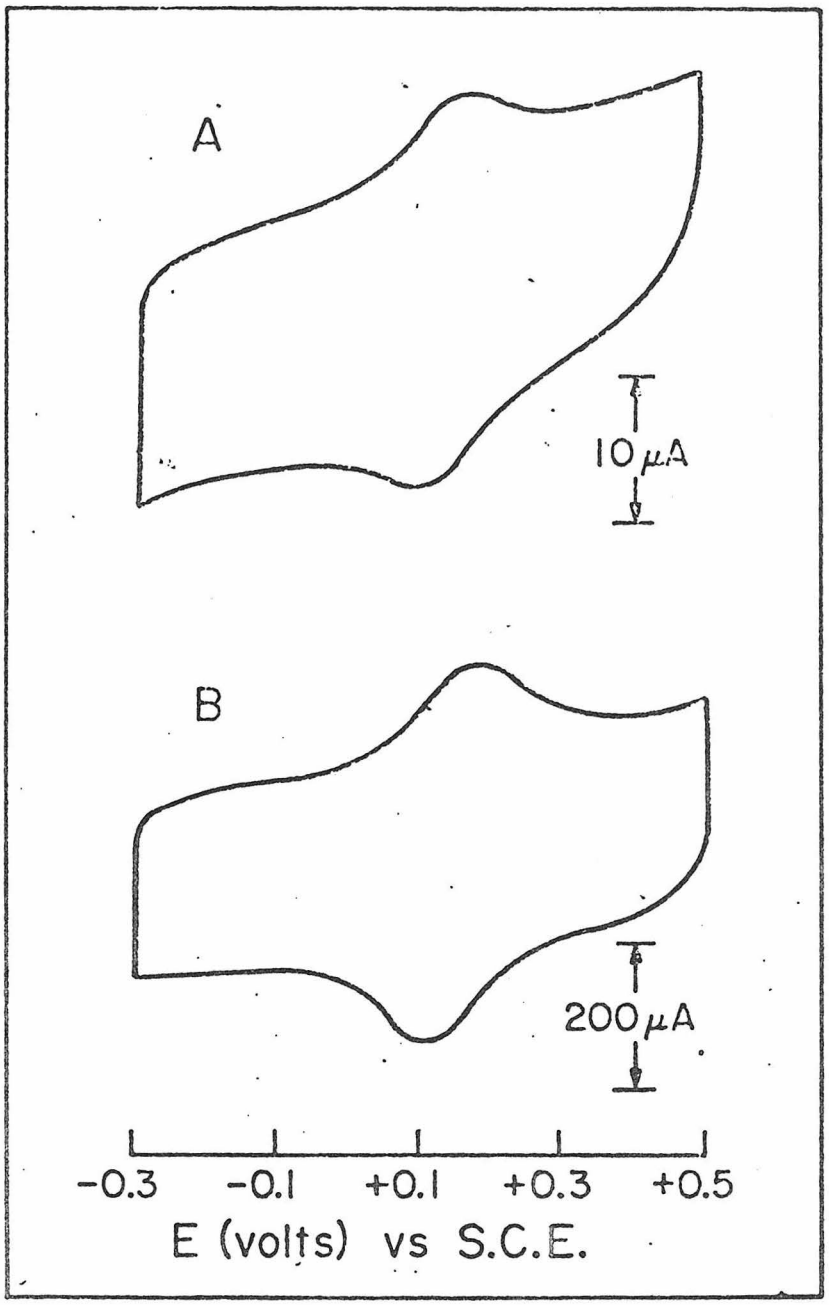

Figure 4

of subsequently recorded voltammograms is decreased markedly. Disks that have undergone Treatments III and V or IV and V can be stored in air for up to a day without significant changes in the wave at +135 mV. As expected, the wave can be entirely eliminated by abrading the electrode with silicon carbide paper.

Control Experiments. The possibilities that during Treatment V the $Ru(NH_3)_5OH_2^{2+}$ might seep into microcrevices in the disks or react with groups present on the surface of the oxidized graphite to (somehow) produce an attached or adsorbed ruthenium complex were examined by exposing disks that had been subjected only to Treatments I or II to the solution of $Ru(NH_3)_5OH_2^{2+}$. The lack of any detectable differential pulse peak using such disks (Figure 3) is strong evidence against these possibilities.

Additional control experiments that produced no sign of attachment included the exposure of disks subjected to the Treatments I, II and III or IV to 0.01 M solutions of $Ru(NH_3)_6^{3+}$, $Ru(NH_3)_6^{2+}$ or $Ru(NH_3)_5Cl^{2+}$. These results confirmed the absence of significant porosity in the pyrolytic graphite employed as well as demonstrating that a labile coordination position in the ruthenium complex is required for the attachment reaction to be successful .

The (remote) possibility that the attachment process, instead of proceeding as suggested in Figure 2, involved a very strong ion-pair interaction between anionic groups on the oxidized graphite surface and the cationic amminomethylpyridine pentaammine ruthenium complex was eliminated by soaking graphite disks in 0.01 M solutions

of $[Ru(NH_3)_5(AMP)](PF_6)_2$ at pH 1 or 7. (Samples of solid $[Ru(NH_3)_5(AMP)](PF_6)_2$ invariably contained $Ru(NH_3)_5(OH_2)(PF_6)_2$ as an impurity. It was therefore necessary to add a slight excess of 4-amminomethylpyridine during these experiments.) Disks subjected to these treatments showed no electrochemical response in the range of potentials where the peaks were obtained in Figure 3.

Peak Potentials. The peak potential (135 mV in 1F HTFA; 115 mV in 1F HCl) of the waves shown in Figure 3 falls in the expected range for a pentaammineruthenium complex in which a π-acid such as pyridine occupies one of the coordination sites. If the sixth coordination site were occupied by a ligand such as an ammine, a halide anion or water the peak potential would appear at potentials 200 to 300 mV more negative (Table I).

In order to compare the peak potentials of the attached ruthenium couple with those of unattached complexes containing a sixth ligand more closely resembling the one which is believed to bind the ruthenium to the graphite surface, the differential pulse voltammetry of the complexes $Ru(NH_3)_5L^{2+}$ (L = AMP, PBA) was examined.

The peak potentials of these complexes, given in Table I, fall very close to that of the corresponding pyridine complex. From this it may be inferred that the 40 to 90 mV difference between the peak potentials of the attached ruthenium complex and unattached model complexes does not result from the presence of the amminomethyl group in the 4 position of the pyridine ligand or from the amidization of this group.

Attachment of $Ru(NH_3)_5L^{2+}$ to Graphite Electrode Surfaces by Means of the Irreversible Adsorption of the Pendant Ligand, L. The preparation of the ligand PPE and its complex with pentaammine-ruthenium(II) was recently reported along with a preliminary description of its electrochemical behavior (12). The phenanthrene group of the ligand serves as an "aromatic anchor" by spontaneously adsorbing on the surface of graphite electrodes and carrying with it the ruthenium complex attached to the pyridine group in the ligand. In contrast to the covalent attachment scheme which depends upon the presence of an adequate number of appropriate functional groups on the electrode surface, attachment by means of pendant aromatic anchors proceeds readily on BPG as well as on EPG electrodes. Figure 5A shows a cyclic voltammogram

obtained with a BPG disk that had been soaked in a dilute solution (less than 1 mM) of $Ru(NH_3)_5(PPE)^{2+}$ in 1:1 acetone-water for 15 min., removed, washed thoroughly with water, and dried in air before being mounted in the electrode holder (Figure 1). The well-formed waves have the symmetrical shape, identical peak potentials and nearly the 90 mV width at half peak height characteristic of reactants which undergo rapid electron transfer and are confined to the surface of an electrode (17). The area encompassed by either the anodic or cathodic wave corresponds to a surface concentration of 5.2×10^{-11} moles cm^{-2} (geometric area).

Figure 5B is a cyclic voltammogram obtained with a EPG disk which was subjected to the same treatment as the BPG disk in Figure 5A. The waves are not as well separated from the background currents, their shape is less symmetrical, the peak potential separation appears to be greater than was true with the BPG electrode, and the width at half peak height is 115 mV. Nevertheless, the apparent surface concentration evaluated by integration of the cyclic voltammogram, 2.8×10^{-10} moles cm^{-2}, is significantly greater than that at the BPG electrode. The differences in the behavior exhibited by the two types of electrode are believed to be the results of the significantly larger microscopic area of the EPG electrode

Figure 5

Cyclic voltammograms of adsorbed $Ru(NH_3)_5(PPE)^{2+}$ on a BPG electrode (curve A) and an EPG electrode (curve B). Supporting electrolyte: 1 M Trifluoroacetic acid. Scan rate: 2.0 volt sec^{-1}.

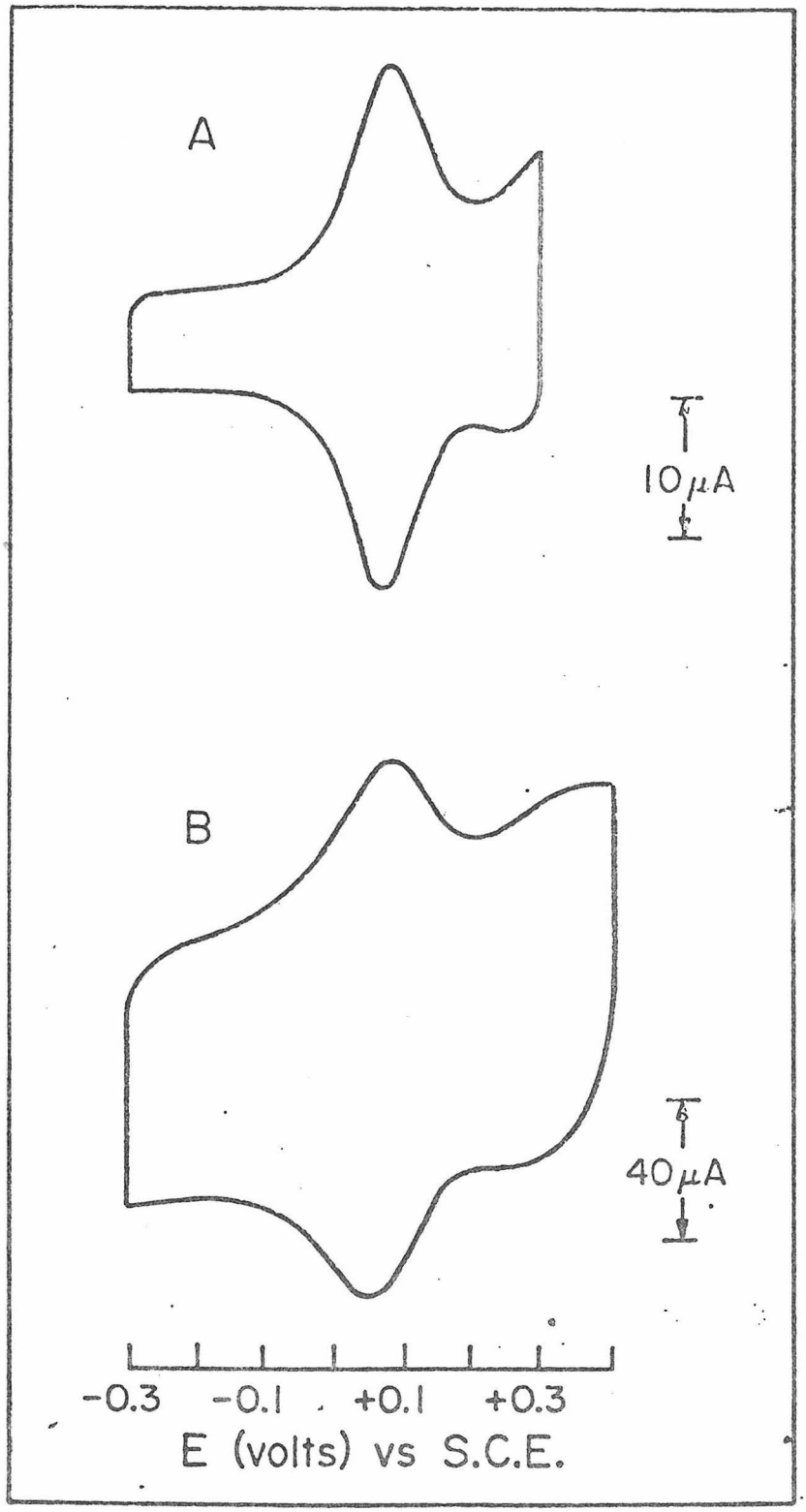

Figure 5

which produces greater background currents associated with double layer charging and surface oxide formation and reduction. These background currents are asymmetric within the potential region where the cyclic voltammetric waves of the adsorbed reactant fall and the resulting asymmetric summing of the background and faradaic currents causes the two peak currents to appear at different potentials. Comparison of the two voltammograms in Figure 5 makes it clear that BPG electrodes are preferable for inspecting the electrochemical response of reactants which are attached to the electrode surface by means of aromatic anchors.

Sweep Rate Dependence of Faradaic Currents for Attached Complexes and Background Currents at Graphite Electrodes. In cyclic voltammetry the relatively small faradaic currents that result with reactants attached to the electrode surface are often obscured by the background currents which are also present. The component of the background current arising from double layer charging, $i_{d.l.}$, is given by Equation 1

$$i_{d.l.} = C_{d.l.} A\nu \qquad (1)$$

where $C_{d.l.}$ is the double layer capacitance, A is the electrode area and ν is the rate of potential scan. The

faradaic current arising from the presence of Γ moles cm^{-2} of an attached reactant that obeys the Nernst equation is (4)

$$i_f = \frac{n^2F^2\Gamma A\nu}{4RT} \qquad (2)$$

Since both currents depend linearly on the rate of potential scan, one would not expect to be able to improve the ratio of faradaic to double layer charging current by increasing the scan rate. However, comparison of the two cyclic voltammograms in Figure 4 shows that the faradaic peak becomes somewhat more prominent at the higher scan rate. This type of behavior was observed with EPG electrodes independent of the mode of attachment of the reactants.

Figure 6 summarizes the observed sweep rate dependence of background and faradaic currents for both EPG and BPG electrodes. (Double layer charging current, $i_{d.l.}$, was measured as one half the distance between anodic and cathodic traces on the cyclic voltammograms.) With the exception of Curve D, all of the data lie close to the straight lines of unit slope expected on the basis of Equations 1 and 2. The smaller slope of Curve D, which represents the background current

at an EPG electrode, means that the faradaic current increases more rapidly than the background with EPG electrodes so that the prominence of faradaic peaks is enhanced at higher scan rates. The origin of this effect is most likely associated with the kinetics of the formation (and removal) of graphite oxides on the EPG electrode surface which constitutes a major component of the background current. Curve A in Figure 6 shows that BPG electrodes yield smaller background currents which exhibit the expected linear dependence on scan rate.

Cyclic voltammetry at appropriate scan rates is a useful procedure with high surface concentrations of attached reactants but at lower concentrations its sensitivity is inadequate at any scan rate and the differential pulse technique becomes preferable (4,11).

Evaluation of Surface Concentrations with Differential Pulse Voltammetry. The general properties of differential pulse voltammograms recorded with reactants attached to electrodes have been discussed recently (11). By restricting measurements to sufficiently slow scan rates (1 mV s^{-1} or less) peak potentials are obtained that fall close to the formal potentials of the attached reactants and are independent of the direction of the scan. Introducing (uncompensated) resistance in series with the indicator electrode produces an enhancement in the peak current and

Figure 6

Log current vs. log scan rate for voltammetric peak and background currents. A: Background current at -200 mV for BPG electrode. B: Peak current for $Ru(NH_3)_5(PPE)^{2+}$ adsorbed on BPG electrode. C: Peak current for covalently attached $Ru(NH_3)_5$(CAAMP) on EPG electrode. D: Background current at -200 mV for EPG electrode. E: Peak current for $Ru(NH_3)_5(PPE)$ adsorbed on EPG electrode.

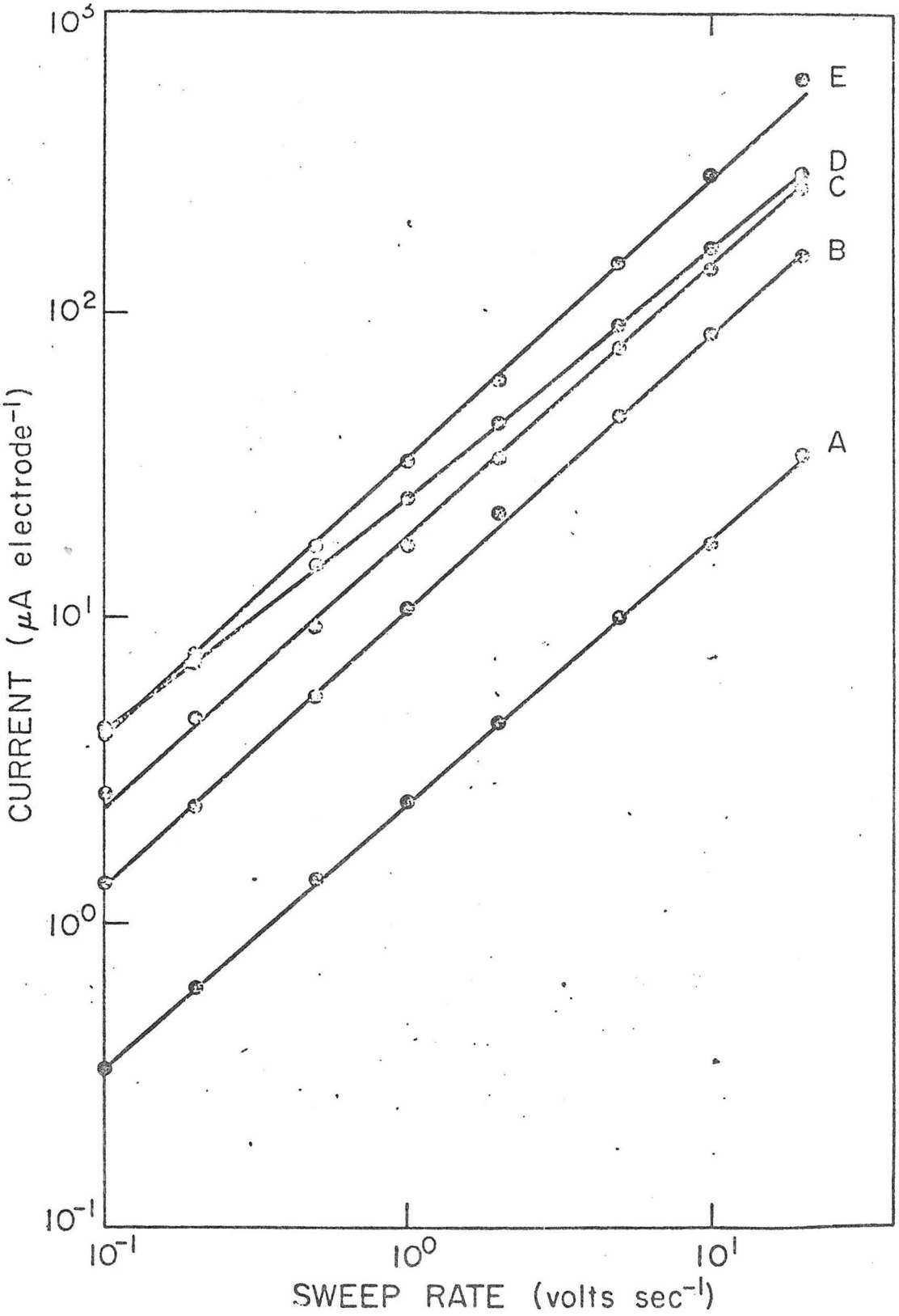
10^3
10^2
10^1
10^0
10^{-1}
CURRENT (μA electrode^{-1})
10^{-1}
10^0
10^1
SWEEP RATE (volts sec^{-1})
E
D
C
B
A

Figure 6

provides a method for estimating the amount of reactant attached to the electrode (11). Figure 7 shows plots of differential pulse voltammetric peak currents for both forms of attached reactant versus the amount of uncompensated resistance present in the circuit controlled by the pulse polarograph. The maximum peak current occurs at the value of the uncompensated resistance, R_u, given in Equation 3 (11):

$$(R_u)_{max} = t(C_{d,l.} + C_f)^{-1} \tag{3}$$

where t is the time at which differential pulse current is sampled and C_f is the faradaic pseudocapacitance which is given by Equation 4 for nernstian reactants (11)

$$C_f = \frac{n^2F^2A\Gamma}{4RT} \tag{4}$$

The surface concentration can then be determined by measuring $(R_u)_{max}$ and $C_{d,l.}$ and applying Equation 5:

$$\Gamma = \frac{4RT}{n^2F^2A}\left(\frac{t}{(R_u)_{max}} - C_{d,l.}\right) \tag{5}$$

As is clear from Figure 5 the effective value of $C_{d.l.}$ obtained from cyclic voltammetry and Equation 1 depends somewhat upon the scan rate employed, especially

Figure 7

Differential pulse voltammetric peak current vs. uncompensated resistance added to the circuit. A: $Ru(NH_3)_5(PPE)^{2+}$ adsorbed on EPG electrode. B: Covalently bound $Ru(NH_3)_5(CAAMP)$ on EPG electrode. C: $Ru(NH_3)_5(PPE)^{2+}$ adsorbed on EPG electrode.

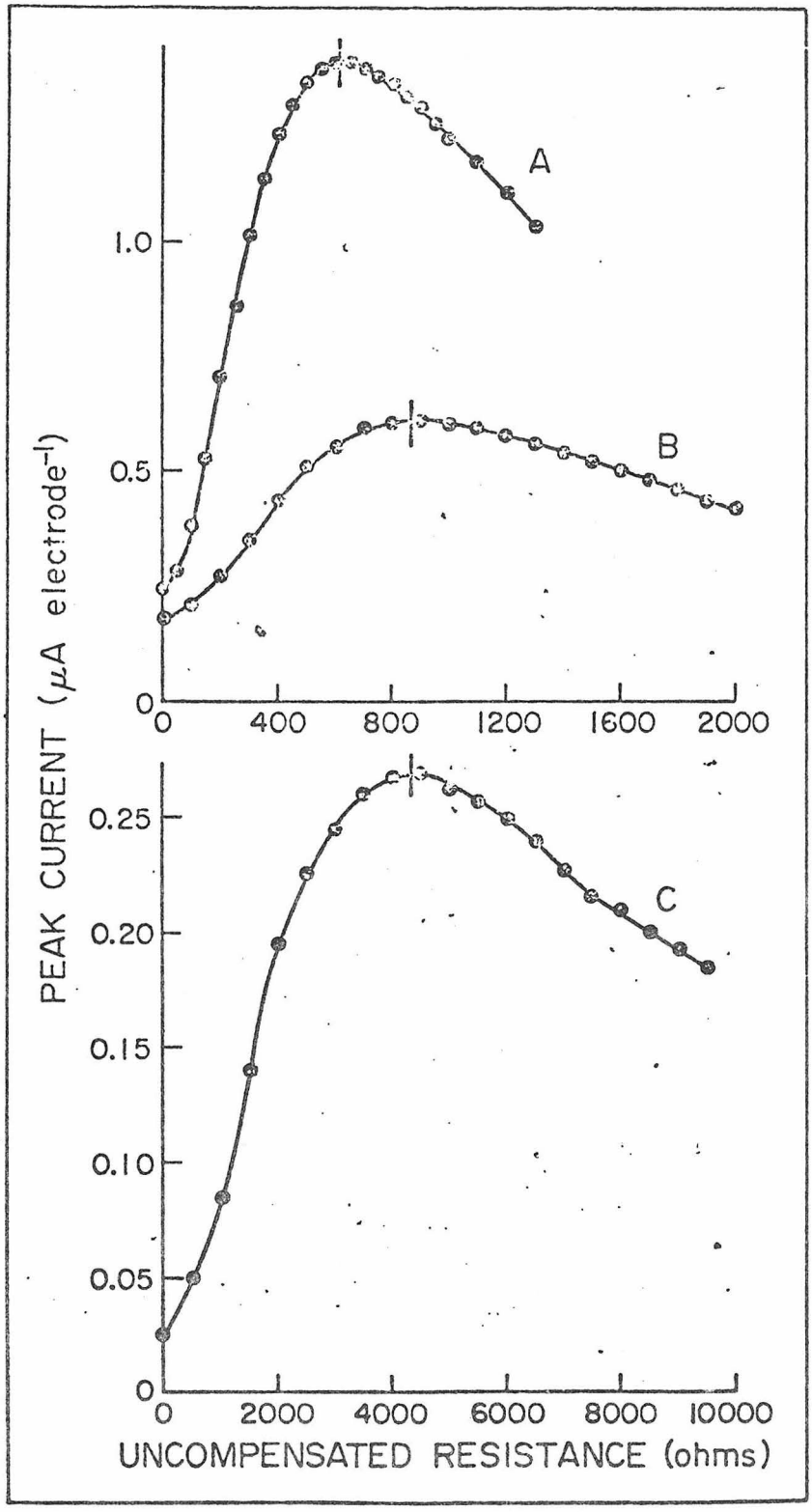
A
B
C
1.0
0.5
0
0
400
800
1200
1600
2000
0.25
0.20
0.15
0.10
0.05
0
2000
4000
6000
8000
10000
PEAK CURRENT (μA electrode⁻¹)
UNCOMPENSATED RESISTANCE (ohms)

Figure 7

with EPG electrodes. The appropriate value of $C_{d.l.}$ to use in Equation 5 seems likely to be that resulting from a voltammogram recorded at a scan rate corresponding to the ratio of the pulse magnitude to the current sampling time employed in the differential pulse voltammetry. For the PAR 174 instrument the current sampling time is 48 msec and 5 mV pulse amplitudes were used so the value of $C_{d.l.}$ was evaluated from cyclic voltammetric currents measured at a scan rate of 5/48 = 0.105 volts s^{-1}. The resulting values of Γ estimated from Equation 5 are 2.9×10^{-10} and 1.0×10^{-9} moles cm^{-2} for $Ru(NH_3)_5(PPE)^{2+}$ adsorbed on BPG and EPG graphite, respectively, and 1.8×10^{-10} moles cm^{-2} for covalently linked $Ru(II)(NH_3)_5(CAAMP)$ (insert drawing 4) on EPG graphite. The corresponding values estimated from the areas of the cyclic voltammograms recorded at the same time as the data in Figure 7 are 4.0×10^{-10}, 2.3×10^{-9} and 1.2×10^{-10} moles cm^{-2}. The agreement between the two sets of values for Γ is well within the estimated uncertainties that are known to be associated with the use of Equation 5 (11).

The considerably greater surface concentration obtained with adsorptive attachment on EPG disks probably reflects the larger microscopic area of this form of graphite. The adsorption of more than a monolayer of the reactant may also be occurring since the aromatic

anchors might be expected to attach to themselves about as readily as to the graphite surface.

Rates of Loss of Attached Reactants from the Electrode Surface. The slow decrease in the magnitude of differential pulse voltammetric peak currents was used to monitor the loss of reactants from the electrode surface. (Between scans the electrodes were potentiostated at -0.15 V. Detached reactants were removed by periodically flushing the cell with fresh electrolyte solution.) The data, plotted semi-logarithmically in Figure 3, indicate that the rates of detachment of both adsorbed and covalently linked reactants follow first-order kinetics only after a significant fraction of the initially attached species has been removed. The half-lives evaluated from the linear portions of the plots for the loss of adsorbed $[Ru(NH_3)_5(PPE)]^{2+}$ and covalently linked $Ru(NH_3)_5(CAAMP)$ were 313 and 1080 min., respectively. The adsorbing reactant, $[Ru(NH_3)_5(PPE)]^{2+}$, can readily be reattached to electrodes from which it has desorbed. However, the diminishing pulse voltammetric waves for the covalently linked complex cannot be restored by exposing the spent electrodes to fresh solutions of $Ru(NH_3)_5OH_2^{2+}$. This might be taken as an indication that it is the rupture of the amide bond holding the ligand to the electrode

surface which determines the rate of loss of the covalently linked complex.

DISCUSSION

The experimental results summarized here make it clear that attachment of electrochemically active reactants to the surface of graphite electrodes can be readily achieved both by spontaneous adsorption via "aromatic anchors" as well as by the controlled synthesis of suitable functionalities on the electrode surface (cf. Figure 2). The two routes to attachment differ markedly in the longevity of the attached reactants (Figure 8) but, at least for the Ru(III)/Ru(II) couples studied here, the electrochemical behavior of the two types of attached reactant is virtually identical. It may be that the very high intrinsic electron transfer rates of ruthenium pentaammine complexes effectively mask real differences in electrochemical reactivities of the two forms of attached reactants so that the attachment of a less reactive redox couple would provide a more sensitive test of this question.

The surface chemistry indicated in Figure 2 is based, in part, on the established presence of carboxylic acid functionality on high area, oxidized graphites (18). The fact that 4-amminomethylpyridine could be successfully

Figure 8

Semilogarithmic plot of differential pulse voltammetric peak current vs. the time the electrode was exposed to the supporting electrolyte solution. A: $Ru(NH_3)_5(PPE)^{2+}$ adsorbed on EPG electorde. B: Covalently attached $Ru(NH_3)_5$(CAAMP) on EPG electrode. Supporting electrolyte: 1 M Trifluoroacetic acid.

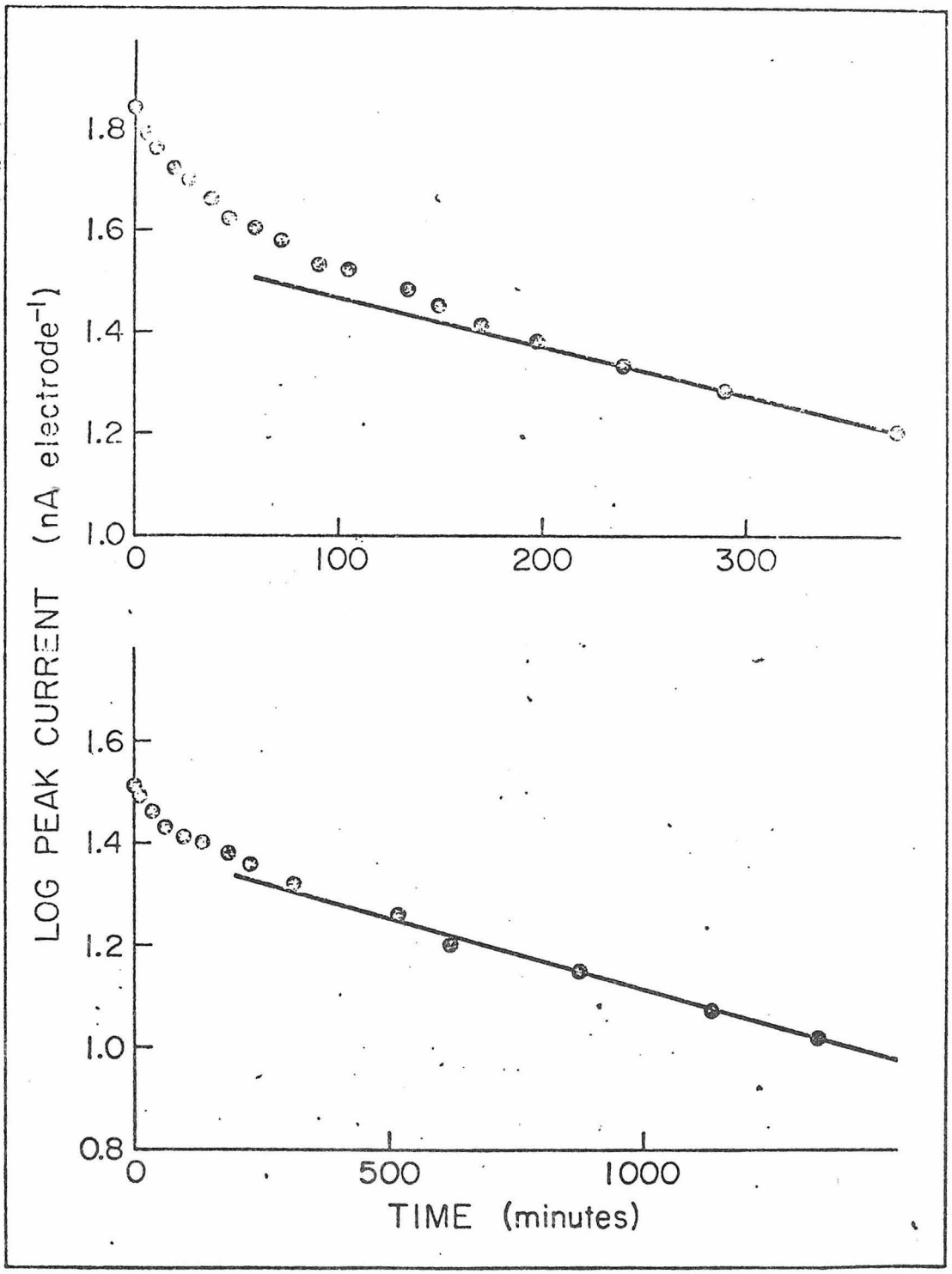
LOG PEAK CURRENT (nA electrode^{-1})
1.8
1.6
1.4
1.2
1.0
0
100
200
300
1.6
1.4
1.2
1.0
0.8
0
500
1000
TIME (minutes)

Figure 8

attached to EPG but not (detectably) to BPG electrodes supports the proposition that the attachment requires an abundance of oxidized functionalities on the surface. However, it is somewhat surprising that the attachment of 4-amminomethylpyridine, if accomplished by means of a simple amide bond, was just as great at oxidized electrodes which were not treated with thionyl chloride as at those which were. Nevertheless, we are convinced that the attachment described does involve a covalent bond because the control experiments clearly rule out spontaneous adsorption of $[Ru(NH_3)_5 (AMP)]$ as well as the possibility of ionic bonding such as (insert drawing 5). Furthermore, the durability of the attached ruthenium complex, $t_{1/2} \sim 18$ hours, is inconsistent with anything but a strong covalent attachment bond.

Finally, it may be worth pointing out that Ru(III)/Ru(II) complexes were selected for this study because their chemistry features several extremely desir virtues: i) Both halves of the redox couple are sufficiently substitutionally inert that the complex is not chemically destroyed within a few cycles of oxidation and reduction; ii) the standard electron transfer rate constant for the Ru(III)/Ru(II) pentaammine complex is quite high (~1 cm sec^{-1})

assuring nernstian behavior with correspondingly sharp differential pulse and cyclic voltammetric responses; iii) the formal potentials of the attached redox couples can be adjusted over a considerable range by selection of the sixth ligand in the metal's coordination sphere. To match these chemical properties with other, particularly first-row, transition metal complexes will probably require the use of multi-dentate ligands.

ACKNOWLEDGEMENTS

We are grateful to Alan Brown for helpful discussions and the synthesis of the ligand PPE.

CREDIT

This work, Contribution No. 5659, was supported by a grant from NSF-RANN.

LITERATURE CITED

(1) R. F. Lane and A. T. Hubbard, J. Phys. Chem., 77, 1401, 1411 (1973).

(2) B. F. Watkins, J. R. Behling, E. Kariv and L. L. Miller, J. Am. Chem. Soc., 97, 3549 (1975).

(3) B. E. Firth, L. L. Miller, M. Mitani, T. Rogers, J. C. Lennox and R. W. Murray, J. Am. Chem. Soc., 98 8271, (1976).

(4) A. P. Brown, C. Koval and F. C. Anson, J. Electroanal. Chem., 72, 379 (1976).

(5) R. J. Burt, G. J. Leigh, C. J. Pickett, Chem. Commun., 1940 (1976).

(6) M. Fujihira, T. Matsue and T. Osa, Chem. Lett., 875 (1976).

(7) P. R. Moses and R. W. Murray, J. Am. Chem. Soc., 98, 7435 (1976); J. Electroanal. Chem., 77, 393 (1977).

(8) J. R. Lenhard and R. W. Murray, J. Electroanal. Chem., 78, 195 (1977).

(9) S. Mazur, T. Matusinovic and K. Cammann, J. Am. Chem. Soc., 99, 3888 (1977).

(10) J. F. Evans, T. Kuwana, M. T. Henne and G. P. Royer, J. Electroanal. Chem., 80, 409 (1977).

(11) A. P. Brown and F. C. Anson, Anal. Chem., 49, 1589 (1977).

(12) A. P. Brown and F. C. Anson, J. Electroanal. Chem., 83, 203 (1977).

(13) P. Ford. D. Rudd, R. Gaunder, and H. Taube, J. Am. Chem. Soc., 90, 1187 (1968).

(14) C. G. Kuehn and H. Taube, J. Am. Chem. Soc., 98, 689 (1976).

(15) H. S. Lim, D. J. Barclay and F. C. Anson, Inorg. Chem., 11, 1460 (1972).

(16) T. Matsubara and P. C. Ford, Inorg. Chem., 15, 1107 (1976).

(17) E. Laviron, J. Electroanal. Chem., 39, 1 (1972) and references therein.

(18) H. P. Boehm, Advan. Catal., 16, 179 (1964).

SECTION I-C

Rotating Ring-Disc Electrode Studies of Oxygen Reduction at Platinum and Modified Pyrolytic Graphite Surfaces

Introduction

Because of possible practical applications to fuel cells and air batteries, the reduction of dioxygen at electrodes has been extensively studied and reviewed (1,2). As explained in the Introduction to Part I of this thesis, this author has taken part in collaborative effort to discover oxygen-reduction catalysts and attach them to conductive supports (3). Considering the importance of this goal, it was necessary to establish a procedure for catalyst evaluation. The electrochemical methods classically used for this purpose have involed use of a rotating ring-disc electrode (RRDE) (1,2,4-7). The rotating ring-disc technique, which is described in a book by Albery and Hitchman (8), is particularly useful in studies of oxygen reduction due to the ease with which electroactive intermediates are detected. The most stable intermediate in the reduction of oxygen to water is hydrogen peroxide. It has been shown (3) that efficient reduction of O_2 to H_2O cannot proceed through H_2O_2; therefore, it is important to ascertain whether or not a catalytic electrode produces this intermediate.

This section contains preliminary attempts to study oxygen reduction on modified pyrolytic graphite electrodes. Included are:

a) descriptions of procedures and experimental conditions,

b) the behavior of a known oxygen electrocatalyst, platinum, under these conditions,

c) two modified surfaces which do not catalyze O_2-reduction, and

d) data for a modified surface that does catalyze O_2-reduction and qualitative comparisons between it and platinum.

Experimental

Materials. Trifluoroacetic acid, HTFA, (Matheson, Coleman, and Bell) and sodium borate decahydrate (J. T. Baker) were used as received. De-ionized water was distilled from a 0.1 M permanganate solution and then from a vessel free of permanganate prior to use.

Compounds. 9-10-phenanthrenequinone (Eastman Organic Chemicals) was recrystallized from benzene. Iron(III) protoporphyrin IX chloride (Eastman Organic Chemicals) was used as received. The procurement and use of polyvinylpyridine (PVP) and Ru(edta) will be published elsewhere (9).

Apparatus. All voltammograms were obtained using a Pine Instrument Company (PIC) Model RDE3 Potentiostat in conjunction with a Hewlett Packard Model 7046A X-Y recorder. Working electrodes were PIC Model DT6 ring-disc electrodes. One electrode contained a platinum disc while the disc on the other electrode was pyrolytic graphite. Both electrodes had platinum rings. Rotation was accomplished with a PIC Model ASR2 analytical rotator. The auxiliary electrode was a platinum wire. The reference electrode was a saturated calomel electrode (SCE), but all potentials reported are with respect to the normal hydrogen electrode (NHE). This conversion is made by subtracting 0.25 V from the raw data.

The electrochemistry cell, which is shown in Figure 1, was fashioned from a 400 ml Pyrex beaker. The upper lip of the beaker was removed and an additional compartment was added to house the reference electrode. The compartments were separated with a medium-porosity sintered glass frit. The cell was covered with a teflon plug which fitted snugly into the top of the beaker. Apertures in the plug allowed for entry of the working and auxiliary electrodes and a glass pipette which was used for deaeration and oxygenation of solutions

Argon was dispersed into two consecutive vanadous solutions and an aqueous solution prior to entry into the cell. Oxygen was dispersed into an aqueous solution prior to use.

Procedures

The ring-disc electrodes were routinely polished with 0.3 micron alumina (Linde) mixed with water on a Microcloth (Buehler) polishing pad. Occasionally, the pyrolytic graphite electrode was resurfaced with 320-grit silicon carbide paper.

Electrode coatings of 9,10-phenanthrenequinone and iron(III) protoporphyrin IX were achieved by allowing the electrodes to soak in dilute (~10^{-3} M) solutions of the materials for ~15 minutes. The solutions were acetone/water (1:1 by volume) and $Na_2B_4O_7$ (0.1 M) in water, respectively. The working electrodes were always washed with copious quantities of water before electrochemical experiments.

Figure 1

Rotating ring-disc electrode cell.

Side View of RRDE Cell

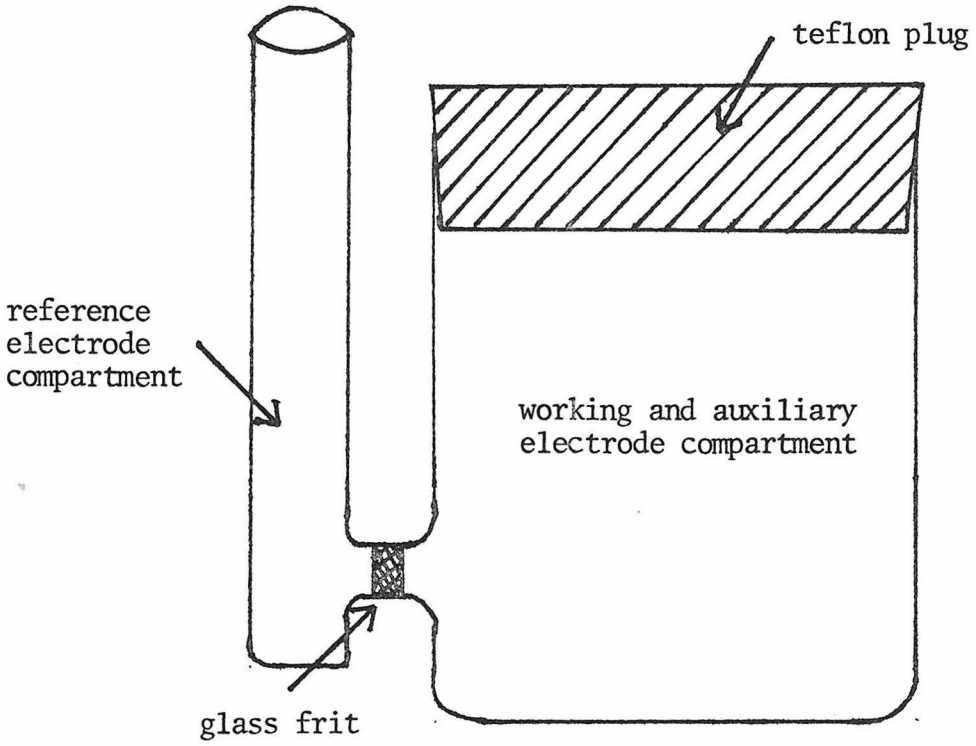

Top View of Teflon Plug

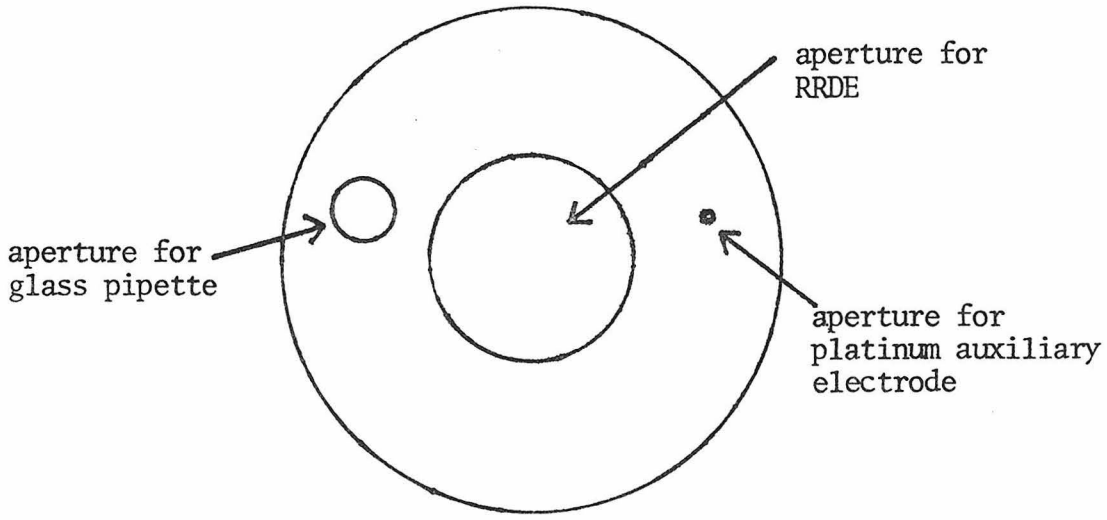

Figure 1

Results and Discussion

Calibration of Electrodes. The two rotating ring-disc electrodes used had the same dimensions and ring material (platinum). One electrode contained platinum as the disc material and the other pyrolytic graphite; these electrodes are forthwith referred to as PG-Pt and Pt-Pt. Table I contains the dimensions of the electrodes given by the manufacturer and the calculated disc area, A.

TABLE I

disc radius, r_1 (cm)	0.382
inside ring radius, r_2 (cm)	0.399
outside ring radius, r_3 (cm)	0.422
disc area, A_{calc} (cm^2)	0.459
collection efficency, N_{calc}	0.177

Included in Table I is the collection efficiency which was calculated using formulae found in the literature (8).

The disc areas and collection efficiencies were also measured experimentally. The systems used for these calibrations were the reduction of $Fe(III)(CN)_6^{3-}$ in HTFA (0.5 M) for the PG-Pt electrode and the oxidation of $Fe(II)(CN)_6^{4-}$ in HTFA (0.5 M) for the Pt-Pt electrode. The areas were obtained using the Levich equation (2):

$$i_L = 199\ nFAD^{2/3}r^{-1/6}\omega^{1/2}c^b$$

where i_L = diffusion-limited current (mA)

n = # of electrons in reaction

F = coulombs/mole = 96484

A = area (cm^2)

D = diffusion coefficient (cm^2/sec)

r = kinematic viscosity (cm^2/sec)

ω = rotation rate (r.p.m.)

c^b = concentration (moles/cm^3)

At 22° C $r = 0.957 \times 10^{-2}$ (10). The Levich equation simplified to:

$$i_L = 4.18 \times 10^7\ nAD^{2/3}\omega^{1/2}c^b$$

Plots of i_L versus $\omega^{1/2}$ for the two electrodes are shown in Figure 2. as expected, i_L has a linear dependence on $\omega^{1/2}$ although least-squares lines calculated from the data have small positive y-intercepts. From the slopes of the least-squares lines and the known diffusion coefficients of $Fe(III)(CN)_6^{3-}$ and $Fe(II)(CN)_6^{4-}$, 0.763×10^{-5} cm^2/sec and 0.641 cm^2/sec (11), respectively, electrode areas can be calculated for the PG-Pt electrode $A_{obs} = 0.406$ cm^2 and for the Pt-Pt electrode $A_{obs} = 0.362$ cm^2. The values are drastically different from $A_{calc} = 0.459$ cm^2, but gave reasonable

Figure 2

Plot of the limiting disc currents i_L versus the square root of rotation rate ($\omega^{1/2}$) for the reduction of $Fe(CN)_6^{3-}$ (1.46 mM) on the PG-Pt electrode (▲) and the oxidation of $Fe(CN)_6^{4-}$ (1.01 mM) on the Pt-Pt electrode (●).

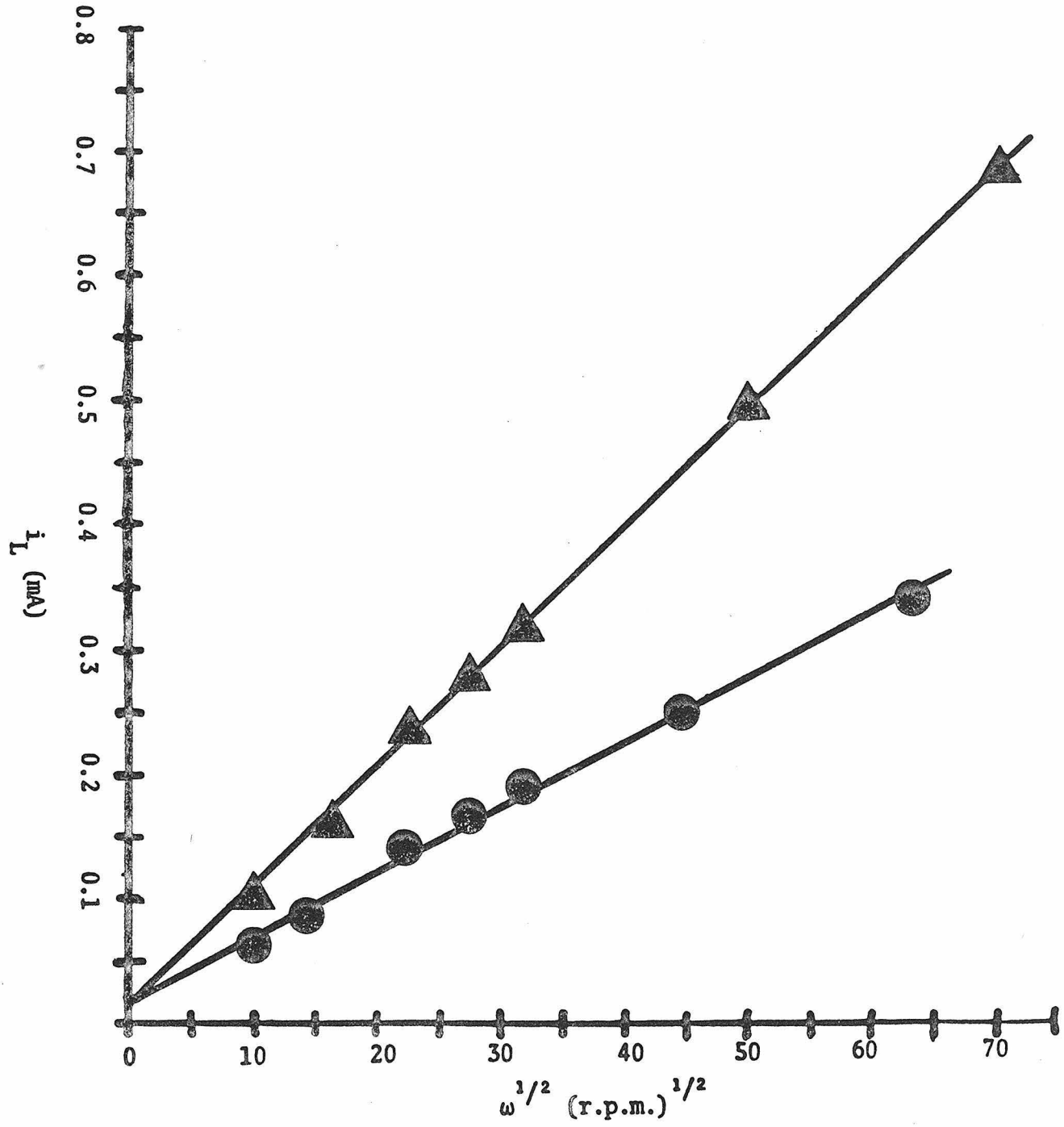

Figure 2

results when used in interpretations of the oxygen reduction data. During the area calibration experiments, collection efficiencies were also measured by holding the ring at the initial potential of the disc scan range. Collection efficiencies are simply the ratio of the ring and disc limiting currents. For both the Pt-Pt and PG-Pt electrodes, N_{obs} varied only slightly with rotation rate. The observed collection efficiencies, $N_{obs} = 0.164$ for the Pt-Pt electrode and $N_{obs} = 0.161$ for the PG-Pt electrode, were fairly close to the calculated value, $N_{calc} = 0.177$.

Oxygen Reduction on Platinum

Because platinum is the best known electrocatalyst for oxygen reduction (2), it was used as a surface with which to calibrate synthetic catalysts. The reduction of O_2 in H_2SO_4 (1 M) at a Pt-Pt ring-disc electrode has been studied by Bockris and coworkers (4). The principal findings are described below:

a) In sulfuric acid solutions that have been rigorously purified, oxygen is reduced at a diffusion-controlled rate in a four-electron process at ~0.5 V. No hydrogen peroxide is produced in this process as evidenced by a lack of current at the ring which is held at +1.4 V where H_2O_2 is known to be oxidized;

b) In sulfuric acid that has not been rigorously purified, the disc current for O_2-reduction reaches a maximum at ~0.6 V, but decays rapidly to a minimum at ~0.4 V. Hydrogen peroxide is detected at the ring throughout the potential region 0.8 - 0.1 V;

c) A kinetic analysis of the ring and disc currents, i_R and i_D, as a function of rotation rate (12) establishes that in unpurified solutions O_2 is reduced in parallel pathways to H_2O_2 and H_2O. The H_2O_2 produced is not destroyed at an appreciable rate.

Bockris' observations about the necessity of purifying sulfuric acid solutions in order to obtain four-electron reduction of O_2 on platinum have been observed in other studies (13). This has led to the general conclusion that elaborate purification of the water and gases used in oxygen reduction studies is required (1). Suspecting that either impurities in the sulfuric acid or else the nature of the acid itself was responsible for the difficulties encountered in platinum studies, this author examined the reduction of O_2 on platinum in HTFA (0.5 M). Only routine procedures for purification of water and gases were used (see Experimental Section). A typical ring-disc scan is shown in Figure 3. The shape of the voltammetric curve for the disc is nearly identical to those reported for purified sulfuric acid solutions. The ring current is small, accounting for <2% of the current produced at the disc (14). Similar scans were recorded at a variety of rotation rates and a plot of i_L vs $\omega^{1/2}$ is shown in Figure 4. At rotation rates $\leq$1000 rpm, i_L is linearly dependent on $\omega^{1/2}$. From the slope of a least-squares line drawn through these data, an n-value of 3.6 can be calculated using the Levich equation. The concentration

Figure 3

Disc and ring currents (i_D and i_R) for the reduction of O_2 in HTFA (0.5 M) on the Pt-Pt electrode (ω = 1000 rpm).

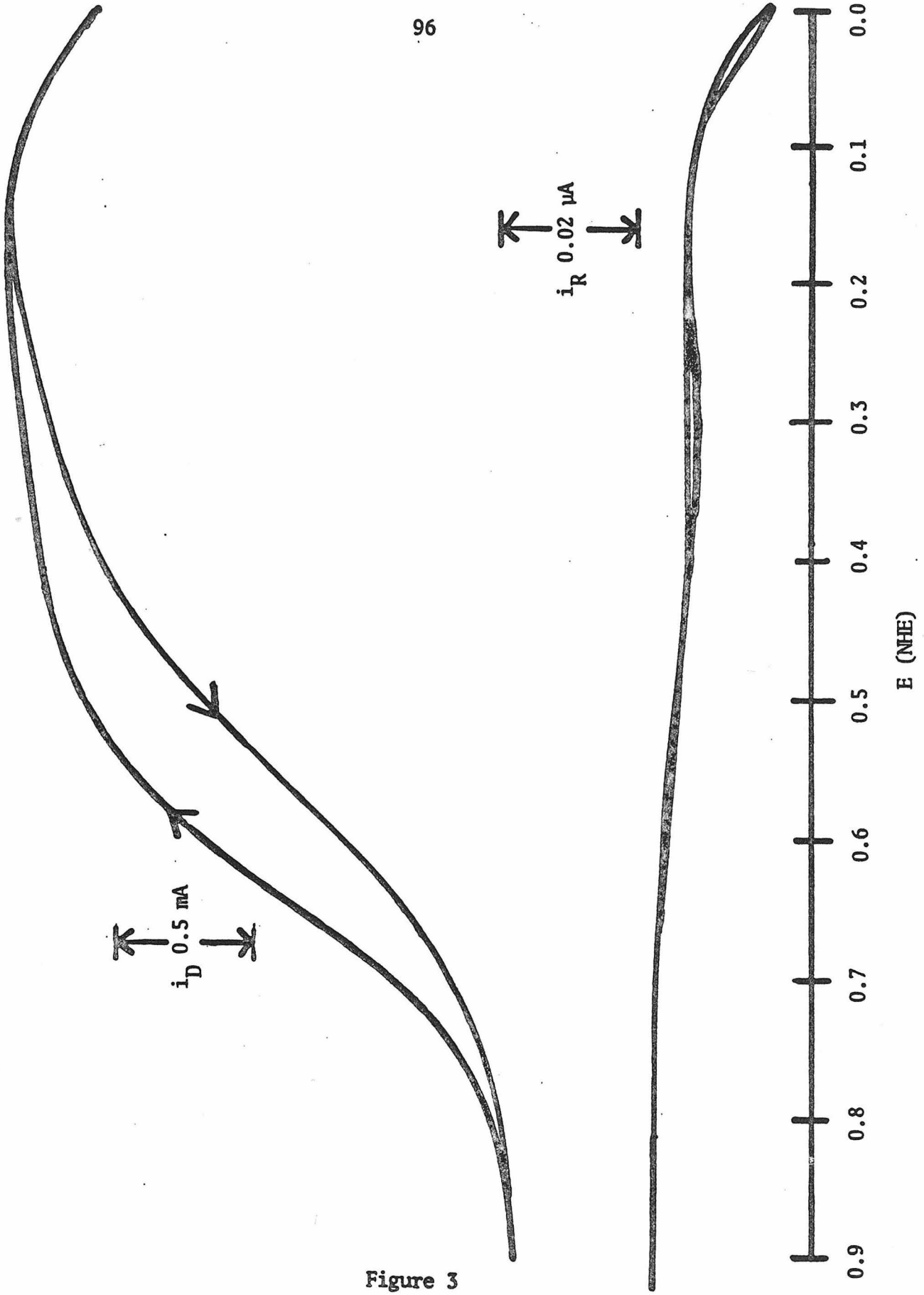

Figure 3

Figure 4

Plots of disc limiting currents, i_D, versus the square root of rotation rate, $\omega^{\frac{1}{2}}$, for the Pt-Pt electrode (●) in oxygen-saturated HTFA (0.5 M) and for the PG-Pt electrode (▲) in oxygen- and Fe(III)(PPCl)-saturated HTFA (0.5 M).

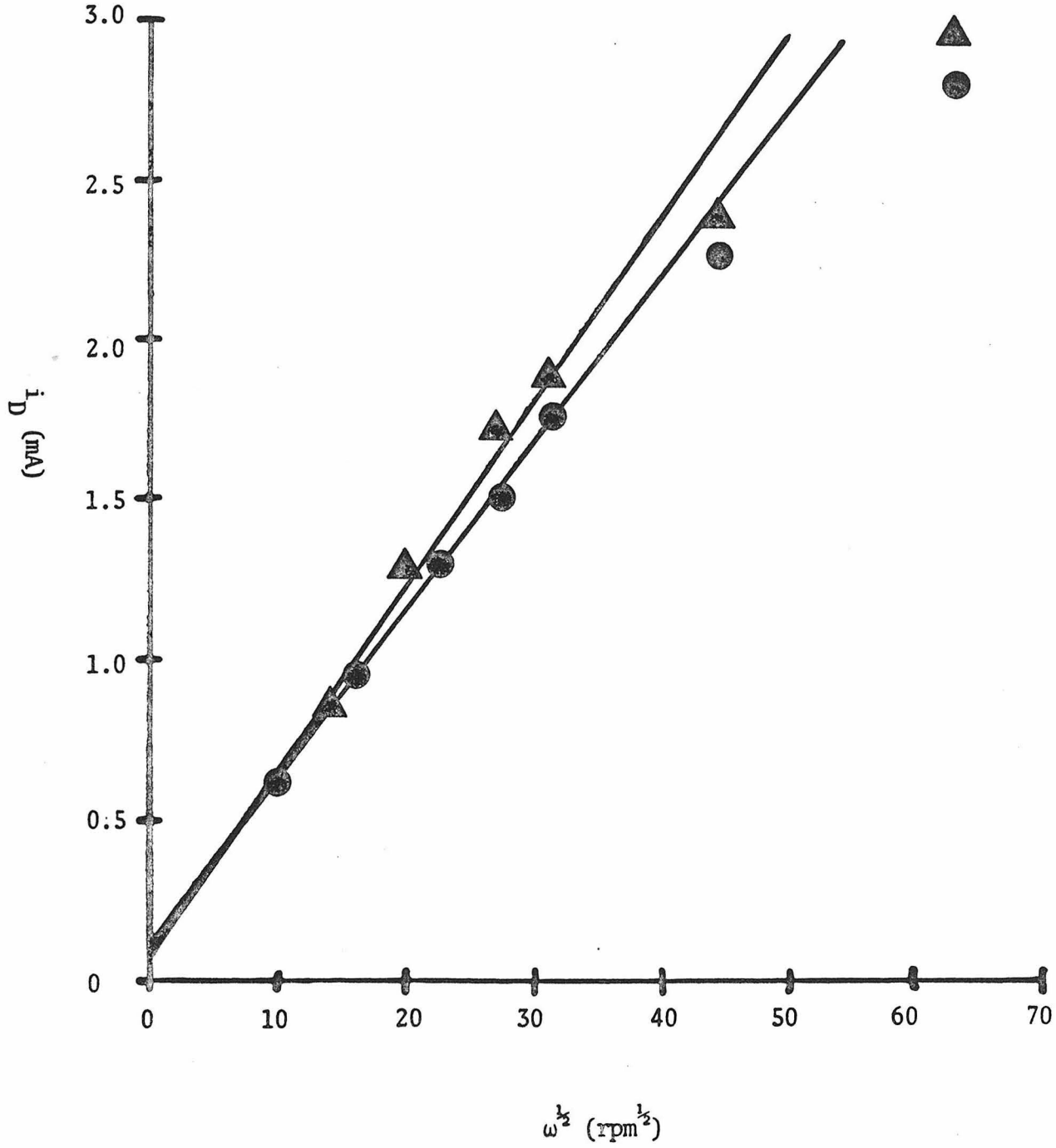
3.0
2.5
2.0
1.5
1.0
0.5
0
i_D (mA)
0
10
20
30
40
50
60
70
$\omega^{\frac{1}{2}}$ (rpm$^{\frac{1}{2}}$)

Figure 4

of O_2 in water at 1 atm is 1.4×10^{-6} mole/cm^3 (11) and the diffusion coefficient of O_2 at 22° C is 1.76×10^{-5} cm^2/sec (15,16). This is consistent with a four-electron reduction of O_2, at least at moderate to slow rotation rates. The unusual behavior at high rotation rates will be discussed later.

The voltammetric curve in Figure 3 shows a large amount of hysteresis. This is apparently due to adsorption on the platinum surface of organics which block O_2-reduction sites (4). Before each scan the electrode must be "activated" by potentiostating at +1.4 V to form an oxide layer, followed by reducing the oxides at 0.0 V. One method used by Bockris to evaluate the amount of organics in the solutions was to measure the current at the disc as a function of time at a fixed rotation rate and potential. This was done for the Pt-Pt electrode in the HTFA solution at the same potential and similar rotation rate. The results are in Figure 5, curve A. It requires ~20 min for the disc current to decay to one-half of its original value. This is a slower decay than Bockris reported for purified H_2SO_4 (4).

No further attempts were made to study the reduction of O_2 on platinum, but several observations were made concerning the "activation" process and the decay of disc currents:

a) The activation process is completely reproducible resulting in identical voltammograms;

b) The process that "deactivates" platinum occurs even at potentials where O_2 is not being reduced;

Figure 5

Disc current, i_D, plotted against time for oxygen reduction in HTFA (0.5 M). Curve A: Pt-Pt electrode; ω = 200 rpm; E = 0.4 V. Curve B: PG-Pt electrode; pre-adsorbed Fe(III)(PPCl); ω = 1000 rpm; E = 0.0 V. Curve C: PG-Pt electrode; solution saturated with Fe(III)(PPCl); ω = 1000 rpm; E = 0.0 V.

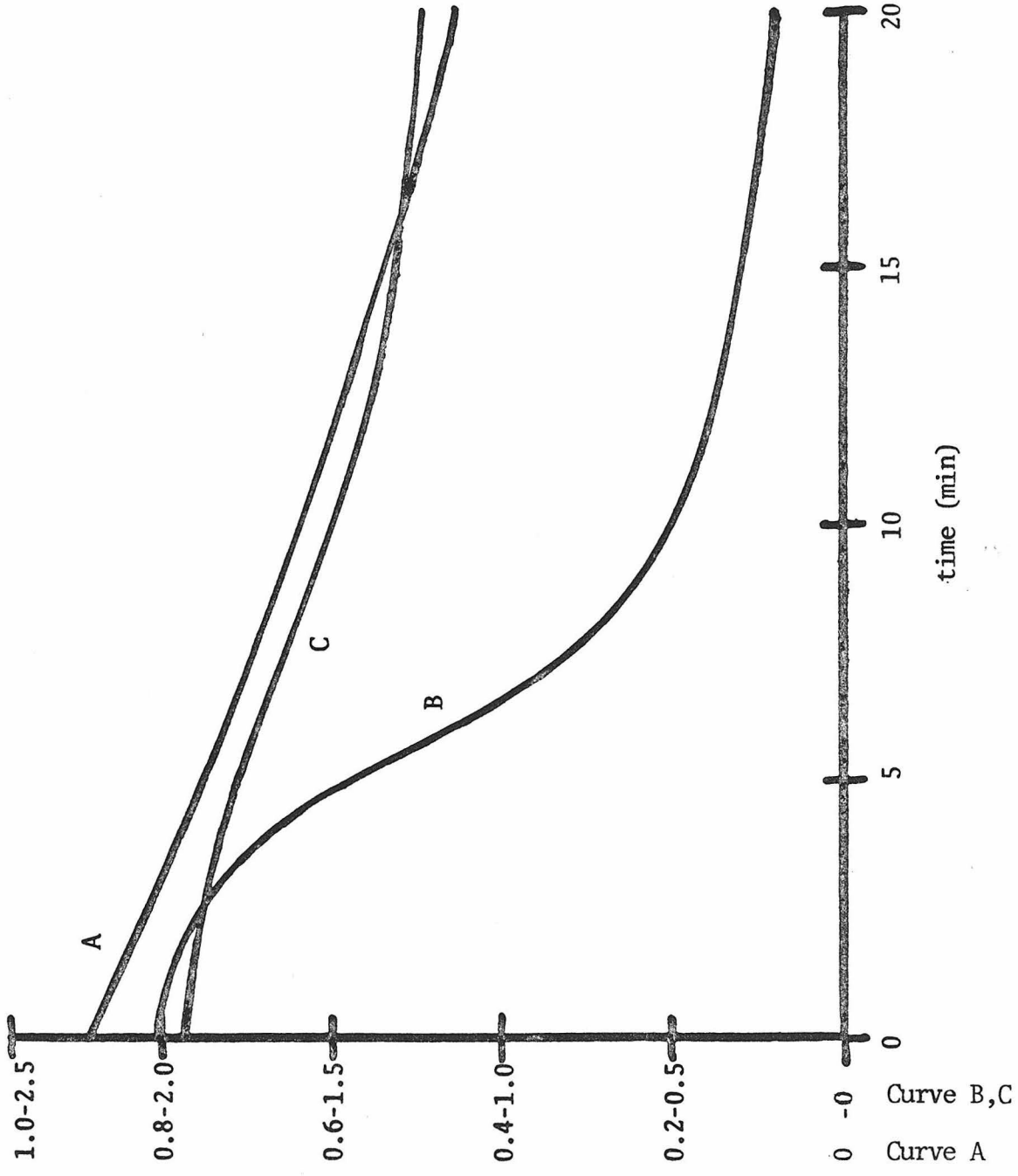
A
B
C
1.0-2.5
0.8-2.0
0.6-1.5
0.4-1.0
0.2-0.5
0
5
10
15
20
time (min)
0 -0 Curve B,C
0 Curve A

Figure 5

c) The decay rate is faster and hysteresis is more noticeable at higher rotation rates.

The final observation might provide an explanation of why the limiting currents for O_2-reduction at high rotation rates did not fall on the line predicted by the Levich equation.

Oxygen Reduction on Pyrolytic Graphite

As opposed to platinum, pyrolytic graphite is a very poor electrocatalyst for oxygen reduction. Voltammograms for the PG-Pt electrode in O_2-free and O_2-saturated solutions are shown in Figure 6. In the absence of O_2, no processes are evident anodic of 0.0 V where hydrogen adsorption begins. Protons apparently are not being reduced to molecular hydrogen because no ring current is observed. In the presence of O_2, a much greater amount of disc current is observed cathodic of 0.0 V. This is apparently due to reduction of O_2 to H_2O_2, because the ring detects current proportional to that seen at the disc. These experiments indicate that any reduction of oxygen on PG positive of 0.0 V is not due to the material itself.

Modified Electrodes That Do Not Catalyze Oxygen Reduction

The attachment of a reversible redox couple does not require that the modified surface will have catalytic properties. The irreversible adsorption of 9,10-phenanthrenequinone on graphite has been described previously (17). Oyama and Anson have developed a method of coating graphite with polyvinylpyridine followed by

Figure 6

Ring and disc currents (i_R and i_D) for the PG-Pt electrode in HTFA (0.5 M). Top - argon saturated. Bottom - oxygen saturated.

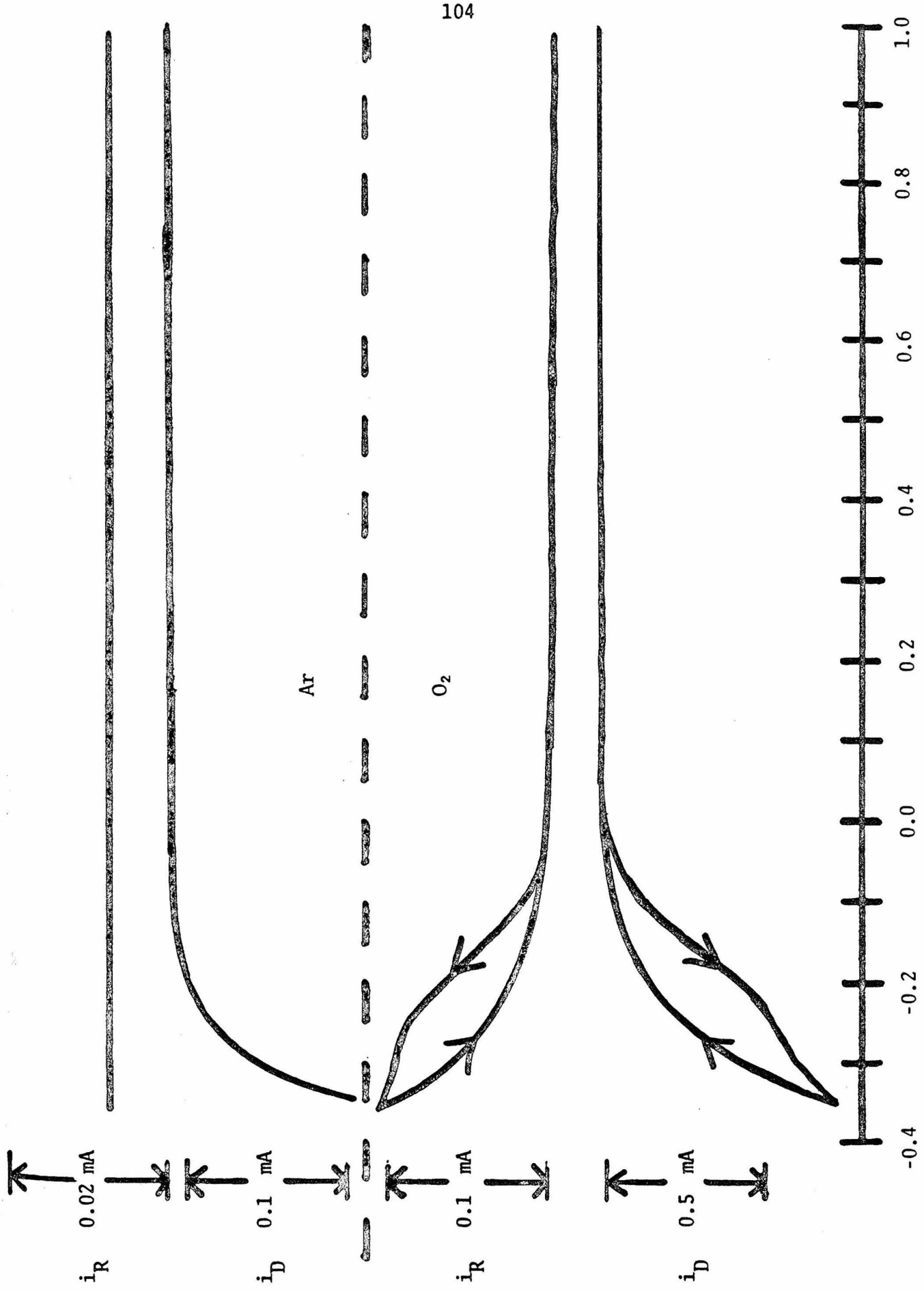

Figure 6

coordination of Ru(edta) (9). The Pg-Pt electrode was coated, in separate experiments, with each of these reagents. Cyclic voltammetry could be used to show that the couples were present and redox active. Rotating studies in the presence of O_2, however, showed absolutely no catalysis.

Oxygen Reduction on Pyrolytic Graphite with Adsorbed Fe(III)-protoporphyrin IX (Cl)

In 1976 Anson and coworkers reported the irreversible adsorption of Fe(III)protoporphyrin chloride (Fe(III)PPCl) and its subsequent surface electrochemistry (17). In $Na_2B_4O_7$ (0.1 M) a wave due to the electrocatalysis of O_2 reduction was observed, which prompted similar investigation in acidic media. A cyclic voltammogram depicting the background for the graphite disc in HTFA (0.5 M) is shown in the top of Figure 7. If, in a separate vessel, Fe(III)PPCl is adsorbed from a borate buffer onto the surface and returned to the acid medium, the voltammogram in the bottom of Figure 7 results. The waves centered at ~0.15 V are due to the reduction of Fe(III) to Fe(II) (17). In the cathodic scan there also appears to be a prewave at ~+0.3 V. In an O_2-free solution these waves persist even if the potential is scanned in the rotating mode. If the solution is then O_2-saturated and a rotating voltammogram is recorded, the behavior shown in Figure 8 is observed. Oxygen begins to be reduced at ~0.4 V and reaches a plateau at ~0.1 V. As in the case of platinum, the wave shows a marked hysteresis. At even

Figure 7

Cyclic voltammograms of the disc in the PG-Pt electrode in argon-saturated HTFA (0.5 M). Top - bare pyrolytic graphite surface. Bottom - after adsorption of Fe(III)(PPCl) from $Na_2B_4O_7$ (0.1 M). Scan rate = 50 mV/sec.

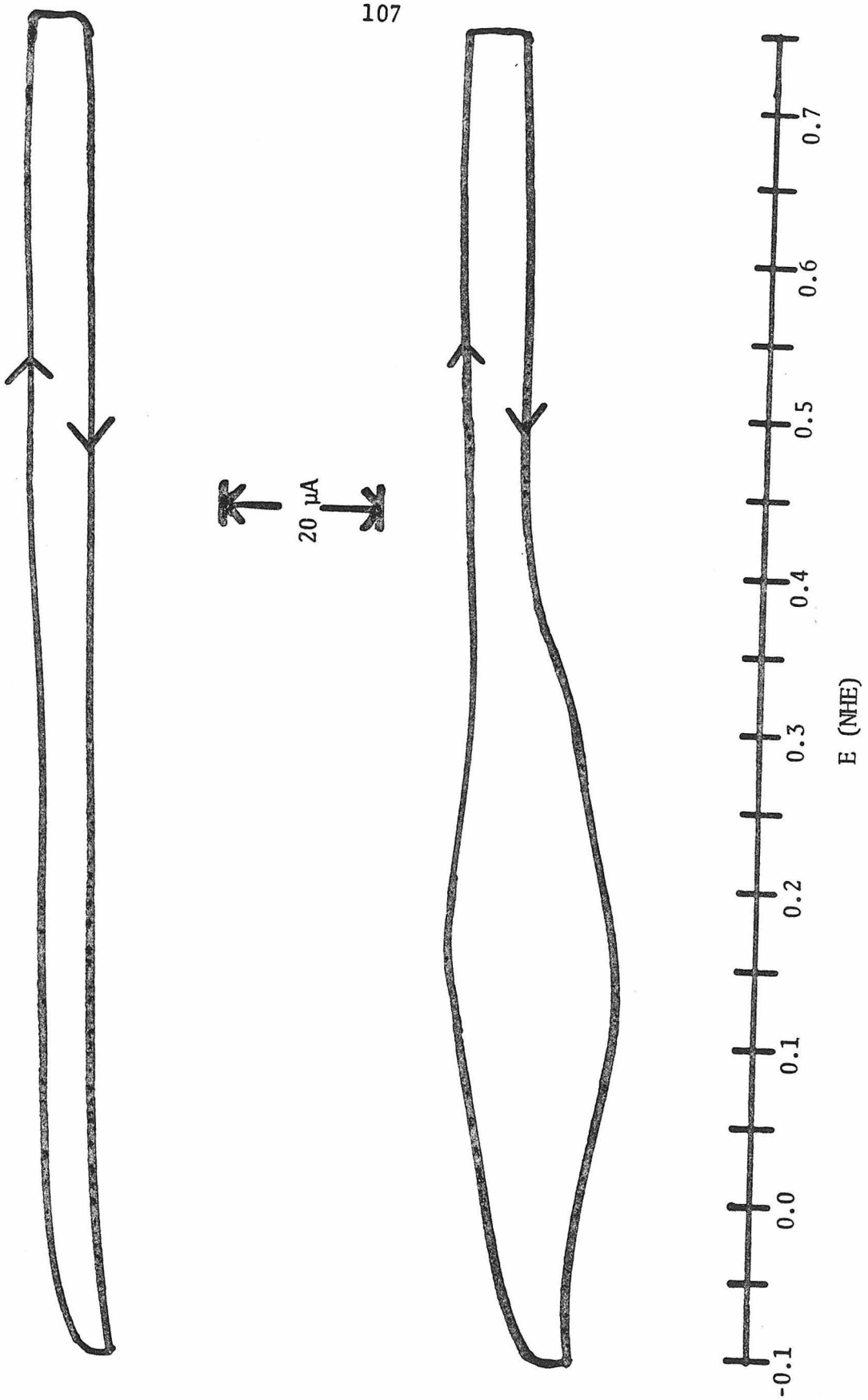

Figure 7

Figure 8

Disc and ring currents (i_D and i_R) for the PG-Pt electrode in oxygen-saturated HTFA (0.5 M). The pyrolytic graphite disc contains pre-adsorbed Fe(III)(PPCl) on its surface.

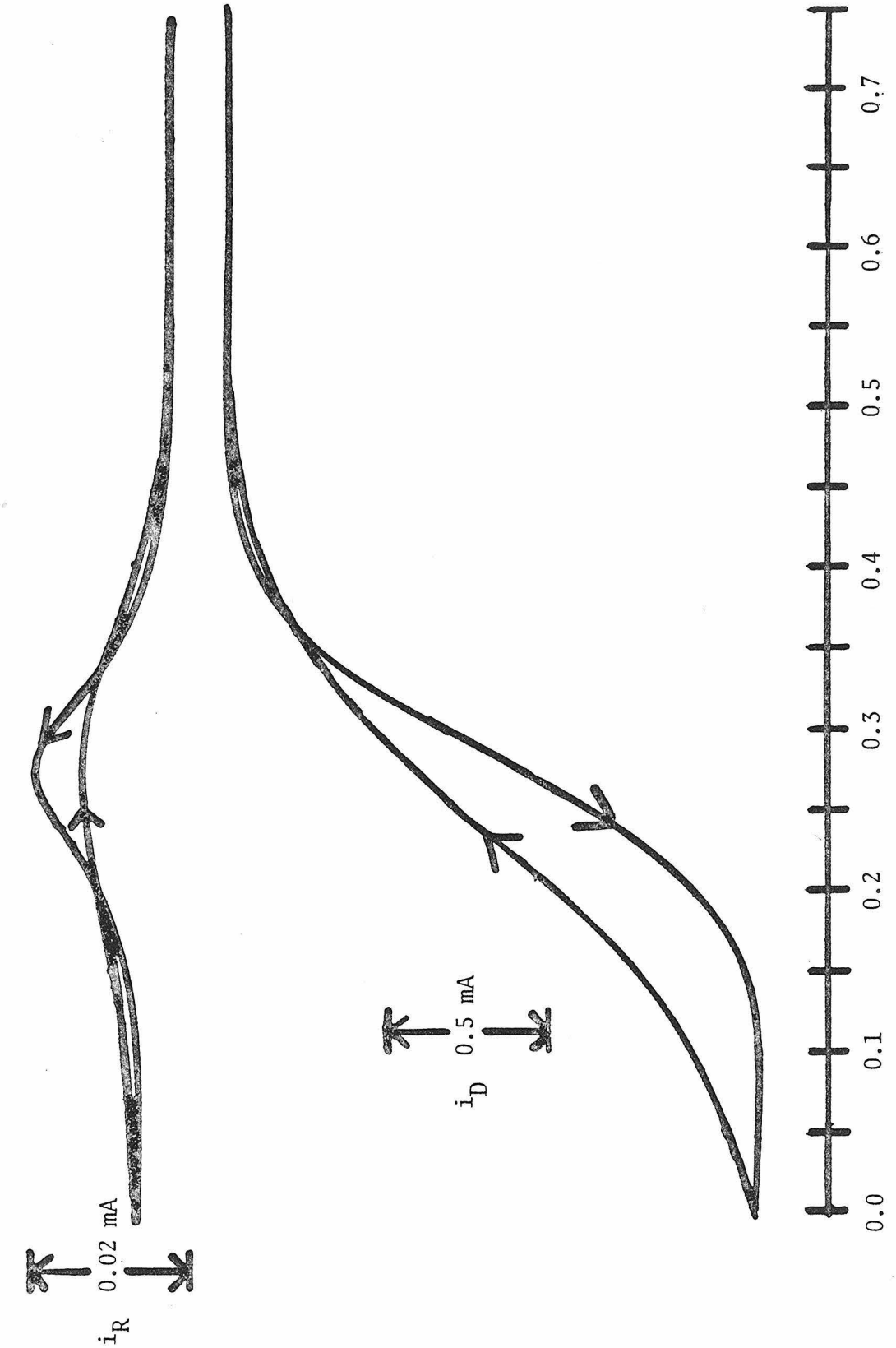

Figure 8

faster rotation rates the hysteresis causes the O_2-reduction wave to become distorted. If the potential is held at 0.0 V and the disc current as a function of time is monitored, Figure 5, curve B results. In less than 20 min, 90% of the catalytic activity is lost. If the electrode is then removed from solution and O_2 is removed, cyclic voltammetry shows that the waves present in Figure 7B have disappeared.

The stability of catalytic waves can be increased by saturating the acid solution with FePPCl. If this is done, the disc current versus time characteristics are shown in Figure 5, curve C. After 25 min. the current has slowly decayed to ~60% of its original value. One would expect that after this decay to a near steady-state catalytic activity, voltammograms free of hysteresis could be recorded. This was not found to be the case.

Saturating the solution with Fe(III)PPCl did allow voltammograms of O_2-reduction with well-defined limiting currents over a wide range of rotation rates to be recorded. At low rotation rates the limiting currents obtained in this manner were identical to those obtained with pre-adsorbed Fe(III)PPCl. This implies that the small amount of Fe(III)PPCl in solution was not affecting the catalytic wave. The saturated solution data is plotted as i_L vs $\omega^{\frac{1}{2}}$ in Figure 4. As with a platinum disc electrode only the data at $\omega \leq 1000$ rpm is linear. Similarly, the n-value calculated from the slope of a least-squares line through the linear data is 3.6.

The ring current, shown in Figure 8, that occurs when O_2 is reduced on a Fe(III)PPCl-coated electrode is unusual. As the wave for O_2 reduction at the disc begins to rise, hydrogen peroxide is detected at the ring. Instead of increasing to a steady value, however, the ring current goes through a maximum at ~0.3 V and decays to a much smaller steady-state value. When the disc current has reached its plateau, 0.1 V, the ring current accounts for <1% of the O_2 being reduced. At 0.3 V the ring current can account for as much as 25% of the disc current.

One explanation for this behavior is that the mechanism of O_2-reduction changes from a two-electron to a four-electron process as a function of potential. A second explanation, which was easily tested, is that the modified electrode was also a catalyst for H_2O_2 reduction. Figure 9 contains the results of rotating ring-disc experiment in a deaerated solution of H_2O_2 (~1 mM) in HTFA (0.5 M). The ring is held at +1.4 V where it is oxidizing H_2O_2 and the disc is scanned cathodically from +1.0 V. For an untreated PG-Pt electrode (Figure 9, top) the ring current decays slowly in a monotonic fashion. The decay is due to a buildup of oxygen bubbles on the ring. For a Fe(III)PPCl coated electrode (Figure 9, bottom) the behavior is initially the same until ~0.4 V where a reduction wave commences at the disc. This wave is due to H_2O_2 reduction as evidenced by the corresponding decrease in current at the ring. This experiment does not prove that oxygen

Figure 9

Disc and ring currents (i_D and i_R) for the PG-Pt electrode in argon saturated HTFA (0.5 M) containing H_2O_2 (~1.5 mM). Top - untreated. Bottom - pyrolytic graphite disc contains preadsorbed Fe(III)(PPCl) on its surface.

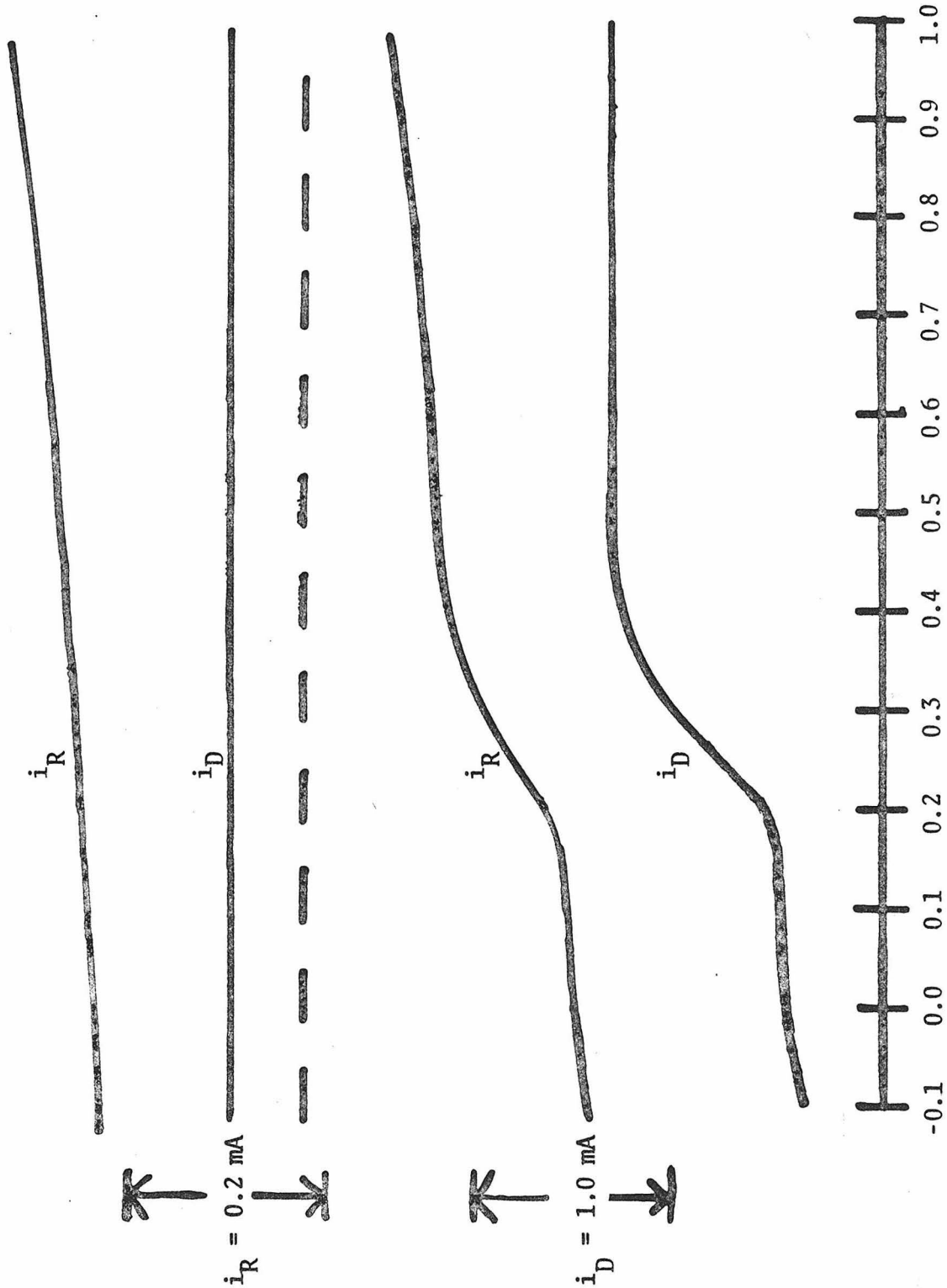

Figure 9

reduction at the Fe(III)PPCl-coated electrodes has H_2O_2 as an intermediate. Any H_2O_2 that is formed, however, will be rapidly reduced possibly accounting for the four-electron wave height.

Conclusions

The results presented in this section are of a descriptive nature. It is possible to extract a much greater amount of mechanistic data from ring-disc experiments (1). This was not attempted here because of the instability in the oxygen reduction waves. If the instability is due to the desorption of Fe(III)PPCl, there are several ways one might attempt to retard this process:

a) Use porphyrins that are less water soluble,

b) Use porphyrins that are water soluble and maintain a solution concentration that would insure a constant surface coverage (1), or

c) Covalently attach the porphyrin to the surface (18).

In all probability the mechanism of O_2-reduction on the Fe(III)PPCl-coated electrodes is a two-electron reduction to H_2O_2 with subsequent reduction to H_2O. If this is true, then this type of electrode cannot ever be engineered to operate at a potential that is very far anodic of the O_2/H_2O_2 couple, 0.68 V. Nevertheless, an inert surface has been modified successfully to increase its catalytic activity. The synthesis of more potent catalysts may eventually lead to a modified electrode capable of cost-efficient oxygen reduction.

References

1. J. Zagal-Moya, Ph.D. Thesis, Case-Western Reserve University (1978) and references therein.
2. J. O'M. Bockris and S. Srinivasan, Fuel Cells - Their Electrochemistry, McGraw-Hill Book Co. N.Y. (1969) and references therein.
3. F. C. Anson, M. Boudart, J. P. Collman, H. Taube, and H. G. Tennent. A proposal concerning this research was originally submitted to and funded by NSF-RANN.
4. A Damjanovic, M. A. Glenshaw, and J. O'M. Bockris, J. Electrochem. Soc. 114, 466 (1967).
5. L. Müller and L. N. Nekrasov, J. Electroanal. Chem. 9, 282 (1965).
6. L. Müller and L. N. Nekrasov, Electrochim. Acta, 9, 1015 (1964).
7. A. N. Frumkin, L. N. Nekrasov, V. G. Levich, and Y. B. Ivanov, J. Electroanal. Chem. 1, 84 (1959).
8. W. J. Albery and M. L. Hitchman, Ring-Disc Electrodes, Oxford Univ. Press, London (1971).
9. N. Oyama and F. C. Anson, submitted to J. Am. Chem. Soc.
10. The Handbook of Chemistry and Physics, 51st edition, The Chemical Rubber Co., Cleveland, Ohio (1970) pp. F-4, F-36.
11. M. V. Stackelburg, M. Pilgrim, and W. Toome, Z. Elektrochem. 57, 342 (1953).

12. A. Damjonovic, M. A. Genshaw, and J. O'M. Bockris, J. Phys. Chem. 45, 4057 (1966).

13. J. S. Mayell and S. H. Langer, Electrochim. Acta 9, 1411 (1964).

14. The percentage of current "accounted for" by the ring is equal to $[i_R/(i_D N_{obs})] \times 100$. In the experiment performed to measure N_{obs}, the ring, by definition, accounts for 100% of the disc current.

15. K. Grubbins and R. Walker, J. Electrochem. Soc. 112, 469 (1965).

16. R. Davies, G. Horvath, and C. W. Tobias, Electrochim. Acta 12, 287 (1967).

17. A. P. Brown, C. A. Koval, and F. C. Anson, J. Electroanal. Chem. 72, 379 (1976).

18. J. C. Lennox and R. W. Murray, J. Electroanal. Chem. 78, 395 (1977).

Introduction to Research on Copper Complexes with Macrocyclic Ligands

Part I of this thesis dealt with attachment of molecules to electrode surfaces, hopefully to create a surface which could catalyze the reduction of dioxygen. While such attachment is now readily accomplished by a variety of methods (1), the more difficult problem of finding adequate oxygen reduction catalysts still remains to be solved (2).

Certainly, ample precedent exists for selecting Cu(I) complexes as worthy candidates for oxygen catalysts. The natural enzyme laccase, which contains four copper atoms per molecule, catalyzes the reduction of oxygen to water (3). Other copper containing enzymes, tyrosinase and hemocyanin, react with oxygen in activation and transport phenomena (4,5). There have been several kinetic studies of the oxidation of Cu(I) by molecular oxygen (6-13), although these processes inevitably yield H_2O_2 as the oxygen reduction product. Despite such promise, however, relatively few Cu(I) complexes with well-defined coordination environments have been isolated in the past (14). The experimental problems that prevented such work were, principally (15):

a) The substitution lability of Cu(I) and Cu(II),

b) The tendency of Cu(I) to disproportionate to Cu(II) and Cu(0),

c) the inability of chemical reagents to reduce Cu(II) complexes to Cu(I), and

d) the air-sensitivity of Cu(I) complexes.

The latter problem is, of course, a desirable one which was essentially solved through the purchase of an inert-atmosphere dry box. Problems with lability and disproportionation were lessened by choosing ligand systems which were tetradentate, contained unsaturated nitrogen donor, and were often closed to form macrocycles.

The problem of reducing Cu(II) complexes selectively to the Cu(I) state was solved through use of electrochemical techniques. The development and use of electrochemistry for copper systems has been this author's major contribution to this research area.

In 1971 Olson and Vasilevskis (16) reported the electrochemistry of Cu(II)(trans-diene)$(ClO_4)_2$, including its electrochemical reduction to a Cu(I) complex which can be isolated.

Using similar procedures, several Cu(II) complexes were examined electrochemically and reduced to the Cu(I) state. For various reasons, further research on most of these systems was judged to be undesirable. For example, three such systems are drawn below.

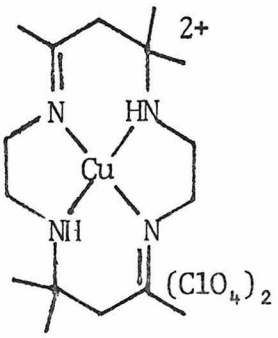

Cu(II)(trans-diene)$(ClO_4)_2$

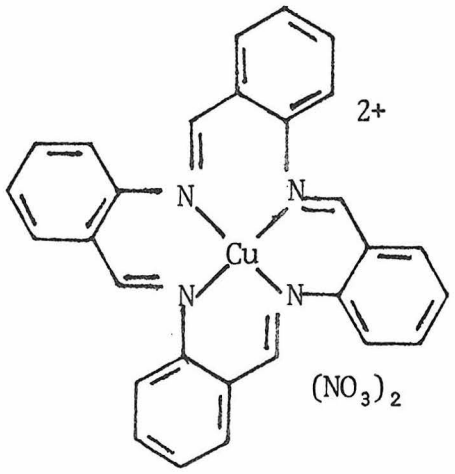

Cu(II)(TAAB)$(NO_3)_2$

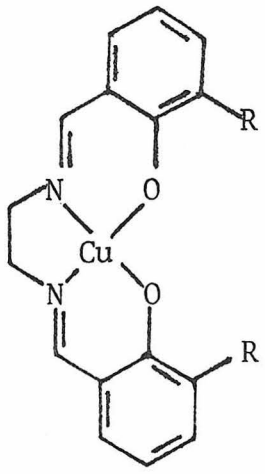

Cu(II)(salen)R_2

R=F, t-butyl

The complex Cu(II)(trans-diene)$(ClO_4)_2$ was isolated in the Cu(I) state, but reaction with oxygen caused ligand oxidation (17). A one-electron reduction product for Cu(II)(TAAB)$(NO_3)_2$ was isolated, but it was unclear whether the ligand or Cu(II) atom was reduced (18). Similarly, the Cu(II)(salen) derivatives were reduced by one electron, but the resulting complexes in solution disproportionated to copper metal before solid material could be isolated (19). Certain other systems were pursued, not primarily for their reactions with oxygen, but rather for their reactions with carbon monoxide.

The ability of certain four-coordinate, 18-electron Cu(I) complexes to form five-coordinate, 20-electron carbonyls was first reported by Gagné in 1976 (20). Later this communication was followed by a full paper (15) which is included as Appendix I to Part II. In that paper, this author was responsible for the ideas concerning the electrochemical measurement of formal potentials and CO bonding constants, along with a significant portion of the manuscript preparation.

It is possible that efficient catalysis of multi-electron reactions such as oxygen reduction will occur only with molecules containing several metal atoms. This notion prompted special interest in binuclear copper complexes. One binuclear Cu(II)Cu(II) complex which is drawn below has been the object of intense research.

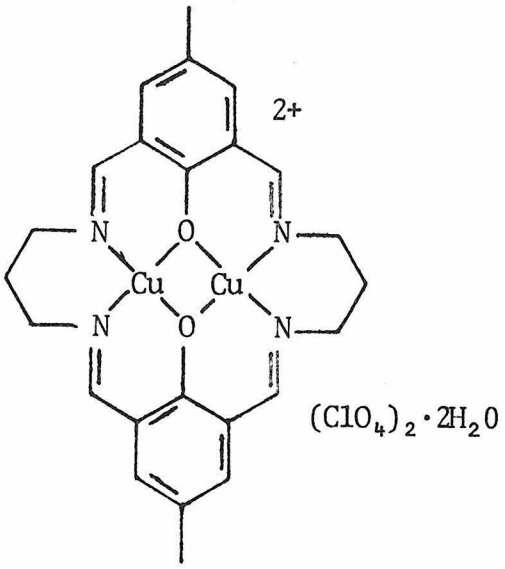

This research included synthesis of Cu(II)Cu(I) and Cu(I)Cu(I) states, electrochemical and CO binding studies, and a variety of physical measurements. A communication has already been published on this case (21) and a full paper is soon to be submitted (22). This author was involved in all facets of the research except the actual EPR experiments.

As use of electrochemistry to study copper complexes increased, the techniques required for electrochemical measurements became more sophisticated. Responsibility for introducing these techniques and for establishing procedures ensuring their correct use fell primarily upon this author. These techniques and procedures, which

are the basis for the electrochemical portions of Sections II-B, II-C and Appendix I, are presented in detail in Section II-A.

Considering that one long-term research goal is to study the reactions of Cu(I) complexes with oxygen, it is disappointing that experiments to date have not yielded characterized products in a reproducible way. This author has been involved in two attempts to investigate the reaction of a Cu(I) complex with oxygen. In one case the reaction resulted in ligand decomposition (17) and in the other reproducible stoichiometries could not be obtained. While these and other attempts to study the interactions of O_2 with Cu(I) complexes have been frustrating at times, attempts to understand the physical properties and coordination chemistry of Cu(I) will, hopefully, lay the groundwork for future success in this area.

References

1. This thesis, Introduction to Part I, and references therein.
2. This thesis, Section I-C, and references therein.
3. J. Fee, Structure and Bonding 23, 1 (1975).
4. R. Lontie, Inorganic Biochemistry, Elsevier, N.Y. (1973) p.344.
5. H. S. Mason, Ann. Rev. Biochem. 35, 595 (1965).
6. M. Guntensperger and A. D. Zuberbuhler, Helv. Chim. Acta 60, 2584 (1977).
7. A. D. Zuberbuhler, Metal Ions in Biological Systems, Vo. 5, H. Siegel, ed., Marcel Dekker, Inc., N.Y. (1976) pp. 325-68.
8. A. L. Crumbliss and L. J. Gestaut, J. Coord. Chem. 5, 109 (1976).
9. A. L. Crumblis and A. T. Poulis, Inorg. Chem. 14, 1529 (1975).
10. R. D. Gray, J. Am. Chem. Soc. 91, 56 (1969).
11. I. Pect and M. J. Anbar, J. Chem. Soc. (A) 1002 (1968).
12. P. M. Henry, Inorg. Chem. 4, 688 (1966).
13. H. Nord, Acta Chem. Scand. 9, 431 (1955).
14. R. H. Jardine, Adv. Inorg. Biochem. 17, 115 (1975).
15. R. R. Gagné, J. L. Allison, R. S. Gall, and C. A. Koval, J. Am. Chem. Soc. 99, 7170 (1977) and references therein.
16. D. C. Olson and J. Vasilevskis, Inorg. Chem. 10, 463 (1971).
17. J. L. Allison and C. A. Koval, unpublished results.

18. D. H. Busch, et al. J. Am. Chem. Soc. 96, 731 (1974).

19. R. S. Gall and C. A. Koval, unpublished results.

20. R. R. Gagné, J. Am. Chem. Soc. 98, 6709 (1976).

21. R. R. Gagné, C. A. Koval, and T. J. Smith, J. Am. Chem. Soc. 99, 8367 (1977), Section II-B of this thesis.

22. R. R. Gagné, C. A. Koval, and T. J. Smith, manuscript in preparation, Section II-C of this thesis.

SECTION II-A

Measurement of Formal Reduction Potentials and CO Binding Constants for a Variety of Copper Complexes

Introduction

The reason behind the extensive use of electrochemistry in a research group primarily concerned with the synthesis, characterization, and reactions of macrocyclic Cu(I) complexes is worth reviewing. Initially, the reason was purely synthetic. While preparation of a variety of Cu(II) complexes was readily accomplished, direct synthesis of the Cu(I) analogs was plagued with non-reaction and disproportionation. Furthermore, chemical reduction of Cu(II) complexes was often unsuccessful. Electrochemical reduction of these same complexes was discovered to be a specific and practical synthetic route into Cu(I) chemistry. During the course of the experiments aimed at Cu(I) synthesis, approximate values of Cu(II) to Cu(I) reduction potentials were inevitably obtained. These reduction potentials were found to be important characterizations of the Cu(I) complexes in and of themselves, and more sophisticated electrochemical techniques were learned solely to facilitate their measurement. The thermodynamic implications of reduction potentials began to be considered in a variety of ways, including the measurement of ligand binding constants (1-3) and the study of metal-metal interactions in binuclear complexes (2,4). The direction of synthetic efforts toward new complexes was, in part, determined by attempts to influence reduction potentials for the purposes of modeling the redox properties of copper containing proteins (5) and

affecting reactivity towards oxygen (6). It should be noted that the expanded use of electrochemistry is not limited to copper chemistry, but is finding increasing popularity in many areas of inorganic chemistry.

Whenever scientists plunge into a new field, mistakes inevitably occur until concepts and procedures become familiar. While the synthetic advantages of electrochemistry were capitalized upon almost immediately, the correct measurement and interpretation of reduction potentials is more difficult.

This thesis chapter has several purposes. The first is to present a brief discussion of the terms relevant to the measurement of reduction potentials and to indicate their use in simple thermodynamic calculations. The second purpose is to describe how reduction potentials can be obtained using several techniques for which instrumentation was available. This is done primarily by example using three inorganic systems. The third purpose is to provide a list of reduction potentials for a variety of Cu(II) complexes. The relationship of these potentials to each other and to copper proteins and their reaction with oxygen is briefly discussed. Finally, a list of CO binding constants for these same complexes is presented to show how ligand binding can be measured by changes in reduction potential. Throughout this chapter, special attention is paid to the experimental problems incurred in doing electrochemistry in non-aqueous solvents. This is done by including a detailed experimental section and by engaging in brief digressions where appropriate.

Most of the procedures in this chapter are not original and might be considered "old-hat" to an experienced electrochemist; nor is the list of Cu(II)/Cu(I) reduction potentials as extensive as others that have been compiled (7). Rather, this chapter is intended to be educational in nature and to establish a framework for the studies contained in Sections II-B, II-C, and Appendix I.

Below are structures and common names for the copper complexes whose electrochemistry is described herein:

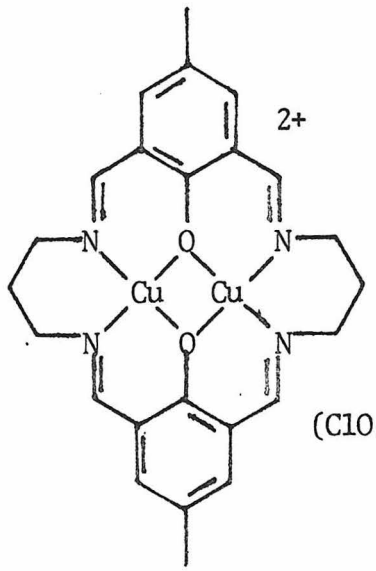

$Cu(II)_2L(ClO_4)_2 \cdot 2H_2O$

$(ClO_4)_2 \cdot 2H_2O$

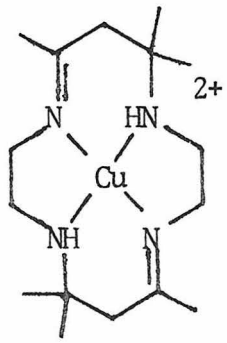

Cu(II)(trans-diene)$(ClO_4)_2$

$(ClO_4)_2$

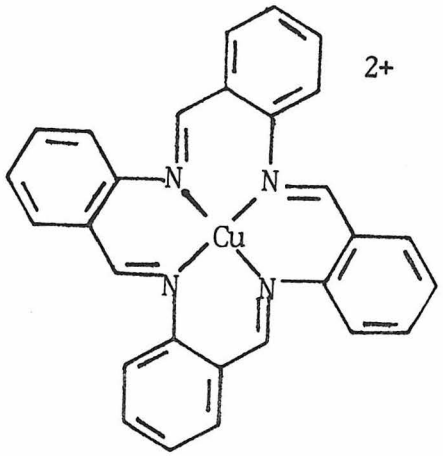

Cu(II)(TAAB)$(NO_3)_2$

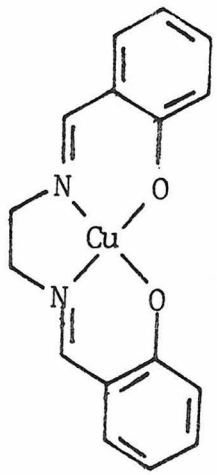

Cu(II)(salen)

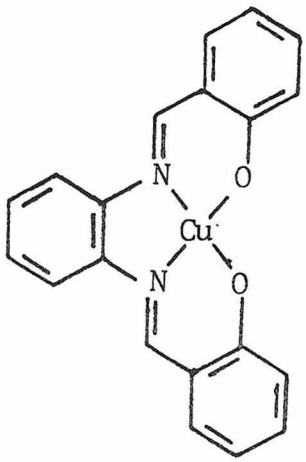

Cu(II)(salophen)

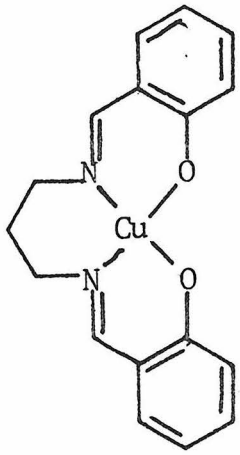

Cu(II)(salpn)

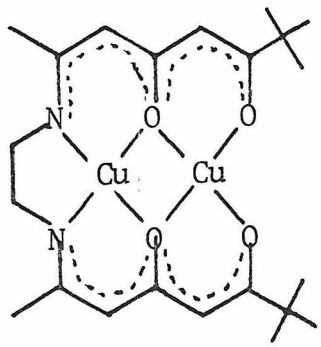

$Cu(II)_2[(PAR)_2en]$

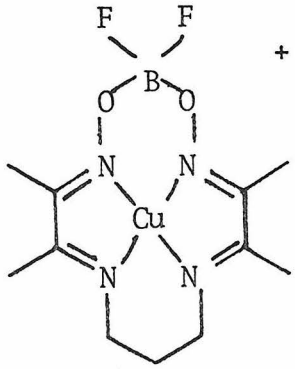

$Cu(II)(DOBF_2)(ClO_4)$

(ClO_4)

Results and Discussion

Definition of Terms

Invariably, discussions concerning half-cell potentials begin with a series of definitions of terms such as electrical potential, electrode potential, electromotive force, electrostatic sign and thermodynamic sign, including their relationship to American, European, and IUPAC sign conventions. That will not be done here; instead, the reader is directed to two such discussions (8,9).

One can simply state that for every reversible half-reaction,

$$ox + ne \rightleftharpoons red,$$

there exists a standard reduction potential, E^o. Values of E^o always refer to the potentials of cells made by combining the half-reaction of interest with the half-reaction

$$H^+ + e^- \rightleftharpoons \tfrac{1}{2}H_2 \uparrow,$$

which has an arbitrarily defined E^o equal to 0. Standard potentials imply all species are present at unit activities and that liquid-liquid junction potentials do not exist. Due to these restrictions, standard potentials are often difficult or impossible to evaluate.

The dependence of cell potential, E, upon the activities of ox and red, a_{ox} and a_{red}, is described by the Nernst equation

$$E = E^{o} - RT/nF \ln \frac{a_{red}}{a_{ox}}$$

where T is temperature and R and F are constants. If concentrations are used instead of activities and liquid junction potentials are implicitly included, the Nernst equation can be re-written as follows:

$$E = E^{f} - RT/nF \ln [red]/[ox] \ .$$

In this equation E^{f} is the formal reduction potential of the half-reaction of interest and is only meaningful if the conditions under which it was measured are known. Since convenient experimental conditions can be chosen arbitrarily, formal potentials are relatively easy to measure.

Reduction potentials are related to free energy changes by the equation $\Delta G^{o} = -nF\ E^{o}$. As is explained in many physical chemistry texts (8,9), the standard potentials for half-reactions can be combined in a way that eliminates electrons and thus allows calculation of free energy changes for overall reactions. Formal reduction potentials can be used in a similar way; however, only E^{f} values obtained under like conditions can be combined and the free energy changes so calculated will only be meaningful under those conditions.

Techniques for Measuring Formal Reduction Potentials

Using the instrumentation available, there were four methods that could be used to determine formal potentials, these being cyclic voltammetry (CV), differential pulse voltammetry (DPV), d.c. polarography and potentiometry. In this section each technique is discussed in terms of extraction of E^f from the data, criteria for reversibility, and values of E^f for three representative redox couples.

Below are the redox couples used as examples:

$$Ru(III)(acac)_3 + e^- \rightleftharpoons Ru(II)(acac)^-$$

$$Fe(Cp)_2^+ + e^- \rightleftharpoons Fe(Cp)_2$$

$$Cu(II)_2L_2^+ + e^- \rightleftharpoons Cu(II)(I)L^+$$

The ruthenium and iron couples were chosen as examples of reversible systems even though their standard electrochemical rate constants, k_s, are unknown. Nonetheless, one can argue that k_s for both systems is probably large (>0.5 cm/sec) because the separate halves of the couples are kinetically stable and geometrically similar. The ferrocene system is relevant because its purported solvent-independent value of E^f (10) is the potential to which all other potentials are compared. Unfortunately, the potential of ferrocene oxidation is far too anodic to be measured with a mercury electrode; therefore, the ruthenium complex was included. Its reduction potential is similar to those of the copper complexes being studied. Finally, the first reduction of $Cu(II)_2L^{2+}$ (11) was selected as typical of most of the copper couples investigated.

Cyclic Voltammetry

Of all the electrochemical techniques which can be used to obtain reduction potentials, cyclic voltammetry is probably the easiest to execute experimentally. Given a solution containing the oxidized form of a reversible redox couple, the cathodic peak potential, E_{p_c}, on the initial scan is related to E^f by Equation 1 (12, 13):

$$E^f = E_{p_c} + (28.5/n)\ mV \qquad 1$$

The anodic peak potential, E_{p_a}, which occurs on the return scan, has a similar relationship to E^f (14) so that the average of E_{p_c} and E_{p_a} is approximately equal to E^f as shown in Equation 2 (15):

$$E^f = (E_{p_a} + E_{p_c}) \div 2 \qquad 2$$

Equation 2 has the advantage that if E_{p_a} and E_{p_c} are shifted symmetrically away from E^f (see below) Equation 2 will still give an accurate value of E^f whereas Equation 1 will not.

In order to have complete confidence in formal potentials calculated from Equations 1 and 2, one needs to ascertain that the redox couples are reversible. The two criteria for determining reversibility are that:

a) the peak currents, i_{p_a} and i_{p_c}, are equal and proportional to the square root of the scan rate, and

b) that E_{p_a}, E_{p_c} and their separation, ΔE_p, which equals 58/n mV, do not vary with scan rate (16).

Cyclic voltammetric data for $Ru(acac)_3$, $Fe(Cp)_2$, and $Cu(II)_2L(ClO_4)_2(H_2O)_2$ are shown in Tables 1A-C. Figures 1 and 2 are plots of data from Tables 1A-C, i_p versus (scan rate)$^{\frac{1}{2}}$ and ΔE_p versus (scan rate)$^{\frac{1}{2}}$, respectively. The behavior in all three systems is similar except that the current in the $Cu(II)_2L^{2+}$ system is not quite proportional to scan rate$^{\frac{1}{2}}$ at fast scan rates. The data show that i_{p_a} is essentially equal to i_{p_c} which, when considered along with Figure 1, indicates that the first criterion for reversibility is being met. The data in Tables 1A-C also show that the second criterion is not met. Peak separations are never equal to 58 mV and increase almost linearly with the square root of scan rate (Figure 2).

Table 1A

Cyclic Voltammetry of $Fe(Cp)_2$ on Pt

Scan Rate[a]	E_{p_a}[b]	E_{p_c}[b]	ΔE_p[b]	E^f[b,d]	i_{p_a}[c]	i_{p_c}[c]	i_p(ave)[c]	$\frac{i_{p_a}}{i_{p_c}}$
.050	.432	.367	.065	.399	.850	.875	8.62	0.97
.075	.432	.364	.068	.398	1.30	1.25	1.27	1.04
.100	.433	.364	.069	.398	1.45	1.40	1.42	1.04
.250	.437	.363	.074	.400	2.20	2.10	2.15	1.05
.500	.441	.365	.076	.403	3.00	2.80	2.90	1.07
.750	.444	.363	.081	.403	3.60	3.60	3.60	1.00
1.00	.443	.359	.084	.401	3.90	4.00	3.95	0.97
2.50	.457	.362	.095	.409	6.50	6.30	6.40	1.03
5.00	.453	.360	.093	.406	8.75	8.50	8.62	1.03
7.50	.459	.353	.106	.406	10.5	10.5	10.5	1.00
10.00	.463	.350	.113	.406	12.0	12.0	12.0	1.00

[a] in volts/sec

[b] in volts

[c] in μA

[d] $(E_{p_a} + E_{p_c}) \div 2$

Table 1B

Cyclic Voltammetry of $Ru(acac)_3$ on Hg

Scan Rate[a]	E_{p_a}[b]	E_{p_c}[b]	ΔE_p[b]	E^f[b,d]	i_{p_a}[c]	i_{p_c}[c]	i_p(ave)[c]	$\frac{i_{p_a}}{i_{p_c}}$
.050	-.801	-.866	.065	-.833	3.80	4.00	3.90	0.95
.075	-.801	-.868	.067	-.834	4.20	4.80	4.50	0.87
.100	-.799	-.873	.074	-.836	5.00	6.00	5.50	0.83
.250	-.805	-.871	.066	-.838	7.80	9.00	8.40	0.87
.500	-.803	-.876	.073	-.839	10.5	11.5	11.0	0.91
.750	-.800	-.878	.078	-.839	14.5	14.5	14.5	1.00
1.00	-.799	-.884	.085	-.841	16.0	16.5	16.2	0.97
2.50	-.789	-.889	.100	-.839	25.0	26.0	25.5	0.96
5.00	-.776	-.893	.117	-.834	35.0	36.0	35.5	0.97
7.50	-.774	-.897	.123	-.835	42.0	44.0	43.0	0.95
10.0	-.772	-.900	.128	-.836	48.0	50.0	49.0	0.96

[a] in volts/sec

[b] in volts

[c] in μA

[d] $(E_{p_a} + E_{p_c}) \div 2$

Table 1C

Cyclic Voltammetry of $Cu(II)_2L(ClO_4)_2 \cdot 2H_2O$ on Hg

Scan Rate[a]	E_{p_a}[b]	E_{p_c}[b]	ΔE_p[b]	E^f[b,d]	i_{p_a}[c]	i_{p_c}[c]	i_p(ave)[c]	$\frac{i_{p_a}}{i_{p_c}}$
.050	-.493	-.564	.071	-.528	4.00	4.00	4.00	1.00
.075	-.493	-.572	.079	-.532	4.80	5.00	4.90	0.96
.100	-.490	-.572	.082	-.531	5.60	5.60	5.60	1.00
.250	-.489	-.575	.086	-.532	8.50	8.50	8.50	1.00
.500	-.486	-.576	.090	-.531	11.0	10.5	10.7	1.04
.750	-.477	-.583	.106	-.530	14.0	13.5	13.7	1.04
1.00	-.477	-.584	.107	-.530	16.0	16.0	16.0	1.00
2.50	-.477	-.594	.117	-.535	24.5	24.0	24.2	1.02
5.00	-.470	-.606	.136	-.538	34.0	33.0	33.5	1.03
7.50	-.464	-.608	.144	-.536	41.0	40.0	40.5	1.03
10.0	-.461	-.612	.151	-.537	46.0	44.0	45.0	1.04

a in volts/sec

b in volts

c in μA

d $(E_{p_a} + E_{p_c}) \div 2$

Figure 1

Plot of i_p(ave) versus (scan rate)$^{\frac{1}{2}}$ for the oxidation of $Fe(Cp)_2$ on Pt (●), the reduction of Ru(acac) on Hg (○), and the reduction of $Cu(II)_2L(ClO_4)_2 \cdot 2H_2O$ on Hg (▲). The data are taken from Tables 1A-C.

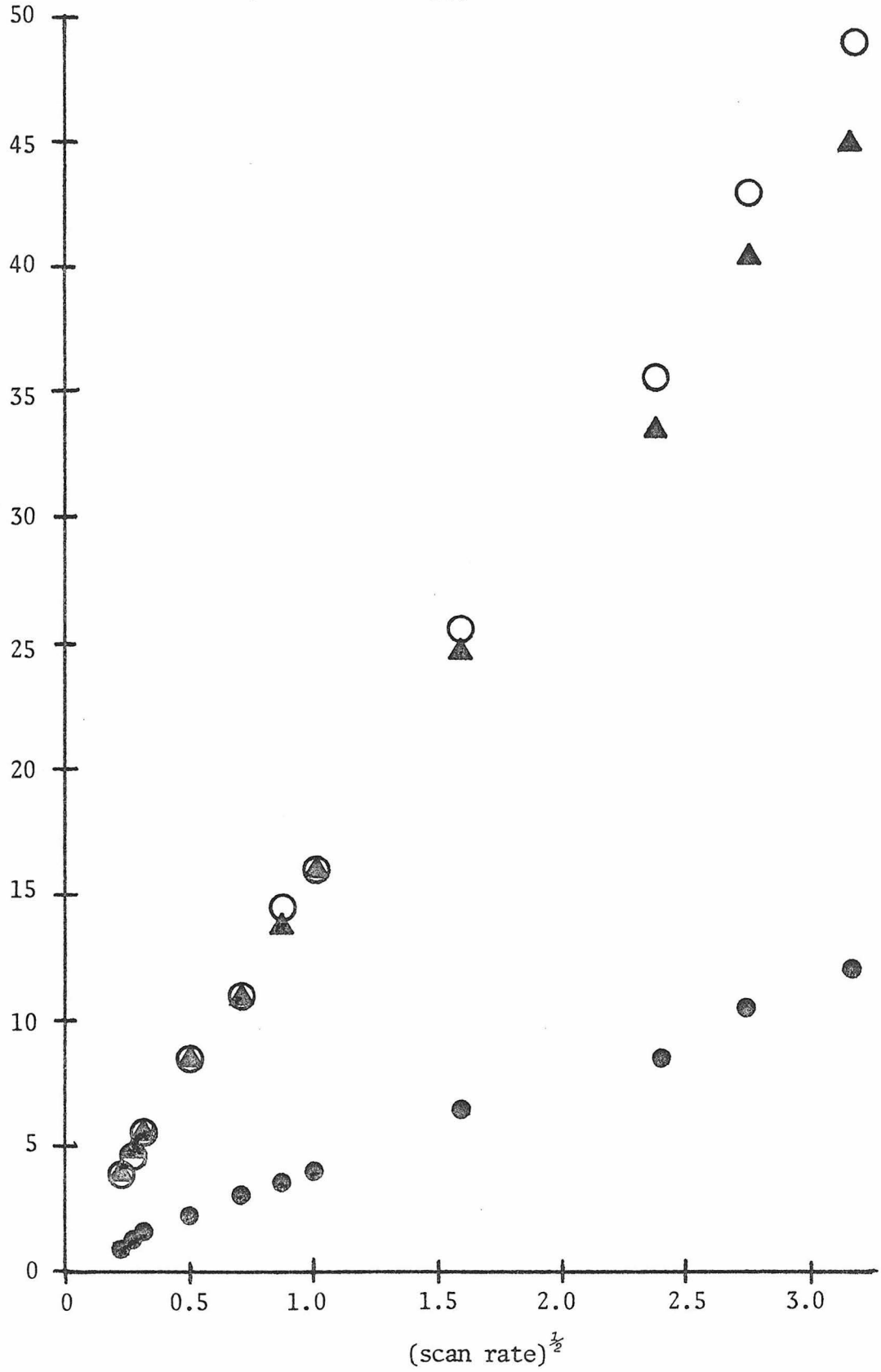

Figure 1

Figure 2

Plot of ΔE_p versus (scan rate)$^{\frac{1}{2}}$ for the oxidation of $Fe(C_p)_2$ on Pt (●), the reduction of $Ru(acac)_3$ on Hg (○), and the reduction of $Cu(II)_2L(ClO_4)_2 \cdot 2H_2O$ on Hg (▲). The data are taken from Tables 1A-C.

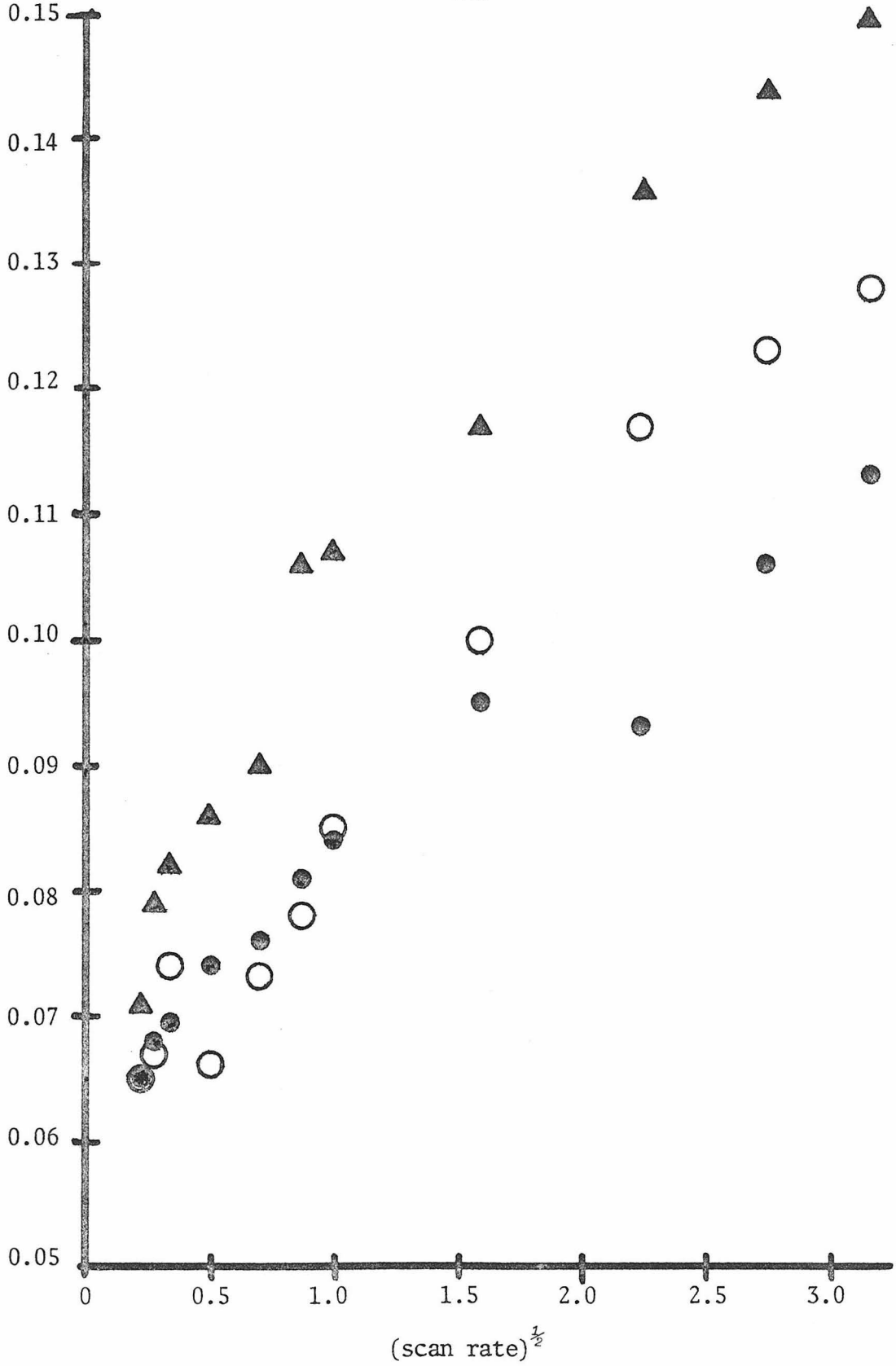
0.15
0.14
0.13
0.12
0.11
0.10
0.09
0.08
0.07
0.06
0.05
0
0.5
1.0
1.5
2.0
2.5
3.0
(scan rate)$^{\frac{1}{2}}$

Figure 2

There are two simple explanations for the behavior described above. One possibility is that the couples are quasi-reversible, which means that the standard electrochemical rate constant, k_s, is small enough so that at rapid scan rates the position of the waves with respect to E^f is not entirely controlled by diffusion. Another explanation would be that in the non-aqueous solvents used, solution resistance caused appreciable ohmic drops between the working and reference electrodes.

Were the former explanation correct, it would be possible to extract values of k_s from peak separations as a function of scan rate using published working curves (17). Such information would be valuable because, using Marcus-Hush theory, one can calculate a lower limit for the homogeneous self-exchange rate, k_{11} from values of k_s (18). Marcus-Hush theory also predicts that k_{11} is an indication of how rapidly a compound will exchange electrons with other molecules (18).

Uncompensated solution resistance, R_{sol}, is an experimental problem that affects the values of ΔE_p in nearly the same way as a low rate constant (19,20). Furthermore, if solution resistance exists in significant and unknown amounts it is impossible to measure k_s. With the equipment available it was impossible to adequately measure, eliminate, or compensate for solution resistance. Measurement of R_{sol} could only be done crudely by recording a cyclic voltammogram of a redox couple that was known to have $k_s \geq 0.5$ and assuming that any difference in the ΔE_p observed and

0.058 V was equal to $2 \cdot i_p \cdot R_{sol}$. Attempts were made to eliminate R_{sol} by increasing supporting electrolyte concentration to 1.0 M and positioning the working and reference electrodes as close together as possible. These efforts did decrease ΔE_p, but only slightly. The PAR Model 179 Digital Coulometer does have the capability for resistance compensation through positive feedback of the current output. Setting the level of this compensation is, however, completely arbitrary. Values of ΔE_p as low as 0.045 V can be obtained by adjusting to the maximum possible compensation. Since the solution resistance problem could not be avoided, efforts to measure k_s were abandoned. Despite the uncertainty surrounding reversibility, one notices that the values of E^f calculated from Equation 2 are fairly constant at all scan rates. The average of these values of E^f is used in comparisons with other techniques.

Differential Pulse Voltammetry (DPV)

In order to maintain a high signal-to-noise ratio, cyclic voltammetry requires reactant concentrations around 10^{-3} M. Compound solubility occasionally is less than this level, but comparable signal-to-noise can be obtained with DPV at concentrations of 10^{-5} M. Problems with solution resistance are also lessened because the amount of current measured in DPV is much smaller than in CV. For example, the peak current equations for CV and DPV are given below (20,21):

$$i_p^{CV} = 269\ n^{3/2} AD^{1/2} C\ r^{1/2} \text{ (amps)} \qquad 3$$

$$i_p^{DPV} = 939\ n^2\ AC\Delta E\sqrt{D/\pi t} \text{ (amps)} \qquad 4$$

n = # of electrons

A = electrode area (cm^2)

D = diffusion coefficient ($cm\ sec^{-1}$)

C = concentration (molar)

r = scan rate ($volt\ sec^{-1}$)

ΔE = DPV modulation amplitude (volts)

t = DPV sampling time ($=48 \times 10^{-3}$ sec)

Assuming that n = 1, A = 0.01 cm^2, D = $10^{-5}\ cm^2\ sec^{-1}$, C = 10^{-3} M and r = 0.2 $volt\ sec^{-1}$, Equation 3 predicts a peak current of 3.8×10^{-6} amp. Assuming that n, A, and D are the same as above and using C = 10^{-5}, ΔE = 0.01 volt, and t = .048 sec, Equation 4 predicts that $i_p^{DVP} = 7.6 \times 10^{-9}$ amp.

Formal potentials can be obtained from the peak potentials of differential pulse voltammograms using Equation 5 (21):

$$E^f = E_p^{DVP} + (\Delta E \div 2) \qquad 5$$

The shape of the wave can also be analyzed for reversibility using the criterion that the peak width at half height, $\Delta E_{\frac{1}{2}i}$, should be 90.4/n mV (21).

Table 2 contains data for the three sample systems (22). All three appear to be reversible, which implies that the large peak separations found with CV were due to ohmic drop. While the scan rates used in DPV are normally 2 mV/sec or less, one should not conclude that DPV is a "slow" technique. A better estimate of the experimental timescale can be found by dividing the modulation amplitude, ΔE, by the sampling time, t (23). For the parameters used in gathering the data in Table 2, the approximate timescale is 0.01 (V) ÷ 0.048 sec = 0.208 (V/sec). This is similar to the timescale of cyclic voltammetry.

Table 2. Differential Pulse Voltammetric Data

Compound	E_p	E^f	$\Delta E_{\frac{1}{2}i}$
$Fe(Cp)_2$	.395	.400	.092
$Ru(acac)_3$	-.830	-.835	.093
$Cu(II)_2L(ClO_4)_2$	-.518	-.523	.092

D.C. Polarography

A technique that measures a relatively small amount of current and that has a slower timescale than CV is d.c. polarography. Concentrations of 0.5×10^{-3} M are easily detectable and with normal parameters diffusion-limited currents are roughly 1.0×10^{-6} amp. Scan rates are usually 1 mV/sec or lower.

Formal potentials are obtained from polarographic waves by finding the potential when the current is one-half of its diffusion-limited value, i_d. For a reversible system this half-wave potential, $E_{1/2}$, is equal to E^f (13,24). The most common analysis for reversibility involves plotting -E vs log $i/(i_d-i)$. For a reversible system a straight line results with a slope of 2.303 RT/nF = 0.058/n V. Table 3 contains data for the polarographic reduction of $Ru(acac)_3$ and $Cu(II)_2L(ClO_4)_2 \cdot 2H_2O$. The data indicate that each is a reversible, one-electron process.

Table 3. Polarographic data

Compound	$E_{1/2}$	Slope
$Ru(acac)_3$	-.822	.058
$Cu(II)_2L(ClO_4)_2$	-.517	.058

Potentiometry

The most direct method of determining formal potentials is by potentiometry, which involves measuring the potential of a solution that contains known amounts of the oxidized and reduced halves of a redox couple. Values of E^f can then be extracted from the Nernst equation. This technique is an equilibrium measurement because no current flows through the cell when E is recorded.

A series of potentiometric measurements can be made during a constant potential electrolysis (CPE) by periodically turning

the potentiostat to open circuit, recording the charge passed, Q, and measuring E. At the end of the electrolysis the total charge passed, Q_t, will be known. For a reduction [red]/[ox] is equal to Q/Q_t-Q. The data are then plotted as E versus log [red]/[ox]. The x-intercept is equal to E^f and, for a reversible system, the slope equals .058/n volts. Upon reoxidation a similar plot is made which should yield the same E^f and Q_t. If the original mass of compound is known, Q_t provides a check on the n-value by using Faraday's Law.

Table 4 contains potentiometric data for the reduction and oxidation of each of the sample systems. While the values of E^f are nearly the same during oxidation or reduction, slope values in two cases are significantly different from .058 V and Q_t values differ by as much as 10%. These discrepancies may be due to solution impurities, compound instability at long times, or to the fact that the potentials recorded were not equilibrium values. It should be noted that this technique is particularly tedious and time-consuming.

Table 4. Potentiometric Data

Compound	Process	E^f	Slope	Q_t
$Fe(Cp)_2$	red.	.389	.061	2.29
$Fe(Cp)_2$	oxid.	.392	.061	2.34
$Ru(acac)_3$	red.	-.821	.066	2.47
$Ru(acac)_3$	oxid.	-.820	.062	2.32
$Cu(II)_2L(ClO_4)_2$	red.	-.523	.067	2.60
$Cu(II)_2L(ClO_4)_2$	oxid.	-.528	.060	2.30

Comparison of Formal Potentials Obtained by Different Techniques

Table 5 contains the formal potentials obtained using the four techniques for the three representative systems. Although agreement between E^f values for each system is good, differences as large as .017 V did occur. These differences appear to be real, because formal potentials obtained by each technique were reproducible to within at least ±0.005 V. It must be remembered, however, that criteria for reversibility were not strictly met in many of these measurements.

Table 5. Comparison of Formal Potentials Obtained by Different Techniques

Compound	Cyclic Voltammetry	DPV	d.c. Polarography	Potentiometry
$Fe(Cp)_2$	.403	.400	---	.390
$Ru(acac)_3$	-.837	-.835	-.822	-.820
$Cu(II)_2L(ClO_4)_2$	-.533	-.523	-.517	-.525

The method judged to be most useful for determining formal potentials for copper complexes was d.c. polarography. This technique offered the following advantages:

a) Excellent reproducility,

b) slow timescale usually allowing reversible behavior to be observed, and

c) only low concentrations of complex being required.

Polarographic Data

Table 6 contains d.c. polarographic data for the reduction of a variety of Cu(II) complexes to the Cu(I) state. Each compound was examined in DMF solutions that were initially deaerated with an inert gas (N_2) and later, in a separate experiment, with carbon monoxide. The significance of the CO data will be discussed in the next section. The meaning of the column headings in Table 6 has already been explained, except for the one labeled "I_d", which is the normalized diffusion-limited current. Rearrangement of the Ilkovic equation is the source of I_d.

$$i_d = 706\ n\ D^{1/2}\ m^{2/3}\ t^{1/6}\ C$$

$$I_d = \frac{i_d}{m^{2/3}\ t^{1/6}\ C} = 706\ n\ D^{1/2}$$

m = mercury flow rate (mg/sec)

t = drop time (sec)

Because D is not expected to vary greatly between complexes, all the one electron reductions are expected to have similar values of I_d.

Table 6

Polarographic Data for Copper Complexes

Complex	Atmosphere	[a] $E_{1/2}$	[b] Slope	[c] r	[d] I_d
Cu(II)(trans-diene)$(ClO_4)_2$	N_2	-.654	.067	.9984	1.67
	CO	-.651	.066	.9990	1.69
Cu(II)(TAAB)$(NO_3)_2$	N_2	-.011	.062	.9997	1.67
	CO	-.009	.058	.9997	1.31
Cu(II)(salen)	N_2	-1.303	.049	.9993	1.89
	CO	-1.239	.054	.9987	2.15
Cu(II)(salophen)	N_2	-1.191	.058	.9998	1.81
	CO	-1.186	.058	.9999	1.81
Cu(II)(salpn)	N_2	-1.099	.058	.9999	1.74
	CO	-1.040	.058	.9999	1.78
Cu(II)[$(PAA)_2$en]	N_2	-.995	.057	.9999	1.51
	CO	-.918	.058	.9999	1.50
Cu(II)$(DOBF_2)(ClO_4)$	N_2	-.452	.057	.9997	1.75
	CO	-.299	.059	.9999	1.78
$Cu(II)_2L(ClO_4)_2 \cdot 2H_2O$	N_2	-.517	.058	.9995	1.34
	CO	-.392	.057	.9999	1.39
$Cu(II)(ClO_4)_2 \cdot 6H_2O$	N_2	-.015	.035	.9993	2.46
	CO	+.114	.061	.9998	1.26
	CO	-.151	.064	.9997	1.24
O_2	Ar	-.774	.069	.9988	

[a] in volts versus NHE.

[b] of -E versus log i/i_d-i plot in volts

[c] regression coefficient of above plot

[d] $706\ n\ D^{1/2} = \dfrac{i_d}{m^{2/3}\ t^{1/6}\ C}$

Many of the complexes in Table 6 have been examined previously using various electrochemical techniques; however, the potentials reported cannot be compared to each other because a variety of reference electrodes and solvents were used. All of the data in Table 6 were collected under identical conditions using ferrocene as an internal, solvent-independent reference couple; therefore, comparison of E^f values are valid. An additional reference potential, the reduction of O_2 to O_2^-, is also included in Table 6.

In most cases the data in Table 6 are in agreement with what has appeared in the literature. Olson and Vasilevskis (25) reported that Cu(II)(trans-diene)$(ClO_4)_2$ could be reduced at a DME in acetonitrile at -.930 V versus the $Ag/AgNO_3$ (0.1 M),CH_3CN reference electrode. They also found a large polarographic slope, 74 mV, and a similar value of I_d, 2.76. The reduction of the Cu(II) atom in Cu(II)$(TAAB)^{2+}$ to Cu(I) has been measured by Busch et al. (26). In acetonitrile, they obtained quasi-reversible (ΔE_p = 65 mV) cyclic voltammogram from which they obtain formal potentials of -0.23 V and +0.13 V versus the $Ag/AgNO_3$ (0.1 M),CH_3CN electrode and SCE, respectively. If the SCE value is corrected to the NHE, E^f is +.375 V which is quite different from the value of -0.009 found in Table 6. This difference is due, primarily, to the choice of reference electrodes, which is discussed in the Experimental Section of this chapter. The difference in E^f for Cu(II)$(TAAB)^{2+}$ and Cu(II)(trans-diene)$^{2+}$ in acetonitrile, as reported in the two

above-mentioned papers, is 0.7 V which is quite similar to the difference in DMF of 0.645 V reported here.

Patterson and Holm reported polarographic data for a variety of Cu(II) chelates in DMF including Cu(II)(salen) and Cu(II)(salophen) (7). They used an aqueous SCE as a reference electrode; therefore, it is not possible to make a direct comparison of $E_{1/2}$ values. Their values of $E_{1/2}$ and slope are -1.21 V and 48 mV for Cu(II)(salen) and -1.11 V and 58 mV for Cu(II)(salophen), values which are consistent with the data in Table 6. For the complexes they investigated, these authors discussed the relative values of $E_{1/2}$ in terms of structural and electronic (primarily donor-atom) effects. Where donor atoms were the same, they concluded that ligands preferring a tetrahedral array would form Cu(II) complexes which had more positive reduction potentials than would those preferring a square-planar array. Cu(II)(salen) and Cu(II)(salophen) are not directly comparable, but the fact that Cu(II)(salpn) is easier to reduce than Cu(II)(salen) supports this idea.

The polarographic data for Cu(II)[$(PAA)_2$en] are in conflict with cyclic voltammetric data reported by Lintvedt (27). In DMF, he finds a two-electron wave at -0.61 V vs the SCE. The polarographic slope of 56.6 mV and I_d value of 1.51 found for this compound can only be interpreted as a one-electron reduction. Constant potential electrolysis of this compound at -1.2 V yields an n-value of 1.0 ± 0.1. Since the two copper atoms in Cu(II)$(PAA)_2$en

have such different ligand environments, the two metal centers would not be expected to reduce at the same potential. Linvedt later agreed that his results may be in error (28).

The first electrochemistry reported for $Cu(II)(DOBF_2)(ClO_4)$ (1) and $Cu(II)_2L(ClO_4)_2 \cdot 2H_2O$ (29) consisted of E^f values derived from quasi-reversible cyclic voltammograms; however, both of these systems are polarographically reversible. The reduction potential of $Cu(II)(DOBF_2)(ClO_4)$ is anodic relative to most of the couples in Table 6, probably due to the four unsaturated nitrogen donors. The first reduction of $Cu(II)_2L(ClO_4)_2 \cdot 2H_2O$ is ~0.5 V anodic of the $E_{\frac{1}{2}}$ found for $Cu(II)_2$(salpn) even though the donor atoms are nearly the same. This could be a structural effect, but is also certainly due in part to the difference in molecular charge.

None of the complexes found in Table 6 reduces in a two-electron step from Cu(II) to Cu(0), a process which occurs for unligated Cu(II) in most solvents other than CH_3CN. This implies that the chelating ligands involved provide at least kinetic stability for the Cu(I) state. Polarographic data for the reduction of $Cu(II)(ClO_4)_2 \cdot 6H_2O$ in DMF is provided in Table 6 to show that two-electron reductions are easily detected by this method. The slope of 35.1 mV is close to the theoretical value of 29 mV and I_d is larger than, although not twice as large as, any of the one-electron processes. The possibility exists that the reduction of Cu(II) to Cu(0) in DMF is not entirely reversible or else that

Cu(I) does enjoy a small region of stability. This in turn implies that the observed wave is the addition of two closely spaced waves. The complex Cu(II)(salen) also has a slope value that is significantly less than 58 mV. It is likely that the Cu(I) compounds derived from this complex will be unstable with respect to disproportionation, as has been found in similar cases (30).

As explained in the introduction to this chapter, the data in Table 6 are not intended to be an extensive list of Cu(II)/Cu(I) potentials, but rather demonstrate the usefulness of the polarographic method and provide a meaningful ordering of the formal reduction potentials of a variety of complexes. Because compounds such as Cu(II)(salen) and Cu(II)(salpn) are included, comparisons can be made to a larger list of Cu(II)/Cu(I) potentials compiled by Patterson and Holm (7).

The $E_{\frac{1}{2}}$ for the reduction of O_2 to O_2^- provides a cathodic limit for complexes that would be expected to have other than a simple electron transfer reaction with oxygen. Complexes with potentials less negative than -.774 V would not be able to reduce oxygen to superoxide ion, but the presence of proton donors makes several other pathways of oxygen reduction possible.

Although the potentials in Table 6 are referenced against the NHE, one cannot conclude that the copper complexes would reduce at these potentials in water. This fact alone, even assuming that the reference electrode correction is meaningful, makes comparison

with reduction potentials for copper proteins difficult. It is, of course, equally unlikely that the proteins would reduce at the same potentials in DMF as in water. This problem is discussed by Holm (31).

CO Binding Constants

When carbon monoxide instead of an inert gas is used for deaerating the DMF solutions, the $E_{1/2}$ values for some of the Cu(II) complexes shift anodically. These shifts indicate that CO is stabilizing Cu(I) relative to Cu(II) in these complexes. If CO were binding to both Cu(II) and Cu(I), information about the binding constants could only be obtained from potential shifts as a function of CO concentration. If, however, CO only binds to Cu(I) in a 1:1 fashion, (which has been shown to be the case for $Cu(DOBF_2)^{+,0}$ and $Cu_2L^{2+,+}$ (1,2,29)) values for the binding constant of CO to the Cu(I) complex can be obtained from a single shift at known CO concentration. The effect of ligand binding on redox potentials can often be derived from the Nernst equation (32), and the expression for the special case of a single CO binding only to Cu(I) is derived below:

Assuming that (33)

$$Cu(II)L^{n+} + e^- \underset{f}{\overset{E^f_{N_2}}{\rightleftharpoons}} Cu(I)L^{(n-1)+}$$

$$Cu(II)L^{n+} + CO + e^- \underset{}{\overset{E^f_{CO}}{\rightleftharpoons}} Cu(I)L(CO)^{(n-1)+}$$

$$Cu(I)L^{(n-1)+} + CO \underset{}{\overset{K_{CO}}{\rightleftharpoons}} Cu(I)L(CO)^{(n-1)+}$$

The Nernst equation under N_2 is

$$E = E^f_{N_2} - \frac{RT}{F} \ln \frac{[Cu(I)L^{(n-1)+}]}{[Cu(II)L^{n+}]}$$

If, under CO, all the Cu(I) exists as $Cu(I)L^{(n-1)+}$ or $Cu(I)L(CO)^{(n-1)+}$

$$[Cu(I)]_{tot} = [Cu(I)L^{(n-1)+}] + [Cu(I)L(CO)^{(n-1)+}] =$$

$$[Cu(I)L^{(n-1)+}] + K_{CO}[Cu(I)L^{(n-1)+}][CO]$$

Dividing through with $[Cu(I)L^{(n-1)+}]$ and solving for the same yields

$$[Cu(I)]_{tot}/[Cu(I)L^{(n-1)+}] = 1 + K_{CO}[CO]$$

$$[Cu(I)L^{(n-1)+}] = [Cu(I)]_{tot}/(1+K_{CO}[CO])$$

Substituting back into the Nernst equation

$$E_{CO} = E^f_{N_2} - \frac{RT}{F} \ln \frac{[Cu(I)]_{tot}}{[Cu(II)L^{n+}](1+K_{CO}[CO])}$$

$$E_{CO} = E^f_{N_2} - \frac{RT}{F} \ln \frac{[Cu(I)]_{tot}}{[Cu(II)L^{n+}]} - \frac{RT}{F} \ln \frac{1}{1+K_{CO}[CO]}$$

At $E_{CO} = E^f_{CO}$, $[Cu(II)L^{n+}] = [Cu(I)]_{tot}$ and the second term above equals zero.

Therefore

$$E^f_{CO} = E^f_{N_2} - \frac{RT}{F} \ln \frac{1}{1+K_{CO}[CO]}$$

$$E^f_{CO} - E^f_{N_2} = \frac{RT}{F} \ln (1+K_{CO}[CO]) \qquad 6$$

Notice in the derivation above that E^f_{CO} can be defined for any known CO concentration, and that if $E^f = E_{1/2}$, K_{CO} can readily be obtained from a single shift in $E_{1/2}$.

Equation 6 and the data in Table 6 allow calculation of CO binding constants for all of the Cu(I) complexes; these are presented in Table 7. This method provides an easy route to values of K_{CO} in that only one measurement is necessary and bulk synthesis of the Cu(I) complexes is not required. Furthermore, the method appears to be accurate in that the value of K_{CO} obtained for

Table 7

CO Binding Constants for Copper Complexes

Complex	Shift[a]	K_{CO}
Cu(II)(trans-diene)$(ClO_4)_2$	.003	~0
Cu(II)(TAAB)$(NO_3)_2$	.002	~0
Cu(II)(salen)	.064	2.4×10^3
Cu(II)(salophen)	.005	~0
Cu(II)(salpn)	.059	1.0×10^3
Cu(II)[$(PAA)_2$en]	.077	4.1×10^3
Cu(II)$(DOBF_2)(ClO_4)$	.153	8.4×10^4
$Cu(II)_2L(ClO_4)_2 \cdot 2H_2O$	.125	2.8×10^4

[a] $E_{1/2}(CO) - E_{1/2}(N_2)$ in volts

Cu(I)($DOBF_2$), 6.7×10^4 is close to the value obtained spectroscopically, 4.7×10^4 (1). Data obtained polarographically, however, should be used only as an indication of ability to bind CO until collaborative evidence for each complex is obtained. Such evidence might include synthesis of the Cu(I) complex and its carbonyl adduct, verification of reversible CO binding (for example, by electronic spectral changes), and proof that only Cu(I) is binding CO in a 1:1 fashion.

One other requirement for the confident use of Equation 6 is that the equilibrium described by K_{CO} is established rapidly on the experimental timescale. If this is not the case, the shifted waves will not be reversible. Indeed, when Cu(II)($DOBF_2$)(ClO_4) was originally examined by cyclic voltammetry (1), the waves recorded under CO were sqewed. Because polarography is a slower technique, however, reversible polarographic waves are obtained for this system. Notice in Table 6 that the slope values for all the complexes measured under CO are as close or closer to 58 mV as the values measured under N_2.

The reasons why CO binds only to certain four-coordinate, 18-electron Cu(I) atoms to form five-coordinate, 20-electron adducts is not yet fully understood (11,35). This question is currently being investigated by J. Allison (3), but it is clear that both electronic and structural factors are involved. Redox potential by itself cannot be used to predict CO binding. Complexes with relatively positive and negative E^f's, Cu(II)($COBF_2$)(ClO_4) and

Cu(salpn), bind CO while Cu(II)(TAAB)$(NO_3)_2$ and Cu(II)(salophen) do not. A well-defined ligand environment is not necessary for CO binding, as evidenced by the behavior of Cu(II)$(ClO_4)_2 \cdot 6H_2O$. Under N_2 this compound is reduced directly from Cu(II) to Cu(0), while under CO the Cu(I) state is stabilized and two one-electron waves result. Of course, the CO adduct in this case need not be five-coordinate.

Experimental

Electrochemical Cells and Accessories

Figures 3 and 4 contain drawings of the two types of cells used for all electrochemical experiments. Figure 5 contains drawings of four pieces of accessory equipment designed for use with the cells. The use and features of the cells and accessories are discussed below.

Figure 3 - Polarographic Cell

This cell had two compartments, separated by a medium sintered glass frit. The large compartment typically contained ~25 ml of solution while the smaller compartment contained ~10 ml. The large compartment housed the working and auxiliary electrodes and the smaller compartment housed the reference electrode. This cell was most often used for d.c. polarography but it was occasionally used for cyclic voltammetry, differential pulse voltammetry, etc. This cell was not used for constant potential electrolysis because, even if the auxiliary electrode was placed

Figure 3

Polarographic Cell

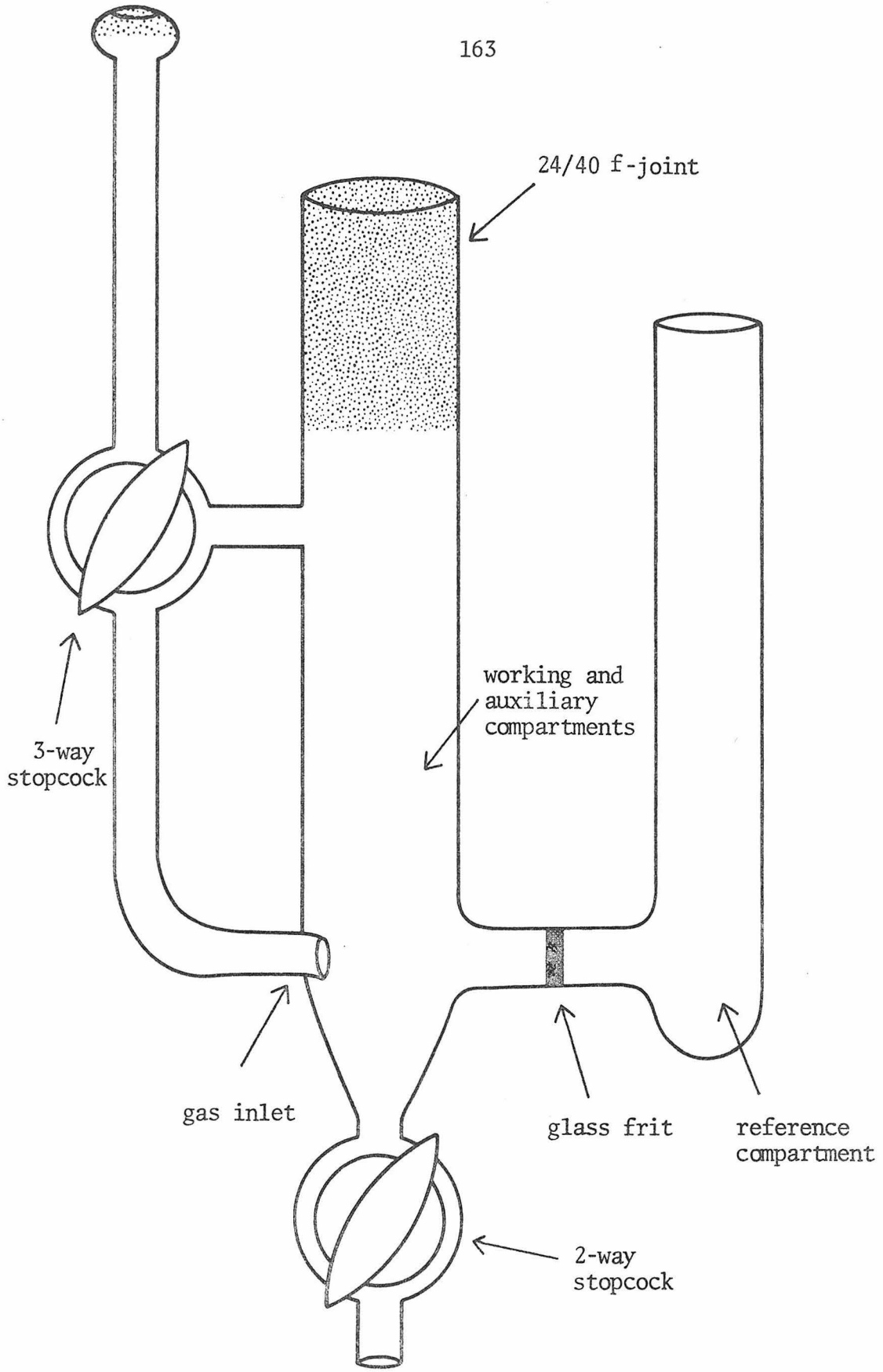
24/40 f-joint
working and
auxiliary
compartments
3-way
stopcock
gas inlet
glass frit
reference
compartment
2-way
stopcock

Figure 3

in the smaller compartment, some mixing of oxidation and reduction products occurred. The glass tubing and 3-way stopcock were used to deaerate the solution or to maintain an inert atmosphere above it. The two-way stopcock at the bottom of the cell was used to drain excess mercury or old solutions without disturbing the reference compartment.

Figure 4 - Electrolysis Cell

This cell had 3 compartments separated by medium sintered-glass frits. The larger end compartments typically contained ~25 ml of solution while the middle compartment contained ~10 ml. The end compartment, which is connected to the 3-way stopcock, contained the working electrode. The auxiliary electrode was housed in the other end compartment during electrolysis. The purpose of the middle compartment is to prevent mixing between the ends. In addition to being used for electrolysis, this cell was used for the same techniques as the polarographic cell. In these cases the auxiliary electrode was usually switched to the working compartment. The port in the middle compartment was normally used only for filling. (The reference electrode could have been placed in the middle compartment, but inevitably would have sensed a large portion of the ohmic drop between the working and auxiliary electrodes.) The reference electrode was normally positioned through the small port in the working compartment in order to be as close to the working electrode as possible.

Figure 4

Electrolysis Cell

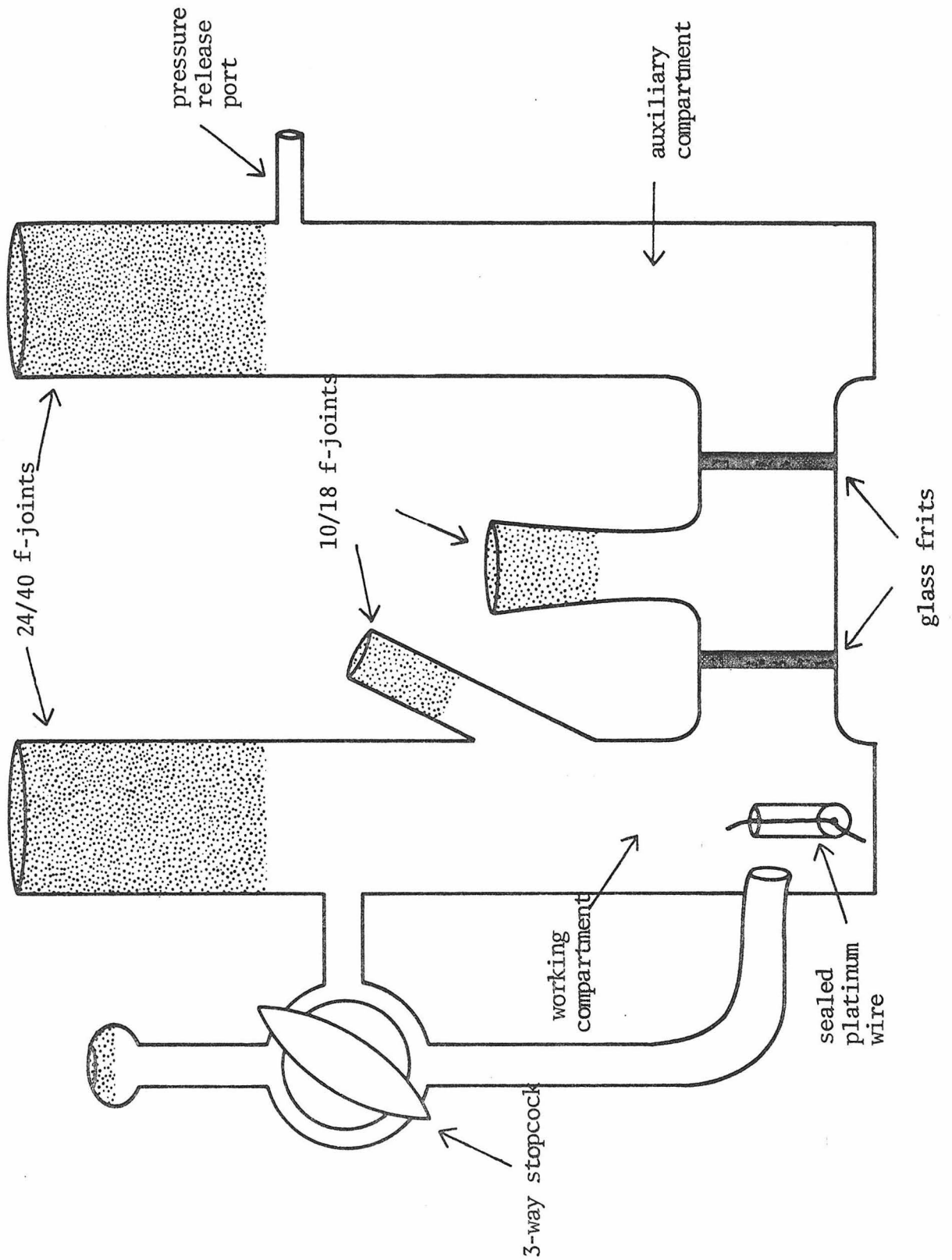
pressure release port
auxiliary compartment
24/40 f-joints
10/18 f-joints
glass frits
working compartment
sealed platimum wire
3-way stopcock

Figure 4

The working compartment also contained a sealed platinum wire at the bottom for connection to a mercury pool. The small horizontal port in the counter compartment is used to release pressure that results when a gas is formed at the counter electrode during electrolysis.

Figure 5 - Accessories

The working compartment adapter fitted into the large ports in the working compartments of the polarographic or electrolysis cells. The accompanying platinum wire served as the auxiliary electrode in all experiments other than electrolysis, and was positioned close to the working electrode. The female joint held either a standard HMDE or the platinum working electrode described below, or allowed insertion of a capillary for polarography. The port ending in a balljiont allowed deaeration gas to escape.

The platinum working electrode was made to fit into the working compartment adaptor and extend down into the working compartment to the level of the frits. The end that contains the platinum-glass seal was polished to a mirror finish with a series of abrasives ending with 0.3 micron alumina (Linde).

The Ag/Ag^{+} reference electrode consisted of a glass tube closed at one end with a fine frit. It was partially filled with solution ($AgNO_3$(0.01 M), TBAP (0.1 M), CH_3CN) into which a silver wire was immersed. Leakage was minimized by closing the open end with a serum cap. This electrode fitted through a

Figure 5

Accessories

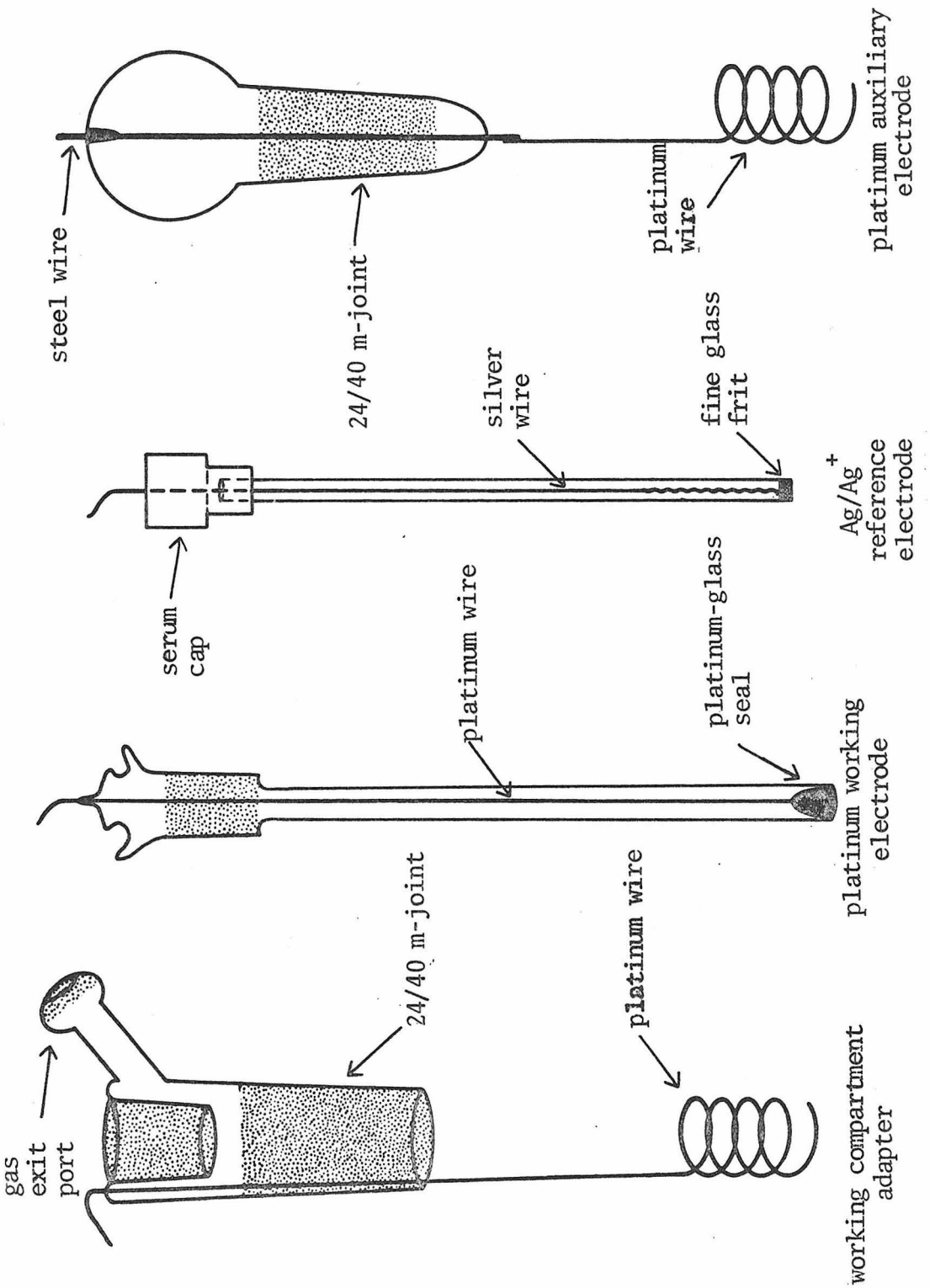
steel wire
24/40 m-joint
platinum wire
platinum auxiliary electrode
silver wire
fine glass frit
Ag/Ag+ reference electrode
serum cap
platinum wire
platinum-glass seal
platinum working electrode
24/40 m-joint
platinum wire
gas exit port
working compartment adapter

Figure 5

thermometer adapter which was placed in the ₹ 10/18 female joint in the working compartment of the electrolysis cell. A stopper or serum cap was used to adapt this electrode to the reference compartment of the polarographic cell.

The platinum auxiliary electrode was designed for use with the electrolysis cell. A platinum wire piercing a large serum cap was occasionally used in its place.

Instrumentation

The apparatus used for constant potential electrolysis and cyclic voltammetry consisted of a Princeton Applied Research Model 173 Potentiostat-Galvanostat coupled with a Model 179 Digital Coulometer, plus a homemade voltage ramp generator. A storage oscilloscope was used for display. A PAR Model 174A Polarographic Analyzer was used for d.c. polarography and differential pulse voltammetry, with a Hewlett-Packard 7004B X-Y recorder for display.

Materials

Spectroquality Acetonitrile (Mathesson, Coleman and Bell) and $AgNO_3$ (Baker and Adamson) were used as received. Tetrabutylammonium perchlorate, TBAP, (Southwestern Analytical Chemicals, Inc.) was dried extensively under an active vacuum prior to use. Bis(pentahaptocyclopentadienyl)iron(II), $Fe(Cp)_2$, (Aldrich) was recrystallized from benzene and gave satisfactory microanalysis. Tris(acelylacetonate)Ru(III), $Ru(acac)_3$ was recrystallized from toluene and petroleum ether and gave satisfactory microanalysis.

N,N-dimethylformamide, DMF (Mathesson, Coleman and Bell) was dried by stirring with $MgSO_4$, $CuSO_4$, and 4A molecular sieves for more than 48 hours prior to distillation at reduced pressure.

Sources of Copper Complexes

The complex, $Cu(II)_2L(ClO_4)_2 \cdot 2H_2O$, was synthesized by a procedure similar to one reported by Robson et al. (36). The exact details are included in Section II-C.

The complexes, $Cu(II)(TAAB)(NO_3)_2$, $Cu(II)(trans\text{-}diene)(ClO_4)_2$, and $Cu(II)(DOBF_2)(ClO_4)$, were synthesized by J. Allison using the literature preparations of Busch et al. (37), Olson and Vasilevskis (25), and Gagné et al. (1), respectively.

The complex, $Cu(II)_2[(PAA)_2en]$, was synthesized by R. Kreh using the method of Linvedt et al. (27).

The complexes, Cu(II)(salen), Cu(II)(salophen) and Cu(II)(salpn), were prepared by E. Kober using the methods of Pfeiffer (38), O'Connor (39), and Lions (40), respectively.

The complex, $Cu(II)(ClO_4)_2 \cdot 6H_2O$ (Research Chemical Corp.), was ground with a mortar and pestal and dried exhaustively under an active vacuum prior to use.

All of the above compounds were analyzed at the Caltech analytical facility and gave satisfactory elemental analyses.

Reference Electrode

All potentials are reported versus the normal hydrogen electrode, NHE. Although the $Ag/AgNO_3$ (0.01 M), TBAP (0.1 M),

CH_3CN electrode (41) was used as the reference electrode in the potentiostatic circuit, potentials were evaluated by recording a differential pulse voltammogram of the oxidation of $Fe(Cp)_2$, a small amount ($\sim 10^{-5}$ M) of which was added to each solution. The $Fe(Cp)_2/Fe(Cp)_2^+$ couple was used as a solvent-independent reference couple, SIRC. Potentials could then be related to the NHE by use of the following formula (10):

$$E_{OR,s} - E_{NHE,w} = (E_{O/R,s} - E_{SIRC,s}) - E_{NHE,w} - E_{SIRC,w})$$

$E_{O/R,s}$ = potential of couple of interest in solvent, s.

$E_{NHE,w}$ = potential of NHE in water.

$E_{SIRC,s}$ = potential of the SIRC in solvent, s.

$E_{SIRC,w}$ = potential of the SIRC in water.

By definition $E_{NHE,w}$ equals 0 and $E_{SIRC,w}$ has been shown to equal +.400 (42). The formula then simplifies to:

$$E_{O/R,s} \text{ versus s.h.e.} = (E_{O/R,s} - E_{Fe(Cp)_2,s}) + .400$$

It is also possible to correct potentials measured against the Ag/Ag^+ reference electrode or SCE to the NHE by using the published potential differences between the Ag/Ag^+ electrode and the SCE,

0.291 V (43), and the SCE and the NHE, 0.245 V (44). The problem with this method is that unknown junction potentials are inevitably included. While the validity of using $Fe(Cp)_2$ to correct potentials to the NHE has been challenged (45), this method of reporting potentials is certainly more reproducible.

References

1. R. R. Gagné, J. L. Allison, R. S. Gall, and C. A. Koval, J. Am. Chem. Soc. 99, 9170 (1977).
2. R. R. Gagné, C. A. Koval and T. J. Smith, manuscript in preparation, Section II-C of this thesis.
3. J. L. Allison, Ph.D. Thesis, California Institute of Technology, Pasadena, California, in preparation.
4. R. R. Gagné and C. Spiro, manuscript in preparation.
5. R. R. Gagné and R. Kreh, manuscript in preparation.
6. To date attempts to characterize the products of Cu(I) + O_2 reactions have been largely unsuccessful.
7. G. S. Patterson and R. H. Holm, Bioinorg. Chem. 4, 257 (1975).
8. J. J. Lingane, "Electroanalytical Chemistry," Interscience Publishers, Inc. N.Y. (1958) pp. 36-67.
9. H. A. Laitinen, "Chemical Analysis," McGraw-Hill Book Company, Inc. N.Y. (1960) pp. 277-283.
10. D. Bauer and M. Breant, "Electroanalytical Chemistry," Vol. 8, Marcel Dekker, Inc. N.Y. (1975) pp. 282-344.
11. Throughout this chapter only the first reduction of this complex is discussed. For a complete discussion of the electrochemistry of this compound see Section II-C.
12. R. S. Nicholson and I. Shain, Anal. Chem. 36, 706 (1964).

13. The diffusion coefficients of the oxidized and reduced species are assumed to be equal.

14. Assuming that the switching potential is at least several hundred millivolts cathodic of E^f.

15. R. N. Adams, "Electrochemistry at Solid Electrodes," Marcel Dekker, Inc. N.Y. (1969) pp. 144,145.

16. A. Weissberger and B. W. Rossiter, "Physical Methods of Chemistry," Part IIA, John Wiley and Sons, Inc. N.Y. (1971) p. 441.

17. R. S. Nicholson, Anal. Chem. 37, 1351 (1965).

18. R. A. Marcus, J. Phys. Chem. 67, 853 (1963); J. Chem Phys. 43, 679 (1965).

19. R. S. Nicholson, Anal. Chem. 37, 667, 1351 (1965).

20. Reference 16, p. 439.

21. E. P. Parry and R. A. Osteryoung, Anal. Chem. 37, 1634 (1965).

22. The value of E^f obtained for $Fe(Cp)_2$ using DPV is arbitrarily assigned a value of +.400 V, because all other experiments were calculated using this technique.

23. C. A. Koval and F. C. Anson, Anal. Chem. 50, 223 (1978).

24. Reference 16, p. 357.

25. D. C. Olson and J. Vasilevskis, Inorg. Chem. 10, 463 (1971).

26. N. Takuoryan, K. Farmery, V. Katovic, F. Lovecchio, E. Gore, L. Anderson, and D. H. Busch, J. Am. Chem. Soc. 96, 731 (1974).

27. R. L. Linvedt, B. Tomlonovic, D. E. Fenton, and M. D. Glich, Adv. Chem. Ser. #150, Chapt. 32, 405 (1975).

28. R. L. Linvedt, private communication.

29. R. R. Gagné, C. A. Koval, and T. J. Smith, J. Am. Chem. Soc. 99, 8367 (1977).

30. C. A. Koval and R. S. Gall, unpublished results.

31. C. L. Hill, J. Renaud, R. H. Holm, and L. E. Mortenson, J. Am. Chem. Soc. 99, 2549 (1977).

32. Reference 9, pp.285-291.

33. This derivation also assumes that [CO] > $[Cu(I)]_{tot}$ so that the [CO] remains constant at any potential. Since [CO] in DMF at 20° C is 4.6×10^{-3} (34) and polarographic concentrations were 0.5×10^{-3}, this assumption was not strictly valid.

34. "Properties and Uses of Dimethylformamide," E. I. DuPont DeNemours and Com., Inc., Industrial Chemicals Department, Wilmington, DE.

35. R. R. Gagné, J. L. Allison, G. S. Luzenski, to be published in J. Am. Chem. Soc.

36. N. H. Pilkington and R. Robson, Aust. J. Chem. 23, 2225 (1970).

37. G. A. Melson and D. H. Busch, J. Am. Chem. Soc. 86, 4834 (1964).

38. P. Pfeiffer, E. Breith, E. Lübbe, and T. Tsumaki, Ann. Chim. 503, 84 (1933).

39. M. J. O'Connor, R. E. Ernst, and R. H. Holm, J. Am. Chem. Soc. 90, 4561 (1968).

40. F. Lions and K. V. Martin, J. Am. Chem. Soc. 79, 1273 (1957).

41. V. A. Pleskov, Zh. Fiz. Khim. 22, 351 (1948).

42. H. M. Koepp, H. Wendt and H. Strehlow, Z. Electrochem. 64, 483 (1960).

43. R. C. Larson, R. T. Iwamoto, and R. N. Adams, Anal. Chim. Acta 25, 371 (1960).

44. H. H. Willard, L. L. Merritt, and J. Dean, "Instrumental Methods of Analysis," Van Nostrand Reinhold Company, N.Y. (1948) p. 537.

45. J. W. Piggle and A. J. Parker, Electrochim. Acta 18, 975 (1973).

SECTION II-B

Binuclear Complexes of Macrocyclic Ligands. A Mixed-Valence Copper(II)-Copper(I) Complex which Exhibits Unusual Temperature-Dependent Behavior

Robert R. Gagné, Carl A. Koval, and Thomas J. Smith

Contribution No. 5595 from the Division of Chemistry and Chemical Engineering, California Institute of Technology, Pasadena, California 91125

(Received May 27, 1977)

Abstract: The binuclear Cu(II) complex resulting from the condensation of 5-methyl-2-hydroxyisophthaldehyde with 1,3-diaminopropane in the presence of $Cu(ClO_4)_2 \cdot 6H_2O$ undergoes two successive one-electron reductions. The mixed-valence complex, $Cu(II)Cu(I)L(ClO_4)$, 1, and the corresponding carbonyl derivative, $Cu(II)Cu(I)L(CO)(ClO_4)$, 2, have been isolated. Complex 1 showed an intervalence-transfer transition (IT) in the near infrared region which is apparently dependent on solvent donor properties (1200 nm in CH_2Cl_2). Seven line epr spectra were seen at 25° but only four lines were observed in frozen solutions. This unusual temperature dependent behavior may be due to axial ligation or macrocyclic-ligand conformational changes which lead to a "locked-in" configuration on the epr timescale.

The carbonyl adduct, 2, showed no apparent IT bands and only four lines in the epr at 25° or in frozen solutions. This complex, 2, apparently contains a five-coordinate Cu(I) carbonyl adduct, an unusual coordination number for Cu(I), and a novel "twenty electron" transition metal carbonyl.

Sir:

Macrocyclic ligands can provide transition metals with unusual ligand environments and consequent novel chemical properties: high and low oxidation states are often stabilized;[1] ligand lability is lessened by the chelating effect;[2] several metal atoms may be held in close steric proximity within the same molecule.[3] Capitalizing on these properties of macrocyclic ligands we are studying the behavior of binuclear copper complexes as models for copper-containing proteins.[4] Herein we report preliminary observations on two mixed-valence, Cu(II)Cu(I), macrocyclic-ligand complexes, one of which exhibited unusual temperature-dependent behavior.

Condensation of 5-methyl-2-hydroxyisophthaldehyde with 1,3-diaminopropane in the presence of $Cu(ClO_4)_2 \cdot 6H_2O$ yielded the binuclear Cu(II) complex, Cu(II)Cu(II)L, 1.[5,6]

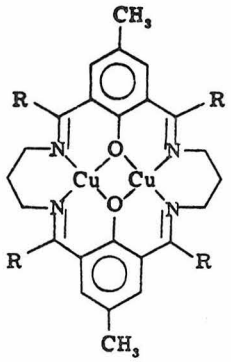

1, Cu(II)Cu(II), n = 2, R = H

2, Cu(II)Cu(I), n , 2, R = H

3, Cu(II)Cu(I)(CO), n = 1, R = H

4, Cu(II)Cu(I), n = 1, R = CH_3

We have been unsuccessful in reducing the complex with chemical reducing agents. Cyclic voltammetry in DMF,[7] however, revealed two quasireversible reduction waves ($E_1^f \simeq -0.52$ V, $E_2^f \simeq -0.91$ V, $n_1 = n_2 = 1.0 \pm 0.1$) by cpe.[8] Electrolysis of green solutions of 1 (-0.7 V, CH_3CN/N_2, $n = 1.0 \pm 0.1$ resulted in a dark brown solution. A nearly black solid, corresponding to the formula Cu(II)Cu(I)L(ClO_4), 2,[6] was precipitated from solution by addition of Et_2O. Saturation of the electrolysis solution with CO followed by addition of Et_2O led to precipitation of a CO adduct, Cu(II)Cu(I)L(CO)ClO_4, 3,[6,10] (ν_{CO} = 2065 cm^{-1}), presumably containing five-coordinate Cu(I).

Representative electronic absorption spectra of 1, 2, and 3 are shown in Figure 1. All three complexes exhibited intense absorptions in the 350-400 nm region (ε = 10-15,000, presumably ligand absorption) and a weaker band at about 600 nm. Since only the 350-400 nm band was observed in zinc complex, Zn(II)Zn(II)L(ClO_4)$_2$(H_2O)$_2$,[6] we tentatively assign the 600 nm absorptions in 1, 3 and 2 (in part) to a ligand field Cu(II) transition.[12] Most notable in the spectra was a broad band in the near infrared seen only for 2. We tentatively assign this as an

Figure 1

Electronic absorption spectra in methanol of $Cu(II)_2L(ClO_4)_2(H_2O)_2$, 1 (——); $Cu(II)Cu(I)LClO_4$, 2 (····) under helium; $Cu(II)Cu(I)(CO)LClO_4$, 3 (– – –) under carbon monoxide. $[Cu(II)_2] = 1.15 \times 10^{-3}$ M; $[Cu(II)Cu(I)] = [Cu(II)Cu(I)(CO)] = 1.10 \times 10^{-3}$ M.

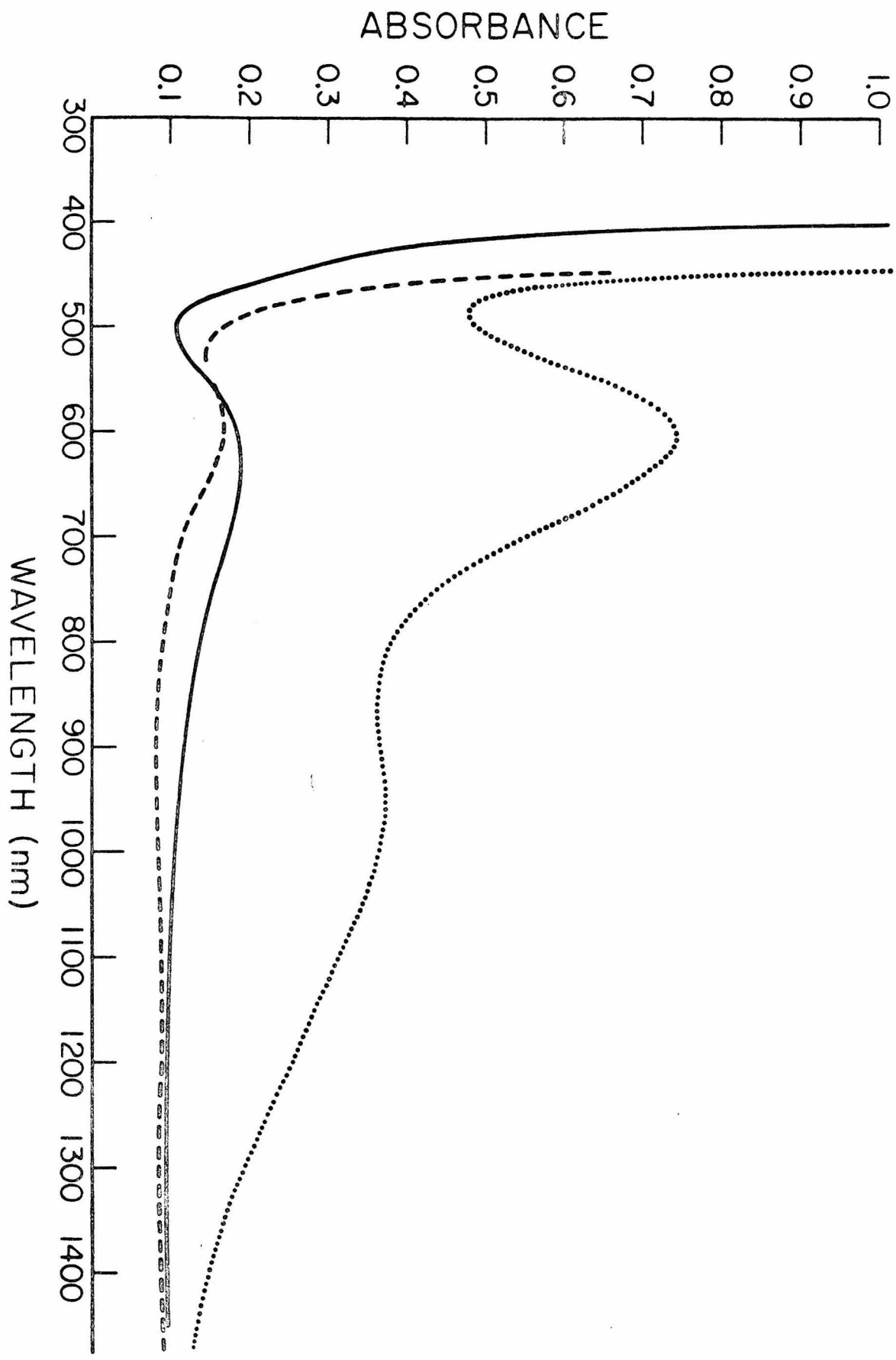
ABSORBANCE
0.1
0.2
0.3
0.4
0.5
0.6
0.7
0.8
0.9
1.0
WAVELENGTH (nm)
300
400
500
600
700
800
900
1000
1100
1200
1300
1400

— Figure 1

intervalence-transfer transition (IT) [Cu(II)Cu(I) → Cu(I)Cu(II)*].[13] The position of the IT band maximum appeared to be dependent on the solvent donor properties. In non-coordinating CH_2Cl_2 the band was at ~1200 nm ($\varepsilon \simeq 80$) while in weakly coordinating CH_3OH, $(CH_3)_2CO$ and CMF the band shifted to ~900 nm. In CH_3CN, which appears capable of forming five-coordinate Cu(I) adducts,[9,10,11] no IT band was observed.

The addition of CO to Cu(II)Cu(I)L, 2, to give the carbonyl adduct, Cu(II)Cu(I)L(CO), 3, was essentially complete (in CH_3OH, $(CH_3)_2CO$, DMF, CH_3CN, CH_2Cl_2) as monitored by electronic absorption spectroscopy and cyclic voltammetry.[14] For example, addition of CO to bluish-green solutions of 2 (CH_3OH) led to yellow solutions with the electronic spectra of 3 (Figure 1). The lack of an observable IT band for 3 appears consistent with the spectra of 2 in donor solvents, i.e., CO adduct formation may shift the IT band to high energies where it is masked by ligand absorption.

Solution epr spectra for Cu(II)Cu(I)L, 2, (Figure 2), consisted of seven lines, consistent with interaction of the odd electron with both Cu centers (I = 3/2). Internally consistent hyperfine splittings in both solvents imply the presence of only a single epr active species. In contrast frozen solutions at

Figure 2

Solution epr spectra (25°) of Cu(II)Cu(I)L(ClO_4), 2, in CH_2Cl_2 (top) and CH_3CN (bottom).

Figure 2

liquid-nitrogen temperature exhibited four-line anisotropic spectra (CH_2Cl_2 or CH_3CN).[15] Similarly, addition of CO to solutions of 2 resulted in a solution of 3 (by electronic spectra) and an epr spectrum having only four lines (25°, CH_2Cl_2). These four-line spectra, whether from frozen solutions of 2 or solutions of 3 at 25°, are consistent with localization of the odd electron on a single copper center, at least on the relatively slow epr timescale (10^{-8} - 10^{-4} sec).[16]

Possible explanations for the temperature-dependent behavior of 2 include: 1) axial ligation by ClO_4^- or solvent (CH_3CN or CH_2Cl_2) at low temperature leads to an asymmetric complex comparable to the carbonyl adduct, 3, or 2) macrocyclic-ligand conformational changes which accompany electron exchange (possible distorted tetrahedral for Cu(I) to distorted square planar for Cu(II)) become more difficult in frozen solutions resulting in a "locked-in" configuration on the epr timescale.[16] The latter explanation is especially attractive for CH_2Cl_2 solutions of 2 in which, presumably, only ClO_4^- and CH_2Cl_2 are available for axial ligation.

These epr results are in contrast to those recently reported by Addison on a similar macrocyclic Cu(II)Cu(I) complex, 4, (R = CH_3) which exhibits four-line epr

spectra even at room temperature in CH_3CN.[17] In this case methyl substitution probably alters the conformational properties of the macrocycle sufficiently to inhibit thermal electron transfer on the epr time scale at temperatures where it occurs with 2.

It should be noted that several Co(III)Co(II) complexes of this macrocycle (R = H) have been prepared and characterized crystallographically although their mixed valence spectral properties were not discussed.[18]

Five coordination for Cu(I) is most unusual. That 2 exhibited an IT band is good evidence for the presence of Cu(I), as opposed to a Cu(II) radical anion. Since the Cu(II)Cu(II)L, complex, 1, does not react with CO, then the CO adduct, Cu(II)Cu(I)L(CO), 3, if five-coordinate as is expected, must also be regarded as containing Cu(I) with a most unusual coordination number.

Acknowledgments. We appreciate assistance by M. Cimolino and R. Richmond. This work was generously supported by the National Institutes of Health, the National Science Foundation, and the Energy Research and Development Administration.

References and Notes

(1) D. C. Olson and J. Vasilevskis, Inorg. Chem., 10, 464, (1971).

(2) J. E. Huheey, "Inorganic Chemistry," Harper and Row, N.Y. (1972), p. 418-423.

(3) For example, see: R. L. Lintvedt, B. Tomlonovic, D. E. Fenton, and M. D. Glick, Adv. Chem. Series, 150, 407 (1975).

(4) Hemocyanin, tyrosinase and laccase all contain a type III, binuclear Cu site.

(5) N. H. Pilkington and R. Robson, Aust. J. Chem., 23, 2225 (1970).

(6) All compounds discussed gave satisfactory elemental analyses.

(7) Abbreviations: DMF, N,N-dimethylformamide; cpe, constant potential electrolysis; Et_2O, diethylether.

(8) Platinum indicating electrodes; 0.1 M in tetrabutylammonium perchlorate; $E^f = (E_{p_a} + E_{p_c})/2$, given vs. s.h.e. as explained in Ref. 9. Full details of the electrochemical properties of these complexes will be forthcoming.

(9) R. R. Gagné, J. L. Allison, R. S. Gall, and C. A. Koval, submitted to the J. Am. Chem. Soc.

(10) We have recently reported five-coordinate Cu(I) species derived from a Cu(I)-macrocyclic ligand complex.[11] Crystallographic analysis[9] of the carbonyl derivative shows Cu to be in a square-pyramidal configuration. We presume that complex 3 contains a similar square-pyramidyl, five-coordinate Cu(I) carbonyl.

(11) R. R. Gagné, J. Am. Chem. Soc., 98, 6709 (1976).

(12) We are at present unable to account for the greater intensity of the 600 nm band in 2.

(13) (a) M. B. Robin and P. Day, Advan. Inorg. Chem. Radiochem., 10, 247 (1967); (b) G. C. Allen and N. S. Hush, Prog. Inorg. Chem., 8, 357 (1967); (c) N. S. Hush, ibid., 8, 391 (1967).

(14) Postive shifts in E^f in the presence of CO permitted an estimation for K_c of 1.1×10^4 M^{-1}. See Ref. 9.

(15) We have not yet obtained solution electronic absorption spectra at low temperatures.

(16) E. L. Muetterties, Inorg. Chem., 4, 769 (1965).

(17) A. W. Addison, Inorg. Nucl. Chem. Lett., 12, 899 (1976).

(18) B. F. Hoskins, R. Robson, and G. A. Williams, Inorg. Chim. Acta, 16, 121 (1976).

Section II-C

Properties of a Binuclear Copper Complex in Cu(II)Cu(II), Cu(II)Cu(I), and Cu(I)Cu(I) States. Synthesis and Characterization Including Electrochemistry, CO Binding, and Measurement of an Intramolecular Electron Transfer Rate by EPR.

Robert R. Gagné, Carl A. Koval, and Thomas J. Smith

Introduction

Studies of polynuclear transition metal complexes promise to impact on bonding, magnetic interaction and electron transfer theories, on catalysis, and on defining the role of multi-metal sites in proteins. Unfortunately investigation of fundamental properties is often thwarted by instabilities in coordination environment which occur upon oxidation state change. For example, Co(III) complexes, relatively substitution inert, can be readily studied in solution but reduction to labile Co(II) may result in ligand substitution. Macrocyclic ligands and other chelates can help to control lability while stabilizing a variety of oxidation states. Recently, creative syntheses have produced a host of remarkably stable binuclear complexes, many containing otherwise labile first-row transition metal ions, derived from polydentate ligands.[1]

In this paper we report the synthesis and characterization of the Cu(II)Cu(I) and Cu(I)Cu(I) derivatives which are formed upon reduction of a previously reported Cu(II)Cu(II) macrocyclic ligand complex. The mixed valence ion, $Cu(II)Cu(I)L^{+}$, exhibits an unusual electronic absorption spectrum and temperature dependent EPR spectra which permit a reasonable estimate of the intramolecular electron transfer rate. Properties of the mixed valence

ion, $Cu(II)Cu(I)L^{+}$, will be compared to those of other well characterized mixed valence species.

A drawing of the parent Cu(II)Cu(II) complex and the derivatives reported herein, along with the nomenclature used throughout this paper, is presented in Figure 1. A preliminary account of this work has already appeared.[5]

Results

Electrochemistry and Synthesis. The binuclear complex, $Cu(II)Cu(II)L(ClO_4)_2 \cdot 2H_2O$, was prepared by condensing 1,3-diaminopropane with 5-methyl-2-hydroxyisophthalaldehyde and $Cu(ClO_4)_2 \cdot 6H_2O$ according to the method of Pilkington and Robson.[2] Under an inert atmosphere, $Cu(II)Cu(II)L^{2+}$ can be reduced electrochemically to $Cu(II)Cu(I)L^{+}$ and Cu(I)Cu(I)L in separate one-electron processes. If a CO atmosphere is used, $Cu(II)Cu(II)L^{2+}$ can be reduced stepwise to $Cu(II)Cu(I)L(CO)^{+}$ and $Cu(I)Cu(I)L(CO)_2$. These processes are outlined in the following scheme:

Scheme

$$Cu(II)Cu(II)L^{2+} + e^{-} \underset{}{\overset{E_1}{\rightleftharpoons}} Cu(II)Cu(I)L^{+} \qquad f^{6}$$

Figure 1

Schematic drawing and nomenclature of the binuclear complexes studied.

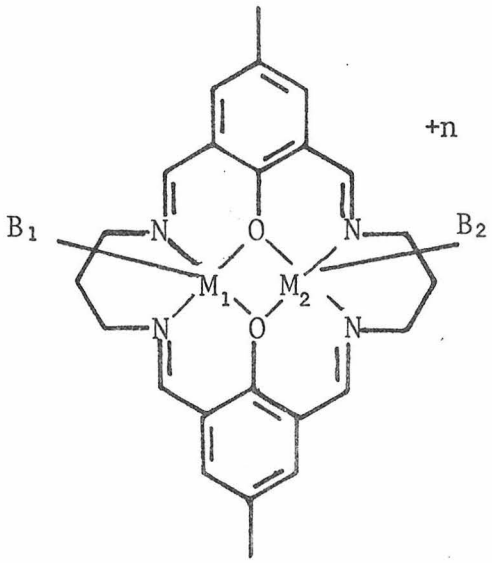

Cpd	M_1	M_2	n	B_1	B_2
$Cu(II)Cu(II)L(ClO_4)_2 \cdot 2H_2O$	Cu(II)	Cu(II)	2	--	--
$Cu(II)Cu(I)L(ClO_4)$	Cu(II)	Cu(I)	1	--	--
$Cu(II)Cu(I)L(CO)ClO_4$	Cu(II)	Cu(I)	1	--	CO
Cu(I)Cu(I)L	Cu(I)	Cu(I)	0	--	--
Cu(I)Cu(I)L(CO)	Cu(I)	Cu(I)	0	CO	CO
$Zn(II)Zn(II)L(ClO_4)_2 \cdot 2H_2O$	Zn(II)	Zn(II)	2	--	--

Figure 1

$$Cu(II)Cu(II)L^{2+} + e^- + CO \overset{E_1{}^f(CO)}{\rightleftharpoons} Cu(II)Cu(I)L(CO)^+$$

$$Cu(II)Cu(I)L^+ + e^- \overset{E_2{}^f}{\rightleftharpoons} Cu(I)Cu(I)L$$

$$Cu(II)Cu(I)(CO)L^+ + e^- + CO \overset{E_2{}^f(CO)}{\rightleftharpoons} Cu(I)Cu(I)L(CO)_2$$

The above processes are all reversible or quasi-reversible. The observed electrochemistry is, however, often complicated by the very low solubility of Cu(I)Cu(I)L. The top of Figure 2 contains cyclic voltammograms of $Cu(II)Cu(II)L^{2+}$ in CH_3CN under N_2 at a platinum electrode. Two reduction processes are evident, occurring at approximately -0.40 and -0.95 V. If the potential scan is reversed at -0.75 V, the wave at -0.40 V is quasi-reversible. The wave at ~-0.95 V does not have the characteristic shape of a diffusion-controlled process. The oxidation waves associated with this reduction, located at ~-0.65 and -0.42 V, are also misshapen. There is little difference between voltammograms recorded using a HMDE[6] or a platinum electrode except in the shape of the two distorted oxidation waves. The compound $Cu(II)Cu(II)L^{2+}$ is not highly soluble in CH_2Cl_2, CH_3OH, or acetone containing 0.1 M TBAP.[6] Nevertheless, cyclic voltammograms of saturated solutions of $Cu(II)Cu(II)L^{2+}$

Figure 2

Cyclic voltammograms of Cu(II)Cu(II)L^{2+} (~ 1 mM) under an inert atmosphere. Top: In CH_3CN; scan rate of 1 V/sec. Bottom: In DMF; scan rate of 3 V/sec.

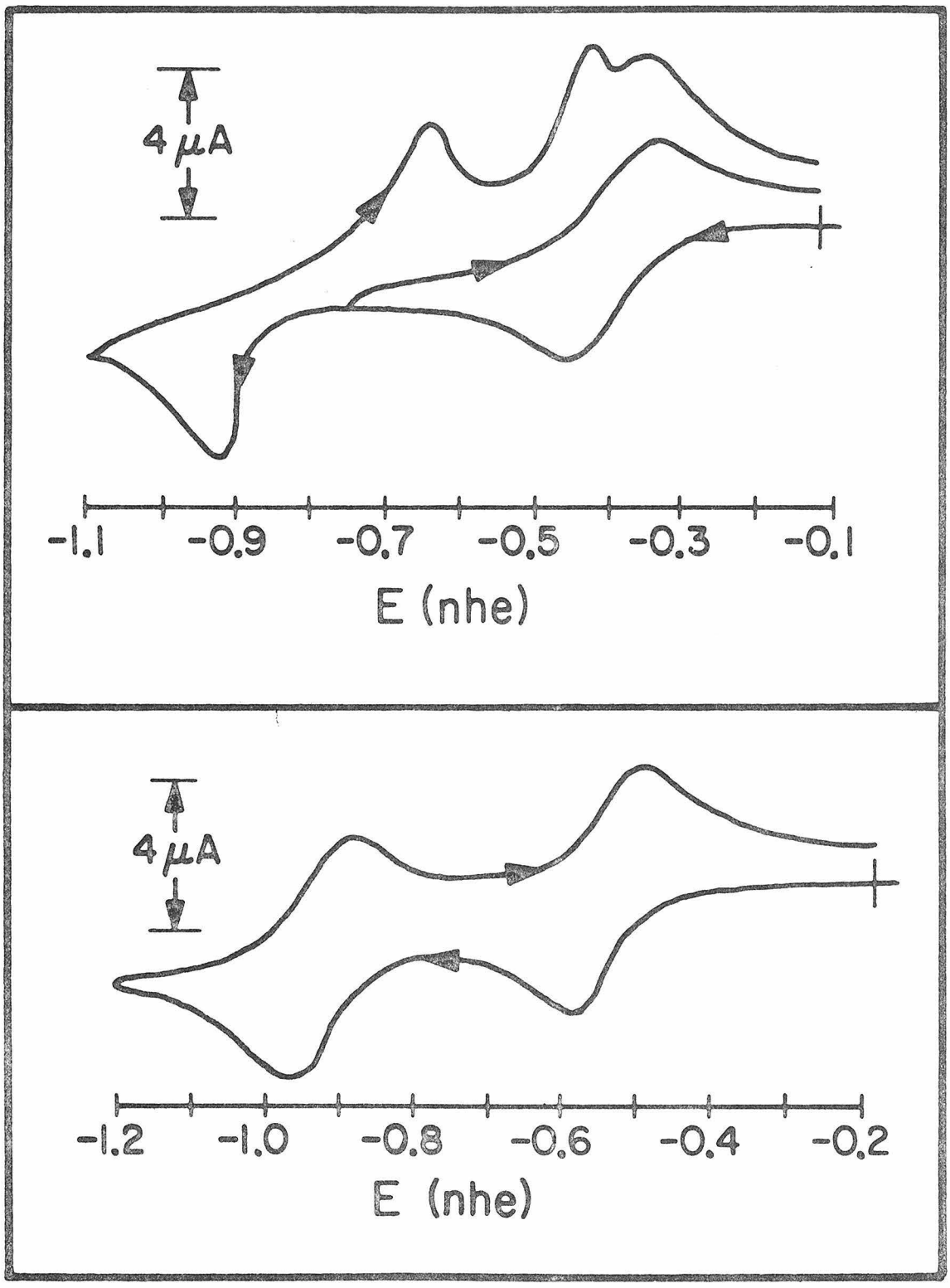

Figure 2

in these solvents resemble those shown in the top of Figure 2.

The compound Cu(I)Cu(I)L is essentially insoluble in CH_3CN, CH_2Cl_2 and CH_3OH, and it is this insolubility which is responsible for the irreversibility of the reduction of $Cu(II)Cu(I)L^+$ to Cu(I)Cu(I)L. This compound is slightly soluble in DMF[6] and a cyclic voltammogram of $Cu(II)Cu(II)L^{2+}$ in this solvent is shown in the bottom of Figure 2. Both reductions are now quasi-reversible, at least at moderately fast scan rates. At slower scan rates (0.1 V/sec), cyclics in DMF begin to resemble the top of Figure 2. Under a CO atmosphere, cyclic voltammograms of $Cu(II)Cu(II)L^{2+}$ in any solvent are similar to the one in the bottom of Figure 1. This is because the CO adduct of Cu(I)Cu(I)L, $Cu(I)Cu(I)L(CO)_2$ is appreciably soluble.

Due, at least in part, to uncompensated solution resistance, the peak separations for the various quasi-reversible cyclic voltammograms of $Cu(II)Cu(II)L^{2+}$ were no smaller than 70 mV and the separations increased with increasing scan rate. For this reason cyclic voltammetry was not used to evaluate formal reduction potentials. Nevertheless, values of E^f calculated using the formula $E^f = (E_{p_a} + E_{p_c})/2$ were close to those obtained using other techniques.

The n-values for the four processes shown in the scheme were found to be 1.0 ± 0.1 by constant potential electrolysis in DMF and CH_3CN. Millimolar solutions could be repeatedly reduced and reoxidized without loss of material. As expected, when Cu(I)Cu(I)L was created as an electrolysis product it was nearly insoluble, forming a precipitate at a Hg pool and coating a Pt gauze electrode with a shiny black film. Constant potential electrolysis of more concentrated solutions of $Cu(II)Cu(II)L^{2+}$ was the basis for the synthesis of $Cu(II)Cu(I)L(ClO_4)$, $Cu(II)Cu(I)L(CO)ClO_4$, and Cu(I)Cu(I)L. The procedures, which are detailed in the Experimental Section, are outlined in Figure 3. Stoichiometries for the addition of CO to $Cu(II)Cu(I)L(ClO_4)$ and Cu(I)Cu(I)L were determined by adding weighed quantities of these compounds to DMF and recording the subsequent uptake of CO. As indicated in Figure 3, $Cu(II)Cu(I)L(ClO_4)$ adsorbed 1.0 ± 0.05 moles of CO per mole of complex and the uptake for Cu(I)Cu(I)L was 2.0 ± 0.1. The compounds $Cu(II)Cu(I)L(ClO_4)$ and Cu(I)Cu(I)L could be prepared as crystalline materials, while $Cu(II)Cu(I)L(CO)ClO_4$ formed a microcrystalline powder. The dicarbonyl complex, $Cu(I)Cu(I)L(CO)_2$, was not isolated from solution.

Figure 3

Synthesis of the reduced forms of $Cu(II)Cu(II)L(ClO_4)_2 \cdot 2H_2O$.

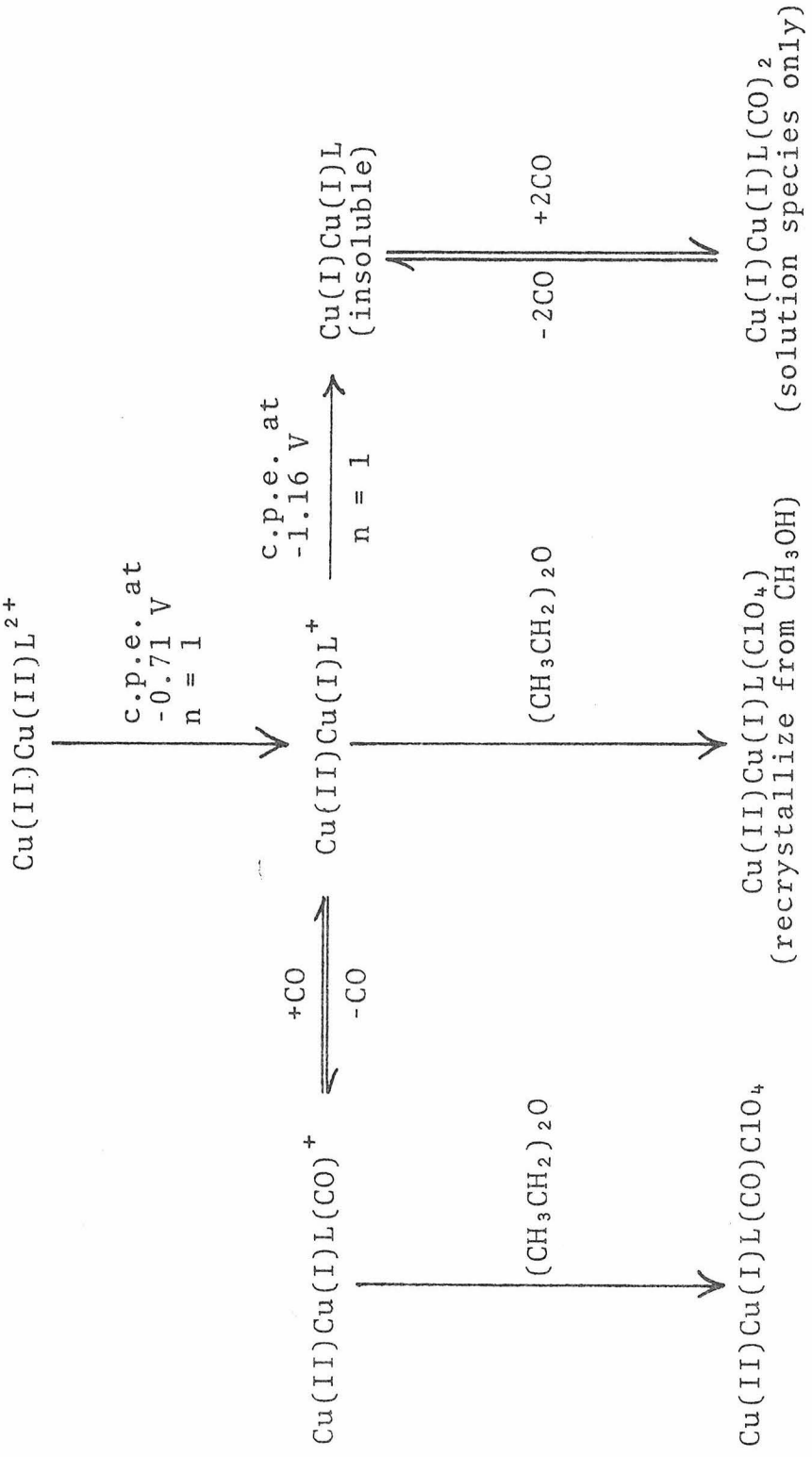
Cu(II)Cu(II)L2+
c.p.e. at
-0.71 V
n = 1
Cu(II)Cu(I)L+
c.p.e. at
-1.16 V
n = 1
Cu(I)Cu(I)L
(insoluble)
-2CO
+2CO
Cu(I)Cu(I)L(CO)2
(solution species only)
(CH3CH2)2O
Cu(II)Cu(I)L(ClO4)
(recrystallize from CH3OH)
+CO
-CO
Cu(II)Cu(I)L(CO)+
(CH3CH2)2O
Cu(II)Cu(I)L(CO)ClO4

Figure 3

The reduction of $Cu(II)Cu(II)L^{2+}$ in DMF was also investigated using d.c. polarography. Polarographic data are summarized in Table I. Again, the insolubility of Cu(I)Cu(I)L caused the wave associated with the reduction of $Cu(II)Cu(I)L^{+}$ to Cu(I)Cu(I)L to be distorted. The reduction of $Cu(II)Cu(II)L^{2+}$ to $Cu(II)Cu(I)L^{+}$ and to $Cu(II)Cu(I)L(CO)^{+}$, however, gave reversible waves as judged by the slope of -E vs log $i/(i_d-i)$ plots which should be 58 mV at 23° C for a one-electron process.[8] Also included in Table I are data for the reductions of O_2, Cu(II)(salpn), and $Zn(II)Zn(II)L^{2+}$.

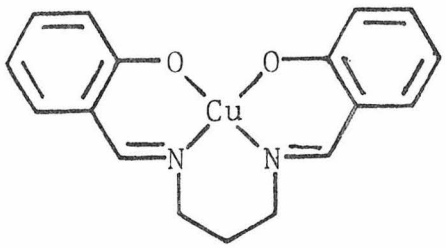

Cu(II)(salpn)

The complex Cu(salpn) might be considered as a monomer for $Cu(II)Cu(II)L^{2+}$, but the difference in charge causes its reduction to occur nearly 0.6 V cathodic of the

TABLE I. Polarographic Data[a]

Compound	Atmosphere	$E_{1/2}$[b]	Slope[c]	I_d[d]	Comments
$Cu(II)Cu(II)L(ClO_4)_2 \cdot 2H_2O$	N_2	-0.517	57.8	1.34	First reduction
	CO	-0.392	56.9	1.39	only
$Zn(II)Zn(II)L(ClO_4)_2 \cdot 2H_2O$	N_2	--	--	--	No waves positive of -1.5 V
Cu(II)(salpn)	N_2	-1.099	57.6	1.74	
	CO	-1.040	58.4	1.78	
O_2	N_2	-0.774	69.0	--	$O_2 + e^- \rightleftharpoons O_2^-$

[a] DMF solution; C ~0.5 mM; TBAP (0.1 m); scan rate = 0.5 mV/sec.

[b] vs NHE.

[c] of -E vs log $i/(i_d-i)$ plot (mV)

[d] $I_d = i_d/(m^{\frac{2}{3}}t^{\frac{1}{6}}C)$: i_d is the diffusion limited current (μA); m is the flow rate (mg/sec); t is the drop time (sec); C is the concentration (mM).

reduction of $Cu(II)Cu(II)L^{2+}$ to $Cu(II)Cu(I)L^{+}$. As expected, since $Zn(II)Zn(II)L^{2+}$ contains no Cu(II) atom, it was not easily reduced. The reduction of oxygen to superoxide ion was not reversible in DMF on Hg, but its half-wave potential is provided as a reference point.

In order to avoid solubility problems, differential pulse voltammetry (DPV) was used to investigate dilute solutions of $Cu(II)Cu(II)L^{2+}$ in DMF. Figure 4 contains DPV scans of $Cu(II)Cu(II)L^{2+}$ on platinum under both nitrogen and carbon monoxide atmospheres. The peak potentials, E_p, from this figure are in Table II along with half-wave potentials that can be calculated using the formula:[9]

$$E_{\frac{1}{2}} = E_p + \frac{MA}{2}$$

where MA is the modulation amplitude or pulse height. Also included are the peak widths at half-height, $\Delta E_{\frac{1}{2}i}$, which are close to the theoretical value of $90.4/n$ mV.[9] The values of $E_{\frac{1}{2}}$ and $E_{\frac{1}{2}}(CO)$ obtained by DPV agree with the polarographic values within a few millivolts.

If differences in diffusion coefficients between the oxidized and reduced halves of redox couples are ignored, values of $E_{\frac{1}{2}}$ obtained in the above electro-

Figure 4

Differential pulse voltammograms of $Cu(II)Cu(II)L^{2+}$ ($\sim 5 \times 10^{-5}$ M).

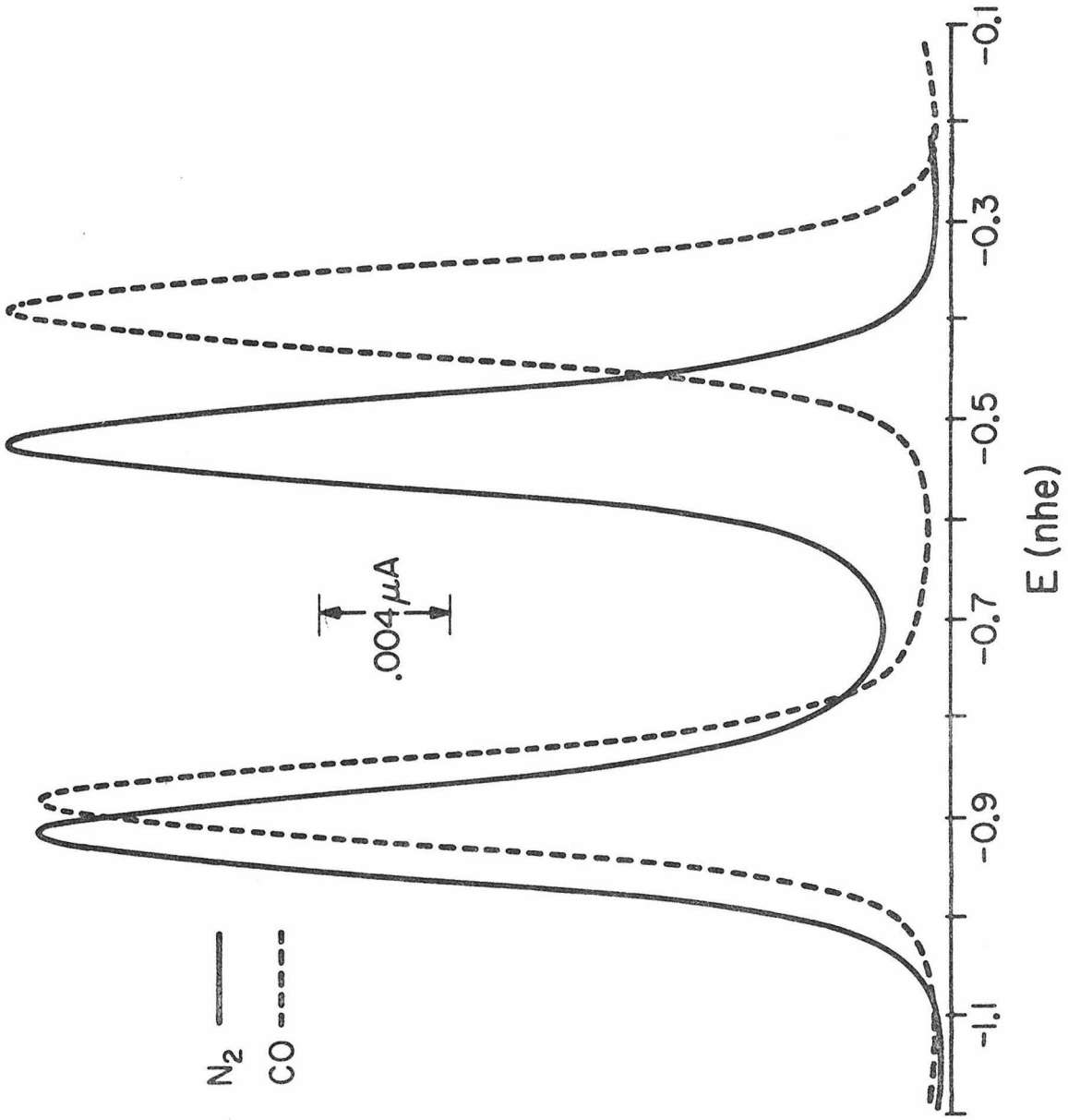

Figure 4

TABLE II. Differential Pulse Voltammetric Data[a]

Process	Atmosphere	E_p[b]	$E_{1/2}$[c]	$\Delta E_{1/2}$[d]
$Cu(II)Cu(II)L^{2+} + e^- \rightleftharpoons Cu(II)Cu(I)L^+$	N_2	-0.518	-0.523	94
$Cu(II)Cu(II)L^{2+} + e^- + CO \rightleftharpoons Cu(II)Cu(I)L(CO)^+$	CO	-0.387	-0.392	93
$Cu(II)Cu(I)L^+ + e \rightleftharpoons Cu(I)Cu(I)L$	N_2	-0.908	-0.913	94
$Cu(II)Cu(I)L(CO)^+ + e^- + CO \rightleftharpoons Cu(I)Cu(I)L(CO)_2$	CO	-0.876	-0.881	93

[a] DMF solution; C_b ~5 x 10^{-5} M; TBAP (0.1 M); scan rate = 2 mV/sec; modulation amplitude (MA) = -10 mV.

[b] Peak potential; vs NHE.

[c] $E_{1/2} = E_p + \frac{mA}{2}$; vs NHE.

[d] Peak width (mV) at half height.

chemical experiments can be used as the E^f's shown in the scheme. Knowledge of these formal potentials enables one to quantify some interesting properties of the system. One is the conproportionation constant describing the equilibrium:

$$Cu(II)Cu(II)L^{2+} + Cu(I)Cu(I)L \overset{K_{con}}{\rightleftharpoons} 2Cu(II)Cu(I)L^{+}$$

The value of K_{con} can be obtained from $E_1{}^f$ and $E_2{}^f$ using the formula:

$$E_1{}^f - E_2{}^f = 0.0591 \quad \log K_{con}$$

The value so calculated is $K_{con} = 3.97 \times 10^6$, using the data in Table II.

Figure 4 and the data in Tables I and II show that the presence of carbon monoxide causes the two reduction waves for $Cu(II)Cu(II)L^{2+}$ to shift anodically. The fact that compound $Cu(II)Cu(II)L^{2+}$ itself does not interact with CO, together with other evidence presented in this paper and in previous work[10,11] indicates that the shifts are due to the binding of CO to Cu(I). Using the formula potentials measured at a CO concentration corresponding to one atmosphere, $E^f_{(CO)}$, certain binding

constants can be calculated. Because compound $Cu(II)Cu(I)L^+$ binds a single CO, the equilibrium constant for the reaction

$$Cu(II)Cu(I)L^+ + CO \overset{K_{CO}}{\rightleftharpoons} Cu(II)Cu(I)L(CO)^+$$

can be found using the following equation:

$$E^f_{(CO)} - E_1{}^f = 0.059 \log (1 + K_{CO}[CO]).$$

The value calculated using the data in Table I is $K_{CO} = 2.82 \times 10^4$. Assuming that the reduced form of Cu(salpn) also binds a single CO, the above formula yields a CO binding constant of 1.95×10^3 for this unisolated Cu(I) complex. Equilibrium constants for the binding of the first and second CO's to Cu(I)Cu(I)L cannot be obtained from an electrochemical measurement at a single CO concentration.

Infrared Spectra. Previously, Robson[2] reported the synthesis of a series of complexes with various dipositive first-row transition elements contained in the binucleating ligand, L. Except for features due to anions and solvent molecules, the IR spectra of the different compounds were found to be very similar.

This is also the case with the compounds formed by reduction of $Cu(II)Cu(II)L^{2+}$. Table III contains selected frequencies from the IR spectra of these compounds. In the column labeled "Imine Stretches" are the positions of the two bands Robson assigned as C=N and phenyl C—C stretches,[2] both of which were shown to have C=N character.[12] Within 40 cm^{-1} these bands are in the same positions in all the compounds. Not included in Table III, but present in all the spectra in the region 1350-650 cm^{-1}, are ten other less intense and unassigned bands. The similarity in the spectra is evidence that the ligand, L, is intact and unreduced throughout the series.

The data in Table III also show that bands due to ClO_4^- and H_2O are present only in the spectra of compounds having these molecules in their formulations. The fully reduced complex, Cu(I)Cu(I)L, has two sharp bands at 1110 and 1070 cm^{-1}. This region is obscured by ClO_4^- adsorption in the spectra of the other compounds, but these bands are also present in spectra of $Zn(II)Zn(II)L(Cl)_2 \cdot 2H_2O$.

The CO stretching frequencies for $Cu(II)Cu(I)L(CO)ClO_4$, $Cu(II)Cu(I)L(CO)^+$ and $Cu(I)Cu(I)L(CO)_2$ are also listed in Table III. The values for ν_{CO} are similar to those

TABLE III. Infrared Data[a,b]

s - strong m - medium w - weak

Compound	Imine	ClO_4^-	Other
$Cu(II)Cu(II)L(ClO_4)_2 \cdot 2H_2O$	1645s, 1572s	1100s, 622m	~3500 (H_2O)
$Cu(II)Cu(I)L(ClO_4)$	1630s, 1555s	1100s, 620m	
$Cu(II)Cu(I)L(CO)(ClO_4)$	1645s, 1565s	1100s, 620m	2064s, 2073[c](CO)
$Cu(I)Cu(I)L$	1620s, 1532s	--	
$Cu(I)Cu(I)L(CO)m$	No Solid-State Spectra		2061[c](CO)
$Zn(II)Zn(II)L(ClO_4)_2(H_2O)$	1650s, 1565s	1100s, 622m	~3400 (H_2O)

[a]All frequencies in cm^{-1}.

[b]All spectra in Nujol mulls except where noted.

[c]DMF solution.

reported for other known Cu(I) carbonyls.[10,13] Although Cu(I)Cu(I)L$(CO)_2$ contains two carbonyls, only a single CO stretch is observed in the solution IR.

EPR. X-band EPR spectra for Cu(II)Cu(I)L(ClO_4) and Cu(II)Cu(I)L(CO)ClO_4 were obtained under a variety of conditions, as summarized in Table IV. Spectra of Cu(II)Cu(I)L^+ in various solvents (CH_2Cl_2, CH_3CN, CH_3OH and $(CH_3)_2CO$) at room temperature display a seven-line isotropic pattern in the g = 2 region with a separation of 40-45 G, (Figure 5). The splitting arises from hyperfine interaction between the odd electron and two copper nuclei ($I = \frac{3}{2}$). Exposure of CH_2Cl_2 solutions of Cu(II)Cu(I)L^+ to carbon monoxide leads to a four-line isotropic spectrum of the carbonyl adduct (Figure 5) for which the hyperfine splitting is now 85 G and is due to localization of the electron at a single copper site. Dissolution of Cu(II)Cu(I)L(CO)ClO_4 in CH_2Cl_2 under a helium atmosphere results in seven-line spectra characteristic of solution spectra of Cu(II)Cu(I)L^+ confirming that coordinated CO is readily released in solution. The magnitude of the splittings in the four-line case is typical for an electron localized on a single Cu site while a splitting of 42 G has also been noted in the seven-line spectrum of a mixed valence

TABLE IV. EPR Parameters for the Mixed Valence Compounds

Sample	Medium	Temperature	g_{avg}	$g_{\|\|}$	$g_{\perp}$	$\|A_{avg}\| \times 10^4$ cm^{-1}	$\|A_{\|\|}\| \times 10^4$ cm^{-1}
Cu(II)Cu(I)L(ClO_4)	solid	15 K	2.085				
	CH_3CN	298	2.262			42.25	
	CH_3CN	77		2.210	2.066		191.0
	CH_2Cl_2	298	2.169			45.57	
	CH_2Cl_2	82		2.228	2.080		187.3
	CH_3OH	292	2.069			38.64	
	$(CH_3)_2CO$	298	2.105			41.77	
Cu(II)Cu(I)L(CO)ClO_4	solid	77	2.089				
	CH_2Cl_2	298	2.113			83.86	
	CH_2Cl_2	79		2.224	2.073		197.3

Figure 5

Room temperature EPR spectra of Cu(II)Cu(I)L(ClO_4) dissolved in CH_2Cl_2 under helium (top) and CO (bottom) atmospheres.

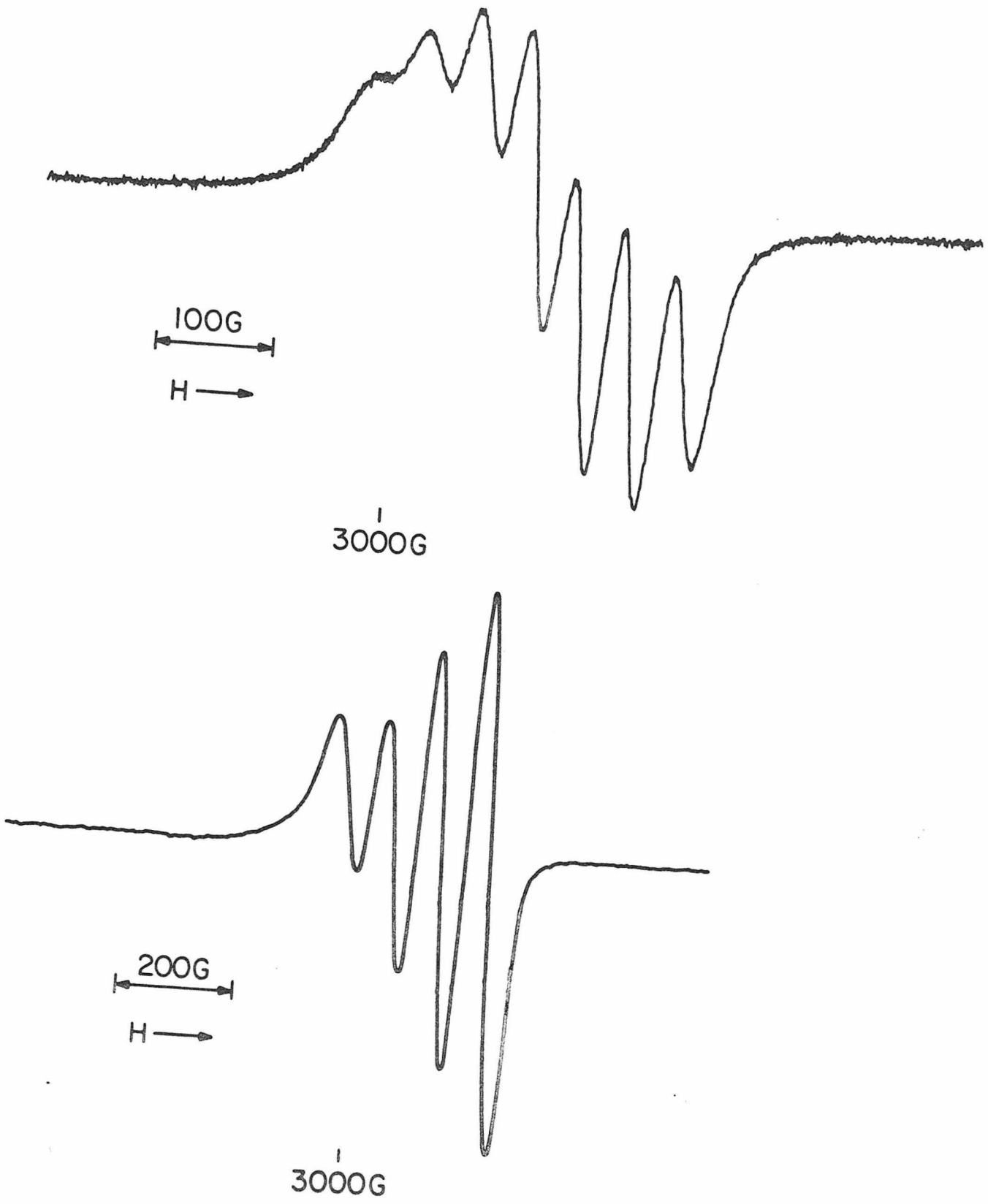

Figure 5

Cu(II)/Cu(I) complex formed from $Cu(I)(CH_3CN)_4^+$ and $Cu(II)(H_2O)_6^{2+}$ (1:1) with acetate ion in methanol.[14,15] The occurrence of a value of A_{avg} for $Cu(II)Cu(I)L^+$ at half that for $Cu(II)Cu(I)LCO^+$ ($A_7 = \frac{1}{2}A_4$) is predicted on theoretical grounds.[16] No hyperfine structure attributable to nitrogen has been seen in these spectra.

The solid state spectra of $Cu(II)Cu(I)L(ClO_4)$ and $Cu(II)Cu(I)L(CO)ClO_4$ exhibit a single symmetrical line at both low and room temperatures with very similar g-values. The lack of any resolution is likely due to dipolar line broadening.

Spectral studies in frozen media met with several experimental complications. The anisotropic spectrum of $Cu(II)Cu(I)L(CO)ClO_4$ in frozen CH_2Cl_2 (solutions of $Cu(II)Cu(I)L(ClO_4)$ exposed to CO before freezing) is straightforward, consisting of a four-line pattern for $g_{||}$ with $g_{\perp}$ not resolved. Frozen solutions of $Cu(II)Cu(I)L(ClO_4)$ in CH_3CN or CH_3CN/toluene (1:1), the latter combination forming good glasses, give essentially the same spectra as for $Cu(II)Cu(I)L(CO)ClO_4$, yet the spectra are often accompanied by two additional features which are indicated by vertical lines in the top of Figure 6. The occurrence of the extra lines varies with conditions. Although they can be observed in solutions frozen

Figure 6

Frozen solution EPR spectra of Cu(II)Cu(I)L(ClO_4) in acetonitrile at 77° K (top) and in ethanol/ methanol (4/1 by volume) at 12° K (bottom). The two vertical lines in the top spectrum indicate contributions from the lower spectrum.

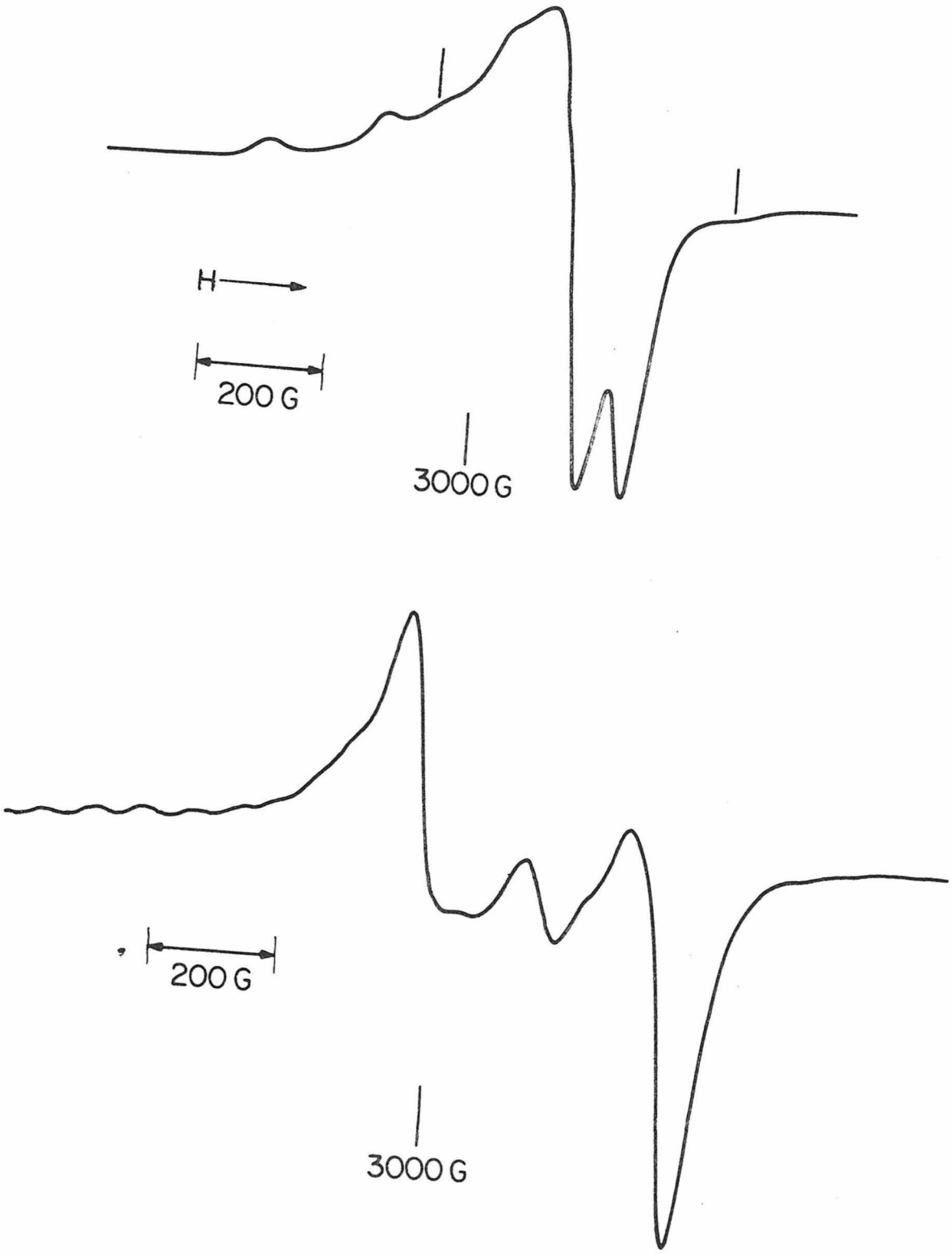

Figure 6

immediately after electrolysis and in concentrations down to about 10^{-3} M, they disappear in very dilute solution (~ 5×10^{-4} M) even though the signal due to the principal absorbing species remains strong. Furthermore, in variable temperature experiments in acetonitrile the intensities of the extra features diminish with respect to the $g_{||}$ lines as the solution is warmed. In frozen CH_2Cl_2 solutions these irregularities occasionally become quite pronounced with intensities exceeding those of the $g_{||}$ features. Another complication which occasionally occurs in experiments with frozen solutions of Cu(II)Cu(I)L(ClO_4) in CH_2Cl_2 is the observation of broad bands, presumably due to precipitated solid. Finally, the bottom of Figure 6 depicts a spectrum of Cu(II)Cu(I)L(ClO_4) in a CH_3CH_2OH/CH_3OH (4:1) glass which bears no resemblance to those recorded in frozen CH_3CN or CH_2Cl_2 media. Instead, the spectrum in the bottom of Figure 6 is characteristic of a spin triplet and is indicative of formation of a dimeric species, i.e., a dimer of macrocyclic complexes involving intermolecular interaction between Cu(II) centers. In addition to the $|\Delta M_s| = 1$ transitions displayed in Figure 6 (bottom) a half-field (1500 G) signal from the $|\Delta M_s| = 2$, $g = 4$ transition which is split into

seven hyperfine components, also diagnostic of a copper triplet spectrum, was observed. On reexamining the low temperature CH_3CN and CH_2Cl_2 solution spectra it was evident that the extra features correspond in relative position to the intense $|\Delta M_s| = 1$ features of the dimer spectrum obtained in alcohol solution. Thus, in CH_3CN and to a greater extent in CH_2Cl_2 it appears that there is frequently some dimerization of $Cu(II)Cu(I)L^+$ in frozen media. This is consistent with the variable concentration and temperature experiments; one would expect the relative amount of dimeric constituent to decrease as the concentration of the complex decreases and temperature increases. Assuming that the triplet spectrum does arise from dipolar through-space coupling of a dimer, the zero-field splitting and $g_{||}$ parameters was used to calculate a Cu-Cu separation of ~4.4 Å.[17]

In spite of these experimental difficulties the principal observation was the change from the seven-line spectrum for $Cu(II)Cu(I)L(ClO_4)$ at room temperature to a four-line pattern at LN_2 temperature or lower in contrast to the apparent localized behavior of $Cu(II)Cu(I)L(CO)ClO_4$ on the EPR time scale at both temperatures. Consequently, spectra of $Cu(II)Cu(I)L(ClO_4)$ in CH_2CL_2 were recorded at various temperatures to

determine if a transition temperature range could be located. The results obtained in a CH_2Cl_2/toluene (3:2) mixture are presented in Figure 7. Spectra were obtained from 84° K (distinct anisotropic four-line spectrum) to 280° K (seven lines, well resolved) although a more limited range is indicated in the figure. To alleviate dimerization and precipitation problems dilute solutions were used, giving less than optimum resolution. Nevertheless, the gross aspects are readily evident. At 154° K the anisotropic spectrum indicative of a localized electron can be seen. At 175° K the low field $g_{||}$ lines have converged somewhat on the central lines. In the 203-227° K range all lines have clearly coalesced. At 250° K new features arise, presumably due to the hyperfine interaction involving two copper centers. The observation of an anisotropic four-line pattern rather than an isotropic spectrum near the coalescence region where the solution is probably fluid may be due to a slow rate of molecular tumbling, such that directional characteristics are not averaged on the EPR timescale.

Under most conditions the spin doublet spectra of frozen solutions of Cu(II)Cu(I)L(ClO_4) have displayed no structure which might be assigned to hyperfine coupling to nitrogen. Dilute CH_2Cl_2 solutions have,

Figure 7

Variable temperature EPR spectra of Cu(II)Cu(I)L(ClO_4) dissolved in CH_2Cl_2/toluene (3/2 by volume).

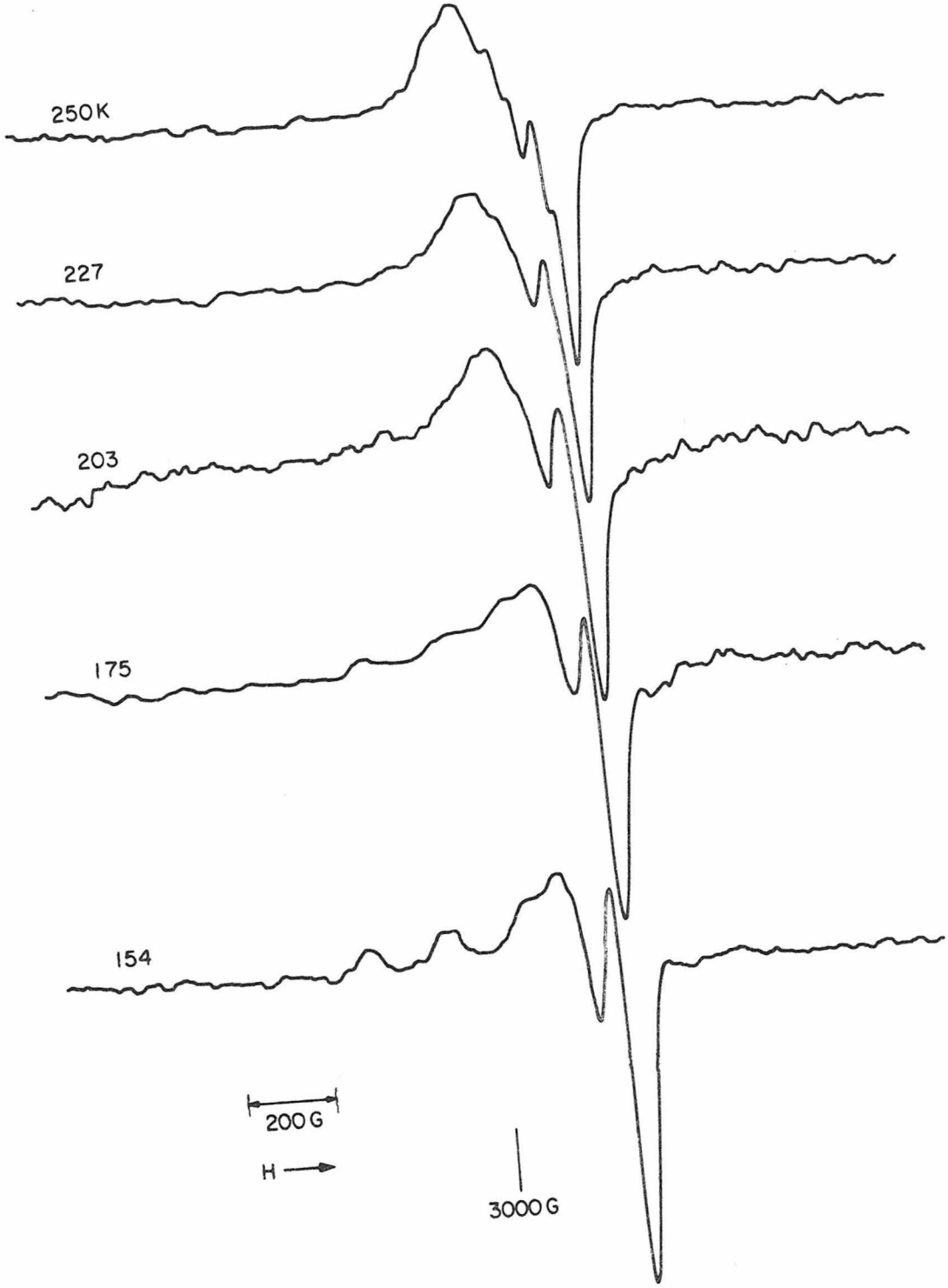

Figure 7

however, occasionally shown such splitting (~15 G) in the $g_{\perp}$ line.

Magnetic Susceptibility. Room temperature magnetic susceptibilities are reported in Table VI. The values for the magnetic moments for Cu(II)Cu(I)L(ClO_4) (1.81μ_β) and Cu(II)Cu(I)L(CO)ClO_4 (1.94 μ_β) are typical of magnetically dilute Cu(II) complexes, although variable temperature measurements may indicate some exchange coupling at lower temperatures. These results contrast with the μ_{eff} for Cu(II)Cu(II)L(ClO_4)$_2 \cdot 2H_2O$ (0.60 μ_β) which indicates quite strong coupling between the Cu(II) centers in agreement with Robson's observations.[2] As expected, Zn(II)Zn(II)L(ClO_4)$_2 \cdot 2H_2O$ and Cu(I)Cu(I)L are diamagnetic, within experimental error.

Electronic Absorption Spectra. Some aspects of the electronic absorption spectra essential to the characterization of Cu(II)Cu(I)L(ClO_4) as a mixed valence species were reported earlier.[5] Representative spectra of Cu(II)Cu(II)L(ClO_4)$_2 \cdot 2H_2O$, Cu(II)Cu(I)L(ClO_4) and Cu(II)Cu(I)L(CO)ClO_4 (Cu(II)Cu(I)L$^+$ exposed to CO) in methanol in the visible and near infrared regions are shown in Figure 8. All three spectra exhibit the tail of an intense absorption in the ultraviolet region with band maxima in the range 350-400 nm (ε ~10,000 M^{-1} cm^{-1}).

TABLE V. Magnetic Susceptibilities at 25°

Compound	μ_{EFF} (B.M)
$Cu(II)Cu(II)L(ClO_4)_2 \cdot 2H_2O$	0.60 ± 0.04
$Cu(II)Cu(I)L(ClO_4)$	1.81 ± 0.04
$Cu(II)Cu(I)L(CO)(ClO_4)$	1.94 ± 0.04
$Cu(I)Cu(I)L$	0.19 ± 0.25
$Zn(II)Zn(II)L(ClO_4)_2 \cdot 2H_2O$	0.00 ± 0.25

Figure 8

Electronic absorption spectra in methanol of $Cu(II)Cu(II)L(ClO_4)_2 \cdot 2H_2O$ (1.15×10^{-3} M) ——; $Cu(II)Cu(I)L(ClO_4)$ (1.10×10^{-3} M) under helium ····; $Cu(II)Cu(I)L(CO)ClO_4$ (1.10×10^{-3} M) under carbon monoxide ----.

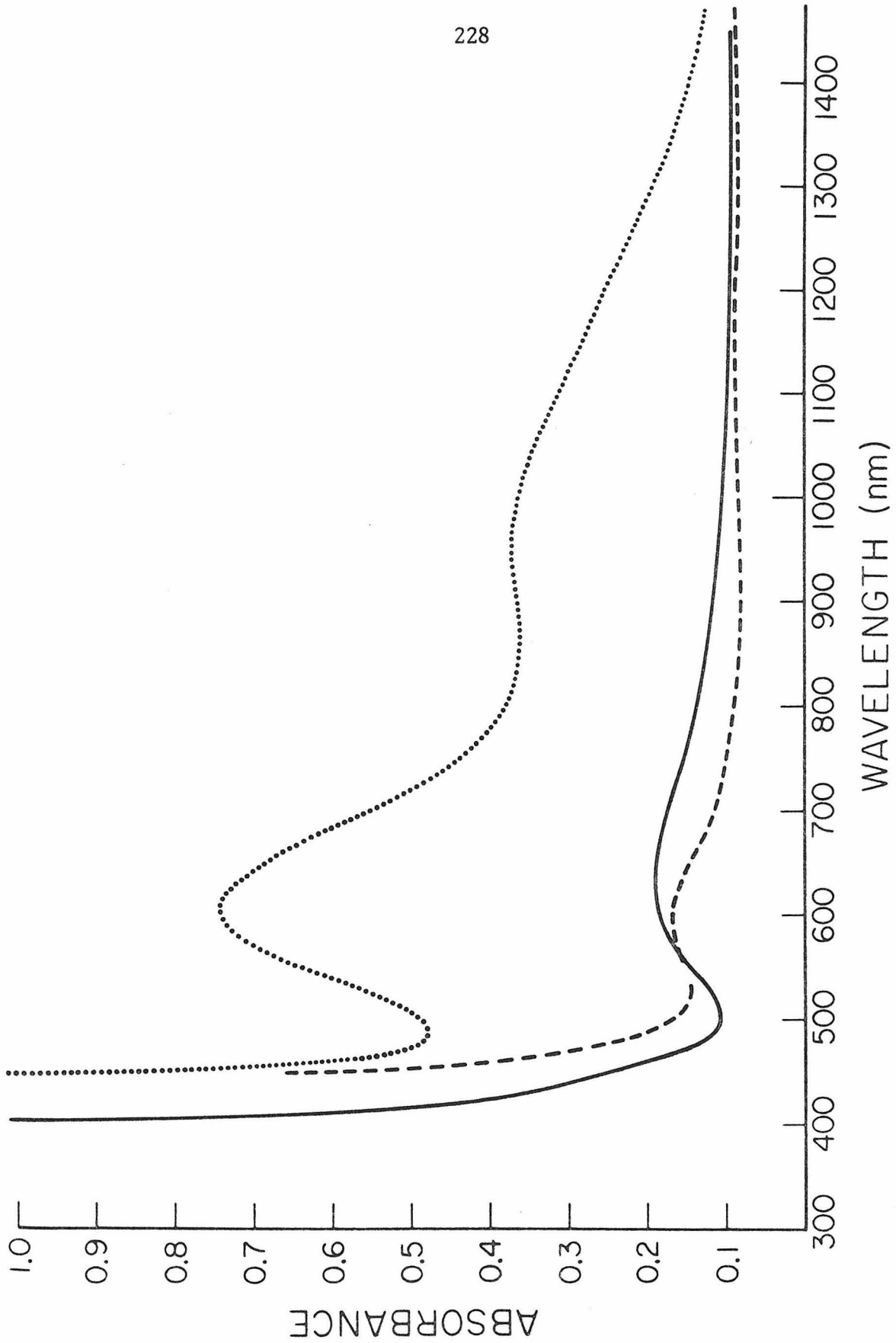
ABSORBANCE
1.0
0.9
0.8
0.7
0.6
0.5
0.4
0.3
0.2
0.1
300
400
500
600
700
800
900
1000
1100
1200
1300
1400
WAVELENGTH (nm)

Figure 8

This band occurs in the yellow complex $Zn(II)Zn(II)L(ClO_4)_2 \cdot 2H_2O$ and is presumably due to an intraligand transition. Some charge transfer character undoubtedly is present in the copper complexes. A band of considerably greater intensity is evident at ~250 nm; it is probably of $\pi \rightarrow \pi^*$ origin. In the visible region $Cu(II)Cu(II)L^{2+}$ (green) displays a much weaker asymmetric band which does not occur in the dizinc complexes, with a maximum at 600 nm(ε = 85 in CH_3CN) and a shoulder at 700 nm (ε = 60 in CH_3CN) in agreement with Robson's observations and presumably due to ligand-field transitions.[2]

Solutions of $Cu(II)Cu(I)L(ClO_4)$ were reported to exhibit a very broad band in the near IR region in certain solvents,which was attributed to an intervalence transfer (IT) transition ($Cu(II)Cu(I) \xrightarrow{h\nu} Cu(I)Cu(II)^*$, the product in a vibrationally-excited state) in addition to an appreciable enhancement of the 600 nm band.[5] The position of the IT band appeared to be solvent dependent; it occurred at 1200 nm in non-coordinating CH_2Cl_2, at 900-1000 nm in the weakly coordinating solvents CH_3OH, $(CH_3)_2CO$ and DMF, while no such band was apparent in CH_3CN which has a strong affinity for Cu(I). Initial spectra were recorded to 1700 nm[5] but the spectral range has now been extended to 2600 nm.

The spectrum of Cu(II)Cu(I)L(ClO_4) in CH_2CL_2 out to this limit is shown in Figure 9 where an additional band can be seen at 1700 nm. Thus, earlier spectra terminated on the plateau of the new band maximum rather than at the true baseline, and the higher energy bands (600 and 1200 nm) are actually much more intense than initially believed. Similar reinvestigation in CH_3OH was complicated by solvent vibrational overtone bands which partially obscure any broad features in the 1700 nm region. Hence it is not clear whether such a band is present in the CH_3OH spectra. In contrast to the bluish-green color of Cu(II)Cu(I)L(ClO_4) in non- or weakly-coordinating solvents, CH_3CN solutions are brown because the tail of the UV band (λ_{max} = 380 nm), which is much broader in this solvent than in CH_2Cl_2, tails off farther into the visible to overlap with the 600 nm band. Initially CH_3CN solutions revealed no feature in the IR region of intensity comparable to that seen in the spectra of the other solutions. On examining more concentrated CH_3CN solutions, however, it appears that the tailing absorption extends farther into the IR than would be expected from Gaussian behavior of the visible and UV bands (Figure 10). Furthermore, there appears to be a very slight band maximum around 1000 nm due to a broad

Figure 9

Electronic absorption spectrum of Cu(II)Cu(I)L(ClO_4) (0.822×10^{-3} M) in dichloromethane under helium.

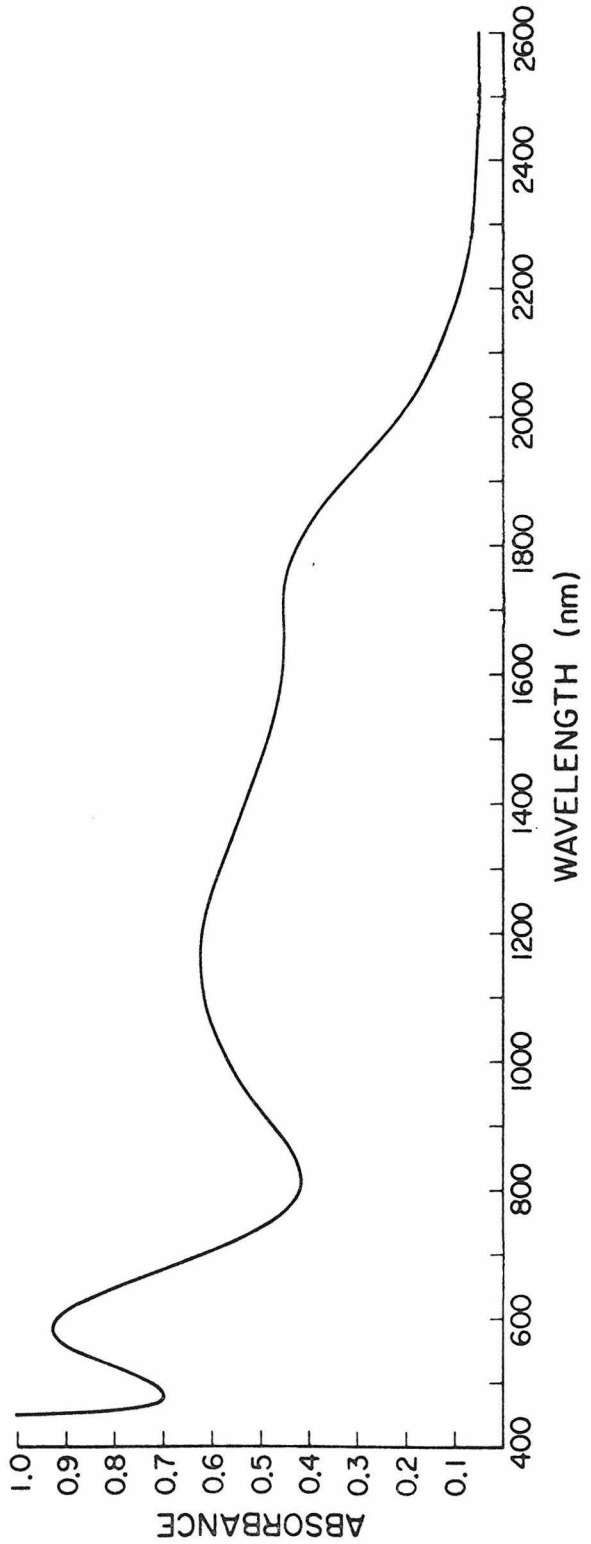
ABSORBANCE
1.0
0.9
0.8
0.7
0.6
0.5
0.4
0.3
0.2
0.1
400
600
800
1000
1200
1400
1600
1800
2000
2200
2400
2600
WAVELENGTH (nm)

Figure 9

Figure 10

Electronic absorption spectrum of Cu(II)Cu(I)L(ClO_4) (1.0×10^{-3} M) in acetonitrile under helium.

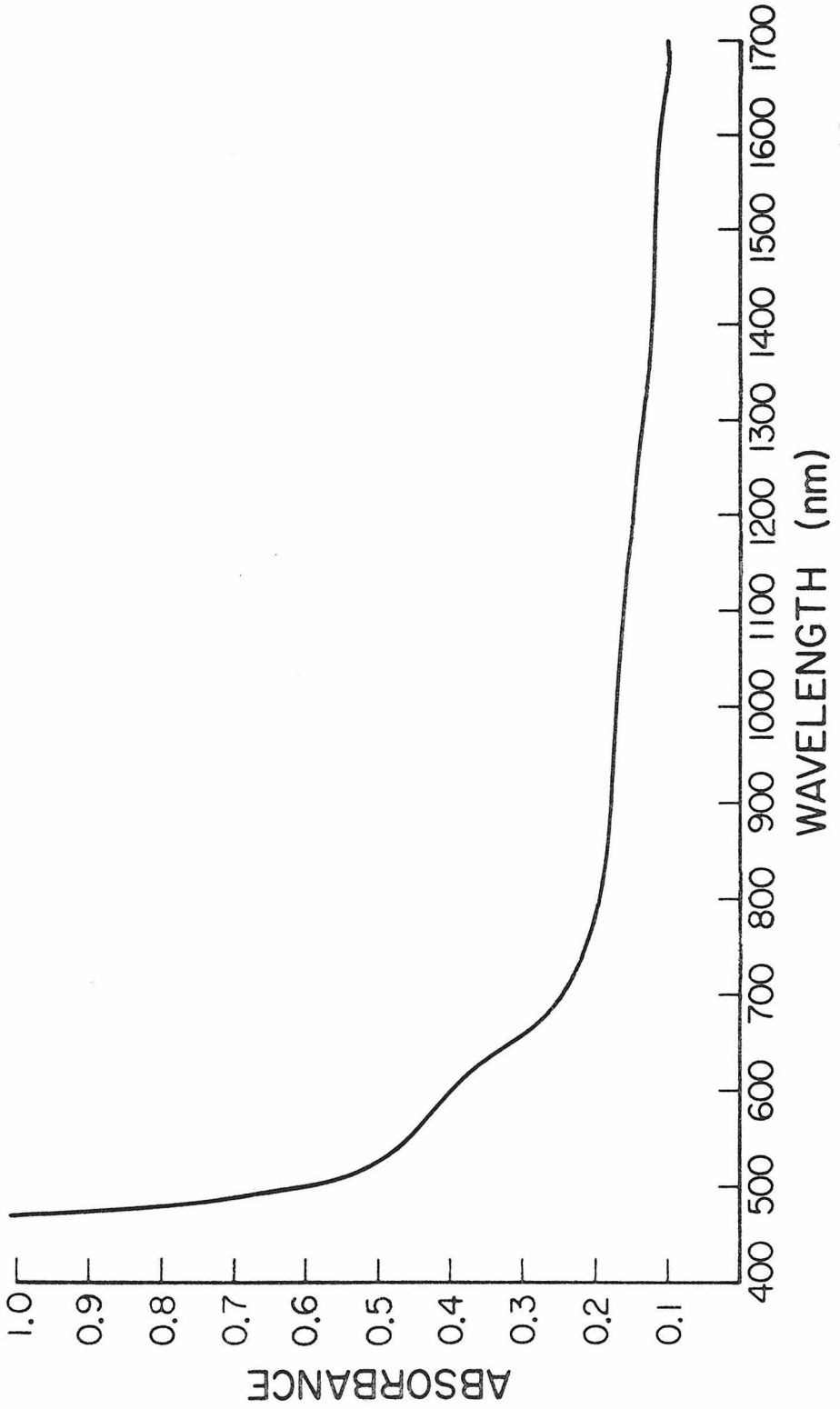
ABSORBANCE
1.0
0.9
0.8
0.7
0.6
0.5
0.4
0.3
0.2
0.1
400 500 600 700 800 900 1000 1100 1200 1300 1400 1500 1600 1700
WAVELENGTH (nm)

Figure 10

band. All solutions of Cu(II)Cu(I)L(ClO_4) turn green rapidly on exposure to oxygen and show only a weak ligand field absorption (λ_{max} ~ 650 nm) in the visible and near IR regions. This observation is consistent with the assignment of the IR bands as intervalence transitions.

As expected from its dark brown color in the solid state, mull spectra of Cu(II)Cu(I)L(ClO_4), Figure 11, resemble those of the CH_3CN solutions. As discussed earlier, Figure 11 shows the near UV band which tails into the visible to overlap the 600 nm absorption. Also, this spectrum clearly exhibits a very broad band in the near IR. Figure 12 shows a very concentrated mull spectrum on a more compressed wavelength scale and farther into the IR. A band at 1800 nm is clearly resolved while another at 1300 nm is accompanied by a shoulder at 1050 nm. Over a period of days (3-5) the mulls turn green in laboratory atmosphere, and again only a weak band due to Cu(II) is observed in the spectra at wavelengths greater than 500 nm.

Since the EPR results demonstrate that dimerization of Cu(II)Cu(I)L^+ occurs in frozen solution under certain conditions, the question arose whether the "IT" bands could result from intermolecular interaction in fluid solution, especially in CH_3OH. Beer's law studies were

Figure 11

Electronic absorption spectrum of Cu(II)Cu(I)L(ClO_4) in a Nujol mull.

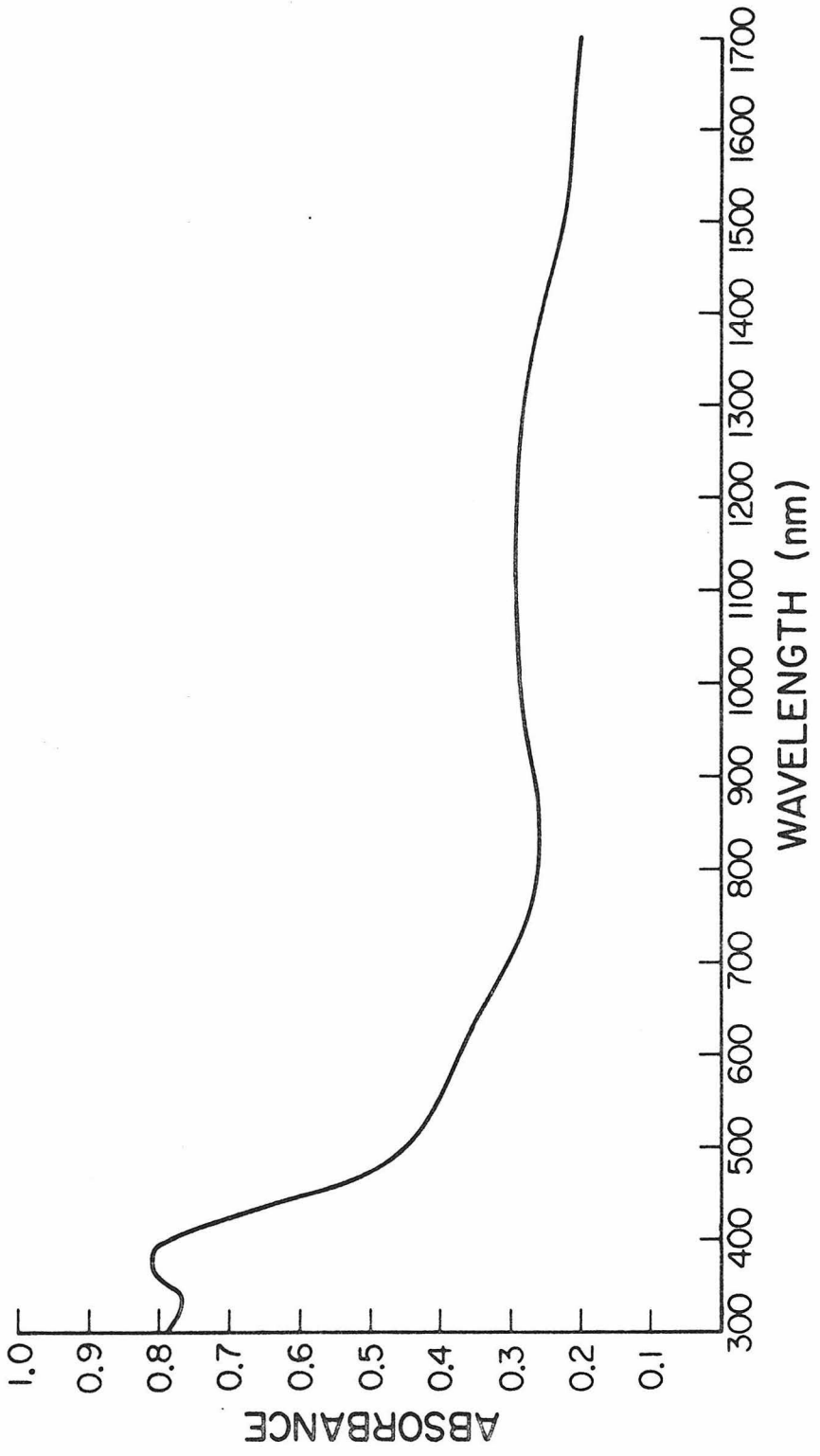
ABSORBANCE
1.0
0.9
0.8
0.7
0.6
0.5
0.4
0.3
0.2
0.1
300
400
500
600
700
800
900
1000
1100
1200
1300
1400
1500
1600
1700
WAVELENGTH (nm)

Figure 11

Figure 12

Electronic absorption spectrum of Cu(II)Cu(I)L(ClO_4) in a Nujol mull (more concentrated mull than in Figure 11.)

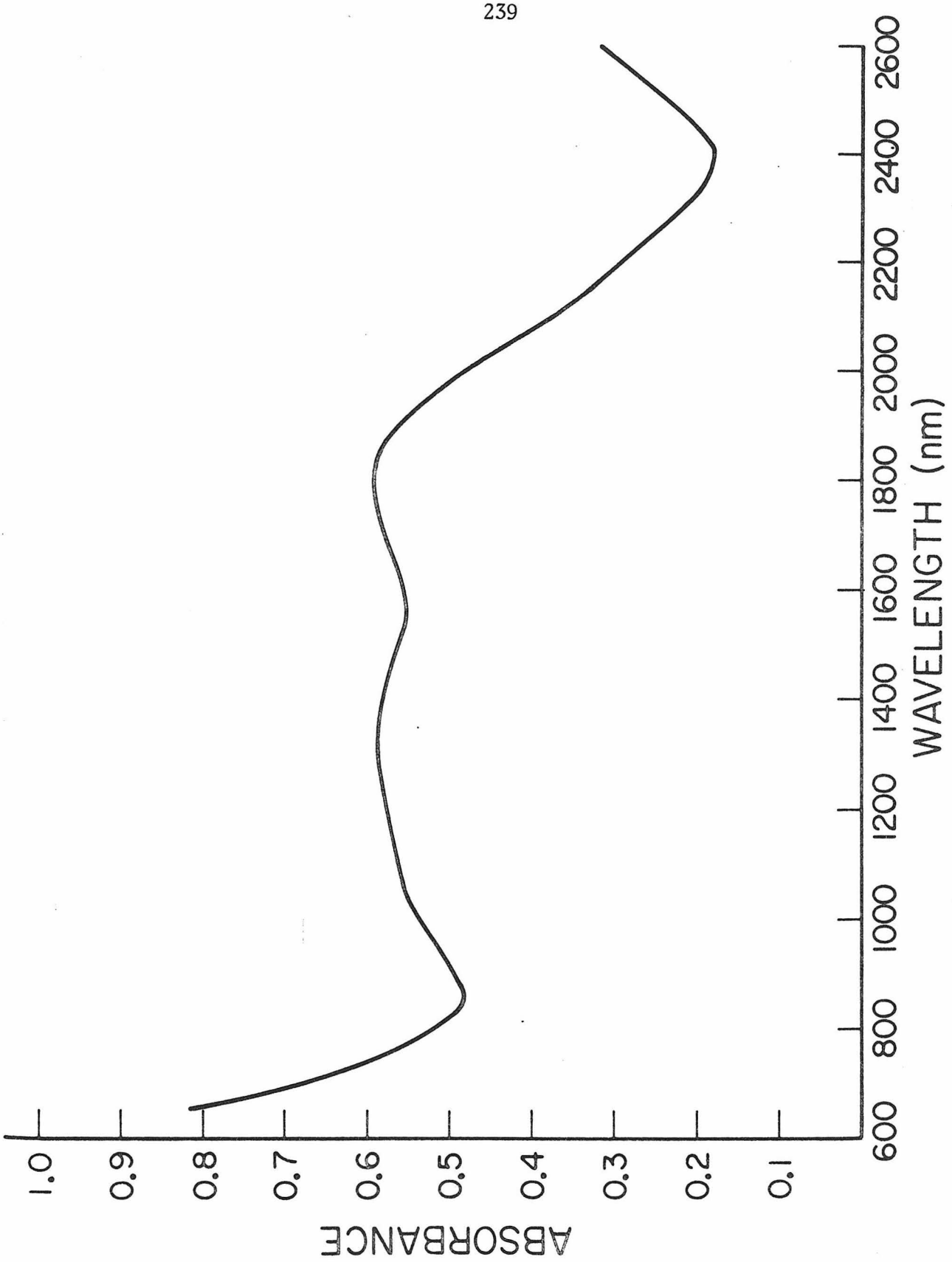
ABSORBANCE
1.0
0.9
0.8
0.7
0.6
0.5
0.4
0.3
0.2
0.1
600
800
1000
1200
1400
1600
1800
2000
2200
2400
2600
WAVELENGTH (nm)

Figure 12

conducted for CH_3OH solutions (600 and 900 nm bands) and CH_2Cl_2 solutions (600, 1200 and 1700 nm bands) over a fifty-fold concentration change (10^{-3}-2×10^{-5} M) at the ambient temperature. For all bands examined the dependence of absorbance on concentration was strictly linear. The lack of any deviation from Beer's law behavior suggests that there is no change in the absorbing species in the concentration range employed. This Beer's law behavior, in light of the observed seven-line isotropic EPR spectrum obtained for $Cu(II)Cu(I)L^+$ in CH_3OH at 25°, suggests that the IR bands are attributable to a monomeric binuclear species. Electronic absorption spectral data for $Cu(II)Cu(I)L(ClO_4)$ are summarized in Table VII.

Exposing $Cu(II)Cu(I)L^+$ in any of the solvents discussed to CO generates yellow solutions of the carbonyl adduct. The spectrum in CH_3OH is shown in Figure 8. It displays only a single weak band (ε = 80 in CH_3OH) at 600 nm (λ_{max} varies slightly in different solvents) which is probably due to a ligand-field transition. Significantly the broad IR bands and the enhanced intensity of the 600 nm band observed for solutions of $Cu(II)Cu(I)L(ClO_4)$ have disappeared.

It is notable that the Cu(II)Cu(I)-acetate system in methanol also exhibits more than one band in the

TABLE VI. Electronic Absorption Spectral Data for Cu(II)Cu(I)L(ClO_4)

Medium	λ_{max}(nm) (~ε)
solid	600 sh, 1050, 1300, 1800,
CH_2Cl_2	580 (980), 1175 (640), 1725 (430)
CH_3OH	605 (930), 975 (430)
DMF	600 (920), 950 (420)
$(CH_3)_2CO$	600 (920), 1000 (480)
CH_3CN	600 , 1000

visible-near IR portion of its spectrum. A sharp band at 509 nm and a broad band centered at 900 nm were reported. The precursor complexes, $Cu(I)(CH_3CN)_4^+$ and $Cu(II)(H_2O)_6^{2+}$, are essentially transparent at these wavelengths.[15]

The spectral observations on $Cu(II)Cu(I)L(ClO_4)$ indicate that similar studies on mixed valence species, particularly those containing copper, should be pursued well into the IR region to ensure that all suspected IT bands have been located.

Cu(I)Cu(I) Compounds. The very low solubility of Cu(I)Cu(I)L limited attempts to obtain solution electronic spectra of this compound. Saturated solutions in DMF showed only a band at 380 nm which tailed into the visible region with no absorption above 700 nm. Mull spectra of this complex also contained the 380 nm band, a shoulder at 475 nm, and an extremely long tail which extended out to 1500 nm. Solution spectra of $Cu(I)Cu(I)L(CO)_2$ contained only an intense band at 410 nm and a prominent shoulder at 600 nm.

Discussion

Electrochemistry

Given the experimental data presented herein for $Cu(II)Cu(I)L(ClO_4)$ and Cu(I)Cu(I)L, along with the fact that $Zn(II)Zn(II)L^{2+}$ has no observable electrochemistry,

it is clear that both electrochemical waves found for $Cu(II)Cu(II)L^{2+}$ are due to the reduction of Cu(II) to Cu(I). Reduction of the two Cu(II) atoms in $Cu(II)Cu(II)L^{2+}$ can be discussed either by treating each site separately or by viewing both atoms and the macrocyclic ligand as a unit. The former method is more useful for comparing the reduction potentials to other monomeric systems, while the latter method is more suitable for comparisons with other multi-metal systems.

As judged by the formal reduction potentials E_1^f and E_2^f, both Cu(I) centers in Cu(I)Cu(I)L are strongly reducing. In fact, the data in Tables I and II indicate that Cu(I)Cu(I)L is a stronger reducing agent than superoxide ion. Since the E^0 for the reduction of Cu(II) to Cu(I) in water is +0.153 V,[21] it appears that the binucleating ligand, L, stabilizes Cu(II) much more than it stabilizes Cu(I). Although anionic oxygen ligands would be expected to favor Cu(II) over Cu(I), unsaturated nitrogen donors can have the opposite effect. For example, the reduction of Cu(II) to Cu(I) in acetonitrile occurs at ~ +0.95 V.[22] The nearly square-planar coordination geometry enforced by the ligand[23] is probably the overriding reason that Cu(II) is stabilized over Cu(I), because the latter prefers a tetrahedral

environment. Because reduction of the copper atoms in $Cu(II)Cu(II)L^{2+}$ to Cu(0) was not observed electrochemically, it is not clear whether the observed solution stability of $Cu(II)Cu(I)L^{+}$ and Cu(I)Cu(I)L towards disproportionation to copper metal is thermodynamic or merely kinetic.

One might expect E_1^f and E_2^f to be similar to the $E_{1/2}$ value of Cu(salpn), -1.099 V, assuming coordination geometries to be similar and ignoring the effects of one copper atom on the other. The observed differences are probably due to molecular charge. The dicationic $Cu(II)Cu(II)L^{2+}$ and cationic $Cu(II)Cu(I)L^{+}$ are, respectively, 0.58 and 0.19 V easier to reduce than the neutral Cu(II)(salpn). A more meaningful comparison can be made between E_1^f and the reduction of $Cu(II)Zn(II)L^{2+}$ which occurs at -0.628 V.[24] Note that the Cu(II)Cu(II) complex is ~0.1 V easier to reduce than Cu(II)Zn(II) complex. A similar situation is found for $[(NH_3)_5Ru(III)$-(pyrazine)$Ru(III)(NH_3)_5]^{6+}$, which is 0.05 V easier to reduce than its best "monomer", $[(NH_3)_5Ru(III)$(pyrazine)-$Rh(III)(NH_3)_5]^{6+}$.[25]

Recently, Patterson and Holm[26] compared the reduction potentials of a series of neutral Cu(II) chelates with potentials for "blue" copper sites in proteins. As with the majority of the neutral chelates, the potentials reported in this paper for $Cu(II)Cu(II)L^{2+}$ are at least

1.0 V more cathodic than the "blue" copper sites, which occur at ~0.5 V. Likewise, the redox potentials for $Cu(II)Cu(II)L^{2+}$ are considerably more reducing than are those for type III copper sites.[27,28] Although type III copper sites and $Cu(II)Cu(II)L(ClO_4)_2 \cdot 2H_2O$, both contain a pair of magnetically coupled copper atoms[2,29] differences in redox potentials argue that ligand environments in the two cases are quite different.

Molecules that contain two or more chemically equivalent and reversible redox sites exhibit electrochemistry which is dictated by the thermodynamic relationships between various molecular redox states. This subject has been examined in the literature both theoretically and experimentally.[30-34] For the case of a molecule with two sites, reduction potentials and the conproportionation constant, K_{con}, are related in the following way:

$$\text{Ox-Ox} + e^- \overset{E_1{}^f}{\rightleftharpoons} \text{Ox-Red}$$

$$\text{Ox-Red} + e^- \overset{E_2{}^f}{\rightleftharpoons} \text{Red-Red}$$

$$\text{Ox-Ox} + \text{Red-Red} \overset{K_{con}}{\rightleftharpoons} 2(\text{Ox-Red})$$

$$E_1{}^f - E_2{}^f = 0.0591 \log K_{con}$$

It is natural to divide the two-site case into three classes based on the value of K_{con}:

K_{con} = 4--This is the totally non-interacting case, i.e., the oxidation state of one site is not affected by the oxidation state of the other. Even though the two sites have the same microscopic redox potentials, notice that E_1^f and E_2^f, which are macroscopic properties, are not equal but are separated by 0.0356 V. This separation is due to statistics and has been observed for certain polyferrocenes.[33,35]

K_{con} < 4--This implies that the second electron is easier to add than the first, $E_1^f - E_2^f < 0.0356$ V, and that the mixed-valence molecule, Ox-Red, will be unstable with respect to disproportionation. If both sites in the molecule do not change geometrically or chemically, it is unlikely that this case will occur because charge should be sequentially more difficult to add. In situations where this case does occur, addition of the first electron is usually followed by some process such as bond-breaking,[36] rotation about a bond,[34] or protonation.[37] The process causes the second site to be easier to reduce than the first.

K > 4--In this case the second electron is more difficult to add than the first, $E_1^f - E_2^f > 0.0356$ V, and Ox-Red is stable. This situation is the most common

and is observed, for example, in many ruthenium dimers,[38] certain biferrocenes,[35] and $Cu(II)Cu(II)L(ClO_4)_2 \cdot 2H_2O$.

The observation that $Cu(II)Cu(II)L^{2+}$ does reduce in two sequential, one-electron steps appears to be in conflict with other electrochemical studies on oxo-bridged, binuclear copper systems. The binuclear complex $Cu(II)Cu(II)([PAA)_2en]$ (drawn below) was reported to reduce in one reversible two-electron step.[42] This result is especially unusual considering the difference in ligands for the two coppers. Indeed we have examined $Cu(II)Cu(II)([PAA)_2en]$ in our laboratory by d.c. polarography and constant potential electrolysis and find that it reduces in a single reversible <u>one</u>-electron process.[43] More recently, Linvedt reported that the two copper atoms in $Cu(II)Cu(II)(BAA)_2$ (drawn below) reduce at exactly the same potential.[44] The conclusion that $E_1^f = E_2^f$ for $Cu(II)Cu(II)(BAA)_2$ does not mean that the two centers reduce with equal ease, because this molecule belongs to the $K < 4$ class and the second electron is microscopically easier to add than the first. The two-electron reduction at a single potential may result from a conformational change accompanying the first one-electron reduction which facilitates the second one-electron process. The electrochemistry for $Cu(II)Cu(II)L^{2+}$ is quite consistent with results on a

similar system $Cu(II)Cu(II)L^{+2}$ (drawn below) reported by Addison in that the molecule is reduced in two one-electron steps.[45]

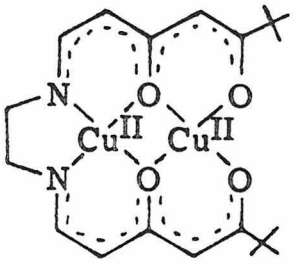

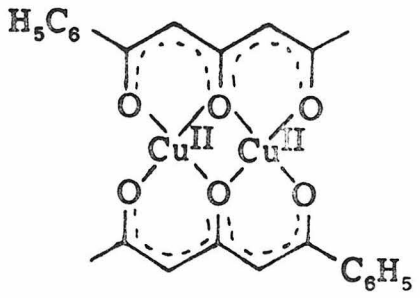

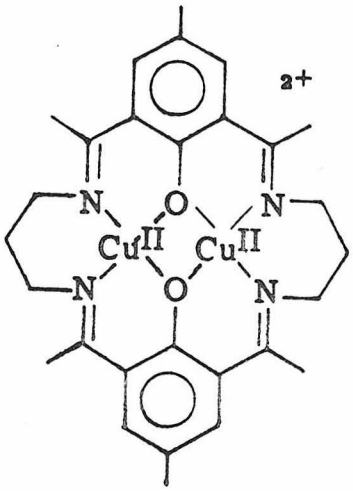

$Cu(II)Cu(II)[(PAA)_2en]$ $Cu(II)Cu(II)(BAA)_2$ $Cu(II)Cu(II)L^{+2}$

Properties of the Mixed Valence Complexes. Our studies of the mixed valence characteristics of $Cu(II)Cu(I)L(ClO_4)$ and $Cu(II)Cu(I)L(CO)ClO_4$ were concerned with their description in terms of existing models. We were especially interested in qualitatively gauging the extent of interaction between the metal centers in the ground state, i.e., are these species better represented as Cu(II)Cu(I) or Cu(1.5)Cu(1.5)? Were the former description appropriate, we hoped to obtain an estimate of the rate of thermal transfer of the odd electron between the two metal sites. Mixed valence materials often exhibit spectral behavior and other physical properties not shown by the isolated ions; in particular, the inter-

valence transfer (IT) transition represents a photo-induced electron transfer from one metal atom to the other. Robin and Day developed a classification scheme of mixed valence systems based on amount of delocalization of the odd electron between metal centers in the ground electronic state.[46] At the same time Hush proposed a coupled harmonic oscillator model for weakly interacting systems which relates the energy of the optical electron transfer (E_{op}) to that of the corresponding thermal activation barrier (E_{th}).[47] For a symmetrical complex this relation is $E_{op} = 4\ E_{th}$. From E_{th} it is possible to calculate a rate constant for the radiationless transfer. Criteria exist for assessing the validity of linking E_{th} to E_{op} in this fashion. These include, principally, agreement between the observed IT spectral band width and that calculated from the model and a solvent dependence of E_{op} such that the media behave as a dielectric continuum. The latter restriction arises because E_{op} represents the inner- and outer-sphere reorganizational energies ($E_{op} = \lambda_i + \lambda_0$) in the Hush model. A number of complexes have met these criteria.[48,49] The application of this model has been challenged for other systems, however, particularly when the calculated rate is at variance with an experimentally determined value such as for biFerrocenium ($Fe(II)Fe(III)^+$).[50,51] The

complex $(NH_3)_5Ru(pyrazine)Ru(NH_3)_5^{5+}$ does not meet either of the spectral tests given above, yet conflicting results from a variety of physical measurements have been reported regarding its definitive classification and corresponding K_{th}.[25,52,53]

The mixed valence copper complexes reported here can be discussed within this context. For the CO complex the observation of a localized odd electron at both high and low temperatures indicates that thermal electron transfer either is prevented entirely or is too slow to be observed on the EPR time-scale at either temperature. This is consistent with the lack of any band in the visible-near IR region of the electronic spectrum assignable to an IT transition. It might, however, occur at higher energy obscured by the high intensity bands of the UV region. The binding of CO to the Cu(I) site would be expected to markedly alter the energy differences between Cu(I) and Cu(II) perhaps to an extent which makes facile electron transfer infeasible. Based on its spectral properties $Cu(II)Cu(I)L(CO)ClO_4$ behaves as though it contains non-interacting metal centers--a Class I species.

The magnitude of K_{con} for $Cu(II)Cu(I)L^+$ (4.83×10^6) can be compared to values for several well-characterized, symmetric ruthenium systems. The mixed-valence ions

$[(NH_3)_5Ru(4,4'\text{-bipyridine})Ru(NH_3)_5]^{5+}$ and $[Cl(bpy)_2Ru\text{-}(pyrazine)Ru(bpy)_2Cl]^{3+}$ (bpy = 2,2 -bipyridine) are Class II systems which obey the Hush model.[39] The values of K_{con} for these compounds are 4-20[40] and 300,[39] respectively. When similar ruthenium systems are oxo-bridged two delocalized Class III ions can be formed, $[Cl(bpy)_2RuORu(bpy)_2Cl]^{3+}$ and $[Cl(bpy)_2RuORu(bpy)_2Cl]^{+}$, with K_{con} equal to 6.49×10^{20} and 3.2×10^{11}.[41] Controversy still exists as to the classification of the ion $(NH_3)_5Ru(pyrazine)Ru(NH_3)_5^{5+}$. Meyer has noted, however, that the value of K_{con} in this system, 1.89×10^7, is much larger than in the weakly-interacting Class II systems.[39] Electrochemical measurements on $Cu(II)Cu(I)L^{+}$ thus indicate a fairly strong interaction but no clear indication as to whether it should be regarded as a Class II or Class III ion.

The complex $Cu(II)Cu(I)L(ClO_4)$ also displays evidence of interaction between Cu(I) and Cu(II) in its electronic and EPR spectra. The room temperature EPR spectra can best be interpreted in terms of intramolecular electron transfer between coppers at a rate which is rapid compared to the relatively slow resonance experiment. In frozen media (solutions where dimerization is not a problem) that exchange is stopped or is too slow to be monitored. The variable temperature experiments reveal

that coalescence takes place at about 200° K which is probably well above the freezing point of a CH_2Cl_2/toluene solution of the complex. Hence, the inhibition of electron exchange is not a consequence of solution freezing. A number of explanations are conceivable for this behavior. First, axial ligation by ClO_4^- or solvent at lower temperatures might lead to an asymmetric complex similar to $Cu(II)Cu(I)L(CO)^+$. Solvent coordination seems likely for CH_3CN but unlikely for CH_2Cl_2, which was utilized for many of the spectroscopic studies. Another cause might be that at the lower temperatures insufficient thermal energy is available to effect macrocyclic conformational changes necessary for the radiationless transfer. According to the accepted picture of thermal electron exchange, geometrical adjustments (bond length changes in simple molecules) to equalize the environments of both metal sites occur prior to electron migration.[54] For $Cu(II)Cu(I)L^+$ this might involve a structure intermediate between square-planar for Cu(II) and square-planar with slight tetrahedral distortion for Cu(I). The molecular structure of a macrocyclic mononuclear Cu(I) complex which is essentially square-planar about copper but exhibits a perceptible tetrahedral twist was recently determined in this laboratory.[55] Such a molecular deformation in solution should require considerably more

energy than in simpler systems, e.g., self-exchange between mononuclear octahedral complexes, and the different coordination geometries for Cu(I) and Cu(II) might be interconvertible at a very slow rate (if at all) at low temperature. Support for the latter interpretation comes from Addison's results on the analogous Cu(II)Cu(I) complex with methyl groups on the imine carbon atoms, $Cu(II)Cu(I)L'^{+}$ (see drawing of $Cu(II)Cu(I)L'^{2+}$ earlier in this paper.)[45] The ambient temperature EPR spectrum for this species displays only four hyperfine lines suggesting the odd electron is localized on one copper atom. The larger methyl substituents may effectively hinder the requisite conformational changes for an EPR-detectable exchange process. Our data do not favor one explanation over the other; indeed both processes may occur. In any event the EPR results favor a designation of $Cu(II)Cu(I)L(ClO_4)$ as a Class II mixed valence system.

The variable temperature spectra permit an estimate of the rate of electron exchange. If k_{th} is taken to be roughly equal to the EPR lifetime ($\sim 10^9$ sec^{-1})[56] at the coalescence temperature ($\sim$200 K), then a value for $E_{th}^{\ddagger}$ can be obtained using the relation

$$k_{th} = \frac{kT}{h} e^{-E_{th}^{\ddagger}/RT}$$

where the symbols have their usual meaning from absolute reaction rate theory, and the transmission coefficient is assumed to be unity for adiabatic electron transfer.[48] This gives a value of 3.3 kcal for the activation barrier and assuming the same value at room temperature yields 2.2×10^{10} sec^{-1} for k_{th} at 298° K. It is to be emphasized that these calculations are merely a rough approximation and are contingent upon the validity of the frequency term and the assumption that no mechaniicistic change occurs between 200 and 298° K.

Other mixed valence systems have been reported to show temperature dependence in their thermal electron transfer properties. The 77° K Mössbauer spectrum of magnetite Fe(III)[Fe(II)Fe(III)]O_4 revealed distinct Fe(III) and Fe(II) ions in octahedral sites while at 300° K they were indistinguishable.[57] In another Mössbauer study the spectra of a series of trinuclear iron clusters Fe(II)Fe(III$_2$)O$(CH_3CO_2)_6 \cdot L_x$ were recorded at several temperatures (77 to 298° K) and the iron valences also became indistinguishable on this time scale (10^{-7} sec).[58]

The electronic spectra of Cu(II)Cu(I)L(ClO_4) in various media are complicated, and definitive interpretation is not possible at present. That the bands in the near

IR and visible regions are due primarily to intervalence-transfer is consistent with the disappearance of the IR bands and the intensity reduction of the 600 nm bands on exposure to CO or O_2 and the lack of these features in the Cu(II)Cu(II) and Cu(I)Cu(I) complexes, although the low solubility of Cu(I)Cu(I)L made it impossible to obtain spectra of solutions of comparable concentration. The intensities of these absorptions are large enough to preclude their assignments as pure ligand-field transitions even for low symmetry environments. Their relatively low energies make them unlikely candidates for charge transfer involving ligands (N and O donors in this macrocycle).

Application of the Hush model to relate the thermal and optical electron transfer processes in a simple fashion is probably inappropriate in this system. For copper complexes the solvent molecules can be regarded as more or less directly involved, depending on their donor strength, in the inner coordination sphere of either or both oxidation states. This would influence the energy of both the thermal and photo-induced processes in a manner different from the effect of a dielectric continuum. Moreover, the varying number of bands observed complicates the use of a simple model. In addition to the basic IT transition involving the same d-orbitals

on different metal atoms, transitions to empty higher-energy orbitals or from filled lower-energy d-orbitals are possible. These additional bands should occur at energies roughly corresponding to the IT transition plus an associated ligand field transition. Such bands have been reported for Prussian blue $KFe(II)Fe(III)(CN)_6 \cdot H_2O$[59] and biferrocenium [Fe(II)Fe(III)][51]. For $Cu(II)Cu(I)L(ClO_4)$ a similar interpretation of the spectra might hold. The variation in the number of bands observed with different solvents and in the solid state is reminiscent of the behavior of the ligand-field spectra of certain square-planar Cu(II) complexes, notably $Cu(acac)_2$ toward solvents of different donor strength.[60] Yet no orbital energy ordering for square-planar or square-pyramidal geometries can satisfactorily account for the solvent independence of the 600 nm band. Furthermore, the lower intensity of CH_3CN solution band(s) remains inexplicable. A less speculative discussion of the electronic spectra of this complex will require additional research.

Cu(I)Cu(I) Compounds. All of the physical studies on Cu(I)Cu(I)L (elemental analysis, IR spectroscopy, and magnetic susceptability) are consistent with its formulation as a Cu(I)Cu(I) compound. Relatively few binuclear Cu(I)Cu(I) compounds are known, although recently attempts to model binuclear copper sites in

proteins have led to the synthesis of several such compounds.[61-64] The lack of solubility for this compound has precluded extensive characterization in solution. On the other hand, since $Cu(I)Cu(I)L(CO)_2$ could not be isolated from solution the evidence for its existence consists of the stoichiometry involved in its preparation and the CO stretching band in the solution IR spectrum. Further study is obviously required for these systems.

Conclusion

Use of a binucleating macrocyclic ligand has led to isolation of mixed valence, Cu(II)Cu(I), and fully reduced, Cu(I)Cu(I), complexes in which each copper ion experiences a similar coordination environment. The mixed valence species, $Cu(II)Cu(I)L^+$ exhibits unusual electronic absorption and temperature dependent EPR spectral properties. The latter permit an estimate of 2.2×10^{10} sec^{-1} for the rate of thermal intramolecular electron transfer. Both $Cu(II)Cu(I)L^+$ and Cu(I)Cu(I)L reversibly bind CO forming $Cu(II)Cu(I)L(CO)^+$ and $Cu(I)Cu(I)L(CO)_2$, respectively, new examples of five coordination for Cu(I).

Experimental

Materials. All chemicals were reagent grade and were used as received unless otherwise noted. Copper(II) perchlorate, ground to a powder then dried to a constant weight in vacuo (25°), was used as $Cu(ClO_4)_2 \cdot 6H_2O$. Tetrabutylammonium perchlorate TBAP (Southwestern Analytical Chemicals) was dried exhaustively in vacuo (25°) before use. Reagent grade N,N-dimethylformamide, DMF, was dried successively over $MgSO_4$ and $CuSO_4$ and then over 4A molecular sieves for 48 hours and vacuum distilled. 5-Methyl-2-hydroxyisophthalaldehyde was prepared by a modification of the literature method.[65]

Physical Measurements. Sample preparation for physical studies on the air-sensitive materials were accomplished in a Vacuum Atmospheres Dri-lab glove box with a helium atmosphere. Thoroughly deaerated spectro-quality solvents were used for solution studies.

Magnetic susceptibility determinations were done with powdered samples at room temperature using a Cahn Instruments Faraday balance; $HgCo(SCN)_4$ was used as a calibrant, and diamagnetic corrections were made using Pascal's constants.

X-band EPR spectra were recorded on a Varian E-line spectrometer. Temperature control was achieved with an

Air Products Heli-Tran liquid helium transfer refrigerator. Samples were contained in cylindrical quartz tubes of 2 or 3 mm diameter equipped with stopcocks and I 14/20 joints. Solutions of the carbonyl complex, $Cu(II)Cu(I)L(CO)^{+}$ were generated from those of $Cu(II)Cu(I)L^{+}$ by evacuating the helium atmosphere in the cell and then admitting carbon monoxide gas.

Electronic spectra were recorded on Cary 14 spectrophotometers. Solid state spectra were obtained with Nujol mulls on filter paper with the mulling agent in the reference compartment. Solution spectra were recorded using 1 cm quartz cells equipped with stopcocks to facilitate addition of CO as described for the EPR procedure. Solvent was run against solvent to obtain a baseline.

Infrared spectra were recorded on a Beckman IR-12 Infrared Spectrophotometer. Solid-state spectra were recorded using Nujol mulls pressed between KBr plates. Solution spectra were obtained using calcium fluoride solution cells (1 mm).

Carbon monoxide stoichiometries were obtained using a modified Warburg Manometer. Both the cell and burette system were water-jacketed at 22° C. The uptakes were performed at a constant pressure of 741 mm Hg.

Electrochemistry. The apparatus used for constant potential electrolysis (CPE) and cyclic voltammetry consisted of a Princeton Applied Research Model 173 potentiostat-galvanostat coupled with a Model 179 digital coulometer, plus a voltage ramp generator of our own design. A PAR Model 174A polarographic analyzer was used for d.c. polarography and differential pulse voltammetry. For display purposes, both a storage oscilloscope and a X-Y recorder were used.

Constant potential electrolysis and cyclic voltammetry were done in a three compartment H-cell. The cell consisted of 25 ml working and auxiliary compartments separated by a small center compartment, all separated by medium porosity sintered glass frits. In all solvents the supporting electrolyte was 0.1 M TBAP.[6] For CPE the working electrode was a mercury pool and for every technique the auxiliary electrode was a coiled platinum wire. The reference electrode consisted of a silver wire immersed in an acetonitrile solution containing $AgNO_3$ (0.01 M) and TBAP (0.1 M), all contained in an 9 mm glass tube fitted on the bottom with a fine porosity sintered glass frit.

All potentials are reported versus the normal hydrogen electrode, NHE. Instead of attempting to correct

potentials measured against the $Ag/AgNO_3$ (0.01 M), TBAP (0.1 M), CH_3CN reference electrode, an internal reference redox couple was used. It has been proposed that the oxidation of ferrocene to ferrocenium ion occurs at the same potential in every solvent.[66] In water the process occurs at +0.400 V versus NHE.[67] Experimentally, small amounts (5×10^{-5} M to 10^{-3} M) of ferrocene were added to solutions containing the compounds of interest and formal potentials for both couples were measured under the same conditions. Ferrocene is not easily reduced and did not react with the reduced forms of the copper complexes. Comparison of potentials to ferrocene oxidation is more reproducible and provides a better estimate of potentials versus the NHE because unknown junction potentials associated with the Ag/Ag^+ or saturated calomel electrodes are avoided.

Cu(II)Cu(II)L$(ClO_4)\cdot 2H_2O$ was prepared via a modification of the method reported by Robson.[2] 1,3-Diaminopropane (1.19 g, 1.34 ml, 16 mmoles) was slowly added to a solution of $Cu(ClO_4)_2\cdot 6H_2O$ (5.9 g, 16 mmoles) in methanol (25 ml). A second solution containing 5-methyl-2-hydroxyisophthalaldehyde (2.5 g, 15.2 mmoles) in boiling methanol was then added dropwise to the copper-amine mixture. The resulting solution was heated to boiling for one hour

and cooled to room temperature. The solution was reduced to a small volume (~20 ml) using a rotary evaporator and was cooled for several hours in a refrigerator. A light green solid formed which was removed by filtration. The filtrate was further reduced in volume by evaporation until just before dryness. During this process more solid formed which was collected and combined with the original precipitate. After being washed with cold water and air-dried, the solid was added to boiling water (~100 ml/g of solid), stirred for about five minutes and filtered. Slow cooling of the filtrate yielded emerald green needles which were isolated by vacuum filtration, washed with cold water and dried under vacuum. Calculated for $C_{24}H_{30}N_4O_{10}Cl_2Cu_2$: C, 37.71, H, 3.96; N, 7.33; Cu, 16.62. Found: C, 37.7; H, 3.8; N, 7.1; Cu, 16.6.

Cu(II)Cu(I)L(ClO_4), was prepared in a helium atmosphere from the Cu(II)Cu(II) complex by constant potential electrolysis at -0.71 V. Details of the electrolysis cell and instrumentation are given earlier in this experimental section. The working compartment initially contained 0.35-0.40 g of the Cu(II)Cu(II) species in DMF (25 ml). During the electrolysis the solution changed in color from green to blue. After completion of the electrolysis (n = 1.0 ± 0.1) the

working compartment solution was transferred to a separate vessel and diethyl ether (50-75 ml) was added causing a dark brown solid to precipitate. After filtration the solid was dried and recrystallized from a saturated solution of boiling methanol, yielding dark brown needles which were dried in vacuo. Calculated for $C_{24}H_{26}N_4O_6ClCu_2$: C, 45.83; H, 4.17; N, 8.9; Cu, 20.20. Found: C, 45.6; H, 4.4; N, 8.7; Cu 19.85.

Cu(II)Cu(I)L(ClO_4)(CO) was synthesized using Schlenk techniques by the addition of carbon monoxide to solutions of the precursor mixed valence complex, Cu(II)Cu(I)L(ClO_4). Under a CO atmosphere solid Cu(II)Cu(I) complex was dissolved in a minimum volume of DMF and the resulting solution was filtered. Diethyl ether, which was deaerated by bubbling with CO, was added slowly to the filtrate until a light brown solid precipitated. The solid was collected by filtration and dried under a stream of CO. Calculated for $C_{25}H_{26}N_4O_7ClCu_2$: C, 45.70; H, 3.99; N, 8.53; Cu, 19.34. Found: C, 45.9; H, 4.25; N, 8.65; Cu, 19.05.

Cu(I)Cu(I)L was synthesized under a helium atmosphere from the Cu(II)Cu(II) complex by constant potential electrolysis at -0.71 V and then at -1.16 V. Initially, electrolysis was carried out at -0.71 V as described in the preparation of the Cu(II)Cu(I) complex, Cu(II)Cu(I)L(ClO_4).

The solution was then further reduced at -1.16 V (n = 1.0 ± 0.1). During the latter process a dark brown, almost insoluble, powder formed which was collected and dried. The compound was redissolved in a small volume of DMF under a CO atmosphere, using Schlenk techniques. After filtration the CO was allowed to slowly (over a 48 hr period) diffuse out of solution into an argon stream. Shiny black crystals formed which were collected and dried in vacuo. Calculated for $C_{24}H_{26}N_4O_2Cu_2$: C, 54.43; H, 4.95; N, 10.58; Cu, 24.00. Found: C, 54.1; H, 5.05; N, 10.75; Cu, 24.4.

Zn(II)Zn(II)L$(ClO_4)_2 \cdot 2H_2O$. 1,3-Diaminopropane (0.5 ml, 6.0 mmoles) followed by $Zn(ClO_4)_2 \cdot 6H_2O$ (2.27 g, 6.1 mmoles) in methanol (25 ml) were added to a solution of 5-methyl-2-hydroxyisophthalaldehyde (1.0 g, 6.1 mmoles) in ethanol (100 ml) with stirring and mild heating. A yellow precipitate formed immediately on addition of the zinc salt but it quickly dissolved giving a yellow solution. The solvent was evaporated to near dryness, with gentle heating, and was cooled to the ambient temperature. The resulting orange-yellow solid was isolated by filtration then recrystallized from 1:1 ethanol/methanol to give a bright yellow microcrystalline powder. Calculated for $C_{24}H_{30}N_4O_{10}Cl_2Zn_2$: C, 37.52; H, 3.94; N, 7.30; Zn, 17.02. Found: C, 37.7; H, 3.9; N, 7.0; Zn, 17.7.

References

1. For example see References 2-4 and references contained therein.

2. N. H. Pilkington and R. Robson, Aust. J. Chem. 23, 225-36 (1970).

3. M. D. Glick and R. L. Lintvedt, Progr. Inorg. Chem. 21, 233-260 (1976); S. E. Groh, Israel J. Chem. 15, 277-307 (1977); George R. Newkome, J. D. Sauer, J. M. Roper and D. C. Hagar, Chem. Rev. 77, 513-97 (1977).

4. H. Okawa, V. Kasempimolporn and S. Kida, Bull. Chem. Soc. Jap. 51, 647-48 (1978); H. O. Okawa, U. Nishida, M. Tanaka and S. Kida, ibid. 50, 127-31 (1977); H. Okawa, T. Tokii, Y. Nonaka, Y. Muto and S. Kida, ibid. 46, 1462-65 (1973); and references therein.

5. R. R. Gagné, C. A. Koval and T. J. Smith, J. Am. Chem. Soc. 99, 8367-68 (1977).

6. Abbreviations used in this paper include: E^f, formal reduction potential; HMDE, hanging mercury drop electrode; TBAP, tetrabutylammonium perchlorate; DMF, N,N-dimethylformamide.

7. R. N. Adams, Electrochemistry at Solid Electrodes, Marcel Dekker, Inc., New York (1969) pp. 144, 145.

8. L. Meites, Polarographic Techniques, John Wiley and Sons, Inc., New York (1965) p. 218.

9. E. P. Parry and R. A. Osteryoung, Anal. Chem. 37, 1634-7 (1965).

10. R. R. Gagné, J. L. Allison, R. S. Gall and C. A. Koval, J. Am. Chem. Soc. 99, 7170-78 (1977).

11. A. W. Addison, M. Carpenter, L. K-M. Lav and M. Wicholas, Inorg. Chem. 17, 1545-52 (1978).

12. G. C. Percy and D. A. Thorton, J. Inor. Nucl. Chem. 34, 3357-67 (1972).

13. M. I. Bruce, J. Orgmet. Chem. 44, 209-26 (1972); M. I. Bruce and A. P. Ostaycwski, J.C.S. Chem. Commun. 1124-5 (1972); M. R. Churchill, B. G. DeBoer, F. J. Rotella, O. M. Abu Salah and M. I. Bruce, Inorg. Chem. 14, 2051-6 (1976); C. Meall, C. S. Arcus, J. L. Wilkinson, T. J. Marks and J. A. Ibers, J. Am. Chem. Soc. 98, 711-18 (1976); R. R. Gagné, R. S. Gall, G. C. Lisensky, R. E. Marsh and L. R. Speltz, Inorg. Chem. 18, 0000 (1979); and reference 10.

14. E. F. Hasty, T. J. Colburn and D. N. Hendrickson, Inorg. Chem. 12, 2414-2421 (1973).

15. C. Sigwart, P. Hemmerich and J. T. Spence, Inorg. Chem. 7, 2545-2548 (1968).

16. C. P. Slichter, Phys. Rev. 99, 478-80 (1955).

17. This treatment was used by Chang in analyzing confacial copper porphyrins.[18] The latter gave EPR spectra essentially the same as that obtained

for the dimer here. From the dimer spectrum $g_{||}$ = 2.591 and $\frac{2D_{||}}{g_{||}\beta}$ = 865 G where $D_{||}$ is the zero field splitting and β is the Bohr magneton.[19] Solving for $D_{||} = 0.0052\ cm^{-1}$. A value for the Cu-Cu distance can be obtained from the relation[20] $r = (0.65\ g_{||}^2/D_{||})^{1/3}$, giving a value of 4.4 Å which is comparable to the 4.2 Å separation found for the porphyrins.[18]

18. C. K. Chang, J. Heterocyclic Chem. 14, 1285-88 (1977).

19. C. -C. Chao and J. H. Lindsford, J. Chem. Phys. 57, 2890-98 (1972).

20. E. F. Hasty, L. J. Wilson, and D. N. Hendrickson, Inorg. Chem. 17, 1834-41 (1978).

21. J. A. Huheey, Inorganic Chemistry, Harper and Row, New York (1972), p. 259.

22. I. M. Kolthoff and J. F. Coetzee, J. Am. Chem. Soc. 79, 1852-58 (1957).

23. B. F. Hoskins, R. Robson and G. A. Williams, Inorg. Chim. Acta 16, 121-33 (1976).

24. R. R. Gagné, T. Smith and C. Koval, unpublished results.

25. C. Creutz and H. Taube, J. Am. Chem. Soc. 95, 1086-94 (1973).

26. G. S. Patterson and R. H. Holm, Bioinorg. Chem. 4, 257-75 (1975).

27. B. R. Reinhammar and T. I. Vänngård, Eur. J. Biochem, 18, 463-68 (1971); B. R. Reinhammar, Biochem. Biophys. Acta 275, 245-59 (1972).

28. N. Makino, P. McMahill and H. S. Mason, J. Biol. Chem. 249, 6062-66 (1974).

29. E. I. Solomon, D. M. Dooley, R. Wang, H. B. Gray, M. Cerdonio, F. Mogno and G. L. Romani, J. Am. Chem. Soc. 98, 1029-31 (1976).

30. F. Ammar and J. M. Savéant, Electroanal. Chem. Interfacial Electrochem. 47, 115-25 (1973); 47, 215-21 (1973).

31. D. S. Polcyn and I. Shain, Anal. Chem. 38, 370-75 (1966).

32. R. L. Myers and I. Shain, Anal. Chem. 41, 980 (1969).

33. J. B. Flanagan, S. Margel, A. J. Bard and F. C. Anson, J. Am. Chem. Soc. 100, 4248-53 (1978).

34. J. Phelphs and A. J. Bard, J. Electroanal. Chem. 68, 313-35 (1976).

35. W. H. Morrison, Jr., S. Krogsrud and D. N. Hendrickson, Inorg. Chem. 12, 1998-2004 (1973).

36. For example, see: R. E. Dessy, P. M. Weissman and R. L. Pohl, J. Am. Chem. Soc. 88, 5117-21 (1966); R. E. Dessy, R. Kornmann, C. Smith and R. Haytor, ibid. 90, 2001-04 (1968).

37. N. H. Furman and G. Stone, J. Am. Chem. Soc. 70, 3055-61 (1948).

38. For example see References 25, 39-41.

39. R. W. Callahan, F. R. Keene, T. J. Meyer and D. J. Salmon, J. Am. Chem. Soc. 99, 1064-73 (1977).

40. G. M. Tom, C. Creutz and H. Taube, J. Am. Chem. Soc. 96, 7827-9 (1974).

41. T. R. Weaver, T. J. Meyer, S. A. Adeylmi, G. M. Brown, R. P. Eckberg, W. E. Hatfield, E. C. Johnson, R. W. Murray, and D. Untereker, J. Am. Chem. Soc. 97, 3039-48 (1975).

42. R. L. Lin vedt, B. Tomlonovic, D. E. Fenton and M. D. Glick, Adv. Chem. Series 32, 407-25 (1975).

43. $E_{1/2}$ = -0.995 V vs nhe; slope of -E vs log $i/(i_d-i)$ plot = 56.6 mV; cpe at -1.2 V yields an n-value of 1.0 ± 0.1; R. R. Gagné, R. P. Kreh and C. A. Koval, unpublished results.

44. D. E. Fenton, R. R. Schroeder and R. L. Linvedt, J. Am. Chem. Soc., 100, 1931-2 (1978).

45. A. W. Addison, Inorg. Nucl. Chem. Lett. 12, 899-903 (1976).

46. M. B. Robin and P. Day, Advan. Inorg. Chem. Radiochem. 10, 247-422 (1967).

47. N. S. Hush, Prog. Inorg. Chem. 8, 391-444 (1967).

48. T. J. Meyer, Accts. Chem. Res. 11, 94-100 (1978).

49. M. J. Powers and T. J. Meyer, J. Am. Chem. Soc. 100, 4393-98 (1978).

50. W. H. Morrison and D. N. Hendrickson, J. Chem. Phys. 59, 380-86 (1973).

51. W. H. Morrison and D. N. Hendrickson, Inorg. Chem. 14, 2331-2346 (1975).

52. J. K. Beattie, N. S. Hush and P. R. Taylor, Inorg. Chem. 15, 992,993 (1976).

53. B. C. Bunker, R. S. Drago, D. N. Hendrickson, R. M. Richman and S. L. Kessell, J. Am. Chem. Soc. 100, 3805-14 (1978).

54. F. Basolo and R. G. Pearson, Mechanisms of Inorganic Reactions, 2nd Ed., John Wiley and Sons, New York (1968) p. 454.

55. R. R. Gagné, J. L. Allison, G. C. Lisensky, Inorg. Chem. in press.

56. Estimated by T. Smith.

57. R. Bauminger, S. G. Cohen, A. Marinova, S. Offer, and E. Segal, Phys. Rev. 122, 1447-50 (1961).

58. D. Lupu, D. Barb, G. Filott, M. Morariu and D. Tarina, J. Inorg. Nucl. Chem. 34, 2803-10 (1972).

59. M. B. Robin, Inorg. Chem. 1, 337-342 (1962).

60. R. L. Belford, M. Calvin and G. Belford, J. Chem. Phys. 26, 1165-74 (1957).

61. J. E. Bulkowski, P. L. Burk, M. F. Ludmann and J. A. Osborn, J.C.S. Chem. Commun. 498-9 (1977).

62. J. M. Lehn, S. H. Pine, E. Watanabe and A. K. Willard, J. Am. Chem. Soc. 99, 6766-68 (1977).

63. A. H. Alberts, R. Annunziata and J. M. Lehn, J. Am. Chem. Soc. 99, 8502-4 (1977).

64. R. R. Gagné, J. Dodge and R. P. Kreh, manuscript in preparation.

65. F. Ullmann and K. Brittner, Chem. Ber. 42, 2539-48 (1909).

66. D. Bauer and M. Breant, Electroanalytical Chemistry, A. J. Bard, ed., Vol. 8 Marcel-Dekker, Inc., New York (1975) pp. 282-344.

67. H. M. Koepp, H. Wendt and H. Strehlow, Zeit. Electrochim. 64, 483-91 (1960).

APPENDIX 1

Models for Copper-Containing Proteins: Structure and Properties of Novel Five-Coordinate Copper(I) Complexes

Robert R. Gagné, Judith L. Allison, Robert S. Gall, and Carl A. Koval

Originally Published: J. Am. Chem. Soc. 99, 7170 (1977)

[Reprinted from the Journal of the American Chemical Society, 99, 7170 (1977).]

Models for Copper-Containing Proteins: Structure and Properties of Novel Five-Coordinate Copper(I) Complexes

Robert R. Gagné,* Judith L. Allison, Robert S. Gall, and Carl A. Koval

Contribution No. 5554 from the Division of Chemistry and Chemical Engineering, California Institute of Technology, Pasadena, California 91125. *Received March 31, 1977*

Abstract: The four-coordinate Cu(I) complex [difluoro-3,3′-(trimethylenedinitrilo)bis(2-butanone oximato)borate]copper(I), $Cu(LBF_2)$, can be produced by electrochemical reduction of the corresponding Cu(II) complex. The Cu(I) complex reacts with monodentate ligands (e.g., CO, 1-methylimidazole, acetonitrile) yielding five-coordinate adducts. The structure of the carbonyl derivative has a square-pyramidal copper displaced 0.96 Å out of the basal nitrogen plane. The Cu–CO distance is 1.780 (3) Å, with a Cu–C–O angle of 177.5 (3)°. The C–O bond length is 1.112 (4) Å. The space group is *Pbca* with a = 13.926 (1) Å, b = 14.209 (1) Å, c = 16.297 (1) Å, Z = 8, and R = 5.5%. Preliminary equilibrium constants were determined by cyclic voltammetry and by absorption spectroscopy. Carbon monoxide ($K_c = 4.7 \times 10^4\ M^{-1}$) binds significantly better than 1-MeIm ($K_c = 16\ m^{-1}$). The possible biochemical significance of five-coordinate Cu(I) is discussed.

Introduction

Numerous copper-containing proteins utilize molecular oxygen in respiratory and biosynthetic functions.[1-3] The best studied copper proteins, hemocyanin and tyrosinase, serve, respectively, in O_2 transport and in activating O_2 for the oxidation of tyrosine.[4] Both tyrosinase and hemocyanin apparently contain a pair of contiguous Cu atoms, commonly designated type III copper, at the active site. The structural nature of the type III copper site is not known for any protein. Stoichiometry,[13,14] EPR,[15-19] and magnetic susceptibility measurements[18-20] on various derivatives of hemocyanin and tyrosinase, however, suggest a strongly antiferromagnetically coupled pair of copper atoms separated by some 3–5 Å.[5-7] The number and identity of ligands bound to either copper are not known. Nonetheless, titration[21,22] and spectroscopic[23,24] studies tend to preclude sulfur and favor nitrogen ligands, probably imidazole nitrogen.

The paucity of structural and mechanistic information for these copper proteins is paralleled by an equally sparse literature on the reactions of Cu(I) complexes, particularly with nitrogen ligands.[25] Extreme lability, facile disproportionation, and air sensitivity have frustrated attempts to explore reactions of copper–nitrogen ligand complexes. For example, there are no well-characterized dioxygen complexes derived from Cu(I)[26] despite the large number of O_2 complexes known for several other metals.[27-30]

To help elucidate possible active site structures and mechanisms of copper protein activity, we are exploring the basic relationships between structure and chemical reactivity in a variety of Cu(I) complexes of predominantly nitrogen ligands. Both mononuclear and binuclear complexes are under investigation, in the hopes of eventually explaining the apparent necessity for a binuclear copper site (type III) for O_2 binding in the proteins.[4] Herein we report the synthesis and properties of novel *five*-coordinate Cu(I) complexes which have been communicated previously.[31]

Results and Discussion

Deducing structure–reactivity relationships for Cu(II) complexes is complicated by a number of factors which can be controlled, as follows.

(1) Both Cu(I) and Cu(II) are rather substitution labile.[25-33] Thus, complexes of monodentate and even bidentate ligands often lead to solutions containing several species including two-, three- and four-coordinate monomers as well as dimers, etc. Use of polydentate ligands, including macrocycles, inhibits both dissociation and dimer formation (via bridging atoms of the polydentate ligand) especially if the chelate is somewhat rigid structurally, as macrocycles are. Explaining solution behavior, especially in reference to solid-state structures, is thus simplified appreciably.

(2) Many Cu(I) complexes disproportionate rapidly at the ambient temperature to Cu(II) and Cu(0).[33] Ligand environments having saturated amines and/or an enforced rigid, square-planar structure destabilize Cu(I) with respect to Cu(II), as shown by electrochemical studies.[34,35] Conversely, employing flexible yet unsaturated nitrogen ligands should preclude disproportionation.

(3) Reducing Cu(II) to Cu(I) without undesirable further reduction to Cu(0) is difficult with most common chemical reducing agents. Likewise, complexing Cu(I) directly by reaction between some appropriate Cu(I) salt and a polydentate ligand most often leads to disproportionation, possibly owing to unstable intermediates.[36-39] Electrochemical reduction at constant potential has, however, been shown[35] to be both specific and practical.

(4) Finally, it must be recognized that most Cu(I) complexes are very air-sensitive. Schlenk, vacuum-line, and modern inert-atmosphere chamber techniques render this a relatively trivial problem.

After examining several other polydentate and macrocyclic ligand systems, the results of which are reported in part elsewhere,[39] we have found the tetradentate ligand **1** to adequately fulfill the requirements above and to yield novel Cu(I) chemistry.[31] The free ligand, 3,3′-(trimethylenedinitrilo)bis(2-butanone dioxime) (**1**, H_2L), has been prepared previously,[40] using boiling diisopropyl ether as solvent, although this procedure is difficult. Large quantities of ligand can be obtained far more simply, however, by combining 2,3-butanedione monoxime with 1,3-diaminopropane in ethanol at 25 °C (eq 1).

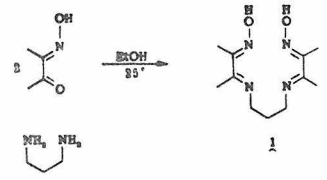

(1)

1

Treating warm acetone or ethanol solutions of the macrocycle **1** with Cu(II) salts gives red to green mixtures depending on the ligand to Cu(II) ratio. With a twofold excess of ligand,

Table I. Cyclic Voltammetric Data for $[Cu(LBF_2)ClO_4]_2$-$C_4H_8O_2$ (5)[a]

Solvent	E_{p_c},[b] V	E_{p_a},[b] V	E^f,[b,c] V	i_{p_c}, μA	i_{p_a}, μA
CH_3CN	−0.432	−0.330	−0.381	18	19
$(CH_3)_2CO$	−0.459	−0.345	−0.402	18	17

[a] Conditions: [Cu] = 2×10^{-3} M under inert atmosphere; sweep rate = 100 mV/s; hanging mercury drop electrode. [b] Potentials are given vs. SHE as calculated in Table X. [c] $E^f = (E_{p_c} + E_{p_a})/2$.

dark red-brown, crystalline $Cu(HL)ClO_4 \cdot H_2O$ (2) can be isolated. The product is contaminated with excess copper, possibly because of small amounts of a binuclear species such as 3. This species may be similar to the Cu(II) complex obtained[41] with salicylaldehydeethylenediamine, 4.

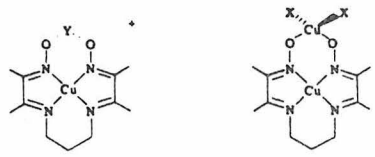

2, Y = H
5, Y = BF_2

3

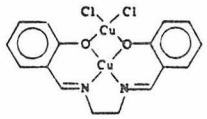

4

To inhibit binding of a second copper atom and to prevent possible hydrogen atom transfer reactions (as to dioxygen coordinated to copper), the bridging oxime hydrogen in 2 was replaced with BF_2 via treatment with boron trifluoride etherate in dioxane. The resulting complex has an analysis consistent with the formulation $[Cu(LBF_2)ClO_4]_2$-$C_4H_8O_2$ (5). It has not been determined whether dioxane is acting as a μ-bidentate bridge between two coppers or is present simply as solvent of crystallization.

The reduction of complex 5 was attempted by several chemical reducing agents, including Na, Zn, Mg, and their amalgams, and hydrazine. In all cases some Cu(0) was produced, by direct reduction of Cu(II) or by disproportionation of intermediate Cu(I) species. For this reason, the electrochemical behavior of the complex was examined.

Cyclic voltammograms of 5 have been obtained both in acetonitrile and in acetone. A scan, representative of the first reduction process in either solvent, is given in Figure 1.[42] While the anodic and cathodic peak currents are nearly equal, the peak potential separation is much larger than the 58 mV expected for a reversible, one-electron process. That this reduction does involve only a single electron is confirmed by constant potential electrolysis at potentials slightly negative of the wave (~ −0.7 V) yielding n values of 1.0 ± 0.05.

The potential of the Cu(II)/Cu(I) couple for 5 (E^f = −0.381; see Table I) is more positive than that for complex 2 (E^f = −0.560; see Experimental Section) indicating a possible stabilization of Cu(I) in the former. Indeed, gram quantities of $Cu(LBF_2)$ (6) can be synthesized by CPE at −0.7 V. During the electrolysis, the original purple solution (Cu(II)) becomes deep blue (Cu(I), λ_{max} 677 nm) with subsequent precipitation of a microcrystalline, red solid. The product, which is blue upon being ground to a powder (an optical phenomenon since there is no other indication of chemical decomposition), is apparently not air-sensitive in the solid state.

In a formal sense the blue Cu(I) complex, $Cu(LBF_2)$, 6, is

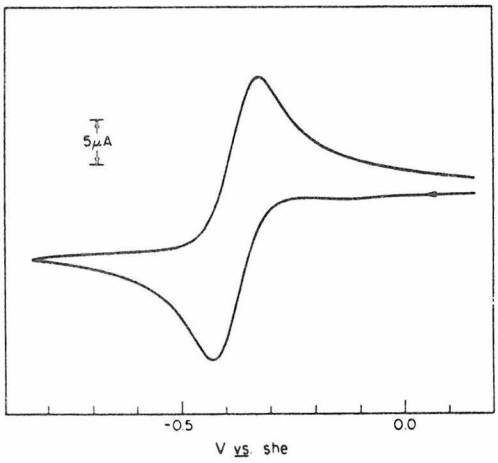

Figure 1. Cyclic voltammetry of $[Cu(LBF_2)(ClO_4)]_2$-$C_4H_8O_2$ (5) in CH_3CN. Scan rate = 100 mV/s. [Cu] = 2×10^{-3} M.

a four-coordinate 18-electron system and as such is coordinatively saturated. Nonetheless, 6 reacts with a number of monodentate ligands to give presumably five-coordinate Cu(I) complexes. For example, addition of 1-methylimidazole, (1-MeIm) to the blue complex 6 in acetone gives a green solution (λ_{max} 420 nm) from which the imidazole adduct, $Cu(LBF_2)$(1-MeIm) (7) can be isolated. Even acetonitrile, usually considered a weak ligand, binds to $Cu(LBF_2)$ (6), giving aquamarine solutions at 25 °C. Green acetonitrile solutions result upon cooling to −40 °C, presumably indicating a greater degree of complex formation at the lower temperature.

Most surprisingly, carbon monoxide reacts rapidly with blue $Cu(LBF_2)$ (6) solutions at 25 °C, yielding light yellow solutions. The reaction is readily reversed upon purging with nitrogen. A stable carbonyl adduct can be isolated from CO treated solutions as a bright yellow microcrystalline material (ν_{CO} 2068 cm^{-1}), $Cu(LBF_2)(CO)$ (8). The solution infrared spectrum of $Cu(LBF_2)(CO)$ (8), (CH_2Cl_2, 1 atm CO) shows only a single peak attributable to coordinated CO (ν_{CO} 2080 cm^{-1}). This is consistent with the presence of a single carbonyl species in solution. Finally, the similarity between ν_{CO} in solution (2080 cm^{-1}) and in the solid state (2068 cm^{-1}) suggests that the solution species is most probably a five-coordinate, monocarbonyl adduct (vide infra).

Crystal Structure

The carbonyl adduct $Cu(LBF_2)(CO)$ (8) was easily crystallized by evaporation of an acetone solution, permitting a structural determination. Figure 2 shows the structure and labeling scheme of the novel copper(I) carbonyl complex while Table II details the crystal data. The structure's uniqueness lies in five-coordination for copper(I) which gives rise to a 20-electron count for the metal atom coordinated to five two-electron donors. Although five-coordination is known for other d^{10} metals,[43] it is not common for copper(I). In addition,

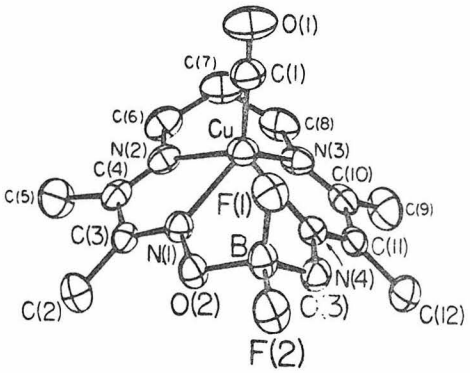

Figure 2. An ORTEP drawing of the structure and numbering scheme of $Cu(LBF_2)(CO)$ (8) with thermal ellipsoids at the 40% probability level. Hydrogen atoms are omitted.

Table II. Crystal Data for $Cu(LBF_2)(CO)$ (8)

Formula	$Cu(BF_2C_{11}H_{18}N_4O_2)CO$
FW	378.64
Space group	D_{2h}^{15}-*Pbca* (no. 61)
a	13.926 (1) Å
b	14.209 (1) Å
c	16.297 (1) Å
V	3224.8 Å^3
Z	8
ρ_{calcd}	1.56 g cm^{-3}
ρ_{obsd}	1.55 (3) g cm^{-3}
λ(Cu K$\bar{\alpha}$)	1.5418 Å
μ(Cu K$\bar{\alpha}$)	23.293 cm^{-1}

Table III. Bond Distances (Å)

Cu-N1	2.165 (2)	N1-C3	1.275 (3)
Cu-N4	2.163 (2)	N2-C4	1.277 (4)
Cu-N2	2.100 (2)	N2-C6	1.459 (4)
Cu-N3	2.108 (2)	C2-C3	1.488 (4)
		C3-C4	1.485 (4)
Cu-C1	1.780 (3)	C4-C5	1.484 (5)
O1-C1	1.112 (4)	C7-C8	1.500 (5)
F1-B	1.386 (4)		
F2-B	1.379 (4)	C2-H1	0.86 (3)
O3-B	1.478 (4)	C2-H2	0.93 (3)
O2-B	1.475 (4)	C2-H3	0.93 (3)
		C5-H4	0.82 (3)
O2-N1	1.374 (3)	C5-H5	1.05 (3)
O3-N4	1.371 (3)	C5-H6	0.89 (3)
		C6-H7	0.85 (3)
N4-C11	1.283 (3)	C6-H8	1.02 (3)
N3-C10	1.269 (4)	C7-H9	0.92 (3)
N3-C8	1.471 (4)	C7-H10	0.91 (3)
C11-C12	1.480 (4)	C8-H11	1.01 (3)
C10-C11	1.494 (4)	C8-H12	0.97 (3)
C9-C10	1.497 (5)	C9-H13	0.98 (3)
C6-C7	1.502 (5)	C9-H14	0.97 (3)
		C9-H15	0.89 (3)
		C12-H16	0.90 (3)
		C12-H17	0.94 (3)
		C12-18	0.87 (3)

Table IV. Bond Angles (Deg)

N2-Cu-N4	124.7 (1)	F1-B-F2	110.7 (3)
N1-Cu-N3	127.6 (1)	F1-B-O2	110.7 (3)
N1-Cu-N4	79.1 (1)	F1-B-O3	110.8 (3)
N2-Cu-N3	85.9 (1)	F2-B-O2	105.1 (3)
N3-Cu-N4	73.8 (1)	F2-B-O3	105.8 (3)
N1-Cu-N2	73.9 (1)	O2-B-O3	113.4 (3)
Cu-N1-O2	126.4 (2)	O3-N4-C11	116.0 (2)
Cu-N4-O3	126.2 (2)	O2-N1-C3	115.7 (2)
Cu-N1-C3	117.5 (2)	N1-O2-B	112.5 (2)
Cu-N2-C4	118.0 (2)	N4-O3-B	112.9 (2)
Cu-N2-C6	120.2 (2)		
Cu-N3-C8	119.4 (2)	N1-C3-C2	123.9 (3)
Cu-N3-C10	118.5 (2)	N1-C3-C4	113.6 (3)
Cu-N4-C11	117.8 (2)	N2-C4-C5	124.3 (3)
		N2-C4-C3	116.3 (3)
N1-Cu-C1	114.9 (1)	N3-C10-C9	125.6 (3)
N2-Cu-C1	114.8 (1)	N3-C8-C7	112.4 (3)
N3-Cu-C1	117.4 (1)	N4-C11-C10	113.3 (3)
N4-Cu-C1	120.3 (1)	N4-C11-C12	124.4 (3)
		C4-N2-C6	121.8 (3)
Cu-C1-O1	177.5 (3)	N2-C6-C7	112.2 (3)
		C8-N3-C10	122.0 (3)
		N_3-C10-C11	116.3 (3)
		C_2-C_3-C_4	122.3 (3)
		C_3-C_4-C5	119.3 (3)
		C9-C10-C11	118.0 (3)
		C10-C11-C12	122.1 (3)
		C6-C7-C8	117.1 (3)

Table V. Root-Mean Square Amplitudes of Vibration along the Principal Axes (Å)

Cu	0.21	0.23	0.24
F1	0.22	0.26	0.28
F2	0.19	0.26	0.34
O1	0.20	0.39	0.40
O2	0.19	0.21	0.27
O3	0.21	0.22	0.26
N1	0.20	0.22	0.23
N2	0.19	0.22	0.27
N3	0.19	0.23	0.27
N4	0.20	0.22	0.23
C1	0.22	0.25	0.28
C2	0.22	0.26	0.29
C3	0.19	0.20	0.24
C4	0.19	0.21	0.27
C5	0.22	0.30	0.35
C6	0.21	0.27	0.32
C7	0.20	0.29	0.34
C8	0.20	0.28	0.34
C9	0.22	0.30	0.35
C10	0.19	0.21	0.29
C11	0.19	0.20	0.27
C12	0.22	0.26	0.32
B	0.20	0.22	0.27

$Cu(LBF_2)(CO)$ (8) is one of the few structurally characterized copper(I) carbonyl complexes and is apparently the only known 20-electron complex containing coordinated carbon monoxide.

Tables III and IV give bond lengths and angles for $Cu(LBF_2)(CO)$ (8). All nonhydrogen intermolecular separations are greater than 3.39 Å. There is no evidence for intermolecular or intramolecular hydrogen bonding.

The carbonyl complex $Cu(LBF_2)(CO)$ (8) exhibits idealized C_s-*m* geometry with no crystallographically imposed symmetry. The copper atom sits in an asymmetrical square-pyramidal environment and is displaced 0.96 Å from the basal plane of the four nitrogen atoms. Two significantly different sets of Cu-N bond lengths which average 2.164 and 2.104 Å characterize the equatorial asymmetry. The trans N-Cu-N angles are 124.7 (1) and 127.6 (1)°; the cis N-Cu-N angles range from 73.8 (1) to 85.9 (1)°.

The carbonyl ligand coordinates at the apex of the square-pyramid with a Cu-CO distance of 1.780 (3) Å and a Cu-C-O angle of 177.5 (3)°. The C-O bond length, which has not been corrected for possible vibrational shortening (Table V), is 1.112

Table VI. Atomic Coordinates[a] for $Cu(LBF_2)(CO)$ (8)

Atom	X	Y	Z
Cu	23458 (3)	10234 (3)	41603 (3)
F1	3529 (1)	1537 (1)	5685 (1)
F2	2753 (1)	1957 (1)	6857 (1)
O1	4321 (2)	962 (2)	3617 (2)
O2	2120 (1)	2451 (1)	5651 (1)
O3	2092 (2)	787 (2)	6083 (1)
N1	1940 (2)	2274 (2)	4836 (2)
N2	1434 (2)	1791 (2)	3383 (2)
N3	1478 (2)	−147 (2)	3874 (2)
N4	1919 (2)	416 (2)	5321 (2)
C1	3568 (2)	986 (3)	3843 (2)
C2	1004 (3)	3726 (2)	4873 (2)
C3	1408 (2)	2873 (2)	4472 (2)
C4	1168 (2)	2609 (2)	3614 (2)
C5	625 (3)	3281 (3)	3094 (2)
C6	1164 (3)	1411 (3)	2584 (2)
C7	1554 (3)	437 (3)	2449 (2)
C8	1206 (3)	−322 (3)	3015 (2)
C9	586 (3)	−1535 (2)	4363 (3)
C10	1182 (2)	−664 (2)	4457 (2)
C11	1425 (2)	−346 (2)	5305 (2)
C12	1071 (3)	−844 (2)	6043 (2)
B	2643 (3)	1675 (2)	6053 (2)

Atom	X	Y	Z	B
H1	135 (2)	422 (2)	479 (2)	5.20
H2	99 (2)	365 (2)	544 (2)	5.20
H3	40 (2)	389 (2)	468 (2)	5.20
H4	8 (2)	307 (2)	310 (2)	6.90
H5	79 (2)	325 (2)	246 (2)	6.90
H6	40 (2)	381 (2)	331 (2)	6.90
H7	136 (2)	178 (2)	220 (2)	6.30
H8	43 (2)	140 (2)	262 (2)	6.30
H9	222 (2)	46 (2)	249 (2)	6.80
H10	134 (2)	24 (2)	195 (2)	6.80
H11	50 (2)	−48 (2)	298 (2)	6.60
H12	146 (2)	−94 (2)	290 (2)	6.60
H13	75 (2)	−180 (2)	383 (2)	7.10
H14	82 (2)	−200 (2)	475 (2)	7.10
H15	1 (2)	−144 (2)	458 (2)	7.10
H16	110 (2)	−47 (2)	648 (2)	5.80
H17	40 (2)	−87 (2)	603 (2)	5.80
H18	136 (2)	−137 (2)	614 (2)	5.80

[a] The X, Y, and Z fractional coordinates are multiplied by 10^5 for the copper atom, 10^4 in the case of the nonhydrogen atoms, and by 10^3 otherwise.

(4) Å. To our knowledge the only other copper(I) carbonyl complex which has been structurally characterized is [hydrotris(1-pyrazolyl)borato]copper(I) carbonyl, [HB(pz)$_3$]CuCO.[44] The latter complex has a four-coordinate copper(I) atom with a closed-shell configuration. Carbon monoxide is bonded linearly; the Cu-CO distance averages 1.765 Å and the C-O bond length is 1.120 Å. Thus, while the average Cu-N distance in $Cu(LBF_2)(CO)$ (8) is 0.09 Å longer than that in [(HB(pz)$_3$)]CuCO, both the Cu-CO and CO distances agree closely in spite of the difference in coordination numbers of the copper atom. As we have previously noted,[31] the carbonyl infrared stretching frequencies also show only a small variation despite the different coordination geometries for copper(I).

Several structural determinations of various metals coordinated to H_2L (1, or its derivatives) have been reported. These include six-coordinate d^6 metals Rh(III)[45a] and Co(III).[45b] A closely related copper(II) complex,[46] which has a saturated Cu-N (amine) bond, is square pyramidal with a perrhenate anion occupying the axial coordination site. The Cu-N bond lengths in $Cu(LBF_2)(CO)$ (8) average 0.16 Å longer than

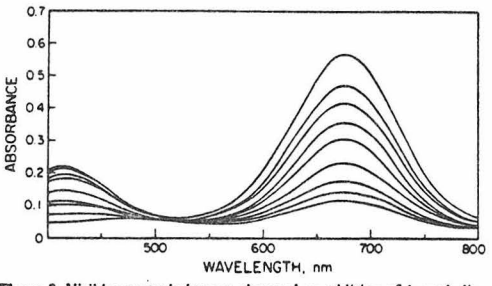

Figure 3. Visible spectral changes observed on addition of 1-methylimidazole to a solution of $Cu(LBF_2)$ (6) in acetone.

those in the copper(II)-amine complex. The copper(II) ion is displaced only 0.24 Å out of the plane of the equatorial nitrogen atoms.[46] Presumably, the larger size of the copper(I) ion accounts for the larger displacement of the metal atom from the plane of the four nitrogen atoms in $Cu(LBF_2)(CO)$ (8).

Rhodium(I) complexes of H_2L (1) have been found to be very reactive toward oxidative addition.[47] In some cases cis addition is indicated which would require distortion of the macrocycle from planarity. The macrocycle is nearly planar in the Rh(III), Rh(I), and Co(III) structures. In $Cu(LBF_2)(CO)$ (8), however, the macrocycle deviates considerably from planarity as evidenced by a dihedral angle of 60.0° between the Ni(1)-C(3)-C(4)-N(2) and N(3)-C(10)-C(11)-N(4) planes. This angle is less than 3° for the d^6 and d^8 complexes.

Other differences in the conformation of the macrocycle in the structures of the six-coordinate BF_2-bridged Rh(III) complex, $Rh[C_2(LBF_2)](CH_3)(I)$,[45a] and of $Cu(LBF_2)(CO)$ (8) are evident. In the latter complex, atom C(7) and the boron atom both lie above the plane of the four equatorial nitrogen atoms. A "boat" conformation is thus produced for the two six-membered rings which include the metal atom. In the Rh(III) complex, however, these atoms are located on opposite sides of the macrocycle plane leading to an overall "chair" conformation. This variation in conformation presumably results from the difference in steric requirements of both the metal atoms and the axial ligands in the Cu(I) and Rh(III) complexes.

The average values of the C=N, C—N, and C—C bond lengths in $Cu(LBF_2)(CO)$ (9) are 1.276 ± 0.006, 1.465 ±

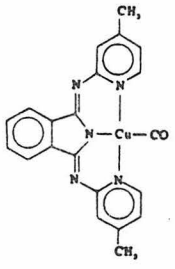

9

0.008, and 1.491 ± 0.008 Å, respectively.[48] For comparison, values of 1.300 ± 0.013, 1.476 ± 0.018, and 1.506 ± 0.025 Å are found for $Rh[C_2(LBF_2)](CH_3)I$.

The refined C-H bond lengths average 0.93 ± 0.06 Å. The H-C-H angles range from 89 to 129° with a mean value of 107 ± 10°.

Tables VI and VII give the atomic coordinates and the anisotropic thermal parameters for $Cu(LBF_2)(CO)$ (8).

Table VII. Anisotropic Thermal Parameters for $Cu(LBF_2)(CO)$ (8)

Atom	U_{11}	U_{22}	U_{33}	U_{12}	U_{13}	U_{23}
Cu	448 (2)	552 (3)	565 (3)	−10 (2)	59 (2)	−18 (2)
F1	51 (1)	68 (1)	74 (1)	2 (1)	−10 (1)	−2 (1)
F2	96 (2)	70 (1)	49 (1)	12 (1)	−28 (1)	−6 (1)
O1	61 (2)	155 (3)	132 (3)	−8 (2)	41 (2)	1 (2)
O2	64 (1)	45 (1)	43 (1)	7 (1)	−11 (1)	−2 (1)
O3	69 (2)	49 (1)	45 (1)	3 (1)	−3 (1)	3 (1)
N1	50 (2)	46 (2)	42 (2)	1 (1)	−4 (1)	3 (1)
N2	52 (2)	68 (2)	38 (2)	−9 (2)	−2 (1)	2 (1)
N3	54 (2)	53 (2)	57 (2)	−4 (1)	5 (1)	−18 (1)
N4	47 (1)	41 (1)	50 (2)	4 (1)	2 (1)	0 (1)
C1	56 (2)	64 (2)	69 (2)	−4 (2)	13 (2)	−2 (2)
C2	70 (2)	55 (2)	74 (2)	10 (2)	−11 (2)	2 (2)
C3	40 (2)	43 (2)	49 (2)	−4 (1)	−1 (1)	8 (1)
C4	45 (2)	64 (2)	46 (2)	−4 (2)	−1 (2)	16 (2)
C5	94 (3)	99 (3)	66 (2)	27 (2)	−13 (2)	15 (2)
C6	82 (3)	92 (2)	44 (2)	−14 (2)	−4 (2)	1 (2)
C7	84 (3)	108 (3)	48 (2)	−6 (3)	2 (2)	−26 (2)
C8	78 (2)	77 (3)	78 (3)	−8 (2)	3 (2)	−37 (2)
C9	85 (3)	54 (2)	125 (4)	−16 (2)	−6 (3)	−8 (2)
C10	41 (2)	40 (2)	83 (3)	2 (2)	3 (2)	−11 (2)
C11	41 (2)	40 (2)	71 (2)	4 (1)	9 (2)	6 (2)
C12	73 (2)	56 (2)	92 (3)	−1 (2)	16 (2)	15 (2)
B	64 (2)	47 (2)	49 (2)	4 (2)	−14 (2)	0 (2)

[a] The form of the thermal ellipsoid is $\exp[-2\pi^2(U_{11}h^2a^{*2} + \ldots + 2U_{23}klb^*c^*)]$. The U_{ij} elements are multiplied by 10^4 for the copper atom and by 10^3 otherwise.

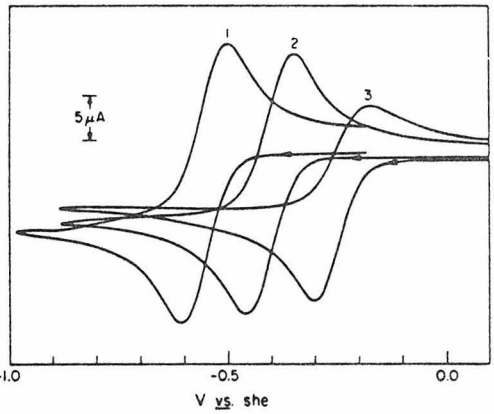

Figure 4. Cyclic voltammetry of $[Cu(LBF_2)(ClO_4)]_2$-$C_4H_8O_2$ (5) in acetone: (1) with 100 equiv 1-MeIm; (2) under N_2; and (3) with 1 atm CO. Scan rate = 100 mV/s. Concentrations of Cu(II) were not held precisely equal, $\simeq 2 \times 10^{-3}$ M.

Equilibrium Constants. Preliminary equilibrium (concentration) constants for the formation of five-coordinate complexes, $Cu(LBF_2)L'$ (eq 2)

$$Cu(LBF_2) + L' \overset{K_c}{\rightleftharpoons} Cu(LBF_2)L' \qquad (2)$$

have been determined via spectroscopic studies and by monitoring changes in electrochemical redox behavior upon addition of ligands, L', as follows.

The blue four-coordinate Cu(I) complex $Cu(LBF_2)$ (6) has a strong absorption at 677 nm (acetone, ϵ 1.03×10^4 M^{-1} cm^{-1}, 25 °C) which disappears upon addition of a large excess of CO or 1-MeIm. Monitoring the absorption at 677 nm as ligand was added was used to determine the extent of formation of the five-coordinate complex (eq 2). Figure 3 depicts the series of spectra obtained upon adding various amounts of 1-MeIm to an acetone solution of the four-coordinate complex, $Cu(LBF_2)$ (6). Only approximate isosbestic behavior was observed due to slight variations in the pathlengths of the sample cells utilized (see Experimental Section). For these preliminary measurements we assume therefore that there are only two principal species in solution, four-coordinate $Cu(LBF_2)$ and five-coordinate $Cu(LBF_2)L'$ (eq 2). Similar measurements with various partial pressures of CO permitted binding constant determinations but, again, no true isosbestic behavior was observed. Table VIII lists the values for the equilibrium constants determined.

Table VIII. Equilibrium Constants for the Formation of Five-Coordinate Complexes $Cu(LBF_2)L'$ in Acetone

$$Cu(LBF_2) + L' \overset{K}{\rightleftharpoons} Cu(LBF_2)L'$$

L'	K	Method
1-MeIm	$K_c = 16\ M^{-1}$	EAS
CO	$K_p = 500\ atm^{-1}$ ($P_{1/2} = 1.5$ mm)	EAS
CO	$K_c \simeq 4.7 \times 10^4\ M^{-1}$	EAS
CO	$K_c \simeq 6.7 \times 10^4\ M^{-1}$	ΔE^f

Changes in electrochemical redox behavior were also employed to determine equilibrium constants. As shown in Figure 4 and in Table IX the cyclic voltammograms obtained using the Cu(II) complex 5 as starting material depend on both the solvent and on other coordinating ligands in solution. A large excess of 1-MeIm causes a significant negative shift in E^f while excess CO results in a positive shift relative to the cyclic voltammogram obtained for 5 under nitrogen (Figure 4). These shifts are attributable to the formation of Cu(I) and Cu(II) adducts of the ligand added. In Figure 4, curves 1 and 3 have approximately the same wave shape as does curve 2. This suggests that the equilibria between Cu(I), Cu(II), and the added ligands are established rapidly compared to the cyclic voltammetry timescale. In the special case where adducts are formed very rapidly and with only one oxidation state of the metal, the shift in E^f can be correlated simply to the degree of

Table IX. Cyclic Voltammetric Data for $[Cu(LBF_2)ClO_4]_2 \cdot C_4H_8O_2$ (5) with Added Ligands[a]

Indicating electrode	Solution atm	L, eq[b]	E_{pc}, V[c]	E_{pa}, V[d]	E^f, V[e]
		In CH_3CN			
Hg	He	None	−0.432	−0.330	−0.381
Pt[f]	N_2	1-MeIm, 5	−0.517	−0.389	−0.453
Pt	N_2	20	−0.548	−0.423	−0.486
Pt	N_2	100	−0.567	−0.437	−0.502
Hg	He	1-MeIm, 100	−0.559	−0.457	−0.508
Hg	CO	CO, satd	−0.274	−0.169	−0.221
		In $(CH_3)_2CO$			
Hg	N_2	None	−0.459	−0.345	−0.402
Pt[f]	He	1-MeIm, 5	−0.561	−0.462	−0.512
Pt	He	20	−0.599	−0.492	−0.546
Pt	He	100	−0.614	−0.502	−0.558
Hg	He	1-MeIm, 100	−0.606	−0.496	−0.551
Hg	CO	CO, satd	−0.298	−0.169	−0.234

[a] Conditions: [Cu] = 2×10^{-3} M; sweep rate = 100 mV/s. [b] L = ligand added, eq = equivalents of L added. [c] Vs. SHE. [d] $E^f \approx E_{pc} + E_{pa}/2$. [e] A Pt indicating electrode was used because with Hg, at approximately +0.035 V, a large reduction wave occurred swamping the Cu(II) + $1e^- \rightarrow$ Cu(I) peak. If the sweep was begun at −0.14 V (CH_3CN) or 0.18 V ($(CH_3)_2CO$) in Hg, the interference was avoided and the cyclical data given were measured. Pt and Hg results agree closely in cases where both were used.

adduct formation.[49] Carbon monoxide as a ligand appears to satisfy these conditions. Addition of CO to the Cu(II) complex 5 causes no observable spectral changes, nor are there any other indications of a Cu(II)-CO adduct. As a first approximation, therefore, the observed shifts in E^f can be totally attributed to formation of the five-coordinate Cu(I) carbonyl $Cu(LBF_2)(CO)$ (8). That this is a reasonable assumption is supported by the close approximation between the equilibrium constant obtained (see Experimental and Table VIII) and that found by spectral measurements (Table VIII). Unfortunately, nitrogen bases, including 1-MeIm, bind to both the Cu(I) and the Cu(II) complexes precluding the use of this electrochemical approach to determine equilibrium constants.

The value of K_c for CO ($\sim 4.7 \times 10^4$ M^{-1}) is significantly greater than that for 1-MeIm (16 M^{-1}). Moreover, the shift in E^f for CO is positive, implying stabilization of Cu(I), while that for 1-MeIm is negative, indicative of either stabilization of Cu(II) or destabilization of Cu(I). It can be argued that this may be attributed to the greater π acidity of CO, which serves to drain the 20-electron system of electron density. Such an explanation is not sufficient to account for a number of observations which are discussed below.

Several Cu(I) complexes of polydentate ligands form carbonyl adducts with very similar ν_{CO}'s despite dissimilar structures. In the tetrahedral [hydrotris(pyrazolyl)borato]copper(I) carbonyl and its dimethyl analogue, [hydrotris(3,5-dimethyl-1-pyrazolyl)borato]copper(I) carbonyl, ν_{CO}'s are 2083 and 2066 cm^{-1}, respectively.[38] The presumably four-coordinate (probably distorted square-planar) isoindoline complex 9 has ν_{CO} 2072 cm^{-1}.[39] As reported here, the five-coordinate complex $Cu(LBF_2)(CO)$ (8) has ν_{CO} 2068 cm^{-1}. The similarity of ν_{CO} for 8 relative to ν_{CO} in the four-coordinate complexes does not suggest a peculiar bonding situation in the five-coordinate complex which might be expected of a 20-electron species.

The formation of five-coordinate adducts from four-coordinate Cu(I)-macrocyclic ligand complexes is apparently not a general phenomenon. For example, the Cu(I) complex 10[35] does not change color when exposed to CO, nor is there any shift in E^f as determined by cyclic voltammetry.[50] In contrast, the binuclear mixed-valence Cu(II)Cu(I) carbonyl complex 11 (ν_{CO} 2067 cm^{-1}), which probably contains a five-coordinate Cu(I), has been isolated.[50]

The very formation of five-coordinate Cu(I) is somewhat enigmatic. The $Cu(LBF_2)(CO)$ (8) structure (Figure 3) may indicate, however, at least one factor helpful in explaining

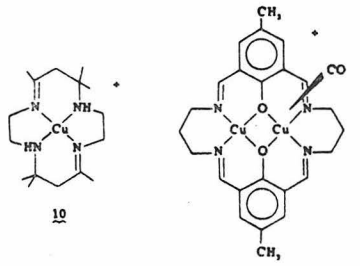

10 11

five-coordination. The Cu atom is seen to be a full 0.96 Å out of the mean plane of the four coordinating nitrogens of the macrocycle. Such a large displacement of a transition metal atom from a macrocycle is unusual and may be due in part to the large radius of Cu(I). In fact it is not unreasonable to expect that the structure of the four-coordinate species, when determined, will reveal Cu(I) to be significantly displaced from the basal plane of the relatively rigid macrocycle by perhaps as much as 0.4 to 0.5 Å. Poor metal-macrocyclic ligand orbital overlap would undoubtedly result. Though bound to four nitrogen atoms and thus formally an 18-electron system, the Cu(I) atom might be better described as coordinatively unsaturated, sterically if not electronically. In contrast, more flexible ligands, as in 10, may better accommodate Cu(I), by producing a more tetrahedral environment.

Oxygen Reactivity

Four-coordinate $Cu(LBF_2)$ (6) is very oxygen sensitive; royal blue acetone solutions rapidly turn yellow brown. The reaction is irreversible and is dependent on temperature, solvent, and electrolyte concentration. Oxidation products have thus far proven intractable but further work is in progress.

Conclusion

The four-coordinate Cu(I)-macrocyclic ligand complex reacts with certain monodentate ligands to give five-coordinate complexes. The available data are insufficient, but this unusual coordination number for Cu(I) may be partly explained by a rigid ligand environment imposed by the macrocycle. Certainly five-coordination for Cu(I) appears viable and worthy of further study. The complexes described herein are not purported to be accurate mimics of the active sites in any copper proteins.

Table X. Reference Electrode Data for Ferrocene Couple in Water, Acetonitrile, and Acetone

Solvent	$E°$, V	Correction, E', V[c]
Water	+0.400[a]	0.000
Acetonitrile	+0.043[b]	−0.043 + 0.400 = +0.357
Acetone	+0.078[b]	−0.078 + 0.400 = +0.322

[a] Vs. SHE. [b] Vs. $Ag|AgNO_3$ (0.1 M) with 0.1 M tetrabutylammonium perchlorate in acetonitrile. [c] Correction needed to bring measured potentials in acetonitrile, acetone originally vs. $Ag|Ag^+$ (0.1 M) in acetonitrile, to potentials vs. SHE.

Rather they suggest that consideration of Cu(I) active site structures must include the possibility of five-coordination. For example, the binuclear copper site in hemocyanin binds one CO. The carbonyl stretching frequency, $^{51}\nu_{CO}$ 2040–2060 cm^{-1}, indicates CO bound to only one Cu; however, that Cu atom could conceivably have as many as five ligands, including CO. Similarly, the resonance Raman spectra of Cu(II) "blue" copper proteins (type I) are interpretable in terms of five-coordination.[52] Since the "blue" copper proteins apparently serve primarily in electron transfer, it seems unlikely that drastic changes occur in the coordination sphere upon reduction of Cu(II) to Cu(I). In any case the present work would be consistent with five-coordination in the reduced, Cu(I), state as well.

Experimental Section

All operations requiring an inert atmosphere were performed in a Vacuum Atmospheres Dri-lab containing either N_2 or He. Electronic absorption spectroscopy (EAS) was performed on a Cary-14 automatic recording spectrometer while infrared spectra were obtained via KBr pellets or in CH_2Cl_2 solution on a Beckman IR-12 spectrometer.

Tetrabutylammonium perchlorate (Southwestern Analytical Chemicals) was dried exhaustively in vacuo before use. Spectroquality acetonitrile and acetone, dried over 4A molecular sieves, were used for cyclic voltammetry. All other solvents were reagent grade.

Electrochemistry. The apparatus used for constant potential electrolysis (CPE) and cyclic voltammetry consisted of Princeton Applied Research's Model 173 potentiostat-galvanostat coupled with Model 179 Digital coulometer, plus a ramp generator of our own design. For display purposes, both a storage oscilloscope and an X-Y recorder were available.

Constant potential electrolyses and cyclic voltammetry were done in a three compartment H-cell. The cell consisted of 25-mL sample and auxiliary compartments separated by a small center compartment, all separated by medium porosity sintered glass frits. In either CH_3CN or $(CH_3)_2CO$, the supporting electrolyte used was 0.1 M TBAP (tetrabutylammonium perchlorate). The $Ag|Ag^+$ reference electrode consisted of a silver wire immersed in an acetonitrile solution containing $AgNO_3$ (0.1 M) and TBAP (0.1 M), all contained in an 8-mm glass tube fitted on the bottom with a fine porosity sintered glass frit. To provide a more general reference, ferrocene's Fe(II)|Fe(III) couple[53] was examined in CH_3CN and $(CH_3)_2CO$. Table X gives measured data and the corrections which were used throughout this paper to adjust the potentials measured against $Ag|Ag^+$ to potentials vs. SHE.

Formal reduction potentials, E', were measured by cyclic voltammetry using the formula $E' = (E_{p_a} + E_{p_c})/2$. The potentials so determined are approximate in that the systems examined did not display strict reversibility, nor were corrections made for diffusion coefficients.

Determination of Binding Constants. Equation 2 gives the equilibrium expression for the reaction of $Cu(LBF_2)$ (6) with ligands, L'. As a first approximation to the equilibrium constant for the formation of five-coordinate species, the equilibrium concentration constant is defined:

$$K_c = [Cu(LBF_2)L']/[Cu(LBF_2)][L'] \quad (3)$$

The equilibrium concentrations of the Cu complexes were determined by use of the Beer's law dependence of the $Cu(LBF_2)$ 677-nm band. It was assumed that $Cu(LBF_2)L'$ did not absorb appreciably at 677 nm. Therefore, when $Cu(LBF_2)$ reacted with L', ΔA ($A_{initial} - A_{equilibrium}$) was taken as a measure of $Cu(LBF_2)L'$ formed.

With L' = 1-MeIm, the cells used had measured pathlengths of about 1 mm. The short pathlength permitted relatively high concentrations of $Cu(LBF_2)$ to be used, thus minimizing decomposition due to residual dissolved oxygen. Preparation of solutions of $Cu(LBF_2)$ ($[Cu(LBF_2)]_{initial} \cong 8 \times 10^{-4}$ M) and addition of 1-MeIm ($[1\text{-MeIm}]_{initial} = 2 \times 10^{-3}$ to 1 M) was effected in the inert atmosphere chamber. The cells were closed with greased, glass stoppers and taped. Spectra were recorded to determine ΔA (677 nm). Measurements were made at 30 ± 2 °C. Only approximate isosbestic behavior was observed, most probably owing to the slight variation in pathlengths of the several cells employed (e.g., see Figure 3). If a 1:1 stoichiometry for adduct formation is assumed (eq 2), the constant K_c is found to be 16 ± 3 M^{-1}.

For CO measurements, the cells used each had approximately 1-mm pathlengths, a 10-mL side-arm reservoir, a Teflon high-vacuum stopper, and a standard taper joint for attachment to a vacuum line. The $Cu(LBF_2)$ ($[Cu(LBF_2)]_{initial} \cong 1.6 \times 10^{-3}$ M) solutions were prepared in the inert atmosphere chamber and closed to the atmosphere. The solutions were then degassed by the freeze-pump-thaw technique (3 cycles) on the vacuum line. The spectra were measured before addition of CO.

The $Cu(LBF_2)$ solution was opened to a system with a mercury manometer and an acetone reservoir. The acetone vapor pressure was measured when the system had equilibrated. Addition of CO (10–80 mmHg) was monitored by use of the manometer. The $Cu(LBF_2)$ solution was stirred under CO for 20 min and the pressure and temperature were then recorded. The spectra were recorded in order to find ΔA (677 nm). A plot of $[Cu(LBF_2)(CO)]/[Cu(LBF_2)]$ vs. P(CO) was extrapolated to give $P_{1/2}(CO) = 1.5$ mm when the $[Cu(LBF_2)(CO)] = [Cu(LBF_2)]$. The equilibrium (pressure) constant, K_p, was calculated as 500 ± 15 atm^{-1}.

Conversion of K_p to K_c for the purpose of comparison to K_c (1-MeIm) utilized data for CO solubility in acetone. Use of a value of 0.2358 mL of CO per mL of acetone at 20 °C[54] and of Henry's law allowed conversion of $P(CO)$ to [CO]. Calculation of K_c resulted in a value of $4.7 \pm 0.2 \times 10^4$ M^{-1}.

The CO binding constant $K_c(CO)$ was also estimated via the shift in E'. Cyclic voltammograms of the Cu(II) complex 5 (acetone/Hg) under 1 atm of CO showed a shift of E' of 0.168 V vs. that found under N_2 (Table IX). Such shifts can be related to the binding of ligand to metal in both the oxidized and the reduced state.[49] A simplified relationship can be derived for the case in which ligand binds, effectively, to only one oxidation state, e.g., eq 4.

$$[Cu(LBF_2)]^+ + CO + e^- \rightleftharpoons [Cu(LBF_2)(CO)] \quad (4)$$

In this equation

$$E°_{(CO)} = E° + (RT/F) \ln (1 + K_c[CO])$$

$E°$ and $E°_{(CO)}$ are the standard potentials for the reduction in the absence and presence of CO, respectively. The equilibrium constant K_c was calculated using the appropriate formal potentials E' in place of the standard potentials $E°$.

X-Ray Data Collection. Crystals of the carbonyl adduct were grown by quick evaporation of an acetone solution under carbon monoxide. Weissenberg photographs revealed orthorhombic symmetry and systematic absences: $h = 2n + 1$, $hk0$ data; $k = 2n + 1$, $0kl$ data; $l = 2n + 1$, $h0l$ data. These extinctions are consistent only with the space group *Pbca*.

A multifaceted crystal of dimensions 0.15 mm × 0.15 mm × 0.30 mm was positioned on a Datex-automated General Electric quarter-circle diffractometer with the [001] direction nearly coincident with the ϕ axis of the diffractometer. The lattice parameters (Table I) were determined by a least-squares fit of 14 manually centered reflections. Data were collected out to $2\theta_{max} = 130°$ above which only a small number of the reflections had measurable intensity. The scan widths were varied linearly from 1.80° at $2\theta = 3°$ to 3.50° at $2\theta = 130°$. The scan speed was 2° min^{-1}. Intensities of 2738 reflections were measured by the moving-crystal, moving-counter techniques using a takeoff angle of 3°. The total background time was 40 s. Three reflections measured every 25 reflections served to monitor crystal and instrumental stability. No significant falloff in the intensities of these reflections was observed.

The measured intensities were reduced to structure factor amplitudes by applying Lorentz and polarization corrections. The standard deviations in the intensities were calculated from the formula: $\sigma^2(I) = S + (B1 + B2)T^2 + (dS)^2$, where S, $B1$, and $B2$ are the scan counts and two background counts, T is a factor which corrects for the difference in time spent on the scan and background counts, and d is the Peterson-Levy[55] factor taken to be 0.02. For the purpose of an absorption correction, the shape of the crystal was approximated by a rectangular prism.

Solution and Refinement of the Structure. The position of the copper atom was determined from a three-dimensional Patterson map. Difference-Fourier syntheses revealed the positions of all the other nonhydrogen atoms. Full-matrix isotropic refinement[56] with data out to 100° in 2θ lowered the R factor to 10%. At this point hydrogen atoms were included. After additional least-squares, a systematically negative disparity between the observed and calculated structure factors was noted. A secondary extinction parameter was included in the refinement as a correction.[61] Least-squares refinement was continued to convergence with two matrices; one matrix contained all nonhydrogen atom coordinates and anisotropic temperature factors, the other contained coordinates of the hydrogen atoms. Isotropic thermal parameters of the hydrogen atoms were fixed at the value of the carbon atom to which they were bonded plus 1.0 Å^2. The R factor[62] at the end of the refinement was 5.5% for 2511 data ($F_o^2 > 0$). No observations other than systematically absent reflections were omitted from the refinement. The goodness of fit was 1.39. A final difference-Fourier synthesis showed no residual electron density greater than 0.34 e Å^{-3}.

Final positional parameters are given in Table VI. Table VII lists the anisotropic thermal parameters.

Preparation of Complexes. 3,3'-(Trimethylenedinitrilo)bis(2-butanone oxime), H_2L (1). 1,3-Propanediamine (37.06 g, 0.5 mol) and 2,3-butanedione monoxime (101.0 g, 1.0 mol) were mixed together in hot ethanol to give a yellow solution approximately 250 mL volume. The solution was allowed to cool to ambient temperature. The resulting white precipitate was isolated immediately by vacuum filtration, washed well with diethyl ether, and dried in air. The ligand was used without further purification.

[3,3'-(Trimethylenedinitrilo)bis(2-butanone oximato)]copper(II) Perchlorate Monohydrate, $(Cu(LH)ClO_4 \cdot H_2O$ (2). A hot acetone solution (20 mL) of $Cu(ClO_4)_2 \cdot xH_2O$ (dried in vacuo at 25 °C, 3.7 g, 10 mmol) was added to a hot acetone solution of the ligand, H_2L, 1 (4.8 g, 20 mmol, in 20 mL), giving a deep red solution. As the solution cooled, a dark red-brown crystalline product precipitated. The solid was isolated by vacuum filtration, washed with diethyl ether, and dried in air. Anal. Calcd for $C_{11}H_{21}ClCuN_4O_7$: C, 31.45; H, 5.00; N, 13.3; Cu, 15.1. Found: C, 31.55; H, 4.75; N, 13.3; Cu, 16.0.

Millimolar solutions of this compound were examined by cyclic voltammetry. A quasireversible wave, complicated by a copper stripping wave, yielded an $E^f \cong 0.56$ V. Constant potential electrolysis at −0.8 V caused the purple solution to become blue with a small amount of copper being plated out on the platinum working electrode. The n values were slightly greater than 1.

Bis[difluoro-3,3'-(trimethylenedinitrilo)bis(2-butanone oximato)]boratecopper(II) Perchlorate] Monodioxane, $(Cu(LBF_2)ClO_4)_2 \cdot C_4H_8O_2$ (5). Boron trifluoride etherate, $BF_3 \cdot Et_2O$ (6 mL, 50 mmol), was added slowly, with stirring, to a mixture of $Cu(LH)ClO_4 \cdot H_2O$ (2) (7.0 g, 17 mmol) in warm dioxane (150 mL, 70 °C). The mixture was heated, with stirring, at a boil for 1 h. The red-violet mixture was cooled slowly to ambient temperature. Dark red-violet solid was isolated by vacuum filtration, washed well with dioxane and diethyl ether, and dried in air. The product was dissolved in a minimum amount of boiling acetone (150 mL). The hot solution was filtered and treated with 5 mL of dioxane. Crystalline product, obtained upon cooling, was isolated and treated as before. A yield of 5.3 g (64%) was obtained. Anal. Calcd for $C_{26}H_{44}B_2Cl_2Cu_2F_4N_8O_{14}$: C, 31.6; H, 4.45; N, 11.35; Cu, 12.85. Found: C, 31.9; H, 4.5; N, 11.25; Cu, 12.6.

[Difluoro-3,3'-(trimethylenedinitrilo)bis(2-butanone oximato)borate]copper(I), $Cu(LBF_2)$ (6). This copper(I) complex was prepared by constant potential electrolysis in a He atmosphere chamber. A simple H-cell was employed with 0.1 M TBAP in acetone in all three chambers. The Cu(II) complex $[Cu(LBF_2)ClO_4]_2 \cdot C_4H_8O_2$, (5) (0.8 g, 15 mmol) was dissolved in the cathodic compartment which also contained a magnetic stir bar and a platinum gauze electrode. A self-contained $Ag|Ag^+$ reference electrode was placed in the middle chamber while a platinum wire was employed in the anodic chamber. Constant potential electrolysis was carried out at −1.0 V vs. $Ag|Ag^+$ (−0.678 V vs. SHE; see Table X) until the current was 1% of the initial value. During electrolysis, red $Cu(LBF_2)$ (6) crystallized from solution. The product was isolated by vacuum filtration, washed with ethanol, and dried under He. Anal. Calcd for $C_{11}H_{18}BCuF_2N_4O_2$: C, 37.65; H, 5.15; N, 16.0; Cu, 18.1. Found: C, 37.8; H, 5.1; N, 16.1; Cu, 18.2; ϵ(acetone, 25 °C, 677 nm) = $1.03 \pm 0.02 \times 10^4$ M^{-1} cm^{-1}. A magnetic susceptibility measurement by the Faraday method showed the compound to be diamagnetic at 25 °C.

Carboxy[difluoro-3,3'-(trimethylenedinitrilo)bis(2-butanone oximato)borate]copper(I), $Cu(LBF_2)(CO)$ (8). A blue solution of $Cu(LBF_2)$ (6) (0.35 g, 10 mmol) in acetone (25 mL) under N_2 was treated with CO (1 atm) yielding a greenish-yellow solution with some green solid. The green solid was removed by filtration and the resulting filtrate was treated with slow additions of heptane. The resulting orange crystalline product was isolated by filtration and dried under a stream of CO. Anal. Calcd for $C_{12}H_{18}BCuF_2N_4O_3$: C, 38.05; H, 4.75; N, 14.8; Cu, 16.8. Found: C, 38.1; H, 4.9; N, 14.7; Cu, 17.1.

[Difluoro-3,3'-(trimethylenedinitrilo)bis(2-butanone oximato)borate](1-methylimidazole)copper(I), $Cu(LBF_2)$(1-MeIm) (7). 1-Methylimidazole (0.1 g, 1.2 mmol) was added under nitrogen to a blue solution of $Cu(LBF_2)$ (6) (0.1 g, 0.2 mmol) in acetone (15 mL). A dark emerald-green solution resulted. Aliquots of heptane (5 mL) were added every 10 min until 30 mL total had been added. After 2 h, red crystalline product (red even when ground to a powder) was isolated by vacuum filtration, washed with 1:1 acetone:heptane, and dried under N_2. Anal. Calcd for $C_{15}H_{24}BCuF_2N_6O_2$: C, 41.6; H, 5.55; N, 19.4; Cu, 14.7. Found: C, 42.0; H, 5.55; N, 19.6; Cu, 14.4.

Note Added in Proof. Crystallographic analysis shows complex 6 to contain essentially square-planar Cu(I) with the four-coordinated nitrogen atoms distorted slightly toward tetrahedrality.[63]

Acknowledgment. We appreciate the assistance of F. Anson, G. Mauk, J. Fujitaki, and J. Koval. This work was supported by the National Institutes of Health and the National Science Foundation.

Supplementary Material Available: Listing of structure factor amplitudes (11 pp). Ordering information is given on current masthead page.

References and Notes

(1) J. Peisach, P. Aisen, and W. E. Blumberg, "The Biochemistry of Copper", Academic Press, New York, N.Y., 1966.
(2) W. H. Vannette and A. Zuberbuhler in "Molecular Mechanisms of Oxygen Activation," O. Hayaishi, Ed., Academic Press, New York, N.Y., 1974, p 371
(3) R. Malkin in "Inorganic Biochemistry", G. L. Eichhorn, Ed., Elsevier, New York, N.Y., 1973, p 689.
(4) In certain copper-containing proteins the copper appears to serve principally in electron transport with no evidence of Cu–O_2 interaction, e.g., as in cytochrome oxidase.[5] In contrast hemocyanin[6–8] and tyrosinase[9] apparently rely on direct, covalent interaction between Cu(I) and O_2, both forming observable dioxygen adducts. The four-copper protein, laccase, may also rely on covalent interaction between O_2 and a binuclear, type III, Cu site.[10–12]
(5) W. S. Caughey, W. J. Wallace, J. A. Volpe, and S. Yoshikawa, *Enzymes*, 12, 299 (1975).
(6) K. E. Van Holde and E. F. J. Van Bruggen in "Biological Macromolecules Series", Vol. 5, S. M. Timasheff and G. D. Fasman, Ed., Marcel Dekker, New York, N.Y., 1971.
(7) R. Lontie and R. Witters in ref 3, p 344.
(8) J. Bonaventura, C. Bonaventura, and B. Sullivan, *J. Exp. Zool.*, 194, 155 (1975).
(9) (a) R. L. Jolley, Jr., L. H. Evans, and H. S. Mason, *Biochem. Biophys. Res. Commun.*, 46, 878 (1972); (b) R. L. Jolley, Jr., L. H. Evans, N. Makino, and H. S. Mason, *J. Biol. Chem.*, 249, 335 (1974).
(10) R. Aasa, R. Brandén, J. Deinum, B. G. Malmstrom, B. Reinhammer, and T. Vanngard, *FEBS Lett.*, 61, 115 (1976).
(11) R. Brandén and J. Deinum, *FEBS Lett.*, 73, 144 (1977).
(12) O. Farver, M. Goldberg, D. Lancet, and I. Pecht, *Biochem. Biophys. Res. Commun.*, 73, 494 (1976).
(13) B. Reinhammar, *Biochim. Biophys. Acta*, 205, 35 (1970).
(14) K. Lerch, *FEBS Lett.*, 69, 157 (1976).
(15) A. J. M. Schoot Uiterkamp, H. VanDerDeen, H. C. J. Berendsen, and J. F. Boas, *Biochim. Biophys. Acta*, 372, 407 (1974).
(16) A. J. M. Schoot Uiterkamp, *FEBS Lett.*, 20, 93 (1972).
(17) A. J. M. Schoot Uiterkamp and H. S. Mason, *Proc. Natl. Acad. Sci. U.S.A.*, 70, 993 (1973).
(18) N. Makino, P. McMahill, H. S. Mason, and T. H. Moss, *J. Biol. Chem.*, 249, 6062 (1974).

(19) E. I. Solomon, D. M. Dooley, R.-H. Wang, H. B. Gray, M. Cerdonio, F. Mogno, and G. L. Romani, *J. Am. Chem. Soc.*, **98**, 1029 (1976).
(20) T. H. Moss, D. C. Gould, A. Ehrenberg, J. S. Loehr, and H. S. Mason, *Biochemistry*, **12**, 2444 (1973).
(21) Y. Engelborghs, S. H. DeBruin, and R. Lontie, *Biophys. Chem.*, **4**, 343 (1976).
(22) B. Salvato, A. Ghiretti-Magaldi, and F. Ghiretti, *Biochemistry*, **13**, 4778 (1974).
(23) J. S. Loehr, T. B. Freedman, and T. M. Loehr, *Biochem. Biophys. Res. Commun.*, **56**, 510 (1974).
(24) T. B. Freedman, J. S. Loehr, and T. M. Loehr, *J. Am. Chem. Soc.*, **98**, 2809 (1976).
(25) R. H. Jardine, *Adv. Inorg. Biochem.*, **17**, 115 (1975).
(26) There are several reports of reversible oxygenation in solution or complexes whose stoichiometry implies possible dioxygen complexation, but these are poorly characterized. See (a) T. Graf and S. Fallab, *Experientia*, **20**, 46 (1964); (b) E. Ochiai, *Inorg. Nucl. Chem. Lett.*, **9**, 987 (1973); (c) C. E. Kramer, G. Davies, R. B. Davis, and R. W. Slaven, *J. Chem. Soc., Chem. Commun.*, 606 (1975); (d) C. S. Arcus, J. L. Wilkinson, C. Masali, T. J. Marks, and J. A. Ibers, *J. Am. Chem. Soc.*, **96**, 7564 ([974(/
(27) R. W. Erskine and B. O. Field in "Structure and Bonding", Vol. 28, Springer-Verlag, New York, N.Y., 1976, p 1.
(28) A. V. Savitskii and V. I. Nelyubin, *Russ. Chem. Rev.*, **44**, 110 (1975).
(29) J. S. Valentine, *Chem. Rev.*, **73**, 235 (1973).
(30) V. J. Choy and C. J. O'Connor, *Coord. Chem. Rev.*, **9**, 145 (1972–73).
(31) R. R. Gagné, *J. Am. Chem. Soc.*, **98**, 6709 (1976).
(32) For an excellent review see: W. E. Hatfield and R. Whyman, *Trans. Metal Chem.*, **5**, 47 (1969).
(33) F. A. Cotton and G. Wilkinson in "Advanced Inorganic Chemistry", 3rd ed, Interscience, New York, N.Y., 1972, p 905.
(34) G. S. Patterson and R. H. Holm, *Bioinorg. Chem.*, **4**, 257 (1975).
(35) D. C. Olson and J. Vasilevskis, *Inorg. Chem.*, **10**, 463 (1971).
(36) There are notable exceptions; see ref 37–39.
(37) M. I. Bruce and A. P. P. Ostazewski, *J. Chem. Soc., Dalton Trans.*, 2433 (1973).
(38) C. Masali, C. S. Arcus, J. L. Wilkinson, T. J. Marks, and J. A. Ibers, *J. Am. Chem. Soc.*, **98**, 711 (1976).
(39) R. R. Gagné, L. Speltz, and R. Gall, manuscript in preparation.
(40) E. Uhlig and M. Friedrich, *Z. Anorg. Allg. Chem.*, **343**, 299 (1966).
(41) R. M. Countryman, W. T. Robinson, and E. Sinn, *Inorg. Chem.*, **13**, 2013 (1974).
(42) Another quasireversible wave, which is comparable in size to the wave depicted in Figure 1, appears at far more negative potentials, $E^{\circ\prime} \simeq -1.2$ V. This process may be attributable to reduction of the ligand.
(43) F. Bigoli, A. Brarbanti, A. Tiripicchio, and M. Tiripicchio Camellini, *Chem. Commun.*, 120 (1970), for example.
(44) M. R. Churchill, B. G. DeBoer, F. J. Rotella, O. M. Abu Salah, and M. I. Bruce, *Inorg. Chem.*, **14**, 2051 (1975).
(45) (a) J. P. Collman, P. A. Christian, S. Current, P. Denisevich, T. R. Halbert, E. R. Schmittou, and K. O. Hodgson, *Inorg. Chem.*, **15**, 223 (1976); (b) S. Bruckner, M. Calligaris, G. Nardin, and L. Randaccio, *Inorg. Chim. Acta*, **3**, 278 (1969).
(46) I. B. Liss and E. O. Schlemper, *Inorg. Chem.*, **14**, 3035 (1975).
(47) (a) J. P. Collman and M. R. MacLaury, *J. Am. Chem. Soc.*, **96**, 3019 (1974); (b) J. P. Collman, D. W. Murphy, and G. Dolcetti, *Ibid.*, **95**, 2687 (1973).
(48) The standard deviation of the mean is calculated by the formula $[\sum^{N}_{i=1}(X_i - \bar{X})^2/N-1)]^{1/2}$.
(49) J. Heyrovski and J. Kuta, "Principles of Polarography", Academic Press, New York, N.Y., 1966, p 157.
(50) R. R. Gagné, C. Koval, T. Smith, and M. Cimolino, manuscript in preparation.
(51) (a) L. Y. Fager and J. O. Alben, *Biochemistry*, **11**, 4786 (1972); (b) J. O. Alben, L. Yen, and N. J. Ferrier, *J. Am. Chem. Soc.*, **92**, 4475 (1970).
(52) V. Miskowski, S.-P. W. Wang, T. G. Spiro, E. Shapiro, and T. H. Moss, *Biochemistry*, **14**, 1244 (1975).
(53) D. Baner and M. Breant, in "Electroanalytical Chemistry", Vol. VIII, A. J. Bard, Ed., Marcel Dekker, New York, N.Y., 1975, p 306.
(54) J. Horiuti, *Sci. Pap. Inst. Phys. Chem. Res. (Jpn.)*, **17**, 125 (1931).
(55) S. W. Peterson and H. A. Levy, *Acta Crystallogr.*, **10**, 70 (1957).
(56) Except for C. K. Johnson's ORTEP program, the computer programs used were from the CRYM system of crystallographic computer programs. The function minimized in the least-squares refinement was $\sum w(F_o^2 - F_c^2)^2$ where F_o and F_c are the observed and calculated structure factors and the weights, w, are $1/\sigma^2(F_o^2)$. Neutral atom scattering factors for Cu were taken from the compilation of Cromer and Waber;[57] those for the other nonhydrogen atoms were from ref 58. Hydrogen atom scattering factors are those of Stewart et al.[59] The real component of the anomalous dispersion correction[60] was included for Cu.
(57) D. T. Cromer and J. T. Waber, *Acta Crystallogr.*, **18**, 104 (1965).
(58) "International Tables for X-Ray Crystallography", Vol. III, Kynoch Press, Birmingham, England, 1962.
(59) R. F. Stewart, E. R. Davidson, and W. T. Simpson, *J. Chem. Phys.*, **42**, 3175 (1965).
(60) D. T. Cromer, *Acta Crystallogr.*, **18**, 17 (1965).
(61) The form of the correction for secondary extinction is $F_c = F_c(1 + cI_c)$. The value from the refinement is $2.00\ (9) \times 10^{-6}\ e^{-2}$.
(62) The R index is $\sum|F_o - F_c|/\sum|F_o|$. The goodness of fit is $\sum w(F_o^2 - F_c^2)^2/(n - p)$, where n is the number of observations and p is the number of parameters.
(63) R. R. Gagné, J. L. Allison, and G. Lisensky, manuscript in preparation.

PROPOSITIONS

Proposition 1

Abstract

It is proposed that one enantiomer of various helicenes be adsorbed on basal plane graphite electrode surfaces, and that this chiral surface be used to electrosynthetically prepare optically active compounds. It is further proposed that certain polyaromatic compounds be synthesized which would allow electroactive ions to be held a specific distance from an electrode in order to study the effect of distance on electron transfer kinetics.

The deliberate chemical alteration of an electrode surface to form so-called "chemically modified electrodes" (CME's) is an area of intense activity (1). The earliest reports in this field (2,3) suggested that CME's might be used for two important purposes:

a) asymmetric electrosynthesis could be induced by attachment of optically active compounds to electrode surfaces, and

b) the effect of distance on heterogenous electron transfer rates could be studied by geometrically constraining electroactive substances at fixed positions from electrodes. To date neither of these goals has been effectively realized.

In his initial paper Miller demonstrated that graphite surfaces can be coated with S-(-)-phenylalanine, presumably through the formation of an amide bond with surface oxides. Such surfaces, when used in the electroreduction of certain ketones, produce alcohols that are optically active (2). Isotropic polycrystalline graphite was used in that work; however, graphite is inherently an anisotropic material. It is made up of layers of carbon atoms having the two-dimensional structure shown below (4,5):

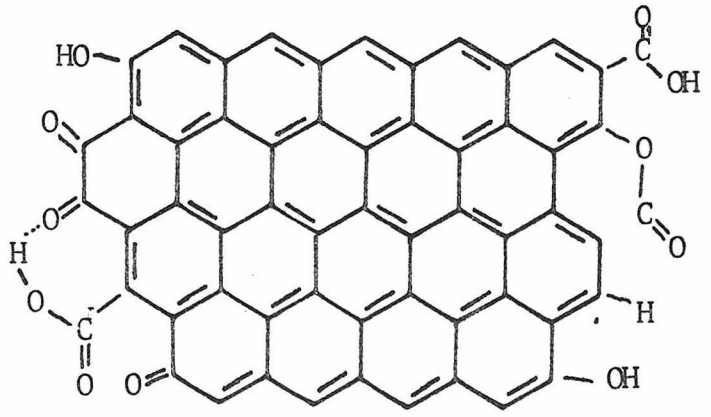

Layers are held together weakly and stack in an ABABAB lattice. Depicted in the drawing are some of the surface oxides that terminate the "edges" of the lattice (6). Bulk quantities of graphite having this isotropic structure can be manufactured; the name used is highly ordered pyrolytic graphite (HOPG). Orientations exposing the oxide functionality are usually referred to as edge plane, with those exposing the polyaromatic face being referred to as basal plane. Recently Miller, using HOPG, showed that, as expected, his treatments only worked on the edge planes (7). Unfortunately, this type of CME has not become a general tool for asymmetric synthesis. This most widely used method for asymmetric electrosynthesis involves relatively weak adsorption of chiral alkaloids at mercury electrodes (8). If surface geometry is responsible for the preferential formation of one enantiomer of the product, then graphite with a completely chiral surface should have general applicability. It is proposed that such a surface can be made by adsorbing molecules generally known as helicenes on basal plane HOPG surfaces.

Helicenes are molecules whose helical structures arise when steric considerations preclude planarity. The first synthesis and resolution of a helicene, hexahelicene, was published by Newman and Lednicher (9). The structure of one entiomer, compatible with proton n.m.r. data, is:

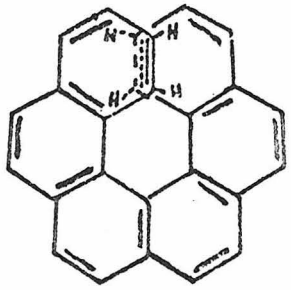

More recently, Martin and coworkers have developed a general procedure leading to the synthesis of hepta-, octa-, and nona-helicenes (10,11). The process involves the photocyclodehydrogenation of 1,2-diarylethylenes:

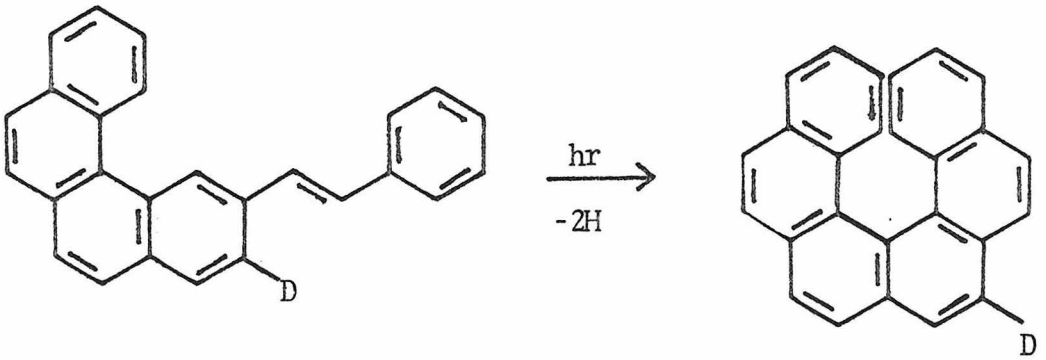

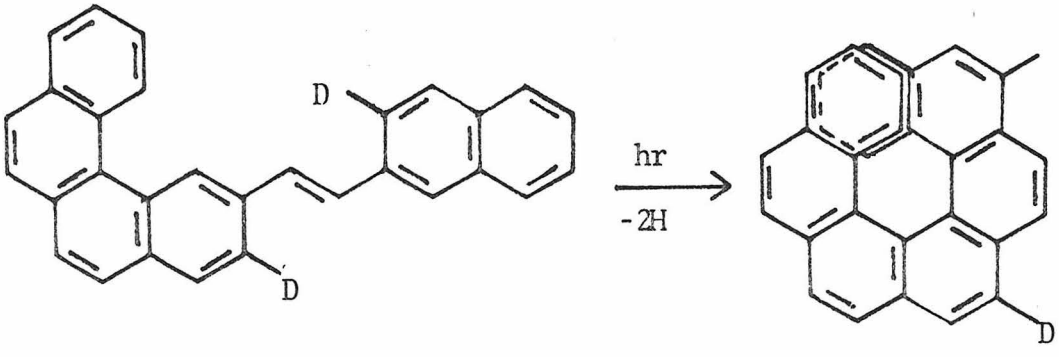

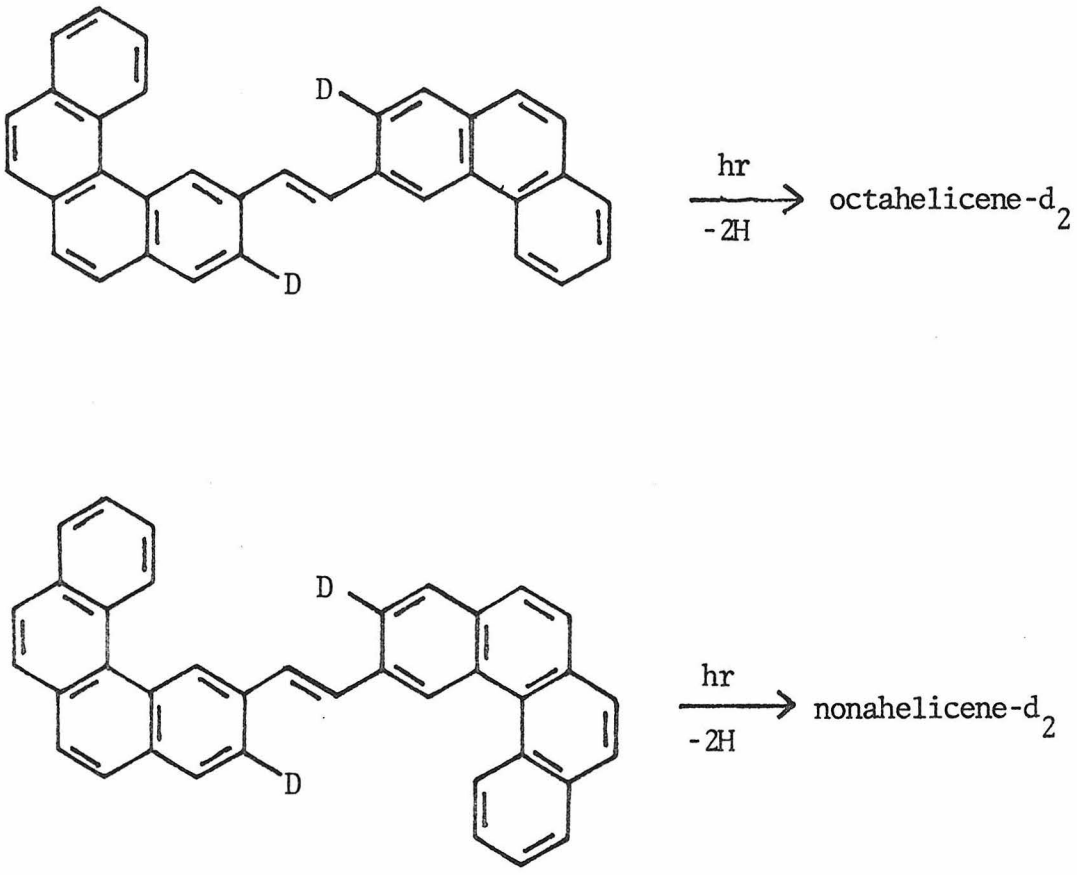

Combinations of deuterium labeling and ^{13}C - NMR spectroscopy have been used to distinguish the helicenes from other isomers whose presence is due to double photocyclizations and isomerizations (12).

Martin et al. have also discovered an interesting method of resolving helicenes through a procedure of repeated crystallization. The maximum rotations measured were (13):

Helicene	$(\alpha)^{25^\circ}_{579}$ ($CHCl_3$)
hepta-	(-) 6900° ± 200
octa-	(-) 6900° ± 200
nona-	(-) 8100° ± 200

These same researchers have studied the racimization of helicenes by what was believed to be a purely conformational pathway. They published the following data (14):

Helicene	$\Delta H^{\ddagger}$ (kcal/mole)	$\Delta S^{\ddagger}$ (e.u.)	$\Delta G^{\ddagger}_{(27^\circ)}$ (kcal/mole)	$Ea_{(27^\circ)}$ (kcal/mole)
hexa-	35.0	-4.2	36.2	35.6
hepta-	40.5	-3.9	41.7	41.4
octa-	41.0	-4.6	42.4	41.6
nona-	41.7	-6.1	43.5	42.3

These results indicate that racimization should not constitute a problem under normal conditions. Furthermore, if the pathway is conformational, racimization would be expected to be slower for an adsorbed species than for a solution species.

There is ample evidence to support the contention that helicenes would be adsorbed on graphite. For over a century it has been known that aromatic molecules such as dyes are strongly adsorbed on graphite and carbons. The reasons for this adsorption are not well-understood, but most evidence indicates that the adsorption takes place on the basal plane (6).

It might be possible to determine adsorption isotherms for the helicenes on the materials one intended to use as electrodes. Adsorption isotherms are graphs of quantity of adsorbate/surface area vs. solution concentration of adsorbate. Isotherms are usually obtained by measuring the intensity of an adsorbate spectral band before and after a solution of known concentration of adsorbate is "washed" with a weighed quantity of the graphite of interest. In the case of helicenes, one could take advantage of the large optical rotations of the molecules. Rotation is proportional to concentrations, and isotherms could be obtained by measuring the change in solution rotation after equilibrium was reached with a known amount of graphite. Of course, these experiments would not determine whether the helicenes were being adsorbed on the edge or basal planes.

If adequate adsorption did not occur spontaneously from solvents in which helicenes are soluble ($CHCl_3$or C_6H_6) one could resort to painting electrodes with such solutions and allowing the solvent to evaporate. In any case, should one be able to attain high surface coverages, the problem of desorption during subsequent electrolysis would not be major. In common practice, electrosynthetic reactions are run in solvents of high dielectric constants, such as H_2O or CH_3CN. The insolubility of helicenes in these solvents would retard their desorption. In addition to being stable to desorption, helicene-coated electrodes should be robust towards oxidation and reduction. The electrochemistry of many

polyaromatic compounds has been studied and tabulations of the results of such research suggest that potentials of ~1.0 V to ~-1.5 V vs SCE in solvents such as DMF or CH_3CN should be accessible (15).

The success of this research will be measured by obtaining yields of optically active compounds. Since it is hoped that the chiral electrode will have general applicability, one will want to test it on a variety of systems. Initially, systems will be selected with the following considerations in mind:

a) The reaction should be known to take place at graphite at a potential within the limits of the modified electrode.

b) The reaction should be carried out in a solvent where helicenes have limited solubility.

c) The reaction should have high yield. (This reduces the ambiguity of results.)

d) The product should have a high, known rotation, as this would facilitate detection of an excess of one enantiomer.

Possible organic electrode reactions can be located in texts on the subject (16). Two possibilities are:

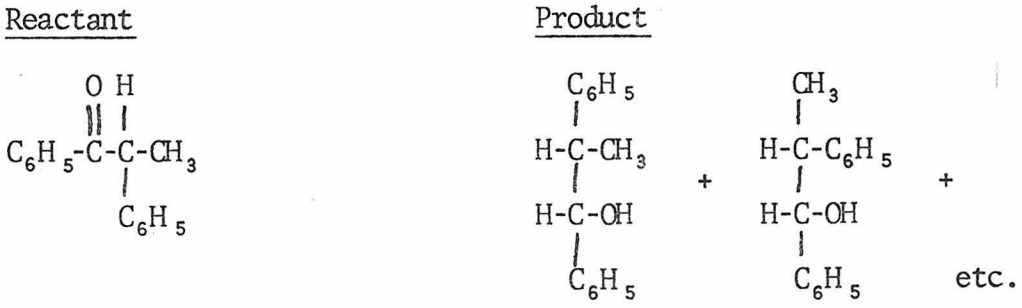

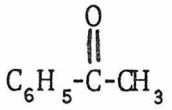

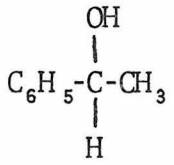

A non-trivial assumption implicit in the research proposed so far is that an adsorbed layer of helicenes will not inhibit electron transfer from the electrode to the substrate. Absorption of organics on platinum or mercury electrodes often causes redox reactions to procede at a slower rate, especially when the reaction proceeds via an inner-sphere pathway. One reason for assuming that monolayer coverages of helicenes would not have a similar effect is that the adsorbate is completely conjugated, identical to the electrode in composition, and similar in structure. Indeed, polyaromatic compounds that, unlike helicenes, are completely planar are essentially the same as a small, single sheet of graphite. Furthermore, if such a molecule were to adsorb flatly onto a graphite basal plane then it might even be considered to be an extension of the surface. This is an intriguing idea because it is almost impossible to imagine any other conducting solid for which isolation of molecular-size portions can be achieved while retaining the ability to replace the molecule in the lattice. If this idea is accepted, one could also imagine doing chemistry on the removable portion before replacement. Creative synthesis of such molecules could provide insight into the distance that an ion must

be from an electrode in order to exchange electrons. As stated previously, this has long been a goal in CME research. Conclusive results have not been obtained for two reasons:

a) Attachment of electroactive species is usually through a "floppy" chain which makes distance from the surface impossible to control, and

b) Even if molecules could be anchored by two or more somewhat rigid chains lack of knowledge about the attachment site on the electrode would still make results ambiguous.

Consider the molecule, L, drawn below:

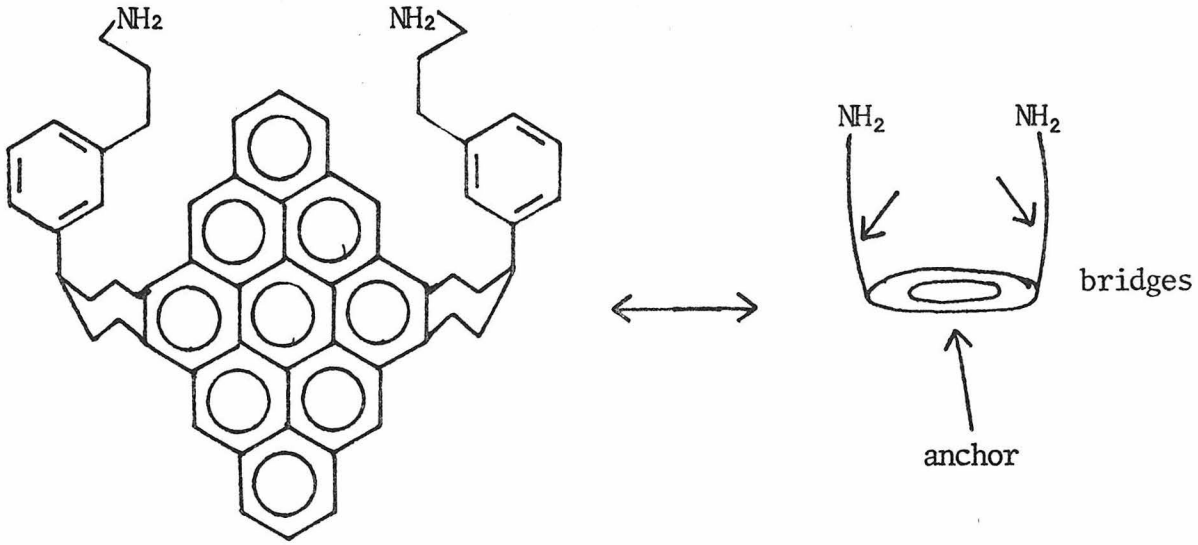

L

Molecular models indicate that if this molecule were complexed with trans-Ru(II)$(NH_3)_4(H_2O)_2$ a rigid structure would result with the ruthenium atom held in a fixed position above the plane of the anchor. Below is a drawing depicting the complex after adsorption on basal plane graphite:

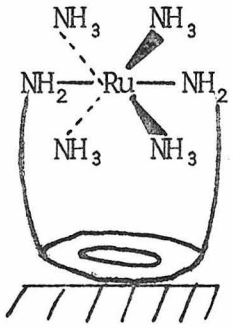

It is proposed that this and other similar complexes be synthesized and adsorbed on graphite electrodes, and that the electron transfer kinetics of the ruthenium atoms then be studied using techniques already in the literature (17).

Ruthenium is chosen as a probe ion in these studies for several reasons. The redox couple

$$Ru(NH_3)_6^{3+} + e^- \rightleftharpoons Ru(NH_3)_6^{2+}$$

has a high heterogenous electron transfer rate constant, k_{et}, that usually causes the couple's electrochemistry to be diffusion-controlled. This, along with the fact that the electrode reaction proceeds by an outer-sphere mechanism (18), would suggest that a decrease in k_{et} was due to a distance effect. Synthesis of the

constrained Ru(II) hexamine complexes should be easily accomplished from either cis or trans$[Ru(NH_3)_4Cl_2]Cl$ (19). High-dilution techniques would probably be necessary to avoid polymer formation, and column chromatography could be used for the purification of the mononuclear complex. Once the complex was formed it would not be expected to be substitution labile either as Ru(II) or as Ru(II) (18).

Synthesis of the ligand, L, or of other ligands for the same purpose would indeed be difficult. Possible syntheses will not be given here because the exact approach would be dictated by what groups made up the bridges. All such ligands would have to contain an anchor of at least six aromatic rings to provide a stable, planar base. The bridge should be rigid, but with as little conjugation as possible to avoid creating an alternate electron pathway.

If distance-dependent values of k_{et} were found for these complexes, x-ray crystallography could be used to find more exact Ru-electrode distances.

References

1. For example see C. A. Koval and F. C. Anson, Anal. Chem. 50, 223 (1978); N. Oyama, A. P. Brown, and F. C. Anson, J. Electroanal. Chem. 87, 435 (1978), and references therein.
2. B. F. Wadkins, J. R. Behling, E. Kariv, and L. L. Miller, J. Am. Chem. Soc. 97, 3459 (1975).
3. A. T. Hubbard and R. F. Lane, J. Phys. Chem. 77, 1401, 1411 (1973).
4. W. Ruland, Chemistry and Physics of Carbon, edited by P. L. Walker, Marcel Dekker, Inc. N.Y. (1969), Vol. 4, pp. 1-83.
5. A. W. Moore, Chemistry and Physics of Carbon, edited by P. L. Walker, Marcel Dekker, Inc. N.Y. (1974), Vol. 11, pp. 69-187.
6. J. A. Mattson and H. B. Mark, Activated Carbon, Marcel Dekker, Inc. N.Y. (1971).
7. B. E. Firth, L. L. Miller, M. Mitani, T. Rodgers, J. Lennox and R. W. Murray, J. Am. Chem. Soc. 98, 8271 (1976).
8. J. Kopilov, E. Kariv, and L. L. Miller, J. Am. Chem. Soc. 99, 3450 (1977), and references therein.
9. M. S. Newman and D. Lednicher, J. Am. Chem. Soc. 78, 4765 (1956).
10. M. Flammang-Barbieux, J. Nasielski, and R. H. Martin, Tetra Lett. 743 (1967).
11. R. H. Martin, M. Flammang-Barbieux, J. P. Cosyn, and M. Gelbcke, Tetra. Lett.3507 (1968).
12. R. H. Martin, and J. J. Schurter, Tetrahed. 28, 1749 (1972).
13. R. H. Martin and M. J. Marchant, Tetrahed. 30, 347 (1974).
14. R. H. Martin and M. J. Marchant, Tetrahed. 30, 347 (1974).

15. C. K. Mann and K. K. Barnes, Electrochemical Reactions in Nonaqueous Solvents, Marcel Dekker, Inc. N.Y. (1970).

16. M. M. Baizer, Organic Electrochemistry, Marcel Dekker, Inc. N.Y. (1973).

17. A. P. Brown and F. C. Anson, Anal. Chem. 49, 1589 (1977).

18. J. F. Endicott and H. Tabue, J. Am. Chem. Soc. 86, 1886 (1964) and Inorg. Chem. 4, 437 (1965).

19. K. Gleu and W. Brevel, Z. Anorg. Allg. Chem. 237, 197 (1938).

Proposition 2

Abstract

An electrochemical study of the reaction of Co(II)(salen) with dioxygen in pyridine is suggested. The intent of the experiments is to obtain thermodynamic and kinetic data for the reaction which could then be used in attempts to synthesize and characterize copper-oxygen complexes.

The interaction of dioxygen with transition metals has been a particularly active research area over the past thirty years. While oxygen complexes are known for many first-row transition elements, by far the greatest number of complexes is known for cobalt (1-5). There are three basic structurally-characterized types of cobalt dioxygen complexes which are diagrammed below (6):

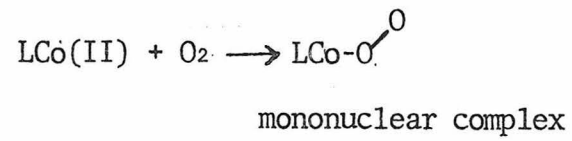

mononuclear complex

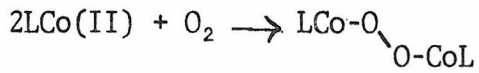

μ-peroxo complex

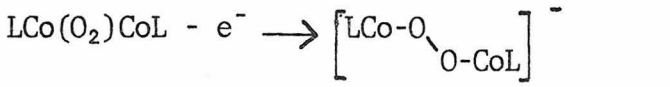

μ-peroxo complex μ-superoxo complex

In contrast to the array of complexes known for cobalt, not a single structurally-characterized dioxygen complex is known for copper, although the existence of such complexes in solution has been suggested (7-10). The inability of synthetic chemists to make copper dioxygen complexes is puzzling in light of the existence of naturally occurring copper-containing enzymes which bind dioxygen (11).

While the properties of cobalt-oxygen complexes have been intensively studied (1-5), the simple dynamics of the formation of these complexes are not understood (12,13). For example, consider the equilibria below:

$$LCo(II) + O_2 \underset{k_{-1}}{\overset{k_1}{\rightleftharpoons}} LCoO_2$$

$$LCoO_2 + LCo(II) \underset{k_{-1}}{\overset{k_2}{\rightleftharpoons}} LCoO_2CoL$$

Despite the amount of work done on cobalt-oxygen complexes, these equilibria have not been fully described for a single system (12,13). This is partially due to the fact that most kinetic studies have been done in aqueous solution, where the presence of protons or hydroxide ion can complicate the above equilibria. Hydroxide ions can form a second bridge in the bi -cobalt complexes (2,4,12) and all of the complexes will probably be thermodynamically unstable in acid. If studies of the reactions of cobalt and oxygen were carried out in aprotic media, these complications should be avoidable.

One reason that there are more cobalt than copper dioxygen compounds is that when cobalt binds to oxygen it usually adopts a formally Co(III)-d_6 configuration (2,3) resulting in strong and inert bonds. For both Cu(II) and Cu(I), ligands are relatively

weakly bound and substitution-labile. If there was greater understanding of the dynamics of the binding of oxygen to cobalt, however, it might be possible to direct experiments toward formation and characterization of copper-oxygen complexes. The remainder of this proposition will attempt to suggest the following:

a) That cobalt systems exist that would lend themselves to thermodynamic and kinetic studies of O_2 binding in non-aqueous media,

b) That electrochemistry might be an excellent way to obtain such data and to characterize dioxygen complexes in solution, and

c) That the literature already contains evidence that similar studies might be possible for copper.

The system that would be chosen for initial study would be the reaction of O_2 in neat pyridine with bis(salicylaldehyde)ethylene-diimino cobalt(II), Co(II)(salen).

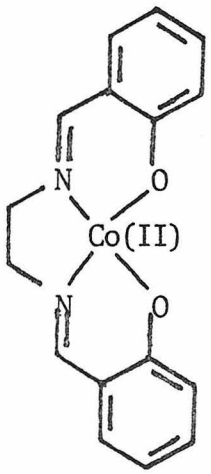

Co(II)(salen) = LCo(II)

This complex forms characterized mononuclear and μ-peroxo complexes, the latter of which can probably be oxidized to a μ-superoxo complex (2). Furthermore, formation of both the mononuclear and μ-peroxo complexes occurs in pyridine at ambient temperatures (14). The oxygen reaction of Co(II)(salen) in pyridine and other solvents has been qualitatively investigated, leading to the following observations (10,17):

a) The reaction occurs at room temperature in pyridine (PY) N,N-dimethylformamide (DMF) and dimethylsulfoxide (DMSO),

b) The μ-peroxo complex is eventually formed in the above solvents, with the mononuclear complex having the most stability in pyridi , and

c) The oxygenation reaction does not occur in tetrahydrofuran (THF), dimethylacetaamide (DMA), toluene or chloroform at room temperature, but the reaction does occur at lower temperatures in these solvents to form the mononuclear complex.

These observations indicate that pyridine would make an excellent solvent for initial studies because it might be possible to examine both the mononuclear and μ-peroxo complexes. The electrochemistry of the mononuclear complex in pyridine has already been the subject of a preliminary investigation (15, 16), the most significant results of which are:

a) In deaerated solutions both the $LCo(III)^{+}/LCo(II)$ and $LCo(II)/LCo(I)^{-}$ couples are electrochemically reversible, and

b) the $LCoO_2$ complex has a reversible reduction process to form $[LCoO_2]^-$.

The electrochemical reduction of O_2 to O_2^- is also reversible in pyridine (18). The binding of O_2 to Co(II)(Salen) to form a mononuclear complex might then be analyzed using the following scheme (19):

#	Process	Thermodynamic Constant
1	$LCo(III)^+ + e^- \rightleftharpoons LCo(II)$	$E_1^f \sim -0.54$
2	$LCo(II) + e^- \rightleftharpoons LCo(I)^-$	$E_2^f \sim -1.57$
3	$O_2 + e^- \rightleftharpoons O_2^-$	$E_3^f \sim -1.08$
4	$LCo(II) + O_2 \underset{k_{-4}}{\overset{k_4}{\rightleftharpoons}} LCoO_2$	K_4
5	$LCo(III)^+ + O_2^- \underset{k_{-5}}{\overset{k_5}{\rightleftharpoons}} LCoO_2$	K_5
6	$LCo(III)^+ + O_2 + e^- \rightleftharpoons LCoO_2$	$E_6^f \sim ?$
7	$LCo(II) + O_2 \underset{k_{-7}}{\overset{k_7}{\rightleftharpoons}} LCo(III)^+ + O_2^-$	K_7
8	$LCo(II) + O_2^- \underset{k_{-8}}{\overset{k_8}{\rightleftharpoons}} (LCoO_2)^-$	K_8
9	$LCo(I)^- + O_2 \underset{k_{-9}}{\overset{k_9}{\rightleftharpoons}} (LCoO_2)^-$	K_9
10	$LCoO_2 + e^- \rightleftharpoons (LCoO_2)^-$	$E_{10}^f \sim -0.87$
11	$LCo(I) + O_2 \underset{k_{-11}}{\rightleftharpoons} LCo(II) + O_2^-$	K_{11}

K_7 can be found immediately by subtracting process 1 from 3; $K_7 = \exp[F(E_3^f - E_1^f)/RT]$. Subtracting process 5 from 4 also gives process 7 which means that $K_7 = K_4/K_5$. The electrochemical reaction depicted in process 6 might provide an easy method for measurement of K_4 and subsequent calculation of K_5. If oxygen binds only to LCo(II) and process 4 is a rapid equilibrium, which it apparently is, measurement of E_6^f under conditions of excess O_2 yields K_4 using the formula (20):

$$E_6^f - E_1^f = .059 \log(1+K_4[O_2]).$$

The use of this method is in some doubt because Costa et al. report no potential shift in E_1^f in the presence of O_2 although they believe that they are operating under the assumptions described above (16). Several explanations are possible. First, O_2 could remain in the coordination sphere of the oxidized cobalt complex, binding with equal strength as in the reduced form. This hypothesis could be tested by changing solvents, because the binding of each solvent to Co(II) would be different. Second, if $[O_2]$ were $\sim 10^{-3}$ M and K was 100 or less, $E_6^f - E_1^f$ would be only a few millivolts. Going to lower temperatures should increase $[O_2]$. Studies on similar complexes suggest that K_4 would also increase because of a large negative entropy term (21). If shifts could be then be seen, variable temperature studies would provide K_4, K_5, and K_7 and their ΔH and ΔS values.

Subtracting process 2 from 3 gives process 11, implying that $K_{11} = \exp[F(E_3^f - E_2^f)/RT]$. Process 11 can also be obtained by subtracting process 8 from 9, which means that $K_{11} = K_9/K_8$. Process 10 provides a possible method of obtaining K_8 and hence K_4. It is possible to view process 10 as the effect of LCo(II) on the reduction of O_2 to O_2^-. If the wave due to process 10 is truly reversible and if $LCoO_2$ and $(LCoO_2)^-$ are the only species involved the ratio of K_4/K_8 can be found from the expression $E_{10}^f - E_3^f = .059 \log K_4/K_8$. If K_4 is known from prior experiments, K_8 and K_9 can be calculated. Again, variable temperature measurements are possible, yielding ΔH and ΔS values. Completion of the analysis described above would constitute a complete thermodynamic description of the mononuclear complex.

With regard to kinetics, knowledge of the various equilibrium constants means that measurement of one rate constant in a particular equilibrium immediately yields the other one. Of processes 4,5,8, and 9, only K_4 could be easily measured using an electrochemical method. For example, a rotating ring-disc electrode (RRDE) could be used to form LCo(II) from $LCo(III)^+$ at the disc and monitor the creation of $LCoO_2$ at the ring by potentiostating at the top of the $LCoO_2/(LCoO_2)^-$ wave (22). Forward rates might be obtained for the other reactions using spectroscopic techniques.

Very little is known about the electrochemistry of the cobalt μ-peroxo complexes, possibly because they tend to have low

solubility (2). This difficulty could possibly be overcome by using normal- or differential-pulse techniques which can detect concentrations of 10^{-5} - 10^{-6} M. Until preliminary studies revealed what electrode processes occurred for a μ-peroxo complex, it would not be worthwhile to attempt an analysis like the one presented above. At the very least, however, one would be interested in obtaining information about the equilibrium

12 $$LCoO_2 + LCo(II) \underset{k_{-12}}{\overset{k_{12}}{\rightleftharpoons}} LCoO_2CoL \qquad K_{12}$$

and about the redox process

13 $$(LCoO_2CoL)^{+} + e^{-} \rightleftharpoons LCoO_2CoL \qquad E^{f}_{13} \quad .$$

The difficulty with regard to measuring k_{12} lies in the fact that k_{-12} is often very small, making it difficult to be certain that a true equilibrium is established. Once again working in anhydrous pyridine should be an advantage because decomposition of the oxygen complexes should not be a problem. Once characteristic electrochemistry for all of the complexes has been established, these electrochemical techniques can be used to determine concentrations of various species in equilibrium mixtures. Finally, it should be noted that it would only be necessary to obtain a constant for the equilibrium

$$14 \qquad 2LCo(II) + O_2 \underset{k_{-14}}{\overset{k_{14}}{\rightleftharpoons}} LCoO_2CoL \qquad K_{14}$$

if an independent value of K_4 were known, since $K_{14} = K_{12}K_4$.

Regardless of the thermodynamic information available, electrochemical observation of process 13 or any reversible reductions of a μ-peroxo complex would be valuable as a method of characterization. The presence of these waves could also be used in an electrochemical kinetic measurement of K_{12}. As the oxidation of μ-peroxo complexes using outer-sphere oxidant has been studied in water, the detection of this process should be possible in pyridine which has an anodic limit of +1.4 V versus an $Ag/AgNO_3$ (1 M), pyridine reference electrode (23).

In addition to its other advantages in the study of Co(II)(salen) reactions with O_2, pyridine is an excellent electrochemical solvent. Although it has a low dielectric constant, many common supporting electrolytes (LiCl,$NaBPh_4$, TEAP, etc.) are soluble in pyridine giving solutions with low resistance. Pyridine is a non-viscous liquid from -41° C to 115° C and is also relatively easy to dry and purify (23).

One final reason for choosing pyridine as a solvent is that it provides a point with which to attempt to relate cobalt-oxygen chemistry to copper-oxygen chemistry. As stated earlier, cobalt-oxygen complexes often possess kinetic stability in water allowing a variety of studies in this solvent (2). The reaction of Cu(I) with oxygen in aqueous media rapidly proceeds to the first

thermodynamic sink, Cu(II) and H_2O_2 (24-31). In pyridine, however, Davies has reported a stable Cu(I) peroxo-complex (9). The key points in this paper are:

a) The overall reaction is:

$$4Cu(I)Cl + O_2 \xrightarrow{\text{pyridine}} 2Cu(II)(py)_2Cl_2 + Cu_2O_2;$$

b) The $Cu(II)(py)_2Cl_2$ is recoverable. Attempts to isolate the Cu_2O_2 species leads to CuO;

c) The Cu_2O_2 species is electroactive in solution, showing a "polarographic wave" at -.95 V which is identical to a wave found for H_2O_2;

d) The Cu_2O_2 species has a sharp Raman band at 856 cm^{-1} (876 cm^{-1} for H_2O_2.);

e) The Cu_2O_2 species has no spectrum in a 10^{-2} M solution.

The brevity of Davies' report causes the conclusion concerning the structure of the Cu_2O_2 species to be less than convincing, and no mention was made of the mechanism of the reaction.

It should be possible to prepare Davies' Cu_2O_2 species electrochemically, avoiding the chromatography procedures which were used. Cupric ion could be generated in the deaerated pyridine by

oxidizing copper metal with various anions, including chloride, present as the supporting electrolyte. After admission of O_2, Cu(I) could be generated at an Hg pool. This process would continue until all the original Cu(II) had reacted, leaving no need to separate a Cu(II) byproduct. Excess oxygen could be removed by deaeration.

Although Davies reports the presence of a "polarographic wave" at -.95 V, he does not say whether it is an oxidation or reduction, whether the process is reversible, or even what the reference electrode is. After determining the open circuit potential of the Cu_2O_2 solution, both oxidation and reductions could be examined. While a formally Cu(I) μ-peroxo complex is not strictly analogous to formally Co(III) complexes, similarities in electrochemistry along with thermodynamic notions derived from cobalt-oxygen studies might suggest further experiments. If the complexes formed by Cu(I) and oxygen in pyridine proved to be too unstable, similar studies using ligands like those described by Osborn (8) and Wilson (7) should be more fruitful.

References

1. For example, see the review articles listed in references 2-5 and further references therein.
2. G. McLendon and A. E. Martell, Coord. Chem. Rev. 19, 1 (1976).
3. F. Basolo, B. M. Hoffman and J. A. Ibers, Acc. Chem. Res. 8, 384 (1975).
4. R. G. Wilkins, Bioinorganic Chem. R. F. Gould, Ed, Amer. Chem. Soc. (1971) pp. 111-34.
5. A. G. Sykes and J. A. Weil, Prog. Inorg. Chem. 13, 1 (1970).
6. The symbol, L, represents all other ligands in the cobalt coordination sphere.
7. M. G. Simmons and L. J. Wilson, Chem. Comm. 634 (1978).
8. J. F. Bulkowski, P. L. Burk, M. F. Ludman and J. A. Osborn, Chem. Comm. 498 (1977).
9. C. E. Kramer, G. Davies, R. B. Davis, and R. W. Slaven, Chem. Comm. 606 (1975).
10. F. Ochiai, Inorg. Nucl. Chem. Lett. 9, 987 (1973).
11. R. Lontie and L. Vanquickenborne, Metal Tons in Biological Systems, Vol. 3, H. Sigel, ed. Marcel Dekker, N.Y. (1974), Ch. 6.
12. G. McLendon and M. Mason, Inorg. Chem. 17, 362 (1978).
13. E. Ochiai, J. Inorg. Nuc. Chem. 35, 1727 (1973).
14. See references 10, 15, 16 and further references therein.

15. G. Costa, A. Puxeddu and L. B. Stefani, Inorg. Nucl. Chem. Lett. 6, 191 (1970).

16. J. Hanzlik, A. Puxeddu and G. Costa, J. Chem. Soc. Dal. 542 (1977).

17. C. Floriani and F. Calderazzo, J. Chem. Soc. A 946 (1969).

18. M. E. Poever and B. S. White, Electrochim. Acta 11, 1061 (1966).

19. The E^f values are approximate ones taken from reference 16.

20. R. R. Gagné, J. L. Allison, R. S. Gall, and C. A. Koval, J. Am. Chem. Soc. 99, 7170 (1970).

21. M. J. Carter, D. P. Rillema, and F. Basolo, J. Am. Chem. Soc. 96, 392 (1974).

22. W. L. Albery and M. L. Hitchman, Ring-Disc Electrodes, Oxford Univ. Press, London (1971) Ch. 6.

23. C. K. Mann, Electroanalytical Chemistry Vol. 3, A. J. Bard, ed. Marcel Dekker, Inc. N.Y. (1969) pp. 57-132.

24. M. Güntensperger and A. D. Zuberbühler, Helv. Chim. Acta 60, 2584 (1977).

25. A. D. Zuberbühler, Metal Ions in Biological Systems, Vol. 5, H. Siegel, ed, Marcel Dekker, Inc. N.Y. (1976) pp. 325-68.

26. A. L. Crumbliss and L. J. Gestaut, J. Coord. Chem. 5, 109 (1976).

27. A. L. Crumbliss and A. T. Poulos, Inorg. Chem. 14, 1529 (1975).

28. I. Pecht and M. Anbar, J. Chem. Soc. A, 1002 (1968).

29. R. D. Gray, J. Am. Chem. Soc. 91, 56 (1969).

30. P. M. Henry, Inorg. Chem.4, 688 (1966).

31. H. Nord, Acta Chem. Scand. 9, 431 (1955).

Proposition 3

Abstract

A rate study of the reaction of binuclear ruthenium complexes with the two-electron oxidant Tl^{3+} is proposed. The results of the study could have implications for catalysis of multi-electron reactions.

The current inorganic literature abounds with reports describing syntheses of multi-metal complexes. These systems often display unusual and fascinating physical properties, but the common rationale for the creation of polynuclear complexes is that they may possess catalytic properties not found in similar mononuclear systems. Invariably the processes that are to be catalyzed involve more than one electron, and there are two basic advantages that a polynuclear catalyst might have over a mononuclear one. The first is the ability to bind a substrate in a geometry that would be impossible for a mononuclear complex. (One can think of this "substrate binding" as substrate activation, or lowering the energy of a transition state or intermediate.) For example, suppose that an oxygen reduction catalyst proceeded by the following mechanism:

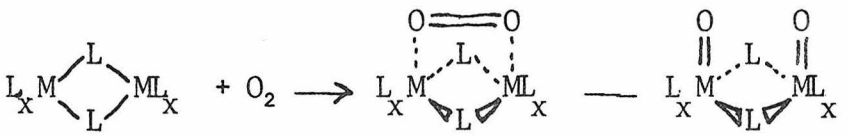

Two analogous mononuclear complexes could not approach dioxygen in the same way for steric reasons, which might lead to different products:

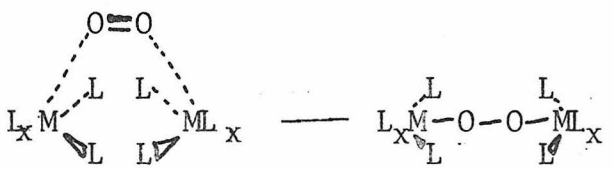

Even if the same geometries are available to both a mononuclear and binuclear catalyst, the latter might have a kinetic advantage:

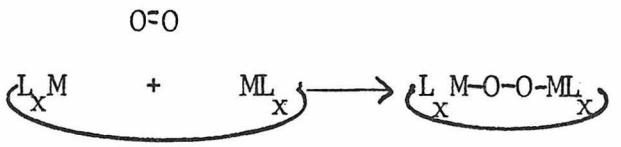

$$L_xM + O=O + ML_x \longrightarrow L_xM - O - O - ML_x$$

$$L_xM\ O=O \longrightarrow L_xM - O - O \xrightarrow{L_xM} L_xM - O - OML_x$$

Notice that the binuclear catalyst completes the process in a single step, while the mononuclear complex requires either a termolecular process or an extra, possible kinetically slow, step.

The second advantage that a polynuclear complex has is the ability to donate the exact number of electrons needed in the multi-electron process in a single step. This advantage is similar to the kinetic one discussed above for substrate binding, yet it can be described less subjectively since the phenomenon is well-known in electron transfer kinetics.

In 1933 P. A. Shaffer observed that while the Ce^{4+}/Ce^{3+} and $Tl^{3+}+Tl$ couples appeared to be electrochemically reversible, implying that they exchange electrons rapidly with electrodes, solutions of ceric sulfate are virtually unreactive towards solutions of thallous sulfate despite a favorable reaction free energy. From this and similar observations Shaffer proposed the principle of equi-valence change (1,2). Simply, reactions between

ions whose stable oxidation states vary by two equivalents will react much more slowly with one-equivalent ions than with other two-equivalent ions. The reasoning behind this principle was summarized by Halpern in 1959 (3). Suppose B is a two-equivalent oxidant with stable oxidation states B^n and B^{n+2}. If B^{n+2} reacts with a two-equivalent reductant A^n whose next stable oxidation state is A^{n+2}, a simple bimolecular mechanism is possible.

$$A^n + B^{n+2} \longrightarrow A^{n+2} + B \qquad \text{mechanism 1}$$

If, however, the only other stable oxidation state of A^n is A^{n+1}, three different mechanisms are possible

$$2A^n + B^{n+2} \longrightarrow 2A^{n+1} + B^n \qquad \text{mechanism 2}$$

$$A^n + B^{n+2} \longrightarrow A^{n+1} + B^{n+1}$$
$$A^n + B^{n+1} \longrightarrow A^{n+1} + B^n \qquad \text{mechanism 3}$$

$$A^n + B^{n+2} \longrightarrow A^{n+2} + B^n$$
$$A^n + A^{n+2} \longrightarrow 2A^{n+1} \qquad \text{mechanism 4}$$

The rate of a process proceeding via mechanism 2 is limited by the low probability of termolecular reactions. Mechanisms like 3 and 4 are rate limited by the unfavorable thermodynamics associated

with the formation of B^{n+1} and A^{n+2}, respectively (4). If the first step in either reaction is an equilibrium, for example,

$$A^n + B^{n+2} \underset{k_{-1}}{\overset{k_1}{\rightleftharpoons}} A^{n+1} + B^{n+1}$$

then the maximum rate of reaction is k_1 which equals $k_{-1}K$ where K is the equilibrium constant. Since k_{-1} has a diffusion-limited maximum value of $\sim 10^{10}$ ℓ mole^{-1} sec^{-1} (5), a small value for K can limit the overall reaction rate.

It is difficult to imagine a simple set of experiments with which to quantify the kinetic implications of binuclear as opposed to mononuclear substrate binding. On the other hand, electron transfer experiments like those used to study the Shaffer principle of equi-valence change should be readily adoptable for the study of binuclear complex reaction kinetics. It is proposed herein to study the reaction of Tl^{3+} with ruthenium(II)-pentaamminepyridine complexes having the general formula

$$(NH_3)_5Ru(II)(py\text{-}B\text{-}py)Ru(II)(NH_3)_5^{4+}$$

along with appropriate monomers, in order to gain insight into one of the catalytic aspects of polynuclear compounds.

The ion Tl^{3+} should serve as an adequate "substrate" in the proposed study. In perchloric acid solutions free of complexing

anions, Tl^{3+} and Tl^{+} exist as aquo ions although $Tl(H_2O)_n^{3+}$ is a fairly strong acid with an acid dissociation constant of 7.3×10^{-2} (6). Fortunately, the reaction rates for $Tl(H_2O)_{n-1}(OH)^{2+}$ are similar to those for $Tl(H_2O)_n^{3+}$ (7) and the concentration of the former can be depressed by working in concentrated acid. The self-exchange reaction between Tl^{3+} and Tl^{+} was measured as early as 1949 (8,9). In molar acid the second order rate constant is approximately 10^{-4} M^{-1} sec^{-1}. Although early kinetic studies could not distinguish between a direct two-electron exchange and a mechanism involving Tl^{2+}, recent pulse radiolysis studies have ruled out Tl^{2+} as an intermediate (10). When Tl^{3+} reacts with a one-electron reductant such as ferrous ion, Tl^{2+} is formed as an intermediate (11) as deduced from kinetic studies which support the following mechanism:

$$Tl^{3+} + Fe^{2+} \underset{k_{-1}}{\overset{k_1}{\longrightarrow}} Tl^{2+} + Fe^{3+}$$

$$Tl^{2+} + Fe^{2+} \longrightarrow Tl^{+} + Fe^{3+}$$

These results are also consistent with pulse radiolysis studies (10). The rate constant k_{-1} is ~1.4×10^{-2} M^{-1} sec^{-1}. Notice that this rate is significantly faster than the Tl^{3+}/Tl^{+} self-exchange rate, in apparent contradiction with the Shaffer principle. Halpern explained this phenomenon by noting that the activation enthalpy is higher for ferrous reaction but a favorable activation entropy,

which is associated with the formation of weakly hydrated Tl^{2+}, is responsible for the faster rate (3). Also, the Tl^{3+}/Tl^{+} exchange reaction has no driving force while the reaction of Tl^{3+} and Fe^{2+} has a E^{o}_{reac} of ~0.5 V.

Ruthenium pentamminepyridine complexes,both mononuclear and binuclear, have several properties which make them logical choices for these studies:

a) The complexes are nearly inert with respect to substitution even in strongly acidic solutions (12,13),

b) The Ru(II)Ru(III) redox couple is usually electrochemically reversible in complexes of this type allowing formal potentials to be easily obtained (14,15), and

c) Electron-transfer reactions involving ruthenium complexes with 6 nitrogen ligands will almost certainly proceed by an outer-sphere mechanism (4).

The synthesis of the ruthenium compounds should not prove difficult. The usual synthetic route involves the reaction of $Ru(II)(NH_3)_5(H_2O)^{+}$ with the appropriate nitrogen heterocycle (16,17). A large number of binuclear complexes has already been synthesized and characterized (16-19). Some of the bridging ligands used are drawn below:

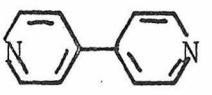

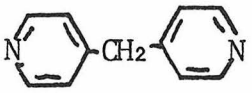

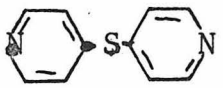

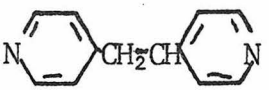

The initial stages of the proposed research would involve the synthesis of several binuclear complexes and appropriate monomers. This would be followed by a brief study of the kinetics of the reaction between the Ru(II) monomers and Tl^{3+} to establish that they are reacting by the same mechanism as Fe^{2+} and to measure their rates. Finally, the kinetics of the reaction of the binuclear Ru(II) complexes with Tl^{3+} would be studied. An attempt would be made to obtain rates for comparison with the monomeric rates and to establish whether or not Tl^{2+} was an intermediate in the binuclear reaction.

In addition to ruling out Tl^{2+} as an intermediate in the Tl^{3+}/Tl^{+} exchange reaction, pulse radiolysis studies have provided additional data about the Tl^{3+}/Tl^{+} couple that allow estimation of the electron transfer rates that might be observed. These data are included in Table 1 along with similar data for other selected processes. Using the Marcus cross-reaction equation without correction for work terms (27)

$$k_{12} = (k_{11}k_{22}k_{12}f)^{\frac{1}{2}}$$

$$\ln f = [[\ln k_{12})^{\frac{1}{2}}/4]/\ln(k_{11}k_{22}/10^{22})$$

One can calculate a number of rates which are given in Table 2. As noted by Schwarz, the Marcus equation provides an excellent estimation of k_{18}, which is the rate determining step in the reduction of Tl^{3+} by ferrous ion. Because $Ru(NH_3)_5(py)^{2+}$ has a faster self-exchange rate and more driving force, the mononuclear rate of reduction of Tl^{3+} is estimated to be ~10^4 M^{-1} sec^{-1}. Evidence exists, however, that suggests that the reaction of mononuclear ruthenium complexes with thallic ion might be slower than predicted. As Taube has recently pointed out (19), the reaction of ruthenium complexes with ferric ion is ~100 times slower than predicted by Marcus theory. Two specific examples demonstrating this point are processes 20 and 21 in Table 2. Furthermore, although the Ce^{4+}/Ce^{3+} exchange reaction is complicated by hydroxide complex formation (28,29), preventing use of the Marcus equation, it is difficult to understand why ceric ion does not react with Tl^{+}. Except for the unknown Ce^{4+}/Ce^{3+} exchange rate, the driving force and complementary self-exchange process is similar to the ferrous ion reaction with Tl^{3+}. Finally, it might be possible to suppress mononuclear rates by using complexes with two pyridine molecules in the ruthenium coordination sphere. As shown in Table 1, processes 6 and 8, t-$Ru(NH_3)_4(py)_2^{2+}$ has ~0.2 V

less driving force than does $Ru(NH_3)_5(py)$. The self-exchange rate for the former is not known.

It is difficult to estimate the rates of binuclear ruthenium complex reaction with Tl^{3+}. The principal problems are estimating exchange rates for the binuclear complexes and deciding whether or not the simplified Marcus equation is meaningful for a two-electron process. If one assumes that the mono- and binuclear exchange rates are the uses the Tl^{3+}/Tl^{+} formal potential to calculate k_{12}, a reduction rate of $\sim 10^6$ can be estimated (Table 2, process 22). While the use of Marcus theory would complement the proposed experiments, the type of reaction being proposed is different enough from simple electron transfer that the actual data would undoubtedly present many surprises.

One experimental difficulty that is certain to complicate analysis of the rate data is the inevitable presence of mixed-valence species. For example, $(NH_3)_5Ru(4,4'\text{-bipy})Ru(NH_3)_5^{5+}$. At best mixed-valence ions will constitute 50% of an equilibrium mixture of the fully oxidized and fully reduced complexes. Their reaction rates with Tl^{3+}, however, should be similar to those found for the mononuclear complexes and their influence on overall rates should be interpretable.

Depending upon the success of these preliminary experiments, a variety of follow-up investigations can be imagined. A few possibilities are: steric effects of the bridging group; the

effect of intra-molecular electron transfer between the ruthenium atoms; and reactivity of asymmetrical systems.

Table 1

#	Process	Exchange Rate (M^{-1} sec^{-1}) or Formal Potential (V)
1	$Tl^{3+} + 2e^- \rightleftharpoons Tl^+$	$E^f = 1.26$ (21)
2	$Tl^{3+} + e^- \rightleftharpoons Tl^{2+}$	$E^f = 0.33$ (10)
3	$Tl^{2+} + e^- \rightleftharpoons Tl^+$	$E^f = 2.19$ (10)
4	$Fe^{3+} + e^- \rightleftharpoons Fe^{2+}$	$E^f = 0.77$ (21)
5	$Ru(NH_3)_6^{3+} + e^- \rightleftharpoons Ru(NH_3)_6^{2+}$	$E^f = 0.05$ (14)
6	$Ru(NH_3)_5(py)^{3+} + e^- \rightleftharpoons Ru(NH_3)_5(py)^{2+}$	$E^f = 0.30$ (14)
7	$Ru(NH_3)_5(isn)^{3+} + e^- \rightleftharpoons Ru(NH_3)_5(isn)^{2+}$	$E^f = 0.37$ (15)
8	$t\text{-}Ru(NH_3)_4(py)_2^{3+} + e^- \rightleftharpoons t\text{-}Ru(NH_3)_4(py)^{2+}$	$E^f = 0.49$ (15)
9	$(NH_3)_5Ru(4,4\text{-bipy})Ru(NH_3)_5^{6+} + 2e^- \rightleftharpoons (NH_3)_5Ru(4\text{-}4\text{-bipy})Ru(NH_3)_5^{4+}$	$E^f \sim 0.35$ (26)
10	$Ce^{4+} + e^- \rightleftharpoons Ce^{3+}$	$E^f = -1.61$ (21)
11	$*Tl^{3+} + Tl^+ \rightleftharpoons *Tl^+ + Tl^{3+}$	$k_{ex} = 1.2 \times 10^{-4}$ (10)
12	$*Tl^{3+} + Tl^{2+} \rightleftharpoons *Tl^{2+} + Tl^{3+}$	$k_{ex} = 3 \times 10^4$ (10)
13	$*Tl^{2+} + Tl^+ \rightleftharpoons *Tl^+ + Tl^{2+}$	$k_{ex} = 1.5 \times 10^4$ (10)
14	$*Fe^{3+} + Fe^{2+} \rightleftharpoons *Fe^{2+} + Fe^{3+}$	$k_{ex} = 4.2$ (22)
15	$*Ru(NH_3)_6^{3+} + Ru(NH_3)_6^{2+} \rightleftharpoons$ etc.	$k_{ex} = 2.8 \times 10^4$ (23,24)
16	$*Ru(NH_3)_5(py)^{3+} + Ru(NH_3)_5(py)^{2+} \rightleftharpoons$ etc	$k_{ex} = 2.2 \times 10^3$ (25,24)
17	$*Ru(NH_3)_5(isn)^{3+} + Ru(NH_3)_5(isn)^{2+} \rightleftharpoons$ etc	$k_{ex} = 4.3 \times 10^5$ (19)

Table 2

#	Process	k_{calc} (M^{-1} sec^{-1})	k_{obs} (M^{-1} sec^{-1})
18	$Tl^{3+} + Fe^{2+} \longrightarrow Tl^{2+} + Fe^{3+}$	2.6×10^{-2}	1.4×10^{-2}
19	$Tl^{3+} + Ru(NH_3)_5(py)^{2+} \rightarrow Tl^{2+}+Ru(NH_3)_5(py)^{3+}$	1.5×10^{4}	?
20	$Fe^{3+}+Ru(NH_3)_6^{3+} \rightarrow Fe^{2+}+Ru(NH_3)_6^{8+}$	3.5×10^{7}	3.4×10^{5}
21	$Fe^{3+}+Ru(NH_3)(isn)^{2+} \rightarrow Fe^{2+}+Ru(NH_3)_5(isn)^{3+}$	1.4×10^{6}	2.6×10^{4}
22	$Tl^{3+}+(NH_3)_5Ru(4\text{-}4'\text{-bipy})Ru(NH_3)_5^{4+} \rightarrow$ $Tl^{+}+(NH_3)_5Ru(4,4'\text{-bipy})Ru(NH_3)_5^{6+}$	1.3×10^{6}	?

References

1. P. A. Shaffer, J. Am. Chem. Soc. 55, 2169 (1933).
2. P. A. Shaffer, J. Phys. Chem. 40, 1021 (1936).
3. A. M. Armstrong and J. Halpern, Can. J. Chem. 37, 148 (1959).
4. H. Taube, Inorg. Chem. 12, 639 (1973).
5. W. C. Gardiner, Rates and Mechanisms of Chemical Reactions, W. A. Benjamin, Inc. Menlo Park, CA (1972) p. 168.
6. G. Biederman, Ark. Kemi, 5, 441 (1953).
7. F. Basolo and R. G. Pearson, Mechanisms of Inorganic Reactions, John Wiley and Sons, Inc. N.Y. (1967) p. 490.
8. R. J. Prestwood and A. C. Wahl, J. Am. Chem. Soc. 71, 3137 (1949).
9. G. Harbottle and R. W. Dodson, J. Am. Chem. Soc. 73, 2442 (1951).
10. H. A. Schwarz, D. Comstock, J. K. Yandell, and R. W. Dodson, J. Phys. Chem. 78, 488 (1974).
11. K. G. Ashurst and W. C. Higginson, J. Chem. Soc. 3044 (1953).
12. P. Ford, D. F. Rudd, R. Gaunder and H. Tabue, J. Am. Chem. Soc. 90, 1187 (1968).
13. P. C. Ford, J. R. Kuempel and H. Taube, Inorg. Chem. 7, 1976 (1968).
14. H. S. Lim, D. J. Barclay and F. C. Anson, Inorg. Chem. 11, 1460 (1972).

15. T. Matsubara and P. C. Ford, Inorg. Chem. 15, 1107 (1976).

16. C. Creutz and H. Taube, J. Am. Chem. Soc. 95, 1086 (1973).

17. G. M. Tom, C. Creutz and H. Taube, J. Am. Chem. Soc. 96, 7827 (1974).

18. G. M. Tom and H. Taube, J. Am. Chem. Soc. 97, 5310 (1975).

19. H. Taube, Bioinorganic Chemistry - II, K. N. Raymond, ed. Amer. Chem. Soc. Washington, D.C. (1977) pp. 127-144.

20. vs. n.h.e.

21. J. E. Huheey, Inorganic Chemistry, Harper and Row, N.Y. (1972) pp. 256-66.

22. J. Silverman and R. W. Dodson, J. Phys. Chem. 56, 846 (1952).

23. E. I. Solomon, P. J. Clendening, H. B. Gray, and F. J. Grunthaner, J. Am. Chem. Soc. 97, 3878 (1975).

24. Corrected to $\mu = 1.0$.

25. D. Cummins and H. B. Gray, J. Am. Chem. Soc. 99, 5158 (1977).

26. G. M. Tom, C. Creutz and H. Taube, J. Am. Chem. Soc. 96, 7827 (1974).

27. R. A. Marcus, J. Phys. Chem. 67, 853 (1963); ibid 43, 679 (1965).

28. J. W. Gryder and R. W. Dodson, J. Am. Chem. Soc. 73, 2890 (1951).

29. F. R. Duke and F. R. Parchen, J. Am. Chem. Soc. 78, 1540 (1956).

Proposition 4

Abstract

A method is proposed for obtaining Raman spectra of the intermediates formed in the photoreduction of trisoxalato complexes of Fe(III), Co(III), and Mn(III). Structural information concerning the intermediates might facilitate clarification of the currently disputed mechanism.

The photoreduction of the trisoxalato complexes of Mn(III), Fe(III), and Co(III) has been extensively studied (1). In solution the overall reaction is (2)

$$2M(III)(ox)_3^{3+} \xrightarrow{h\nu} 2M(II)(ox)_2^{2-} + ox^{2-} + 2CO_2$$

M = Fe, Co, Mn ox = oxalate

Two similar photoprocesses occur for the compounds in the solid state where the stoichiometries are (3)

$$2K_3M(III)(ox)_3 \cdot 3H_2O \xrightarrow{h\nu} 2K_2Mn(II)(ox)_2 + K_2ox + 2CO_2 + 6H_2O$$

M = Mn, Co

$$2K_3M(III)(ox)_3 \cdot 3H_2O \xrightarrow{h\nu} 2M(II)(ox)_2 + 3K_2ox + 6H_2O$$

These processes occur using light from ~550 nm up to ~250 nm. The quantum yields, which can be greater than 1, decrease with decreasing wavelength. The high-energy portion of this spectral range is dominated by LMCT bands for all of the complexes; however, the photoreduction also occurs upon irradiation of ligand field bands.

Many attempts have been made to determine the mechanism of these reactions in solution. One of the earlier mechanisms proposed was (5-7)

$$M(III)(ox)_3^{3-} \xrightarrow{h\nu} {}^*M(III)(ox)_3^{3-}$$

$${}^*M(III)(ox)_3^{3-} \longrightarrow M(II)(ox)_2^{2-} + ox^{\cdot-}$$

$$ox^{\cdot-} + M(III)(ox)_3^{3-} \longrightarrow M(III)(ox)_2(ox^{\cdot-})^{2-} + ox^{2-}$$

$$M(III)(ox)_2(ox^{\cdot-}) \longrightarrow M(II)(ox)_2^{2+} + 2CO_2$$

$$2ox^{\cdot-} \longrightarrow 2CO_2 + ox^{2-}$$

More recent kinetic studies on solutions using flash photolysis have suggested increasingly complex mechanisms requiring a host of intermediates. Such studies on the photoreduction of $Fe(III)(ox)_3^{3+}$ have been done by Cooper and Degraff (8,9) and Jamieson and Perone (10,11). Recent work on $Co(II)(ox)_3^{3-}$ includes that by DeJaegere (12), Hoffman (13), and their coworkers. Some of the intermediates suggested in these papers are:

$ox^{\cdot-}$ $\quad$ $CO_{2}^{\cdot-}$ $\quad$ $M(II)(ox)_3^{4-}$

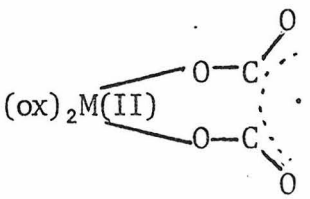

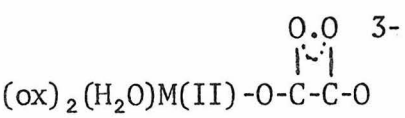

$(ox)_3M(II)(ox^{\cdot})^{5-}$ $(ox)_2M(II)(CO_2^{\cdot})^{3-}$

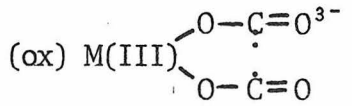

These intermediates were suggested to explain transient electronic spectra and some of them were detected by electrochemistry and ESR. Although much less conclusive studies have been completed on the solid state reaction, similar pathways and intermediates are usually proposed (3).

Considering the disagreement concerning the mechanism and the nature of the intermediate in trisoxalato M(III) photoreduction, spectra containing structural information on these species would be valuable. It is proposed herein that it might be possible to obtain Raman spectra of some of the intermediates which would provide such information.

Texts are available on Raman spectroscopy (14,15) and the subject will not be discussed at length here. Raman spectra contain information similar and complementary to infrared spectra. Because a minute portion of incident light undergoes Raman scattering, the technique has not been as widely used as has infrared spectroscopy; however, as high intensity laser sources are becoming more common, Raman spectroscopy is increasing in popularity. By using as a light source a laser with a frequency that is contained within an electronic

adsorption band of the sample, one can obtain enhancement of Raman signals that is as great as 10^5-10^6. This is the resonance Raman effect, which is particularly useful for inorganic systems (16,17) especially now that lasers with a variety of incident frequencies are available.

Raman spectroscopy has an additional advantage over infrared in that H_2O is a poor Raman scatterer making aqueous studies possible. Van Duyne and coworkers (18) have obtained resonance Raman spectra of species generated electrochemically in millimolar solutions.

In the proposed experiments, one would attempt to obtain Raman spectra of intermediates in the photoreduction of the tris-oxalato-complexes both in solution and in the solid state. Initially, the laser light used would be the source of both Raman scattering and photolysis. The solid samples would be in pressed discs and the solution would be in common round cells with flat bottoms. In both cases one would attempt to achieve the situation depicted below:

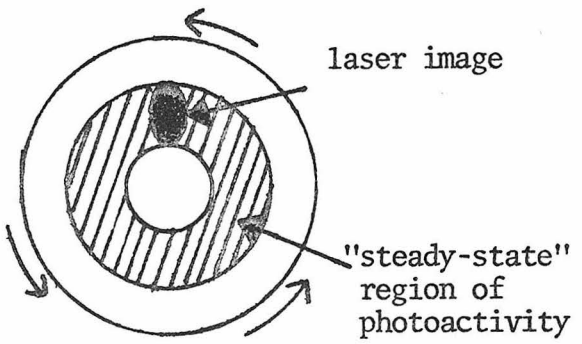

As indicated above, the sample will be spinning; therefore, species formed by photolysis will be swept through the laser beam a number of times and new species will continually be formed. Sample rotation is commonly used in Raman spectroscopy to prevent sample heating. A recent review by Kiefer, which contains useful illustrations and photographs, describes this and other Raman techniques (19). In a more complicated experiment, two laser sources might be used, one to cause photolysis and the other to study photoproducts:

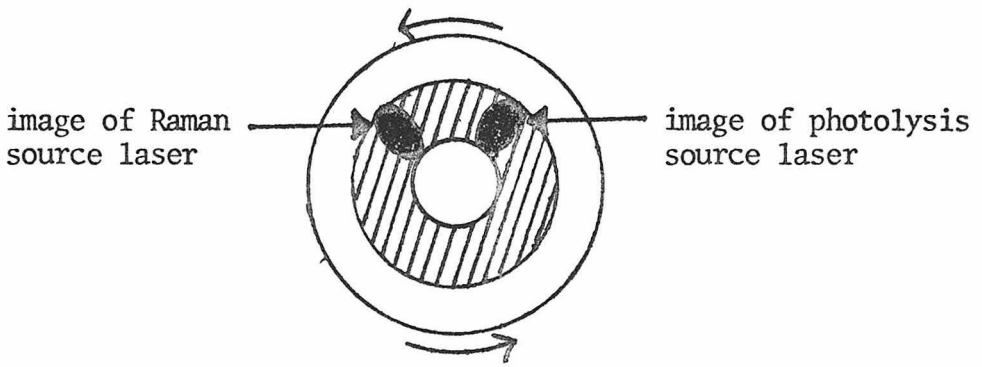

With both of the above set-ups, the experimental objectives would be the same. These would be to:

a) Obtain Raman spectra of the starting materials, $Mn(III)(ox)_3^{3-}$, and the photoproducts, $Mn(II)(ox)_2^{2-}$, ox^{2-} and CO_2, under separate conditions using laser light that caused no photolysis,

b) Attempt to generate some of the simple proposed intermediates such as ox^- and $CO_2^{\cdot-}$ by means other than photolysis and obtain their

Raman spectra,

c) Record spectra during photolysis, eliminating bands due to starting materials and photoproducts, and

d) Attempt to interpret the remaining bands in terms of the proposed intermediates.

References

1. For example, see references 2-4 and further references therein.
2. V. Balzani and V. Carassity, Photochemistry of Coordinatation Compounds, Academic Press, N.Y. (1970) pp. 138-40, 167-72, 221-4.
3. A. W. Adamson and P. D. Fleischer, Concepts of Inorganic Photochemistry, John Wiley and Sons, Inc. N.Y. (1975) pp. 395-7.
4. Z. Stasicka and A. Marchaj, Coord. Chem. Rev. 23, 131 (1977).
5. C. A. Parker, Proc. Roy. Soc. Ser. A 220, 104 (1953).
6. C. A. Parker, Trans. Far. Soc. 50, 1213 (1954).
7. C. A. Parker and C. G. Harchard, J. Phys. Chem. 63, 22 (1959).
8. G. D. Cooper and B. A. Degraff, J. Phys. Chem. 75, 2897 (1971).
9. G. D. Cooper and B. A. Degraff, J. Phys. Chem. 76, 2618 (1972).
10. R. A. Jamieson and S. P. Perone, J. Phys. Chem. 76, 830 (1972).
11. J. I. Patterson and S. P. Perone, J. Phys. Chem. 77, 2437 (1973).
12. L. Cordemans, J. D'Olieslager, J.Henrix and S. DeJaegere, J. Phys. Chem. 78, 1361 (1974).
13. N. S. Rowan, M. Z. Hoffman and M. Milburn, J. Am. Chem. Soc. 96, 6060 (1974).
14. D. A. Long, Raman Spectroscopy, McGraw-Hill, Inc. England (1977).
15. H. A. Szymanski, ed. Raman Spectroscopy, Vol I and II, Plenum Press, N.Y. (1967, 1970).

16. R. J. Clark, Adv. Infr. Ram. Spec. 1, 143-72 (1975).

17. R. S. Tobias, The Raman Effect, Vol. 2, A. Anderson, ed., Marcel Dekker, Inc. N.Y. (1973) pp. 405-518.

18. D. L. Jeanmaire, M. R. Suchanski and R. P. Van Duyne, J. Am. Chem. Soc. 97, 1699 (1975).

19. W. Kiefer, Adv. Infr. Ram. Spec. 3, 1-42 (1977).

Proposition 5

Abstract

A calculation of the bond energies of 1/1 complexes composed of Ni(0), Cu(I) and Zn(II) and five simple ligands is proposed. Trends in these bond energies could be used to help elucidate simple concepts in transition metal bonding. Experiments that would complement the calculations are also proposed.

When ligands bind to transition metals the most common orientation is for an orbital on the ligand, which contains a non-bonding or "lone" pair of electrons, to point directly at the metal atom. One idea used to explain why certain ligand-metal bonds are stronger than others is to treat the bond like the reaction of a Lewis acid and base:

Lewis acid Lewis base

An empirical concept which is used to explain why certain Lewis acid/base pairs bind more strongly than others is the hard and soft classification. Huheey's inorganic textbook contains a discussion of the hard/soft concept (1), the main points of which are presented below:

a) The term "hard" as applied to both acids and bases implies a small and relatively unpolarizable species, while the term "soft" implies a large and polarizable species;

b) In general, hard acids bind more strongly to hard bases than to soft bases and vice versa.

The hard/soft concept works well for ligands like amines and halides, but for other small-molecule ligands (e.g., carbon monoxide, cyanide ion, and isocyanides) an important concept is that of π-acidity. This subject is discussed in Cotton and Wilkinson's

text in terms of the following drawings (2):

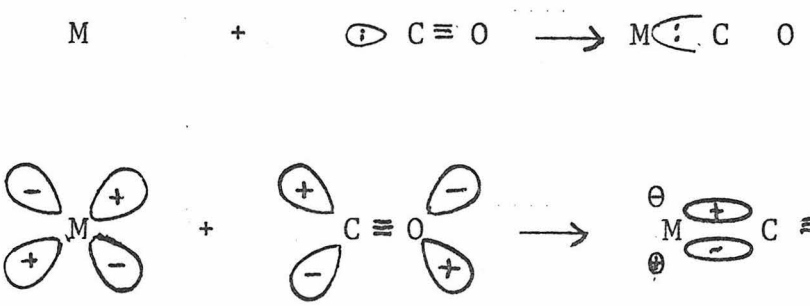

The top half of the drawing depicts the usual lone pair σ-donation toward the metal, while the bottom half suggests that filled metal d-orbitals can back-dontate into unfilled π*-orbitals on the CO. Evidence for this back-donation is found by examining the IR stretching frequencies of the ligand triple bond in the coordinated and uncoordinated states. The presence of electrons in the lone pair orbital is antibonding with respect to the triple bond; donation of these electrons toward the metal should strengthen the triple bond, resulting in a higher stretching frequency (3). On the other hand, back-donation of metal electrons into an orbital which is antibonding with respect to the triple bond should produce a lower frequency (2). In the case of carbon monoxide, which is usually considered to be a poor σ-donor and an excellent π-acceptor, stretching frequencies (γ_{CO}) are always found to be lower in metal complexes (1850-2125 cm^{-1}) than in free CO (2143 cm^{-1}) (2). When Co is bound to a strong Lewis acid which cannot back-donate, such as BH_3, γ_{CO} increases to 2164 cm^{-1} (4). With cyanide and

isocyanides, which are both σ-donors and π-acceptors, these same trends can be seen by using metals with different abilities to back-donate (5). For free CN_7^- γ_{CN} = 2080 cm^{-1} and in complexes γ_{CN} ranges from 1910 to 2185 cm^{-1} (5). Similar trends are found for isonitriles. Nitriles, which are very poor π-acceptors, normally have higher stretching frequencies in the coordinated state (5).

A further consideration in a discussion of metal-ligand binding is the ability of the ligands to lower the energy of the system through crystal field stabilization energy (CFSE) (6). Consideration of CFSE is the main factor involved in the creation of another ordering of ligand binding strengths, the spectrochemical series.

With all of the above-mentioned factors in play at once, it is difficult to isolate the effect of any individual factor on a metal ligand bond. It is proposed herein that one could attempt this isolation by applying theoretical calculations to the 1/1 complexes made up of the metal atoms and ligands shown below:

Metal atoms	Ligands
Ni(O)	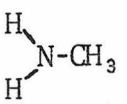
	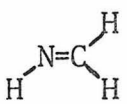
Cu(I)	N≡C-H
Zn(II)	C≡N-H
	C≡O

The isoelectronic series of metal atoms Ni(0), Cu(I) and Zn(II) was chosen for several reasons. The most important is that in their normal complexes these metals have a closed-shell, d^{10} configuration which will eliminate the need to worry about crystal field effects. Furthermore, because of their position at the right side of the transition series these elements have relatively tightly bound d-orbitals which implies only slight ability to overlap with π^* ligand orbitals. This assertion is supported by the fact that $Ni(CO)_4$ is the last stable zero-valent carbonyl complex encountered proceeding to the right across the first transition series, (2), as well as by the fact that only recently have simple mono-carbonyls been discovered for Cu(I) (7). No Zn(II) carbonyls are known. Working with metals in this borderline region of back-donation should provide interesting insights into the process. Finally, this group of metal atoms forms a reasonable series of Lewis acids from the hard Zn(II) to the soft Ni(0).

The ligands were also chosen to represent a series going from the hard ammine to the softer immine to the soft nitrile. While the nitrile is a σ-donor and poor π-acceptor, the isoelectronic isonitrile is both a good σ-donor and π-acceptor. Finally, the poor σ-donor and good π-acceptor, CO, ends the series. For the immine, nitrile, and isonitrile ligands, R-groups instead of hydrogens would be necessary in order to make the synthesis of the complexes possible. These were not included in the chosen ligands in order to simplify calculations.

The principal purpose of the proposed calculations is to obtain bond energies for the fifteen metal-ligand pairs. This would be done using the generalized valence bond (GVB) method. Goddard and coworkers have written an overall description of the GVB method (8) and a GVB calculation of one of the metal-ligand pairs, Ni(0)-CO, has already appeared (9). The GVB description of CO is not unusual and similar descriptions should be possible for the other ligands. In the description of the metal, an additional technique is used in conjunction with the GVB method. This technique uses effective potentials to describe the inner 18-electrons of the metal atoms (10), an approximation which greatly simplified such calculations.

One problem certain to arise in the calculations is that the ground state configurations for the metal atoms both free and complexed, would not be d^{10}. This is due to electron-electron repulsion in the tightly bound d-orbitals which can be alleviated by promotion of one or two electrons to the 4s orbital. For example, in Ni(0) the ground state is s^2d^8 with the s^1d^9 state slightly higher (11). In Ni(0)-CO, the s^1d^9 configuration becomes the ground state (9). One could, however, use the excited state d^{10} configuration in the calculations. This would result in the situation drawn below:

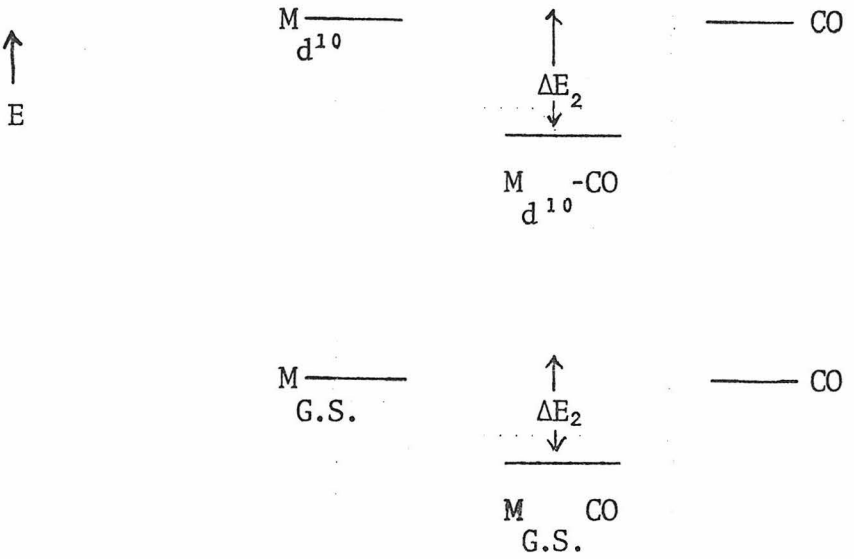

The bond energy for the d^{10} state, ΔE_2, would not be expected to be same as the ground state bond energy, ΔE_1, yet the relative values of ΔE_2 for the different metal-ligand pairs would be more useful in comparisons to real inorganic systems. Systematic differences in ΔE_1 and ΔE_2 might also be revealing, serving as an evaluation of the important of d-orbitals in the bonding.

Two other methods of gaining insight into the role of back-bonding in these complexes can be envisioned. When the metal atom and ligand are brought together, one could essentially "freeze" the d-orbitals into their atomic descriptions and see what effect this had on ΔE_2. An even more drastic approach would be to attempt to describe the entire metal atom as an effective potential and see if bonding still occurred.

Regardless of the success of the additional calculations, the main result would be the relative ordering of the ΔE_2 values.

A priori, one would expect that Zn(II) would bond most strongly to the ammine and only weakly to the π-acids, with Ni(O) doing just the opposite. The Cu(I) bonding preferences should be intermediate between Ni(O) and Z(II).

Theoretical calculations are usually more interesting when the results can be compared to experimental values. This would be difficult in the case of the ΔE_2 values because even if the bond energies for the complexes could be measured they would correspond to values of ΔE_1. Trends in ΔE_1 and ΔE_2 might be the same, however, which would make it worthwhile to obtain relative bond energies for the complexes experimentally. For the Cu(I) and Zn(II) complexes this could be done using ion cyclotron resonance spectroscopy (ICR). This technique has been reviewed by Beauchamp (12) and has recently been used to measure the binding of various ligands to Li^+ (13). In these experiments a more logical series of ligands would be:

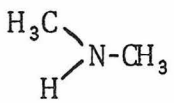

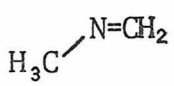

$N\equiv C-CH_3$

$C\equiv N-CH_3$

$C\equiv O$

Since Ni(0) is not an ion, it could not be examined with this technique. Instead, Ni(0)-ligand complexes using the above ligands could be formed by using frozen maxtrix techniques to examine the complexes spectroscopically (14). The complex Ni(0)-CO has already been examined in this way (15). While these experiments would not provide bond energies, properties such as stretching frequencies could be compared to those afforded by the calculations.

References

1. J. E. Huheey, Inorganic Chemistry, Harper and Row, N.Y. (1972) Ch. 6.
2. F. A. Cotton and G. Wilkinson, Advanced Inorganic Chemistry, Interscience Publishers, N.Y. (1972) Ch. 22.
3. W. England, L. S. Salmon and K. Ruedenberg, Topics in Current Chemistry, 23, 31 (1971).
4. R. D. Cowan, J. Chem. Phys. 18, 1101 (1950).
5. K. Nakamoto, Infrared and Raman Spectra of Inorganic and Coordination Compounds, John Wiley and Sons, N.Y. (1978) pp. 259-270.
6. See reference 1, Ch. 8 and reference 2, Ch. 20.
7. R. R. Gagné, J. L. Allison, R. S. Gall, and C. A. Koval, J. Am. Chem. Soc. 99, 7170 (1977), and references therein.
8. W. A. Goddard, T. H. Dunning, W. J. Hunt and P. J. Hay, Acc. Chem. Res. 6, 368 (1973).
9. S. P. Walch and W. A. Goddard, J. Am. Chem. Soc. 98, 7908 (1976).
10. C. F. Melius, B. D. Olafson, W. A. Goddard, Chem. Phys. Lett. 28, 457 (1974).
11. C. E. Moore, Atomic Energy Levels, Vol. II, National Bureau of Standards (1952).
12. J. L. Beauchamp, Ann. Rev. Phys. Chem. 22, 527 (1971).

13. R. L. Woodin and J. L. Beauchamp, J. Am. Chem. Soc. 100, 501 (1978).

14. G. A. Ozin, Acc. Chem. Res. 10, 21 (1977).

15. M. Moskovits, G. A. Ozin, and J. R. Durig, ed., Vib. Spectra. Struct. 4, 187 (1975).